BNL-108392-2015-JA

Do TFSA Anions Slither?

Pressure Exposes the Role of TFSA Conformational Exchange in Self-Diffusion

Sophia N. Suarez,*[†] Armando Rúa,[‡] David Cuffari,[†] Kartik Pilar,[‡] Jasmine L. Hatcher,[§,‖]

Sharon Ramati[‖] and James F. Wishart*[‖]

[†]Physics Department, Brooklyn College, Brooklyn, NY 11210

[‡]Department of Physics, Hunter College, New York, NY 10021

[§]CUNY Graduate School, New York, NY 10016

[‖]Chemistry Department, Brookhaven National Laboratory, Upton, NY 11973

* To whom correspondence should be addressed: S.N.S.: SNSuarez@brooklyn.cuny.edu; J.F.W.: wishart@bnl.gov

Abstract

Multi-nuclear (^{1}H, ^{2}H, and ^{19}F) magnetic resonance spectroscopy techniques as functions of temperature and pressure were applied to the study of selectively deuterated 1-ethyl-3-methylimidazolium bis(trifluoromethylsulfonyl)amide (EMIM TFSA) ionic liquid isotopologues and related ionic liquids. For EMIM TFSA, temperature-dependent ^{2}H T_1 data indicate stronger electric field gradients in the alkyl chain region compared to the imidazolium ring. Most significantly, the pressure dependences of the EMIM and TFSA self-diffusion coefficients revealed that the displacements of the cations and anions are independent, with diffusion of the TFSA anions being slowed much more by increasing pressure than for the EMIM cations, as

shown by their respective activation volumes (28.8 ± 2.5 cm^3/mol for TFSA vs. 14.6 ± 1.3 cm^3/mol for EMIM). Increasing pressure may lower the mobility of the TFSA anion by hindering its interconversion between *trans* and *cis* conformers, a process that is coupled to diffusion according to published molecular dynamics simulations. Measured activation volumes ($\Delta V^{\ddagger}$) for ion self-diffusion in EMIM bis(fluoromethylsulfonyl)amide and EMIM tetrafluoroborate support this hypothesis. In addition, ^2H T_1 data suggests increased ordering with increasing pressure, with two T_1 regimes observed for the MD_3 and D_2 isotopologues between 0.1-100 and 100-250 MPa respectively. The activation volumes for T_1 were 21 and 25 (0-100 MPa) and 11 and 12 (100-250 MPa) cm^3/mol for the MD_3 and D_2 isotopologues, respectively.

Introduction

There is great interest in studying ionic liquids (ILs) on a fundamental level as models for the transport properties of complex liquid systems, as well as for possible applications in several industries, including textiles, energy and nuclear waste recycling. With regards to energy, ILs comprised of imidazolium-based cations and their counter anions have formed the basis of many research projects geared towards the development of alternative electrolyte materials for energy storage devices such as batteries[1-4] and supercapacitors.[5-8] This is because of their useful combination of chemical, thermal and physical properties such as low volatility, combustion resistance and ionic conductivity. Another attractive feature of ILs is their tunability. Depending on the application, desired performance can be achieved by combining the right cation and anion to produce the required properties. Theories for controlling properties by design have been advanced based on trends observed in particular classes of ILs.[9-11] For example, it has been

proposed that if one desires better transport properties, the choice should be ions of small size, greater charge delocalization and multiple conformations that differ slightly in energy. However, experience has shown that empirical relationships are poor predictors of what properties will result from particular pairings for many cations and anions. Nevertheless, the bis(trifluoromethylsulfonyl)amide (TFSA, $(CF_3SO_2\text{-}N\text{-}SO_2CF_3)^-$) anion has become very popular in ionic liquid science for its tendency to form lower melting, lower viscosity and higher conductivity salts than many other anions. When combined with imidazolium cations, TFSA can produce fluid room temperature ILs with high ionic conductivity.[11]

Various techniques have been applied towards understanding the factors that control the fluid properties of ILs, including molecular dynamic simulations,[12-14] conductivity,[15,16] viscosity,[15-17] Raman spectroscopy[18-20] and nuclear magnetic resonance (NMR).[12,16,21-26] As a tool, NMR is able to provide nucleus-specific microscopic and macroscopic translational and rotational dynamics through determination of the spin-lattice relaxation time T_1 and the self-diffusion coefficient D, over a wide temperature and frequency range. Most NMR studies have been done as a function of temperature, which causes both changes in energy and density. However, when done as a function of pressure, NMR allows separation of the density effects from energy-related ones, which oftentimes control the transport dynamics of mobile systems, especially ones in which viscosity effects play a role. In this study we report multi-nuclear NMR (^1H, ^2H, and ^{19}F) T_1 relaxation and (^1H and ^{19}F) self-diffusion data as functions of temperature and pressure for the deuterated isotopologues of 1-ethyl-3-methylimidazolium (EMIM) cation with the TFSA anion, and for comparison, EMIM bis(fluoromethylsulfonyl)amide (FSA, also known as FSI) and EMIM tetrafluoroborate (BF_4). The selective deuteration allows us to analyze the fundamental dynamics of the cation through ^1H (I = ½) and ^2H (I = 1) probe nuclei. The quadrupole ^2H

nucleus is extremely sensitive to rotational dynamics and reflects the interaction between the nuclear quadrupole moment and its electric field gradient. The advantage of determining both T_1 and D data comes from the fact that analysis of T_1 data and associated correlation times often require an assumption about the relaxation mechanism and its relation to the translational motion of the probe species, while D data provides a direct determination of the translational motion.

Variable pressure has been used in vibrational spectroscopic studies of ILs[27-31] comprised of various anions and cations including EMIM and TFSA[18-20] and results show several behaviors, including conformational changes, enhancement of cation-anion hydrogen bonding interactions and shifts of vibrational frequencies to higher values. In this manuscript we present our findings of variable pressure and temperature NMR T_1 and D studies for EMIM TFSA, and pressure studies on EMIM FSA and EMIM BF_4. To the authors knowledge there have been no published variable-pressure NMR studies on these ILs. The initial objective for this study was to use selective deuteration to probe the local environment of each segment of the EMIM cation to identify each contribution to the transport properties of the IL. One question of interest was whether the motion of the anion is coupled to that of the cation at higher pressures. As increasing pressure is expected to affect the packing (molecular order) and possibly screening – two factors that affect the structure of ILs,[30] we expected to see these changes in both the short- and long-range dynamics of the system. Remarkably, as will be explained below, we found that the conformational dynamics of the TFSA anion dominate the effects of pressure on self-diffusion in EMIM TFSA.

One of the key molecular interactions in ILs is hydrogen bonding[30,32] through the C-H•••X and C-H•••O groups. Although weak in comparison with Coulombic interactions, hydrogen bonding plays a role in the structure and therefore dynamics of ILs. In general, strong hydrogen

bonding can produce order in systems and one example of this are the O-H•••O bonds in water. Because of this, numerous efforts has been directed towards determining its precise nature. While it is not the intention of this manuscript to explore explicitly the hydrogen bonding in the EMIM TFSA system, we will use it to explain our results where applicable. As hydrogen bonds are known to increase in strength with increasing pressure, our reasoning of their effect on the system's dynamics is applicable.

Experimental Section

Sample Preparation

Three partially-deuterated 1-ethyl-3-methylimidazolium bis(trifluoromethylsulfonyl)amide ILs were prepared by reaction of 1-methylimidazole with the appropriately deuterated ethyl bromide or the reaction of 1-ethylimidazole with methyl iodide-d_3, followed by metathesis to the TFSA salts using aqueous Li TFSA. Complete details regarding the synthesis can be found in the Supporting Information of Shkrob, *et al*.[33] Their structures are shown in Figure 1. The syntheses of EMIM FSI and EMIM BF_4 are reported in the Supporting Information. The samples were dried in a vacuum oven until their water content was below 200 ppm and stored in a dry argon-filled glove box to avoid absorption of atmospheric moisture.

Nuclear Magnetic Resonance

The ^{1}H spectra for EMIM TFSA were recorded using a Bruker Avance III 400 MHz SB spectrometer, using $CDCl_3$ as the ^{2}H lock and a small amount of TMS (^{1}H δ = 0 ppm) as the chemical shift reference.

The T_1 and D measurements were conducted on a Chemagnetics CMX-300 spectrometer as a function of temperature from 296 to 373 K and pressure (up to 2.5 kbar) with a 7.3T superconducting magnet. For this magnetic field, ^{1}H, ^{2}H and ^{19}F resonances occur at frequencies of 309, 47 and 283 MHz respectively. For both the ^{1}H and ^{19}F variable temperature T_1 and D measurements, the ILs were inserted into a 5 mm NMR tube. The experiments were performed in a 5mm Nalorac gradient probe and a current amplifier provided by Magnetic Resonance Instruments, Inc. The NMR spectra were obtained by collecting free induction decay following $\pi/2$ pulse and Fourier transforming the data.

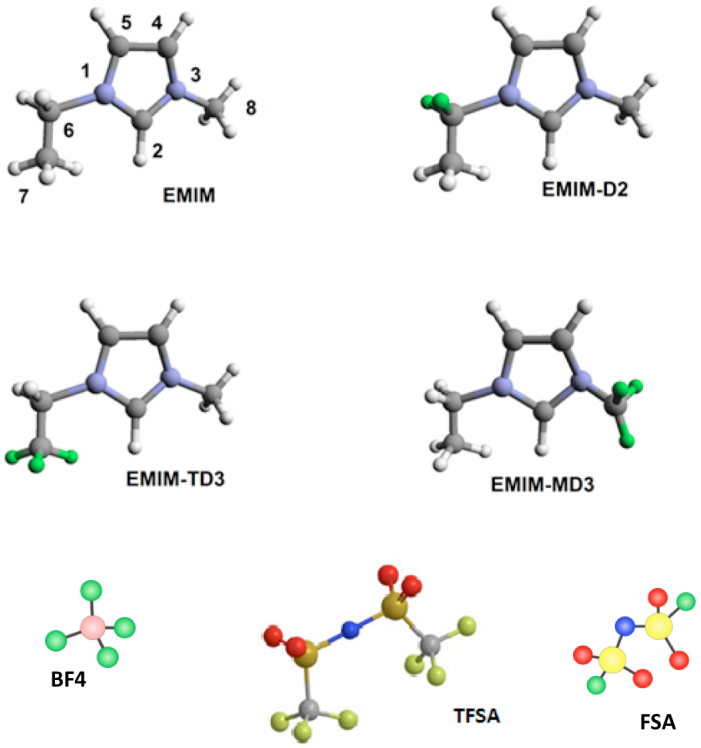

Figure 1. Structures of the deuterium-labeled (indicated in green) EMIM cations and the BF_4, FSA and TFSA anions (*cis* conformation shown).

Multinuclear spin-lattice relaxation measurements (T_1) were determined using the inversion recovery (180°-τ-90°-Acq) sequence for about 15 values of τ. At least five T_1s were allowed between repetitions of the pulse sequence and uncertainties were ~5%. Self-diffusion coefficients (D) can be obtained by using either static or pulsed field gradients with the Hahn spin-echo pulse sequence ($\pi/2$ - τ - π). For the pulsed field gradient technique, D values were obtained using the Hahn spin-echo pulse sequence with square-shaped gradient pulses of equal amplitude g, duration δ and separation Δ after the *rf* pulses. The values of δ and Δ are chosen to allow sufficient attenuation of the echo amplitude. The resulting attenuation depends on the change in positions and associated frequencies of the spins during the separation interval Δ and was shown to be represented by the equation:

$$A(g) = A_0 \exp[-2\tau/T_2] \exp[-D(\gamma\delta g)^2(\Delta-\delta/3)] \qquad 1$$

Here γ is the magnetogyric ratio, g is the gradient strength (dB/dz) and A_0 is the value of the echo amplitude at zero gradient. The values of both Δ and δ were adjusted at each new temperature setting and once optimized, g was varied to measure diffusion. The value of D was obtained by fitting the echo attenuation data for about 15 values of g ranging from ~0.2 – 3 T/m and uncertainties were ~ 5%. For D values determined by the static field gradient method, the echo attenuation profile is determined from:

$$A(\tau) = A_0 \exp[-2\tau/T_2] \exp[-2D(\gamma\tau g)^2\tau/3)] \qquad 2$$

For all D values calculated, single exponential attenuation profiles were obtained.

For the multi-nuclear variable pressure measurements, the ILs were hermetically sealed in a plastic bag, placed in an *rf* coil and immersed in the pressure transmitting fluid (Fluorinert FC-3283 and vacuum oil for ^{1}H and ^{19}F, respectively) inside a copper-beryllium pressure vessel. The pressure was generated using a manual pump that is capable of reaching pressures up to 2.5 kbar.

The probe used was home built with a tuning circuit with an effective range of 60-80 MHz, which corresponds to a static field gradient of 27.5-35 T/m. All variable pressure experiments were performed at 80 MHz using a 35 T/m gradient.

Calculation of activation volumes from literature data

Activation volumes for comparison with our experimental results were obtained from analysis of literature data sets of diffusion constants and viscosities measured versus pressure and temperature. Data sets were selected for analysis based on their relevance to the focus of the study and the availability of sufficient data for accurate fitting. All the data used, their sources, and the resulting fits are tabulated in Supporting Information Section 2.

Results and discussion

Ambient pressure experiments

Before presentation of our novel pressure dependence results we shall compare our T_1 relaxation results on the EMIM TFSA isotopologues at ambient pressure with previous reports. The ^{1}H NMR peak assignments are consistent with those of Hayamizu, *et al*.[22] and are tabulated in Table 1 following the scheme shown in Figure 1. A representative NMR spectrum for the MD_3 EMIM TFSA IL is shown in Figure S1 of Supporting Information Section 1. ^{19}F and ^{2}H NMR spectra (not shown) had single peaks.

Table 1. ^{1}H NMR parameters of each proton site of the EMIM cation in neat EMIM TFSA.

H label	**2**	**4**	**5**	**6**	**7**	**8**
δ (ppm)	8.45	7.39	7.32	4.14	1.42	3.84
Multiplicity	Triplet	DxD	DxD	Quadruplet	Triplet	Singlet
	$^4J_{H2-H4} = {}^4J_{H2-H5} =$ 1.60Hz $^3J_{H4-H5} = 2.00$Hz			$^3J_{H6-H7} = 7.34$Hz		

Variable-temperature diffusion and T_1 relaxation studies

The ^{1}H and ^{19}F spin-lattice relaxation times (T_1s) for EMIM TFSA are shown in Figure 2 as functions of inverse temperature. (Similar graphs for three deuterated isotopologues of EMIM are shown in Figures S2-S4 of Supporting Information Section 1.) For a heterogeneous spin I = ½ system, the magnetization recovery can have non-exponential behavior, making it difficult to determine a definitive T_1. Fortunately, for the samples studied all magnetization recoveries were exponential and the general behavior shows increasing T_1 with increasing temperature. The behavior for the adjacent ring protons H4 and H5 are identical and were the longest for all samples, while the NCH_3 and CH_2 protons had the shortest T_1s. The ^{19}F T_1s for CF_3 groups of TFSA were linear for all the samples. The data observed for the EMIM TFSA sample is consistent with that in the literature.[22]

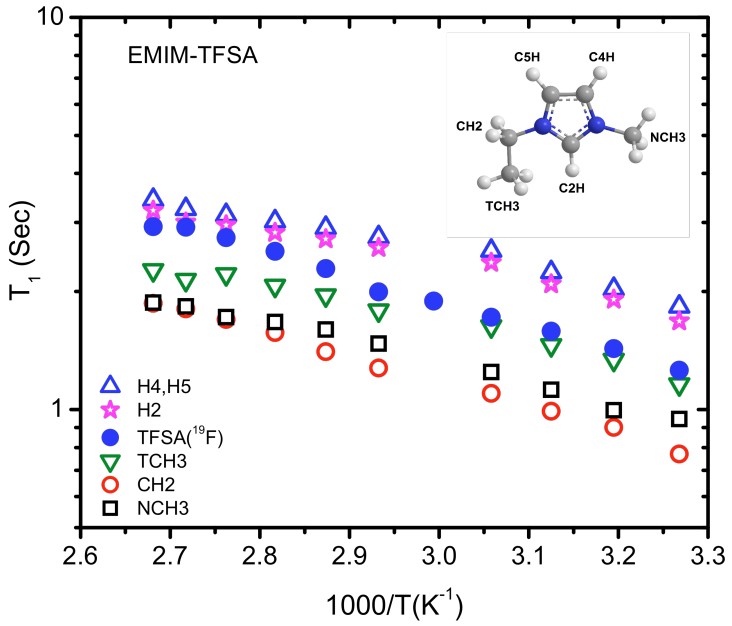

Figure 2. Arrhenius plots of ^{1}H and ^{19}F T_1 relaxation times for the assigned peaks of EMIM TFSA.

Over the temperature range studied, no T_1 minimum was observed. Because of this, it was not possible to determine correlation times associated with the motions. Regardless, for mobile media the dynamics of the diffusing species cause fluctuations of the local fields that, depending on the spin, could be magnetic or electric in nature. In the case of magnetic fluctuations, the fields may be due to dipole-dipole interactions, chemical shift anisotropy, scalar couplings, and spin rotations. All four produce modulations that create mechanisms for relaxation. While the motions may be translational and/or rotational in nature, for viscous media such as ionic liquids where the timescale for viscosity-affected motions are long, the expectation is that the T_1s obtained represent the reorentational motion of the whole molecule. Additionally, for ^{1}H spins, the dipole-dipole interactions are the main source of relaxation. Since the dipole-dipole interaction depends inversely on the cube of atomic internuclear distances, intramolecular interactions are stronger than intermolecular ones.[34,35] Although this does not however entirely exclude the intermolecular interactions, they shall be considered negligible. This further supports our interpretation of the T_1s as broadly indicative of the rate of motion of molecules bearing nuclei.

Activation energies were determined from the T_1 data for all the samples and the values are summarized in Table 2. Values range from ~8 – 17 kJ/mol, and the all-proteo EMIM IL had lower activation energies compared to D_2, TD_3 and MD_3. The difference in values may be due to the perturbation of the hydrogen bonding by the presence and location of the deuterons. Hydrogen bonding and its effect on ion transport is extremely sensitive to the breakage and formation of bonds, which facilitate ion transport. The placement of a larger moment of inertia within the network affects the rotational motions and rates of formation and breakage, thereby the effective hydrogen bonding.[36] Early single crystal studies on the effect of substituting

deuterium for hydrogen in O-H•••O hydrogen bonded crystals showed a change in the lattice dimensions, the general trend being an increase.[37,38] Such an increase could reduce the strength of the hydrogen bonding by increasing the distances between the interaction sites on the cations and anions. Disturbance of the hydrogen bonding was also observed by Chang, *et al.*,[39] whose work showed the presence of D_2O affecting the IR vibrational frequencies for the both the alkyl and imidazolium C-H groups.

Table 2. Activation energies for reorientational motion in EMIM TFSA determined from ^{1}H, ^{2}H and ^{19}F T_1 data (kJ/mol).

Position	EMIM-MD_3	EMIM-TD_3	EMIM-D_2	EMIM
H4, H5	11.8 ± 0.8	10.3 ± 0.2	10.0 ± 0.2	8.3 ± 0.5
H2	9.9 ± 0.7	10.3 ± 0.3	10.8 ± 0.3	8.4 ± 0.5
TCH_3	12.4 ± 0.4	-	12.3 ± 0.3	9.1 ± 0.5
CH_2	16.9 ± 0.8	11.2 ± 0.3	-	12.3 ± 0.2
NCH_3	-	10.3 ± 0.3	11.2 ± 0.4	10.1 ± 0.4
TFSA (^{19}F)	11.8 ± 0.2	12.2 ± 0.3	12.6 ± 0.5	12.3 ± 0.3
^{2}H T_1 data	15.0 ± 0.3	16.2 ± 0.2	11.6 ± 0.1	-

Shown in Figure 3 are the linear Arrhenius plots of ^{2}H and ^{19}F T_1 relaxation data for the three deuterated isotopologues. The ^{19}F relaxation times were identical as expected, while the ^{2}H T_1s were in the order MD_3 > TD_3 > D_2 at each temperature, the same pattern observed for the activation energies for ^{1}H relaxation. The MD_3 and TD_3 had similar activation energies (~15 and 16 kJ/mol) while that for the D_2 group was lower (~12 kJ/mol). Deuterons relax through quadrupolar interactions, which the T_1 results indicate are more efficient in the D_2 isotopologue, meaning the electric field gradient is strongest in the location of CD_2, followed by MD_3. Additionally, the fact that different T_1s are observed for the various deuterated groups suggests asymmetry in the interactions between each group and its surroundings, which is comprised

mainly of anions in the first solvation shell. Both the TFSA and EMIM ions are asymmetric with regards to their charge distributions.[40-42] This asymmetry was demonstrated for the TFSA anion by *ab initio* calculations from which the natural charge was determined and electrostatic potential (ESP) based charge calculated for the various points of interactions (N, O and F).[41,42] While the values of the charges determined by the two methods differed, the pattern observed was the same, with the order N > O > F for favorable interaction locations. The fact that the fluorine atoms had the lowest charge means they are most 'ionic', less restricted and therefore more able to effect conformational changes.

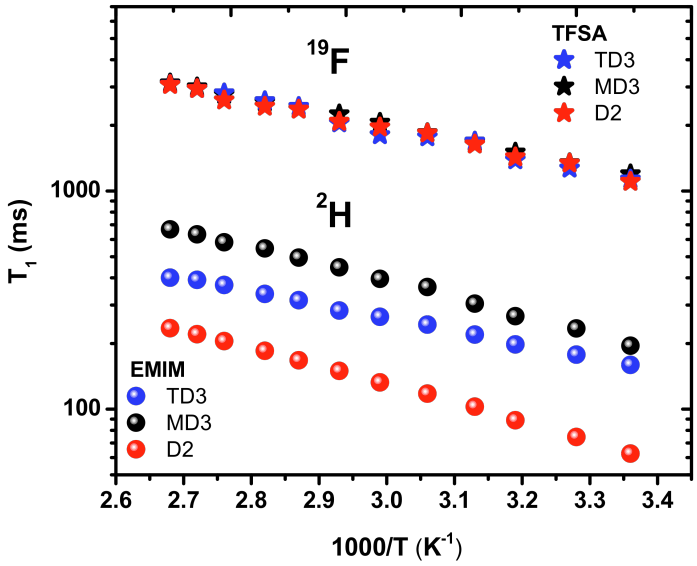

Figure 3. Arrhenius plots of ^{2}H and ^{19}F T_1 relaxation times for the assigned peaks of deuterated EMIM TFSA samples.

Self-diffusion coefficients D were determined as a function of temperature using the PGSE NMR technique for the cations (^{1}H) and anions (^{19}F), and the Arrhenius plots are shown in Figure 4. Slightly faster diffusion was observed for the cations over the entire temperature range and results are comparable with those of Hayamizu *et al.*,[22] Noda *et al.*[16] and Borodin et al.[12]

While acknowledging that the diffusion coefficients are best fit using the Vogel-Tamman-Fulcher equation,[12,16,22] linear fits over the measured temperature range obtain an activation energy for all the ^{1}H diffusion data taken as one set of 22.5 ± 1.0 kJ/mol and that for all the ^{19}F data taken as one set is 20.5 ± 0.6 kJ/mol.

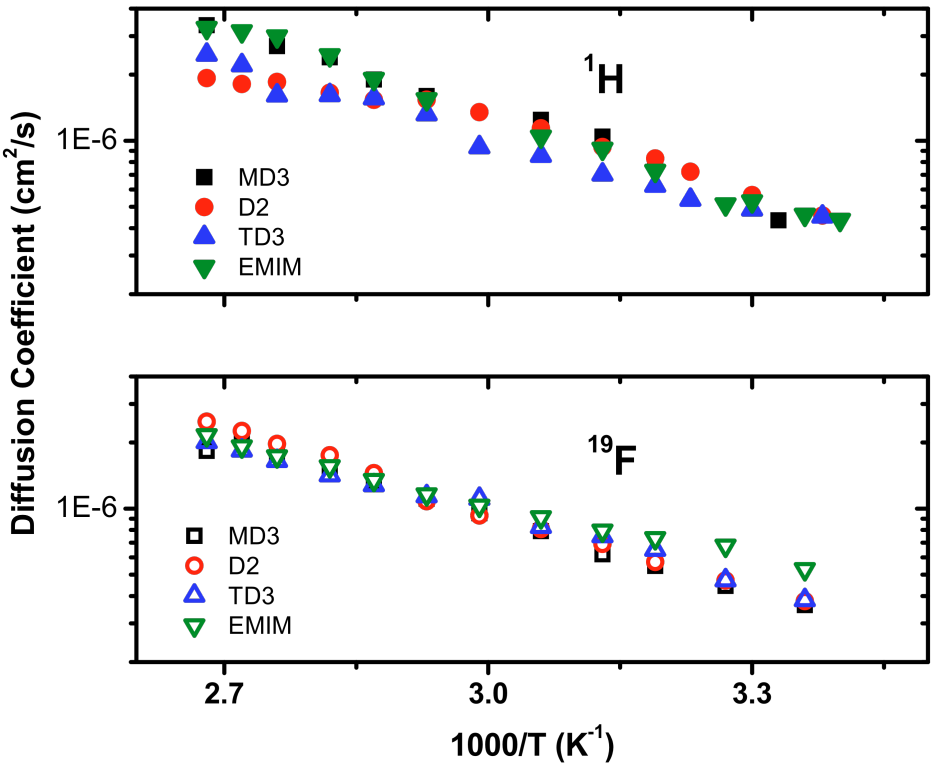

Figure 4. Arrhenius plots of ^{1}H and ^{19}F self-diffusion coefficients for all four EMIM TFSA isotopologues.

Variable-temperature diffusion studies on EMIM TFSA[16,22] have shown that the diffusion correlates well with the inverse of the viscosity through the Stokes-Einstein relationship: $D = kT/\pi c\eta r$, where k is the Boltzmann constant, T is the absolute temperature, c is a constant (4-6) and r is the effective hydrodynamic radius. As shown in Figure 5, when D is plotted against T/η the result is linear and shows the TFSA anion having a greater hydrodynamic radius than the

EMIM cation.[16] The viscosity data used for the figure was taken from Noda *et al.*[16] and considered the same for all isotopologues.

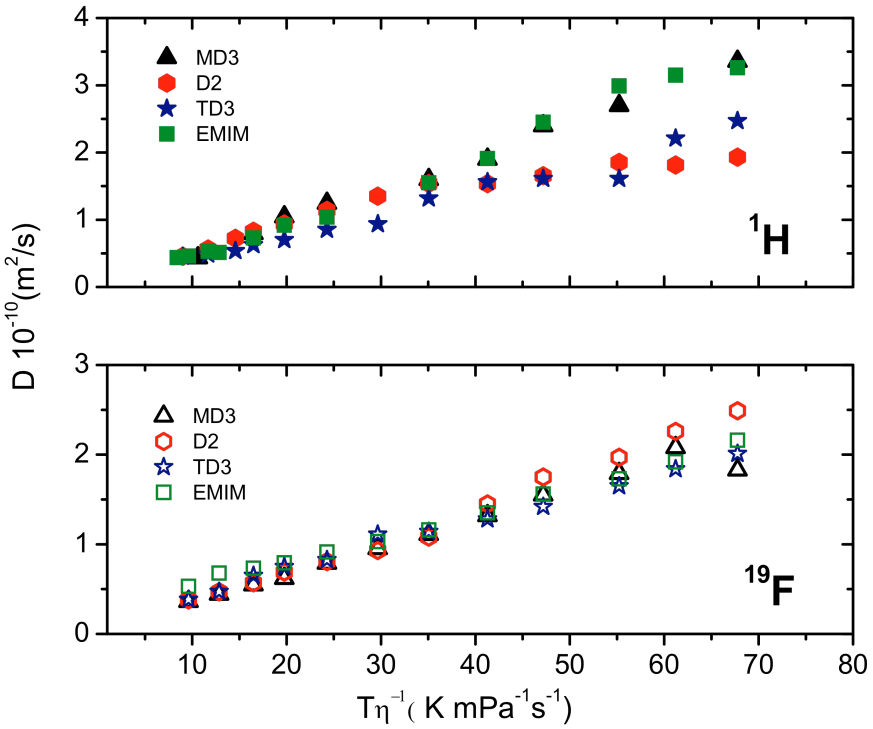

Figure 5. ^{1}H and ^{19}F diffusion constants vs. T/η for the EMIM TFSA isotopoloques.

Variable-pressure diffusion and T_1 relaxation studies:

Variable pressure data for T_1 (^{2}H) relaxation and ion (^{1}H and ^{19}F) self-diffusion are reported in Tables S19 and S20 of Supporting Information Section 1. The data are depicted in Figures 6 and 7 below, and the relaxation times and diffusion constants both decrease with increasing pressure as expected. The use of pressure as a variable allows the changing of the inter- and intra-molecular interactions without affecting the frequency (temperature) or causing compositional changes. *As shown, no saturation was observed for either T_1 or D over the*

pressure range studied, which suggests that whatever dynamical changes are taking place have not yet reached their limits. While the D data is monotonic, the T_1 plots for the two isotopologues that are deuterated adjacent to the imidazolium ring exhibit two distinct linear regions between the pressure ranges 0.1-100 and 100-250 MPa, which could indicate two different packing arrangements for both the MD_3 and D_2 deuterated samples. The linearity of the TD_3 group could be due to its distance away from the ring, or the fact that the alkyl chain is a less favorable interaction site compared to both MD_3 and D_2 for hydrogen bonded imidazolium cation-anion interactions.[40-42]

Activation volumes for relaxation and diffusion as determined by fitting the T_1 or D vs. pressure data according to equation (3) are given in Table 3.

$$\Delta V = -RT(\partial \ln\alpha/\partial P)_T \qquad 3$$

Here α can be $1/T_1$ or D, P is the pressure, T is the temperature and R is the gas constant. There are rearrangements in the local environment to accommodate ion rotation that depend on local density fluctuations. Activation volume is therefore an indicator of the ease of mobility, with higher values oftentimes being attributed to more restricted motion, possibly due to greater interactions between the species. The values obtained for the MD_3 and D_2 isotopologues are similar, with that for the 100-250 MPa region being almost half that of the 0.1-100 MPa region. The TD_3 isotopologue showed the smallest activation volume and monotonic behavior over the entire pressure range.

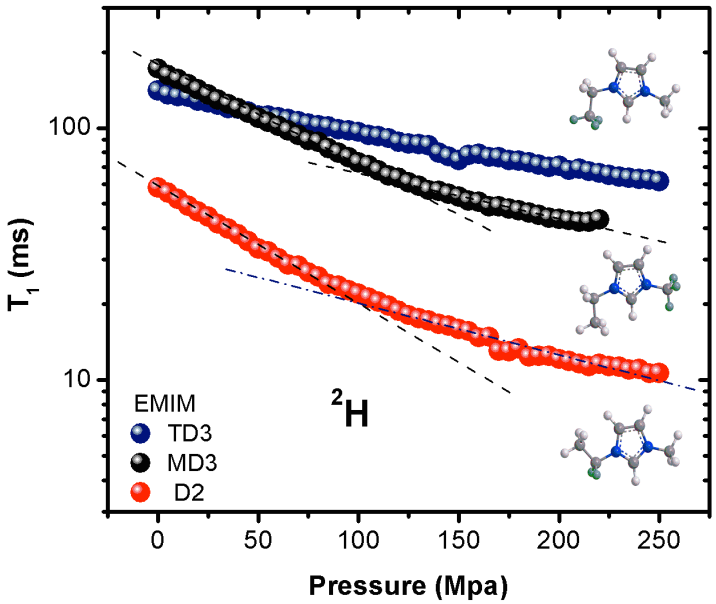

Figure 6. ^{2}H T_1 relaxation times for deuterated EMIM TFSA isotopologues as functions of pressure.

Table 3: Activation volumes determined from variable-pressure ^{2}H T_1 data at 22 ˚C.

Deuteration site	**ΔV (cm^3/mol) (0.1-100 MPa)**	**ΔV (cm^3/mol) (100-250 MPa)**
MD_3	21 ± 1	11 ± 1
D_2	25 ± 1	12 ± 1
TD_3	8 ± 1 (0.1-250 MPa)	

Figure 7 illustrates a remarkable finding about the pressure-dependent behavior of the EMIM cation and TFSA anion diffusion coefficients. At ambient pressure the self-diffusion coefficients, measured by ^{1}H and ^{19}F respectively, are essentially the same. However, with increasing pressure the diffusion of the anion slows faster than for the cation, resulting in an activation volume that

is almost twice as large for TFSA compared to EMIM (28.8 vs. 14.6 cm^3/mol, respectively, see also Table 4).

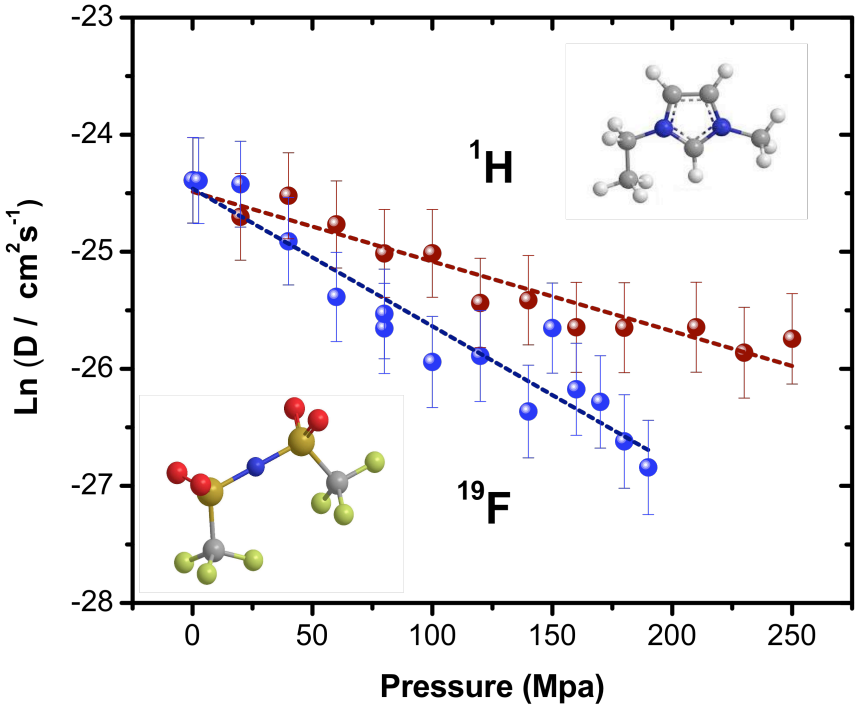

Figure 7. ^{1}H and ^{19}F self-diffusion coefficients for EMIM TFSA as functions of pressure.

In *fluid* (as opposed to crystalline) ionic liquids, the TFSA anion exists in equilibrium between two conformational states about the C-S-S-C dihedral angles - described as *trans* or *anti* (C_2 symmetry) and *cis* or *gauche* (C_1 symmetry). (In crystals, typically only one conformer is present although there can be exceptions.) This equilibrium has been studied experimentally by Raman spectroscopy[20,43] and by electronic structure and molecular dynamics (MD) simulations.[12,43-48] Under ambient conditions the trans conformer is slightly favored[20,43] and the enthalpy change from the *trans* conformer to *cis* is positive by about 3.5 kJ/mol according to temperature-dependent Raman spectroscopy[43] and supported by MD simulations.[12] Pressure-dependent Raman spectroscopy[20] on *N,N*-diethyl-*N*-methyl-*N*-(2-methoxyethyl)ammonium

(DEME) TFSA showed an increasing *trans*/*cis* ratio with increasing pressure, finding that the partial molar volume of the *trans*-TFSA anion conformer is 0.7 cm^3/mol smaller than that of the *cis* one for that system.

Molecular dynamics simulations by Borodin *et al.*[12] showed that artificially increasing the barrier for *trans*-*cis* conversion of the anion in EMIM TFSA and *N*-methyl-*N*-propylpyrrolidinium TFSA by 12.5 kJ/mol resulted in slowing down of the anion and cation transport by 40-50%. No similar effect was found in the case of the smaller FSA anion. They showed that in the case of TFSA the ionic self-diffusion is coupled to conformational exchange. Although the +0.7 cm^3/mol reaction volume for *trans*-to-*cis* TFSA conversion cited above is relatively small, the activation volume for conformational exchange could be much larger, and thus contribute to the larger activation volume for TFSA anion self-diffusion compared to the EMIM cation. Borodin and coworkers[12] did not note a difference in self-diffusion between the cations and the TFSA anion when they artificially increased the TFSA conformational exchange barrier in their simulations, however the difference is quite evident in our pressure data.

The conformation and shape of the cation and its alkyl chain have also been shown to affect the self-diffusion coefficients of the ions, which Tsuzuki *et. al*. demonstrated for EMIM cation TFSA and other ILs using molecular dynamics simulations.[49] Simulated D values of both the EMIM cation and TFSA anion were reduced by 39% and 34% respectively when the conformational flexibility of the alkyl chain was restricted along the C_2-N_1-C_7-C_8 torsional angle.

Consequently, molecular dynamics simulations predict that restriction of conformational exchange results in slowing self-diffusion for both the TFSA anion and the EMIM cation to similar degrees, regardless of whether the restriction is imposed on the anion or the cation, although the effects may be larger in the case of restricting the anion. This situation left open the

question of whether the remarkable effect shown in Figure 7 could be due to pressure-induced conformational restriction of the anion, the cation or both ions. We therefore set out to measure activation volumes for the related ILs EMIM FSA and EMIM BF_4 and to compare our results with activation volumes for other ILs available in the literature. We selected EMIM FSA in order to test the predictions of Borodin *et al.*[12] in contrast to EMIM TFSA, and EMIM BF_4 was selected to provide a small anion with no conformational exchange and also because pressure-diffusion data for longer-chain imidazolium BF_4 ILs was available in the literature for comparison. The results are shown in Table 4 along with selected results derived from the literature. A much larger $\Delta V^{\ddagger}$ set for self-diffusion and fluidity (= 1/viscosity), calculated from literature data and covering 18 ILs, is presented in Supporting Information Section 2.)

Table 4. Activation volumes for ionic self-diffusion and fluidity for selected ILs, and calculated ionic volumes. All volumes are in cm^3/mol and measured at 25 °C unless noted.

Ionic Liquid	$\Delta V^{\ddagger}_{cation}$	$\Delta V^{\ddagger}_{anion}$	$\Delta V^{\ddagger}_{fluidity}$	V_{cation} [a]	V_{anion} [a]
EMIM TFSA	14.6 ± 1.3 [b] (22 °C)	28.8 ± 2.5 [b] (22 °C)	25.9 ± 0.7 [d]	70.2	95.6
BMIM TFSA [i]	19.2 ± 1.4 [b] (27 °C)	22.6 ± 2.7 [b] (27 °C)	27.3 ± 0.2 [e]	90.6	95.6
HMIM TFSA [i]	–	–	27.4 ± 0.2 [d] 25.4 ± 0.3 [d] (50 °C)	111.1	95.6
EMIM FSA	12.9 ± 0.9 [b] (22 °C)	11.0 ± 1.5 [b] (22 °C)	–	70.2	65.0
EMIM BF_4	14.0 ± 1.0 [b] (22 °C)	15.3 ± 1.4 [b] (22 °C)	24.4 ± 1.0 (20 °C) [f]	70.2	30.4
BMIM BF_4 [i]	22.0 ± 0.4 [c] 19.0 ± 0.2 [c] (50 °C)	No data at 25 °C 18.9 ± 0.7 [c] (50 °C)	25.0 ± 0.1 [g] 21.4 ± 0.2 [g] (50 °C)	90.6	30.4
HMIM BF_4 [i]	–	–	29.5 ± 0.6 [d] 23.2 ± 0.2 [d] (50 °C)	111.1	30.4
OMIM BF_4 [i]	25.3 ± 0.8 [c] (50 °C)	24.7 ± 0.4 [c] (50 °C)	29.2 ± 0.2 [h] 25.5 ± 0.2 [h] (50 °C)	131.6	30.4

[a] Ref. 50. [b] This work. [c] Ref. 51. [d] Ref. 52. [e] Ref. 53. [f] Ref. 54. [g] Ref. 55. [h] Ref. 56. [i] BMIM = 1-butyl-3-methylimidazolium, HMIM = 1-hexyl-3-methylimidazolium, OMIM = 1-octyl-3-methylimidazolium.

Several trends are evident from the data in Table 4. First, the activation volumes for ionic self-diffusion in EMIM FSA and EMIM BF_4 are very similar for anions and cations in the same IL. The $\Delta V^{\ddagger}$ values for EMIM cation self-diffusion are slightly smaller for the FSA and BF_4 ILs than for the TFSA salt. Significantly, the activation volumes for FSA and BF_4 self-diffusion in the EMIM IL series are much smaller than that of TFSA, and $\Delta V^{\ddagger}$ is larger for BF_4 than for FSA despite the former anion having less than half the ionic volume of the latter one. These results comport with the predictions of Borodin *et al.*[12] that conformational restriction of the anion would have no effect on diffusion in EMIM FSA, whereas it would have a strong effect in EMIM TFSA. Comparison of EMIM FSA and EMIM BF_4 shows that the primary $\Delta V^{\ddagger}$ effect is not related simply to anion size, so the dynamics of the TFSA anion is the key factor.

However, the MD simulations summarized above predict that diffusion of both ions would be affected comparably but that is not observed in EMIM TFSA. In the case of BMIM TFSA, $\Delta V^{\ddagger}$ for cation diffusion is more than 4 cm^3/mol larger than for EMIM, whereas $\Delta V^{\ddagger}$ for the TFSA anion is more than 6 cm^3/mol larger than for EMIM than for BMIM, although the uncertainties for both are fairly large. As the alkyl chain on the cation grows longer, pressure effects on its conformational dynamics can also influence the activation volumes. Thus, the EMIM cation would appear to be particularly suited for exposing the role of conformational dynamics in the diffusion of TFSA anion.

The effects of increasing imidazolium alkyl chain length on $\Delta V^{\ddagger}$ for self-diffusion can be seen among the entries for the BF_4 salts in Table 4. Comparison of the results we obtained for EMIM BF_4 with those for BMIM BF_4 with OMIM BF_4 calculated from the literature show that the activation volumes for self-diffusion of the cation and anion in a given IL are the same within the error limits, and they increase significantly as the alkyl chain length increases. The increases

with chain length have to be inspected carefully because of the temperature differences in the measurements. As seen in with $\Delta V^{\ddagger}_{BMIM}$ for BMIM BF_4, in the fourth column of Table 4 and in many examples in Supporting Information Section 2 Table S22, the activation volumes decrease with increasing temperature, since the free volume increases as the density decreases.

The effects of alkyl chain length in the BMIM, HMIM and OMIM PF_6 series (see Table S22, Supporting Information Section 2) are harder to compare due to the scarcity of data sets at temperatures in common. Clear increases with chain length are seen in $\Delta V^{\ddagger}_{PF6}$ but the pattern in $\Delta V^{\ddagger}_{cation}$ is less clear. Also, $\Delta V^{\ddagger}_{PF6}$ is clearly larger than $\Delta V^{\ddagger}_{HMIM}$ at 50 °C and $\Delta V^{\ddagger}_{OMIM}$ at 75 and 80 °C, but $\Delta V^{\ddagger}_{PF6}$ and $\Delta V^{\ddagger}_{cation}$ are approximately the same for BMIM and for HMIM at higher temperatures. A differential effect on the PF_6 anion cannot arise from conformational exchange since it has none, however MD simulations have shown that there are profound changes in the structural organization of this family of ILs as the alkyl chains lengthen.[57,58] Longer alkyl chains lead to increasing degrees of polar-nonpolar domain segregation, and as the chains grow longer the polar domain where the PF_6 anions reside changes from an essentially isotropic 3-dimensional space to a network of ionic channels that confine diffusion of the anion (see the void spaces in Figure 6 of Reference 58), which may produce a relative increase in $\Delta V^{\ddagger}_{PF6}$ with chain length. The reason why the BF_4 and PF_6 IL families differ in their behavior (at least within the limited amount of available data) is beyond the scope of this discussion but it may involve differences in the interactions of the respective anions with the imidazolium cations.

N-butyl-*N*-methylpyrrolidimium TFSA (BMpyrr TFSA) is the only non-imidazolium IL for which pressure-dependent self-diffusion constants are available,[59] and it is distinguished from the imidazolium salts by the fact that the saturated pyrrolidine ring undergoes its own conformational exchange (pseudorotation)[47] while the planar aromatic imidazolium cations are

rigid. (Calculated activation volumes for BMpyrr TFSA are presented in Supporting Information Section 2 Table S22.) Consequently, there are three types of conformational exchange occurring in BMpyrr TFSA, cation alkyl chain reorientation, cation ring pseudorotation and anion *cis-trans* isomerization. The activation volume for BMpyrr diffusion in BMpyrr TFSA (30.5 ± 0.3 cm^3/mol at 30 °C) is significantly larger than the one we measured for BMIM in BMIM TFSA (19.2 ± 1.4 cm^3/mol at 25 °C). Since BMpyrr and BMIM have the same number of non-hydrogen atoms, the large difference in activation volumes clearly exposes the dynamical consequences of the non-planarity and conformational lability of the BMpyrr cation on the transport properties of the IL.

The activation volume results for ionic self-diffusion thus serve as important experimental corroboration of the findings from molecular dynamics simulations described above that conformational exchange plays a major role in ion transport within ILs. With its small size and minimal configurational dynamics, the EMIM cation turns out to be very useful for exposing dynamical effects of its counterions. Effects that are observable in ILs containing small ions can get washed out as the ions increase in size, and they can also be overshadowed by the effects of structural inhomogeneity as the ions become elaborated enough to induce domain segregation or other types of specific interactions.

It is unfortunate that the number of results for pressure-dependent IL self-diffusion coefficients available in the literature is limited only to the examples discussed above (as far as we could find using resources including SciFinder, ILThermo[60] and Web of Science), but it is not surprising due to the specialized equipment and copious instrument time required for the measurements. To expand the range of activation volume data for transport phenomena in ILs we examined the reported pressure dependences of the viscosities of the ILs for which we had

diffusion data and related ones sharing the same cations and/or anions. The results are presented in the right-hand columns of Supporting Information Section 2 Table S22 and the fits are individually presented in Section 2 as well. In order to keep the sign of the calculated activation volumes consistent with the diffusion results, the natural log of the fluidity, or inverse viscosity, was plotted versus pressure. In most cases the activation volume for viscous flow $\Delta V^{\ddagger}_{fluidity}$ for a given IL is slightly larger than the self-diffusion activation volumes $\Delta V^{\ddagger}_{cation}$ and $\Delta V^{\ddagger}_{anion}$ at the same temperature. There is also more scatter in the $\Delta V^{\ddagger}_{fluidity}$ results, owing to measurements by different methods and groups that sometimes disagree and in other instances concur. (Data with too few observations or with obvious problems such as inconsistency with the preponderance of published ambient-pressure data were not included in Table S22. In some cases data from multiple sources was analyzed and reported.)

Generally speaking, the $\Delta V^{\ddagger}_{fluidity}$ results support the more limited self-diffusion results in terms of trends among families sharing common anions and differences between anion families. As expected, the trend of decreasing $\Delta V^{\ddagger}_{fluidity}$ with higher temperature also occurs to a similar degree as with the self-diffusion results. Two points deserve specific mention. First, $\Delta V^{\ddagger}_{fluidity}$ values for EMIM BF_4 at 20 and 30 °C (24.4 and 23.0 cm^3/mol, respectively) are much larger than $\Delta V^{\ddagger}_{EMIM}$ (14.0 cm^3/mol) and $\Delta V^{\ddagger}_{BF4}$ (15.3 cm^3/mol) at 22 °C. To our knowledge there is no pressure-dependent viscosity data available for EMIM FSA at present, so we cannot be sure whether the EMIM BF_4 results are unique or part of a trend. Second, our calculations revealed huge $\Delta V^{\ddagger}_{fluidity}$ values for two salts of the tris(pentafluoroethyl)trifluorophosphate (FAP) anion, namely 1-butyl-2-methyl-3-methylimidazolium (BMMIM) FAP and *N*-butyl-*N*-methoxyethylpyrrolidinium ((EOM)Mpyrr) FAP, 45.4 and 41.8 cm^3/mol respectively at 40 °C. The FAP anion is significantly larger than any of the other anions we studied however it is

nominally matched in size by the OMIM and C_{10}MIM cations, but not by the $\Delta V^{\ddagger}_{fluidity}$ values for their respective ILs in Table S22. Clearly the transport dynamics of FAP ILs will be a fruitful area for further studies.

Conclusion

Complete NMR T_1 and D measurements were performed on selectively-deuterated EMIM TFSA samples as a function of both temperature (20-100 °C) and pressure (0.1-250 MPa). Selective deuteration of the various sites (TD_3, MD_3 and D_2) allowed assessment of local short-range motions through determination of the ^{2}H T_1s. The values ranked in the order $MD_3 > TD_3 > D_2$ at each temperature and the activation energies determined followed the same order. The differences in the T_1 activation energies are possibly due to variations in the strength of the hydrogen bonds at the deuterated sites in the network of cations and anions.

Several theoretical studies on the gas-phase interactions of the imidazolium cation and TFSA anion reveal an expanded network whereby anions and cations interact through hydrogen bonds, the strongest of which exist through the hydrogen at the C2 location on the imidazolium ring.[40-42] Central to formation of these bonds are the conformations of both the cation and anion and the sites of interactions. For the imidazolium-based cation, nine sites of interactions are favored by the anions.[40,41] However, due to several factors that include Coulombic repulsion and anion size, not all sites can be occupied simultaneously. The fewer sites occupied, the weaker and less ordered the network.[40,41] For TFSA, it takes only two anions to fully encapsulate the cation, which results in a weakly linked network of ions with a high degree of disorder due to its conformations.

It is expected that frequent fluctuations of these bonds can cause fluctuations in ionic positions and orientations, thereby affecting the transport of the ionic species. In addition to

reducing bond distances as shown by Raman spectroscopy,[27-31] increasing pressure will also strengthen hydrogen bonds, thereby creating a more rigid network. We see this in the variable pressure ^2H T_1 data, which shows two activation volumes for both D_2 and MD_3 in the pressure ranges 0.1-100 and 100-250 MPa. One could consider these two regions as having different local structures, with 100 MPa being the transition point. It is interesting that the TD_3 group does not show this type of behavior, which may be due to its distance from the electron-withdrawing cationic imidazolium ring.

The measurements of ionic self-diffusion constants as a function of pressure produced the provocative finding that the activation volume for TFSA diffusion in EMIM TFSA is approximately twice that of the EMIM cation. The difference in activation volumes is far smaller for BMIM TFSA and there are few examples in the literature data we analyzed (Table S22) where the difference between ions in the same IL is statistically significant, and none that are comparably dramatic. To probe the factors contributing to this remarkable difference, we determined activation volumes for self-diffusion in EMIM FSA and EMIM BF_4. In both ILs we found that the activation volumes of *both* ions were small (11-15 cm^3/mol) and comparable to that of EMIM in EMIM TFSA. The apparently small inherent activation volume for EMIM thus provides contrast to observe the much larger ΔV_{diff} for TFSA, and provokes reflection about its origins.

As described above, MD simulations of Borodin[12] predicted that restriction of TFSA conformational exchange in EMIM TFSA would lead to reduced transport of both ions but that the same type of restriction on the FSA anion in EMIM FSA would have no effect. Canongia Lopes and coworkers also noted that the conformational change in FSA is subtle compared to TFSA.[61] By probing the effect of increasing pressure on self-diffusion rates, we tested this

hypothesis by using pressure to reduce the free volume available to accommodate interconversion between the *cis* and *trans* conformers of TFSA. Compared to EMIM FSA, we did indeed see a dramatic effect, but only in the ΔV_{diff} for TFSA anion and not for the EMIM cation. TFSA anion has trifluoromethyl groups that FSA anion lacks, and the displacement of the CF_3 groups during *cis-trans* interconversion consequently places greater steric demands on diffusion that show up in ΔV_{diff}. We believe this is solid evidence for the connection between TFSA conformational exchange and diffusion. Thus, the TFSA anion ambulates through an ionic liquid by twisting between its two conformers, similar to how a snake moves by slithering.

We suggest that our experimental activation volume results provide support for theoretical interpretations of how configurational interconversion is important for diffusion in ionic liquids, which are not easy to validate by other experimental approaches. Activation volume results have proven very valuable for detailed mechanistic studies in ionic liquids[62] as well as many other areas of chemistry.[63,64] The results we have obtained so far suggest promising avenues for further investigations, which we hope will be enhanced by complementary molecular dynamics studies.

Supporting Information. Section 1: Syntheses of EMIM FSI and EMIM BF_4. Figure S1 showing the ^{1}H NMR spectrum of EMIM TFSA (MCD_3) IL. Figures S2-S4 showing Arrhenius plots for T_1 relaxation for the deuterated isotopologues of EMIM TFSA. Figures S5-S8 showing pressure dependence plots for T_1 relaxation and self-diffusion in EMIM FSA and EMIM BF_4. Tables S1-S21 of measured diffusion constants and T_1 relaxation times as functions of temperature and pressure. **Section 2:** A tabulation of 42 activation volumes for self-diffusion and 64 for viscous flow (fluidity) for eighteen ionic liquids at various temperatures, obtained from this work and by analysis of primary diffusion or viscosity vs. pressure data from the literature,

with individual pages showing all fits and attributions. This material is available free of charge via the Internet at http://pubs.acs.org.

Acknowledgments

The work at Brooklyn College was supported by a PSC CUNY grant. The work at Hunter College was supported by the Office of Naval Research and the Hunter NIH-supported RISE program. The work at BNL (JLH, SR and JFW) was supported by the US-DOE Office of Science, Division of Chemical Sciences, Geosciences and Biosciences under contracts DE-AC02-98CH10886 and DE-SC0012704. JLH originally prepared the selectively deuterated imidazolium TFSA ILs and BMIM TFSA for the work described in Ref. 33. SR prepared the EMIM FSA and EMIM BF_4 salts.

References:

1. Seki, S.; Kobayashi, Y.; Miyashiro, H.; Ohno, Y.; Usami, A.; Mita, Y.; Watanabe, M.; Terada, N. Highly reversible lithium metal secondary battery using a room temperature ionic liquid/lithium salt mixture and a surface-coated cathode active material. *Chem. Commun.* **2006,** , 544-545.

2. Shin, J. H.; Henderson, W. A.; Passerini, S. Ionic liquids to the rescue? Overcoming the ionic conductivity limitations of polymer electrolytes. *Electrochem. Commun.* **2003,** *5*, 1016-1020.

3. Garcia, B.; Lavallee, S.; Perron, G.; Michot, C.; Armand, M. Room temperature molten salts as lithium battery electrolyte. *Electrochim. Acta* **2004,** *49*, 4583-4588.

4. Galinski, M.; Lewandowski, A.; Stepniak, I. Ionic liquids as electrolytes. *Electrochim. Acta* **2006,** *51*, 5567-5580.

5. Alam, M. T.; Islam, M. M.; Okajima, T.; Ohsaka, T. Capacitance Measurements in a Series of Room-Temperature Ionic Liquids at Glassy Carbon and Gold Electrode Interfaces. *J. Phys. Chem. C* **2008,** *112*, 16600-16608.

6. Aurbach, D.; Levi, M. D.; Salitra, G.; Levy, N.; Pollak, E.; Muthu, J. Cation trapping in highly porous carbon electrodes for EDLC cells. *J. Electrochem. Soc.* **2008,** *155*, A745-A753.

7. Bao, Q.; Bao, S.; Li, C. M.; Qi, X.; Pan, C.; Zang, J.; Lu, Z.; Li, Y.; Tang, D. Y.; Zhang, S.; Lian, K. Supercapacitance of solid carbon nanofibers made from ethanol flames. *J. Phys. Chem. C* **2008,** *112*, 3612-3618.

8. Fedorov, M. V.; Kornyshev, A. A. Ionic liquid near a charged wall: Structure and capacitance of electrical double layer. *J. Phys. Chem. B* **2008,** *112*, 11868-11872.

9. Tokuda, H.; Tabata, S. I.; Susan, M.; Hayamizu, K.; Watanabe, M. Design of polymer electrolytes based on a lithium salt of a weakly coordinating anion to realize high ionic conductivity with fast charge-transfer reaction. *J. Phys. Chem. B* **2004,** *108*, 11995-12002.

10. Tokuda, H.; Hayamizu, K.; Ishii, K.; Susan, M. A. B. H.; Watanabe, M. Physicochemical properties and structures of room temperature ionic liquids. 2. Variation of alkyl chain length in imidazolium cation. *J. Phys. Chem. B* **2005,** *109*, 6103-6110.

11. Armand, M.; Endres, F.; MacFarlane, D. R.; Ohno, H.; Scrosati, B. Ionic-liquid materials for the electrochemical challenges of the future. *Nat. Mater.* **2009,** *8*, 621-629.

12. Borodin, O.; Gorecki, W.; Smith, G. D.; Armand, M. Molecular Dynamics Simulation and Pulsed-Field Gradient NMR Studies of Bis(fluorosulfonyl)imide (FSI) and Bis[(trifluoromethyl)sulfonyl]imide (TFSI)-Based Ionic Liquids. *J. Phys. Chem. B* **2010,** *114*, 6786-6798.

13. Kobrak, M. N.; Znamenskiy, V. Solvation dynamics of room-temperature ionic liquids: evidence for collective solvent motion on sub-picosecond timescales. *Chem. Phys. Lett.* **2004,** *395*, 127-132.

14. Margulis, C. J. Computational study of imidazolium-based ionic solvents with alkyl substituents of different lengths. *Molec. Phys.* **2004,** *102*, 829-838.

15. Hayamizu, K.; Aihara, Y.; Nakagawa, H.; Nukuda, T.; Price, W. S. Ionic conduction and ion diffusion in binary room-temperature ionic liquids composed of [emim][BF_4] and $LiBF_4$. *J. Phys. Chem. B* **2004,** *108*, 19527-19532.

16. Noda, A.; Hayamizu, K.; Watanabe, M. Pulsed-gradient spin-echo H-1 and F-19 NMR ionic diffusion coefficient, viscosity, and ionic conductivity of non-chloroaluminate room-temperature ionic liquids. *J. Phys. Chem. B* **2001,** *105*, 4603-4610.

17. Kanakubo, M.; Harris, K. R.; Tsuchihashi, N.; Ibuki, K.; Ueno, M. Effect of pressure on transport properties of the ionic liquid 1-butyl-3-methylimidazolium hexafluorophosphate. *J. Phys. Chem. B* **2007,** *111*, 2062-2069.

18. Penna, T. C.; Faria, L. F. O.; Matos, J. R.; Ribeiro, M. C. C. Pressure and temperature effects on intermolecular vibrational dynamics of ionic liquids. *J. Chem. Phys.* **2013,** *138*, 104503.

19. Pison, L.; Costa Gomes, M. F.; Padua, A. A. H.; Andrault, D.; Norman, S.; Hardacre, C.; Ribeiro, M. C. C. Pressure effect on vibrational frequency and dephasing of 1-alkyl-3-methylimidazolium hexafluorophosphate ionic liquids. *J. Chem. Phys.* **2013,** *139*, 054510.

20. Yoshimura, Y.; Takekiyo, T.; Imai, Y.; Abe, H. Pressure-Induced Spectral Changes of Room-Temperature Ionic Liquid, N,N-Diethyl-N-methyl-N-(2-methoxyethyl)ammonium Bis(trifluoromethylsulfonyl)imide, DEME TFSI. *J. Phys. Chem. C* **2012,** *116*, 2097-2101.

21. Chung, S. H.; Lopato, R.; Greenbaum, S. G.; Shirota, H.; Castner, E. W.; Wishart, J. F. Nuclear magnetic resonance study of the dynamics of imidazolium ionic liquids with -$CH_2Si(CH_3)_3$ vs -$CH_2C(CH_3)_3$ substituents. *J. Phys. Chem. B* **2007,** *111*, 4885-4893.

22. Hayamizu, K.; Tsuzuki, S.; Seki, S.; Umebayashi, Y. Nuclear magnetic resonance studies on the rotational and translational motions of ionic liquids composed of 1-ethyl-3-methylimidazolium cation and bis(trifluoromethanesulfonyl)amide and bis(fluorosulfonyl)amide anions and their binary systems including lithium salts. *J. Chem. Phys.* **2011,** *135*, 084505.

23. Sangoro, J.; Iacob, C.; Serghei, A.; Naumov, S.; Galvosas, P.; Karger, J.; Wespe, C.; Bordusa, F.; Stoppa, A.; Hunger, J.; Buchner, R.; Kremer, F. Electrical conductivity and translational diffusion in the 1-butyl-3-methylimidazolium tetrafluoroborate ionic liquid. *J. Chem. Phys.* **2008,** *128*, 214509.

24. Kimura, H.; Yasaka, Y.; Nakahara, M.; Matubayasi, N. Nuclear magnetic resonance study on rotational dynamics of water and benzene in a series of ionic liquids: Anion and cation effects. *J. Chem. Phys.* **2012,** *137*, 194503.

25. Kosters, J.; Schonhoff, M.; Stolwijk, N. A. Ion Transport Effects in a Solid Polymer Electrolyte Due to Salt Substitution and Addition Using an Ionic Liquid. *J. Phys. Chem. B* **2013,** *117*, 2527-2534.

26. Huang, J. F.; Chen, P. Y.; Sun, I. W.; Wang, S. P. NMR evidence of hydrogen bonding in 1-ethyl-3-methylimidazolium-tetrafluoroborate room temperature ionic liquid. *Inorg. Chim. Acta* **2001,** *320*, 7-11.

27. Takekiyo, T.; Imai, Y.; Hatano, N.; Abe, H.; Yoshimura, Y. Conformational preferences of two imidazolium-based ionic liquids at high pressures. *Chem. Phys. Lett.* **2011,** *511*, 241-246.

28. Chang, H. C.; Jiang, J. C.; Su, J. C.; Chang, C. Y.; Lin, S. H. Evidence of rotational isomerism in 1-butyl-3-methylimidazolium halides: A combined high-pressure infrared and Raman spectroscopic study. *J. Phys. Chem. A* **2007,** *111*, 9201-9206.

29. Su, L.; Zhu, X.; Wang, Z.; Cheng, X. R.; Wang, Y. Q.; Yuan, C. S.; Chen, Z. P.; Ma, C. L.; Li, F. F.; Zhou, Q.; Cui, Q. L. In Situ Observation of Multiple Phase Transitions in Low-Melting Ionic Liquid BMIM BF_4 under High Pressure up to 30 GPa. *J. Phys. Chem. B* **2012,** *116*, 2216-2222.

30. Chang, H. C.; Jiang, J. C.; Tsai, W. C.; Chen, G. C.; Lin, S. H. Hydrogen bond stabilization in 1,3-dimethylimidazolium methyl sulfate and 1-butyl-3-methylimidazolium hexafluorophosphate probed by high pressure: The role of charge-enhanced C-H•••O interactions in the room-temperature ionic liquid. *J. Phys. Chem. B* **2006,** *110*, 3302-3307.

31. Su, L.; Li, M.; Zhu, X.; Wang, Z.; Chen, Z. P.; Li, F. F.; Zhou, Q.; Hong, S. M. In Situ Crystallization of Low-Melting Ionic Liquid [BMIM][PF_6] under High Pressure up to 2 GPa. *J. Phys. Chem. B* **2010,** *114*, 5061-5065.

32. Desiraju, G. R.; Steiner, T. *The Weak Hydrogen Bond*. Oxford University Press: Oxford, 1999.

33. Shkrob, I. A.; Marin, T. W.; Chemerisov, S. D.; Hatcher, J. L.; Wishart, J. F. Radiation Induced Redox Reactions and Fragmentation of Constituent Ions in Ionic Liquids. 2. Imidazolium Cations. *J. Phys. Chem. B* **2011,** *115*, 3889-3902.

34. Kowalewski, J.; Maler, L. *Nuclear spin relaxation in liquids: theory, experiments and applications*. CRC Press: Boca Raton, 2006.

35. Price, W. S. *NMR Studies of Translational Motion Principles and Applications*. Cambridge University Press: New York, 2009.

36. Jeffrey, G. A. *An Introduction to Hydrogen Bonding*. Oxford University Press: New York, 1997.

37. Ubbelohde, A. R.; Woodward, I. Structure and Thermal Properties of Crystals. VI. The Role of Hydrogen Bonds in Rochelle Salt. *Proceedings of the Royal Society of London Series A-Mathematical and Physical Sciences* **1946,** *185*, 448-465.

38. Thomas, J. O.; Tellgren, R.; Olovsson, I. Hydrogen-bond studies. LXXXIV. An X-ray diffraction study of the structures of $KHCO_3$ and $KDCO_3$ at 298, 219 and 95 K. *Acta Cryst. B* **1974,** *B30*, 1155-66.

39. Chang, H. C.; Jiang, J. C.; Chang, C. Y.; Su, J. C.; Hung, C. H.; Liou, Y. C.; Lin, S. H. Structural organization in aqueous solutions of 1-butyl-3-methylimidazolium halides: A

high-pressure infrared spectroscopic study on ionic liquids. *J. Phys. Chem. B* **2008,** *112*, 4351-4356.

40. Hunt, P. A. Why does a reduction in hydrogen bonding lead to an increase in viscosity for the 1-butyl-2,3-dimethyl-imidazolium-based ionic liquids? *J. Phys. Chem. B* **2007,** *111*, 4844-4853.

41. Hunt, P. A.; Gould, I. R.; Kirchner, B. The structure of imidazolium-based ionic liquids: Insights from ion-pair interactions. *Aust. J. Chem.* **2007,** *60*, 9-14.

42. Qiao, B.; Krekeler, C.; Berger, R.; Delle Site, L.; Holm, C. Effect of anions on static orientational correlations, hydrogen bonds, and dynamics in ionic liquids: A simulational study. *J. Phys. Chem. B* **2008,** *112*, 1743-1751.

43. Fujii, K.; Fujimori, T.; Takamuku, T.; Kanzaki, R.; Umebayashi, Y.; Ishiguro, S. I. Conformational equilibrium of bis(trifluoromethanesulfonyl) imide anion of a room-temperature ionic liquid: Raman spectroscopic study and DFT calculations. *J. Phys. Chem. B* **2006,** *110*, 8179-8183.

44. Borodin, O. Polarizable Force Field Development and Molecular Dynamics Simulations of Ionic Liquids. *J. Phys. Chem. B* **2009,** *113*, 11463-11478.

45. Santos, C. S.; Annapureddy, H. V. R.; Murthy, N. S.; Kashyap, H. K.; Castner, E. W., Jr.; Margulis, C. J. Temperature-dependent structure of methyltributylammonium bis(trifluoromethylsulfonyl) amide: X ray scattering and simulations. *J. Chem. Phys.* **2011,** *134*, 064501.

46. Canongia Lopes, J. N.; Padua, A. A. H. Molecular force field for ionic liquids composed of triflate or bistriflylimide anions. *J. Phys. Chem. B* **2004,** *108*, 16893-16898.

47. Canongia Lopes, J. N.; Shimizu, K.; Padua, A. A. H.; Umebayashi, Y.; Fukuda, S.; Fujii, K.; Ishiguro, S. I. A tale of two ions: The conformational landscapes of bis(trifluoromethanesulfonyl)amide and *N,N*-dialkylpyrrolidinium. *J. Phys. Chem. B* **2008,** *112*, 1465-1472.

48. Paulechka, Y. U.; Kabo, G. J.; Emel'yanenko, V. N. Structure, Conformations, Vibrations, and Ideal-Gas Properties of 1-Alkyl-3-methylimidazolium bis(trifluoromethylsulfonyl)imide Ionic Pairs and Constituent Ions. *J. Phys. Chem. B* **2008,** *112*, 15708-15717.

49. Tsuzuki, S.; Matsumoto, H.; Shinoda, W.; Mikami, M. Effects of conformational flexibility of alkyl chains of cations on diffusion of ions in ionic liquids. *Phys. Chem. Chem. Phys.* **2011,** *13*, 5987-5993.

50. Kaintz, A.; Baker, G.; Benesi, A.; Maroncelli, M. Solute Diffusion in Ionic Liquids, NMR Measurements and Comparisons to Conventional Solvents. *J. Phys. Chem. B* **2013,** *117*, 11697-11708.

51. Harris, K. R.; Kanakubo, M.; Tsuchihashi, N.; Ibuki, K.; Ueno, M. Effect of pressure on the transport properties of ionic liquids: 1-alkyl-3-methylimidazolium salts. *J. Phys. Chem. B* **2008,** *112*, 9830-9840.

52. Ahosseini, A.; Scurto, A. M. Viscosity of imidazolium-based ionic liquids at elevated pressures: Cation and anion effects. *Int. J. Thermophys.* **2008,** *29*, 1222-1243.

53. Harris, K. R.; Kanakubo, M.; Woolf, L. A. Temperature and pressure dependence of the viscosity of the ionic liquids 1-hexyl-3-methylimidazolium hexafluorophosphate and 1-butyl-3-methylimidazolium bis(trifluoromethylsulfonyl)imide. *J. Chem. Eng. Data* **2007,** *52*, 1080-1085.

54. Sanmamed, Y. A.; Gonzalez-Salgado, D.; Troncoso, J.; Romani, L.; Baylaucq, A.; Boned, C. Experimental methodology for precise determination of density of RTILs as a function of temperature and pressure using vibrating tube densimeters. *J. Chem. Thermodyn.* **2010,** *42*, 553-563.

55. Harris, K. R.; Kanakubo, M.; Woolf, L. A. Temperature and pressure dependence of the viscosity of the ionic liquid 1-butyl-3-methylimidazolium tetrafluoroborate: Viscosity and density relationships in ionic liquids. *J. Chem. Eng. Data* **2007,** *52*, 2425-2430.

56. Harris, K. R.; Kanakubo, M.; Woolf, L. A. Temperature and pressure dependence of the viscosity of the ionic liquids 1-methyl-3-octylimidazolium hexafluorophosphate and 1-methyl-3-octylimidazolium tetrafluoroborate. *J. Chem. Eng. Data* **2006,** *51*, 1161-1167.

57. Canongia Lopes, J. N.; Padua, A. A. H. Nanostructural organization in ionic liquids. *J. Phys. Chem. B* **2006,** *110*, 3330-3335.

58. Costa Gomes, M. F.; Canongia Lopes, J. N. C.; Padua, A. A. H. Thermodynamics and Micro Heterogeneity of Ionic Liquids. In *Ionic Liquids*, Springer-Verlag Berlin: Berlin, 2009; Vol. 290, pp 161-183.

59. Harris, K. R.; Woolf, L. A.; Kanakubo, M.; Ruther, T. Transport Properties of N-Butyl-N-methylpyrrolidinium Bis(trifluoromethylsulfonyl)amide. *J. Chem. Eng. Data* **2011,** *56*, 4672-4685.

60. Kazakov, A. M., J.W.; Chirico, R.D.; Paulechka, E.; Diky, V.; Muzny, C.D.; Kroenlein, K.; Frenkel, M. "NIST Standard Reference Database 147: NIST Ionic Liquids Database - (ILThermo)", Version 2.0. http://ilthermo.boulder.nist.gov.

61. Canongia Lopes, J. N.; Shimizu, K.; Padua, A. A. H.; Umebayashi, Y.; Fukuda, S.; Fujii, K.; Ishiguro, S. I. Potential energy landscape of bis(fluorosulfonyl)amide. *J. Phys. Chem. B* **2008,** *112*, 9449-9455.

62. Hubbard, C. D.; Illner, P.; van Eldik, R. Understanding chemical reaction mechanisms in ionic liquids: successes and challenges. *Chem. Soc. Rev.* **2011,** *40*, 272-290.

63. van Eldik, R.; Hubbard, C. D., *Chemistry Under Extreme and Non-Classical Conditions*. John Wiley & Sons: New York, 1997.

64. van Eldik, R.; Klärner, F.-G., *High pressure chemistry : synthetic, mechanistic, and supercritical applications*. Wiley-VCH: Weinheim, 2002.

Supporting Information (Section 1)

for

Do TFSA Anions Slither?

Pressure Exposes the Role of TFSA Conformational Exchange in Self-Diffusion

Sophia N. Suarez,* Armando Rua, David Cuffari, Kartik Pilar, Jasmine L. Hatcher,

Sharon Ramati and James F. Wishart*

Contents

Experimental Section: Synthesis of EMIM FSA and EMIM BF_4.

Figure S1. Proton NMR spectrum of *N*-methyl deuterated (MD_3) EMIM TFSA.

Figures S2 to S8. Plots of T_1 relaxation times and diffusion constants as functions of temperature and pressure.

Tables S1 to S21. Tables of T_1 relaxation times and diffusion constants as functions of temperature and pressure.

Experimental Section: Synthesis of EMIM FSA and EMIM BF_4.

1-Ethyl-3-methylimidazolium tetrafluoroborate. 1-ethyl-3-methylimidazolium bromide (4.04 g, 0.0211 mol) and 10 mL of anhydrous acetone were added to a 250 mL round bottom flask fitted with a magnetic stir bar. Sodium tetrafluoroborate (Aldrich, 2.32 g, 0.0211 mol) was diluted with 10 mL of anhydrous acetone and added to the mixture with stirring. Neither of the reagents completely dissolved in the acetone. The reaction mixture was left to stir at room temperature for two days, resulting in a yellow liquid with white crystals. The reaction mixture was gravity filtered to separate the white solid, and the liquid was washed repeatedly with anhydrous acetone and filtered to remove residual solid. The yellow liquid was rotary evaporated under reduced pressure at 50 °C. The product was a yellow liquid (3.05 g, 72.8 %). ^{1}H NMR (400 MHz, DMSO- d_6) δ = 1.39-1.43 (t, 3H, NCH_2CH_3); 3.84 (s, 3H, NCH_3); 4.16-4.21 (q, 2H, NCH_2CH_3); 7.66-7.75 (d, 2H, NC*H*CH*H*N); 9.07 (s, 1H, NC*H*N).

1-Ethyl-3-methylimidazolium bis(fluorosulfonyl)amide. 1-ethyl-3-methylimidazolium bromide (4.36 g, 0.0228 mol) and 3.5 mL of deionized water were added to a 100 mL round bottom flask fitted with a magnetic stir bar. Potassium bis(fluorosulfonyl)amide (also known as potassium bis(fluorosulfonyl)imide, TCI Chemicals, 5.0 g, 0.0228 mol) was diluted with 10 mL of anhydrous acetone and added to the mixture with stirring. The reaction mixture was left to stir at room temperature for two days, resulting in a yellow liquid with white crystals. The reaction mixture was gravity filtered to separate the white solid, and the liquid was washed repeatedly with anhydrous acetone and filtered to remove residual solid. The yellow liquid was rotary evaporated under reduced pressure at 50 °C. The product was a yellow liquid (3.05 g, 72.8 %). was repeated until the test was negative. Residual water was removed from the IL by rotary evaporation under high vacuum and the final product was dried in a vacuum oven at 68 °C for 24 hours to obtain a light yellow liquid (4.86 g, 73.2 %). ^{1}H NMR (400 MHz, DMSO- d_6) δ = 1.40-1.44 (t, 3H, NCH_2CH_3); 3.84 (s, 3H, NCH_3); 4.16-4.21 (q, 2H, NCH_2CH_3); 7.66-7.74 (d, 2H, NC*H*CH*H*N); 9.09 (s, 1H, NC*H*N)**.**

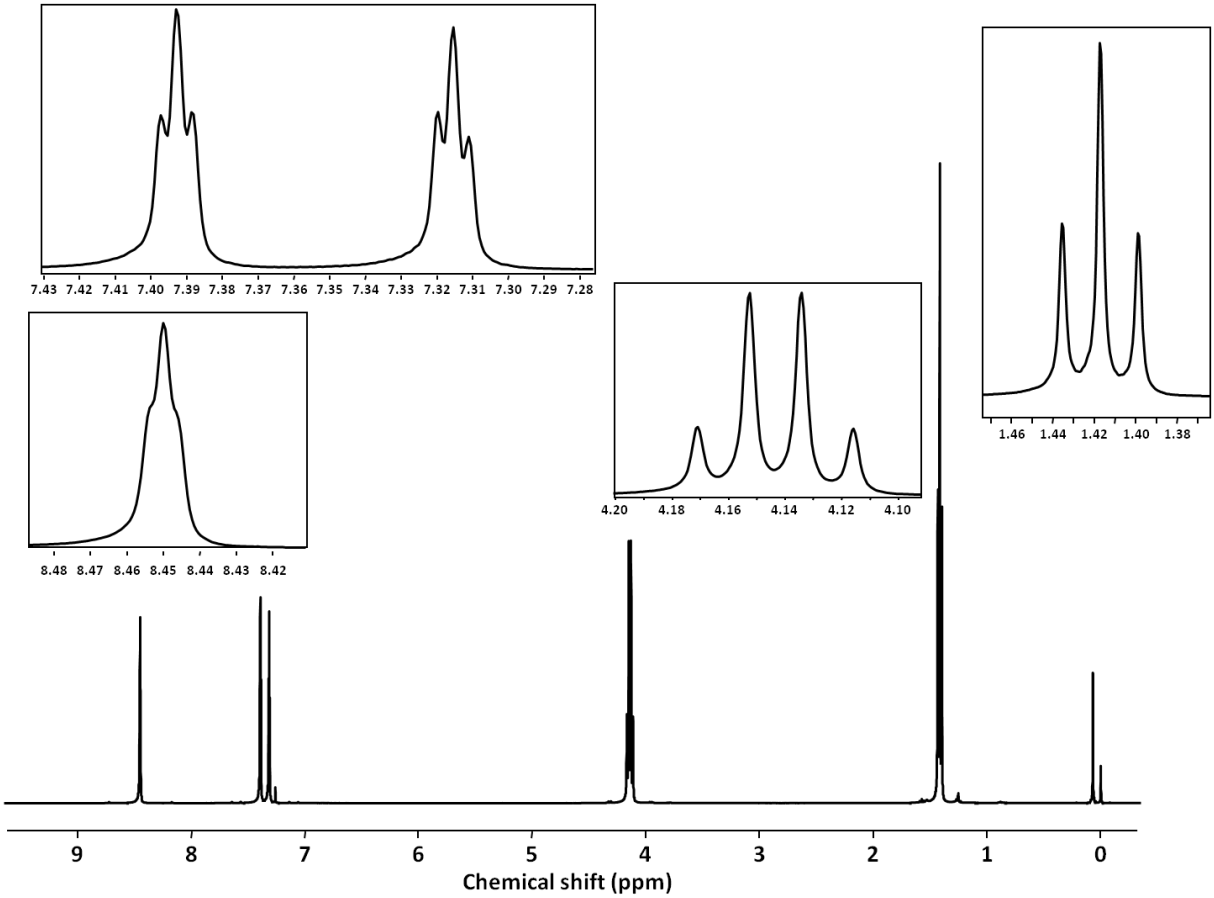

Figure S1. Proton NMR spectrum of *N*-methyl deuterated (MD_3) EMIM TFSA. Regions of interest are expanded in the inserts.

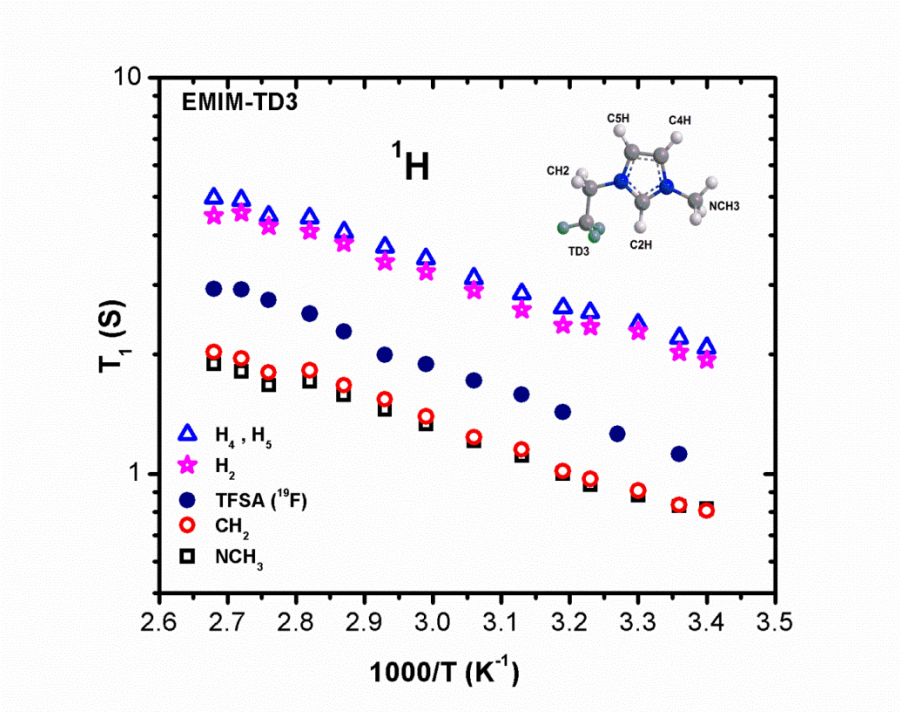

Figure S2. Arrhenius plots of ^{1}H and ^{19}F T_1 relaxation times for the assigned peaks of TD_3 EMIM TFSA.

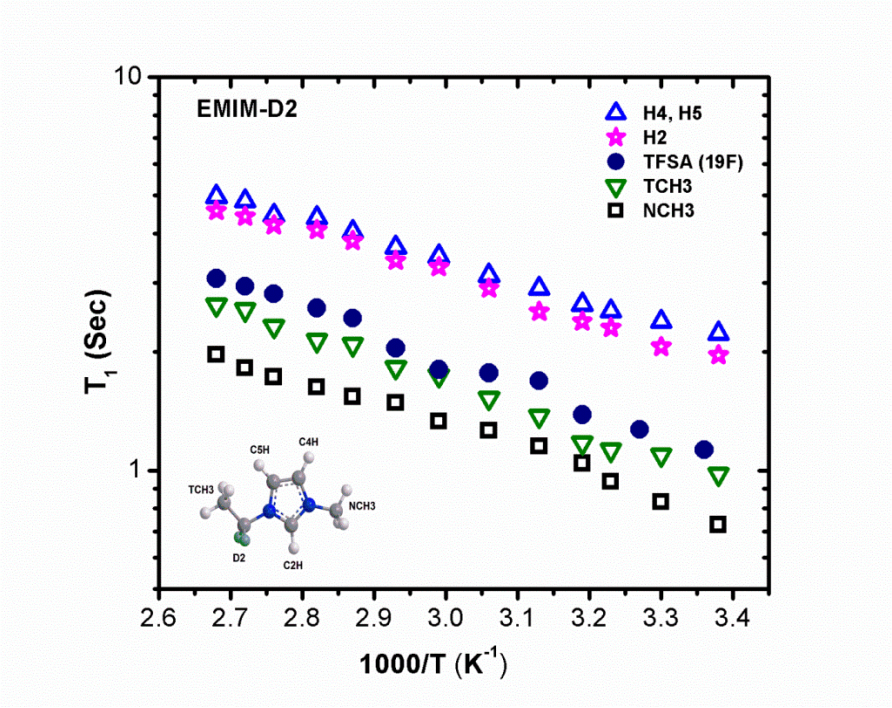

Figure S3. Arrhenius plots of ^{1}H and ^{19}F T_1 relaxation times for the assigned peaks of CD_2 EMIM TFSA.

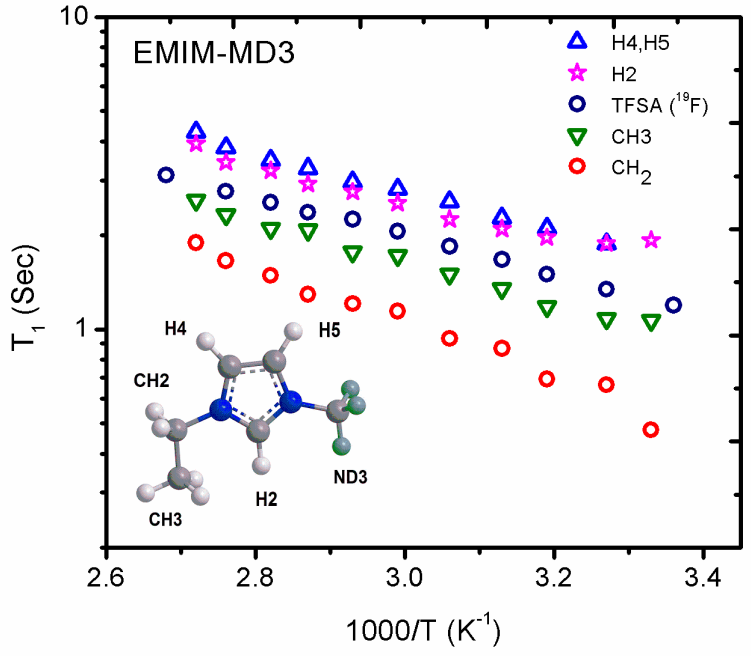

Figure S4. Arrhenius plots of ^{1}H and ^{19}F T_1 relaxation times for the assigned peaks of MD_3 EMIM TFSA.

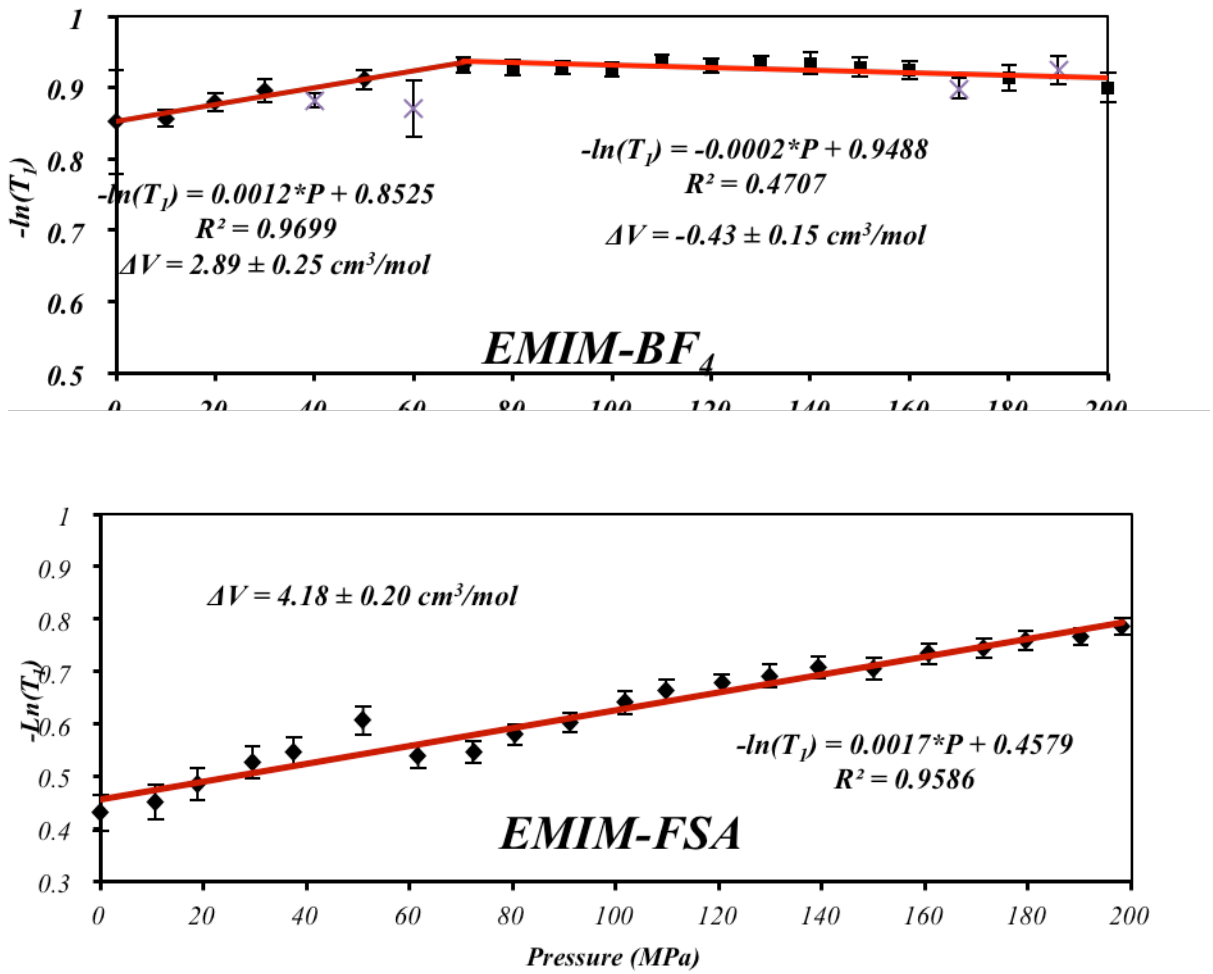

Figure S5. Variable-pressure ^{1}H T_1 relaxation time plots for EMIM BF_4 (top) and EMIM FSA (bottom).

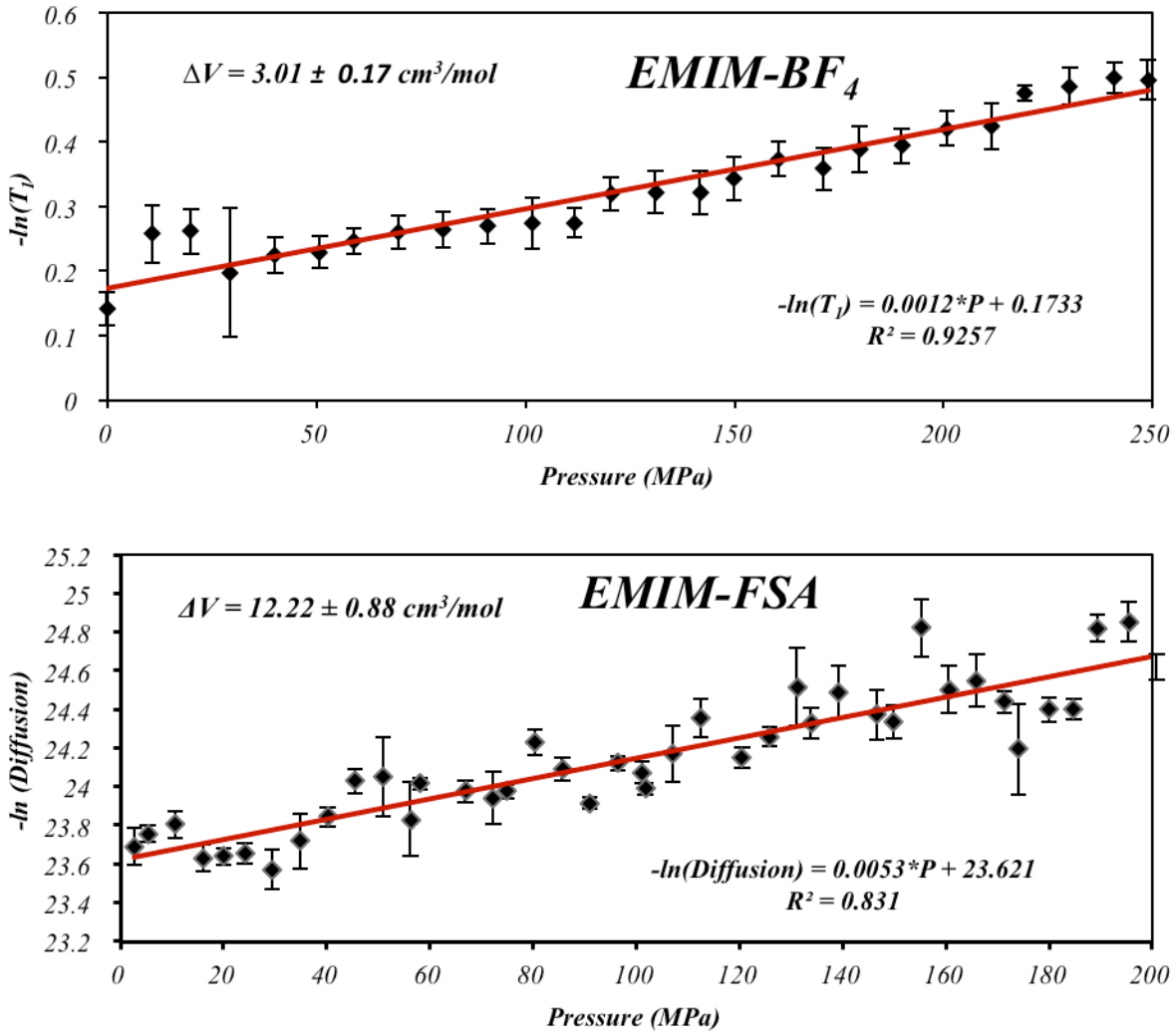

Figure S6. Variable-pressure ^{19}F T_1 relaxation time plots for EMIM BF_4 (top) and EMIM FSA (bottom).

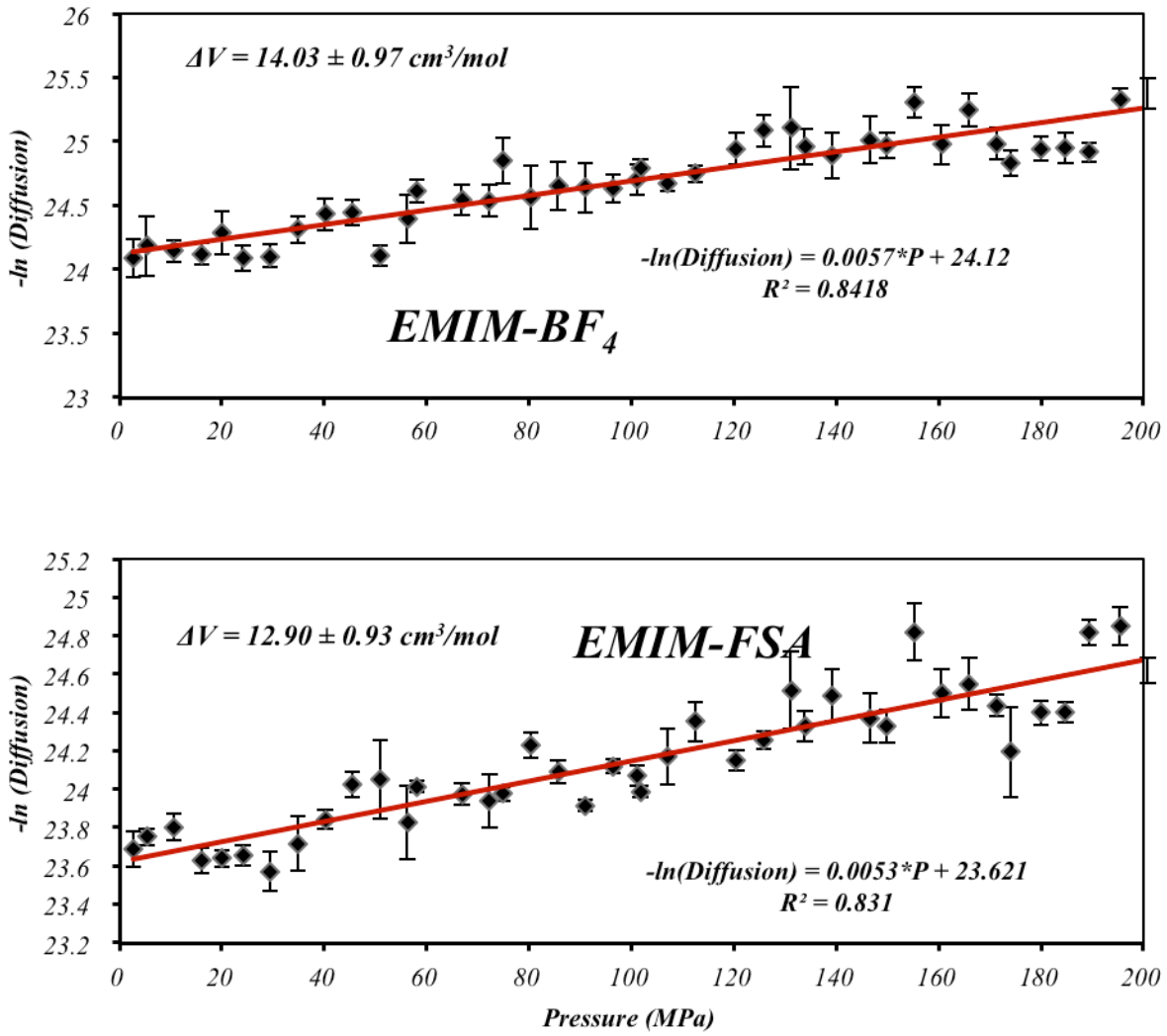

Figure S7. Variable-pressure ^{1}H (cation) diffusion constant plots for EMIM BF_4 (top) and EMIM FSA (bottom).

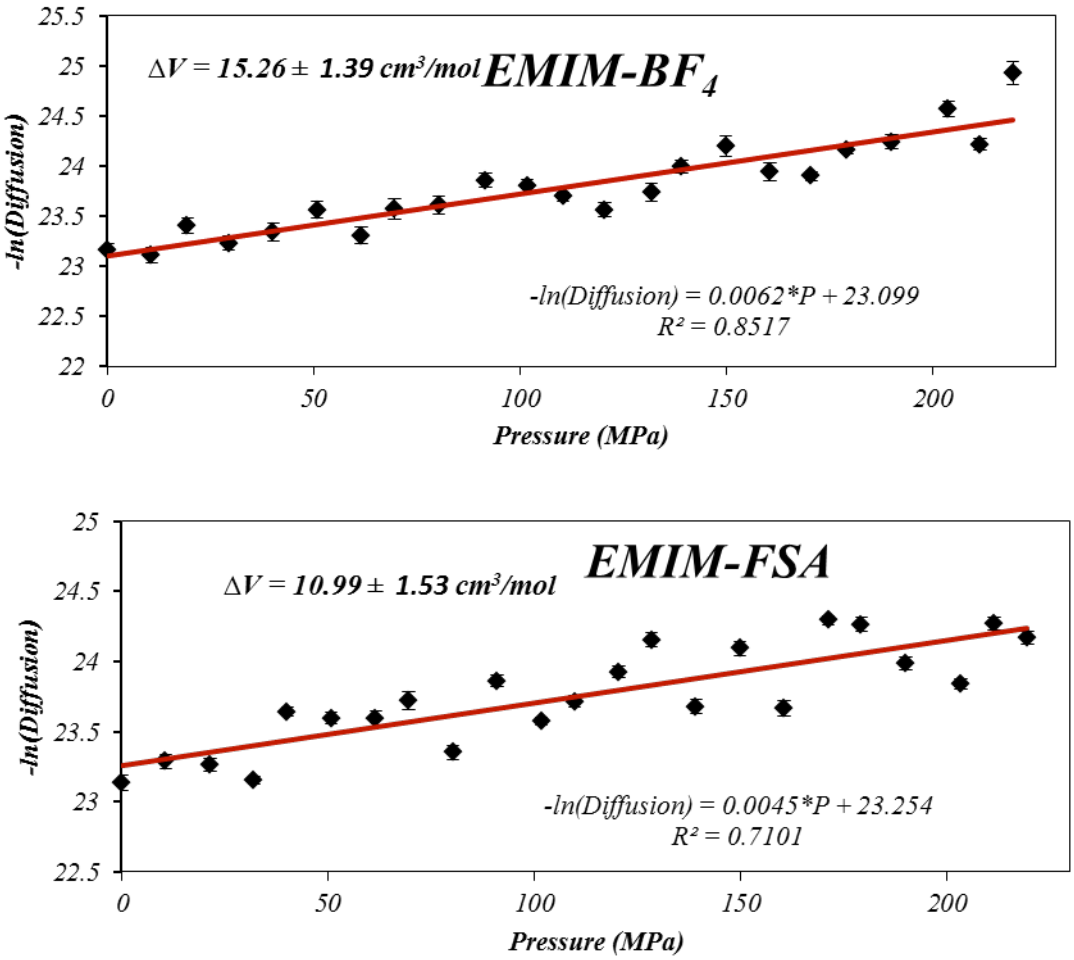

Figure S8. Variable-pressure ^{19}F (anion) diffusion constant plots for EMIM BF_4 (top) and EMIM FSA (bottom).

Please note: all tables are embedded Excel files. Double-click them to open in Excel.

Table S1. Variable-temperature ^{1}H T_1 relaxation data for EMIM TFSA. T_1 data are in seconds.

Temperature (K)	CH2	TCH3	H4,H5	H2	NCH3
306	0.77	1.16	1.83	1.68	0.95
313	0.90	1.34	2.03	1.91	1.00
320	0.99	1.46	2.24	2.09	1.12
327	1.10	1.63	2.54	2.37	1.25
341	1.28	1.79	2.75	2.59	1.47
348	1.40	1.95	2.91	2.72	1.60
355	1.57	2.07	3.02	2.83	1.67
362	1.70	2.21	3.13	2.95	1.72
368	1.81	2.14	3.24	3.00	1.83
373	1.87	2.27	3.43	3.22	1.87

Table S2. Variable-temperature ^{1}H T_1 relaxation data for MD_3-deuterated EMIM TFSA. T_1 data are in seconds.

Temperature (K)	CH2	CH3	H4,H5	H2
300	0.48	1.07	--	1.93
306	0.66	1.08	1.88	1.88
313	0.69	1.18	2.11	1.97
319	0.87	1.35	2.28	2.10
327	0.93	1.50	2.57	2.25
334	1.14	1.72	2.81	2.54
341	1.21	1.77	2.97	2.75
348	1.29	2.08	3.28	2.92
355	1.49	2.10	3.47	3.23
362	1.66	2.33	3.82	3.42
367	1.89	2.59	4.29	3.93

Table S3. Variable-temperature ^1H T_1 relaxation data for TD_3-deuterated EMIM TFSA. T_1 data are in seconds.

Temperature (K)	NCH3	CH2	H4, H5	D2
294	0.82	0.81	2.08	1.94
298	0.83	0.83	2.20	2.03
303	0.88	0.91	2.39	2.29
310	0.94	0.97	2.55	2.35
313	1.00	1.02	2.62	2.37
320	1.11	1.15	2.85	2.59
327	1.21	1.24	3.11	2.90
334	1.33	1.39	3.49	3.24
341	1.45	1.54	3.74	3.43
348	1.58	1.67	4.07	3.81
355	1.71	1.82	4.43	4.10
362	1.67	1.80	4.48	4.22
367	1.81	1.96	4.91	4.56
373	1.89	2.03	4.97	4.49

Table S4. Variable-temperature ^1H T_1 relaxation data for D_2-deuterated EMIM TFSA. T_1 data are in seconds.

Temperature (K)	NCH3	TCH3	H4, H5	H2
296	0.73	0.98	2.23	1.96
303	0.83	1.09	2.39	2.06
310	0.94	1.12	2.54	2.30
313	1.04	1.18	2.64	2.39
319	1.15	1.37	2.90	2.53
327	1.26	1.52	3.13	2.90
334	1.33	1.74	3.50	3.29
341	1.49	1.82	3.69	3.41
348	1.54	2.09	4.04	3.83
355	1.63	2.14	4.38	4.08
362	1.73	2.32	4.45	4.20
367	1.82	2.56	4.84	4.42
373	1.97	2.63	4.96	4.56

Table S5. Variable-temperature ^{19}F T_1 relaxation data for four isotopologues of EMIM TFSA. T_1 data are in seconds.

Temperature (K)	EMIM MD3	EMIM D2	EMIM TD3	EMIM
298	1.19	1.13	1.10	1.12
306	1.34	1.27	1.34	1.26
313	1.50	1.39	1.43	1.43
320	1.67	1.69	1.64	1.58
327	1.85	1.77	1.84	1.72
334	2.06	1.81	1.96	1.89
341	2.25	2.05	2.08	2.00
348	2.37	2.43	2.37	2.29
355	2.55	2.59	2.44	2.53
362	2.76	2.81	2.61	2.74
368	2.99	2.94	2.94	2.92
373	3.12	3.07	3.07	2.93

Table S6. Variable-temperature ^{19}F (anion) self-diffusion data for four isotopologues of EMIM TFSA. D values are in cm^2/s.

Temperature (K)	EMIM MD3	EMIM D2	EMIM TD3	EMIM
298	3.63E-07	3.79E-07	3.83E-07	5.30E-07
306	4.44E-07	4.70E-07	4.72E-07	6.78E-07
313	5.48E-07	5.71E-07	6.50E-07	7.33E-07
320	6.19E-07	6.90E-07	7.49E-07	7.93E-07
327	7.89E-07	8.07E-07	8.26E-07	9.14E-07
334	9.53E-07	9.31E-07	1.11E-06	1.03E-06
341	1.11E-06	1.08E-06	1.14E-06	1.16E-06
348	1.32E-06	1.45E-06	1.28E-06	1.35E-06
355	1.55E-06	1.75E-06	1.42E-06	1.56E-06
362	1.79E-06	1.97E-06	1.65E-06	1.73E-06
368	2.08E-06	2.26E-06	1.84E-06	1.92E-06
373	1.83E-06	2.49E-06	2.01E-06	2.16E-06

Table S7. Variable-pressure ^{1}H T_1 relaxation data for EMIM BF_4 at 22 °C. T_1 data are in seconds.

Pressure (MPa)	T1 (s)	T1 Uncertainty (±)
0	0.427	0.031
10	0.425	0.005
20	0.415	0.005
30	0.408	0.007
40	0.414	0.004
50	0.402	0.005
60	0.418	0.016
70	0.394	0.004
80	0.395	0.004
90	0.395	0.003
100	0.396	0.004
110	0.392	0.003
120	0.394	0.004
130	0.392	0.004
140	0.393	0.006
150	0.395	0.005
160	0.397	0.005
170	0.414	0.004
180	0.401	0.007
190	0.397	0.008
200	0.406	0.008

Table S8. Variable-pressure ^{19}F T_1 relaxation data for EMIM BF_4 at 22 °C. T_1 data are in seconds.

Pressure (MPa)	T1 (s)	T1 Uncertainty (±)	
0.10	0.868	0.023	
10.76	0.773	0.034	
20.06	0.770	0.027	
29.44	0.821	0.082	
40.20	0.799	0.022	
50.88	0.795	0.020	
58.95	0.782	0.016	
69.64	0.771	0.021	
80.32	0.768	0.021	
91.01	0.764	0.020	
101.77	0.761	0.031	
111.76	0.760	0.017	
120.52	0.726	0.018	
131.21	0.725	0.024	
141.89	0.725	0.024	
149.96	0.710	0.024	
160.65	0.689	0.019	
171.40	0.699	0.023	
180.02	0.678	0.024	
190.09	0.675	0.018	
200.84	0.657	0.018	
211.53	0.655	0.024	
219.60	0.622	0.008	
230.28	0.615	0.018	
240.97	0.607	0.014	
249.04	0.610	0.019	

Table S9: Variable-pressure ^{1}H (cation) self-diffusion data for EMIM BF_4 at 22 °C.

Pressure (MPa)	Diffusion (*10^-6 cm^2/s)	Diffusion Uncertainty (±)
2.69	0.705	0.105
5.38	0.643	0.150
10.69	0.668	0.057
16.06	0.687	0.059
20.06	0.580	0.097
24.13	0.709	0.070
29.44	0.698	0.064
34.82	0.564	0.059
40.20	0.502	0.061
45.51	0.495	0.051
50.88	0.694	0.056
56.26	0.519	0.098
58.12	0.419	0.038
66.95	0.449	0.053
72.33	0.453	0.057
74.95	0.330	0.059
80.32	0.441	0.109
85.70	0.402	0.076
91.01	0.408	0.078
96.39	0.411	0.044
101.08	0.384	0.046
101.77	0.352	0.026
107.08	0.395	0.026
112.45	0.366	0.023
120.52	0.301	0.037
125.83	0.261	0.032
131.21	0.256	0.083
133.90	0.295	0.041
139.21	0.317	0.056
146.58	0.281	0.052
149.96	0.292	0.028
155.27	0.209	0.025
160.65	0.291	0.044
166.03	0.222	0.029
171.33	0.289	0.035
174.02	0.337	0.033
180.02	0.301	0.029
184.78	0.299	0.035
189.40	0.309	0.023
195.47	0.205	0.019
200.84	0.196	0.023

Table S10. Variable-pressure ^{19}F (anion) self-diffusion data for EMIM BF_4 at 22 °C.

Pressure (MPa)	Diffusion (*10^-6 cm^2/s)	Diffusion Uncertainty (±)
0.10	0.871	0.051
10.69	0.918	0.071
19.37	0.688	0.053
29.44	0.816	0.054
40.20	0.728	0.067
50.88	0.583	0.046
61.57	0.754	0.066
69.64	0.580	0.056
80.32	0.559	0.052
91.70	0.435	0.032
101.77	0.459	0.028
110.45	0.513	0.021
120.52	0.585	0.040
131.90	0.494	0.044
139.21	0.381	0.025
149.96	0.308	0.031
160.65	0.400	0.035
170.65	0.417	0.018
179.40	0.322	0.014
190.09	0.296	0.021
203.88	0.214	0.016
211.53	0.304	0.019
219.53	0.149	0.017

Table S11. Variable-pressure ^{1}H T_1 relaxation data for EMIM FSA at 22 °C. T_1 data are in seconds.

Pressure (MPa)	T1 (s)	T1 Uncertainty (±)
0.10	0.650	0.022
10.69	0.636	0.021
18.75	0.615	0.019
29.44	0.591	0.018
37.51	0.579	0.017
50.88	0.545	0.015
61.57	0.583	0.013
72.33	0.579	0.012
80.32	0.560	0.011
91.01	0.547	0.010
101.77	0.526	0.011
109.76	0.514	0.011
120.52	0.508	0.009
129.83	0.501	0.011
139.21	0.492	0.010
149.96	0.494	0.011
160.65	0.480	0.009
171.33	0.475	0.008
179.40	0.468	0.008
190.09	0.464	0.007
198.16	0.455	0.007

Table S12. Variable-pressure ^{19}F T_1 relaxation data for EMIM FSA. T_1 data are in seconds.

Pressure (MPa)	T1 (s)	T1 Uncertainty (±)
0.10	0.686	0.012
5.38	0.666	0.017
10.69	0.640	0.019
16.06	0.643	0.021
20.06	0.625	0.019
24.13	0.586	0.018
29.44	0.580	0.019
34.82	0.595	0.014
40.20	0.561	0.018
45.51	0.565	0.016
50.88	0.540	0.013
56.26	0.535	0.024
61.57	0.526	0.016
66.95	0.519	0.014
72.33	0.508	0.022
74.95	0.500	0.022
80.32	0.483	0.014
85.70	0.448	0.010
89.01	0.451	0.016
96.39	0.434	0.014
99.08	0.429	0.018
104.46	0.411	0.022
109.76	0.411	0.018
115.14	0.407	0.012
117.83	0.398	0.014
125.83	0.369	0.020
131.21	0.366	0.016
133.97	0.372	0.013
139.21	0.365	0.010
144.58	0.350	0.010
149.96	0.351	0.015
152.72	0.348	0.025
160.65	0.341	0.012
166.03	0.336	0.014
171.40	0.342	0.008
174.02	0.328	0.011
180.02	0.322	0.007
184.78	0.309	0.007
190.09	0.309	0.007
195.47	0.306	0.010

Table S13. Variable-pressure ^{1}H (cation) self-diffusion data for EMIM FSA at 22 °C.

Pressure (MPa)	Diffusion (*10^-6 cm^2/s)	Diffusion Uncertainty (±)
2.69	1.054	0.100
5.38	0.988	0.042
10.69	0.940	0.066
16.06	1.119	0.077
20.06	1.107	0.047
24.13	1.091	0.059
29.44	1.187	0.122
34.82	1.024	0.145
40.20	0.904	0.045
45.51	0.751	0.049
50.88	0.735	0.151
56.26	0.917	0.176
58.12	0.761	0.024
66.95	0.791	0.044
72.33	0.819	0.113
74.95	0.791	0.028
80.32	0.614	0.040
85.70	0.706	0.042
91.01	0.842	0.026
96.39	0.684	0.025
101.08	0.718	0.040
101.77	0.781	0.023
107.08	0.651	0.096
112.45	0.542	0.055
120.52	0.664	0.034
125.83	0.597	0.030
131.21	0.462	0.094
133.90	0.556	0.044
139.21	0.474	0.065
146.58	0.532	0.068
149.96	0.554	0.048
155.27	0.340	0.051
160.65	0.467	0.058
166.03	0.447	0.061
171.33	0.498	0.029
174.02	0.636	0.148
180.02	0.518	0.032
184.78	0.517	0.027
189.40	0.341	0.024
195.47	0.330	0.033
200.84	0.416	0.028

Table S14. Variable-pressure ^{19}F (anion) self-diffusion data for EMIM FSA at 22 °C.

Pressure (MPa)	Diffusion (*10^-6 cm^2/s)	Diffusion Uncertainty (±)
0.10	0.896	0.049
10.69	0.769	0.039
21.44	0.790	0.036
32.13	0.878	0.025
40.20	0.540	0.018
50.88	0.567	0.014
61.64	0.568	0.048
69.64	0.499	0.031
80.32	0.722	0.036
91.08	0.433	0.017
101.77	0.579	0.015
109.83	0.503	0.021
120.52	0.406	0.015
128.52	0.323	0.016
139.27	0.521	0.026
149.96	0.344	0.018
160.65	0.527	0.029
171.40	0.281	0.006
179.40	0.290	0.009
190.16	0.381	0.018
203.53	0.443	0.016
211.53	0.288	0.013
219.60	0.318	0.024

Table S15. Variable-temperature ^{2}H T_1 relaxation data for EMIM TFSA isotopologues. T_1 values are in seconds.

Temperature (K)	MD3	TD3	D2
278	0.1953	0.06256	0.1596
305	0.23439	0.07456	0.17781
313	0.26688	0.08902	0.19791
319	0.30439	0.10264	0.21965
327	0.36278	0.11781	0.24417
334	0.39592	0.13262	0.26518
341	0.44673	0.14977	0.28333
348	0.49487	0.16763	0.31599
355	0.54532	0.18522	0.3373
362	0.58216	0.20518	0.37107
367	0.63256	0.22064	0.39147
373	0.66742	0.23493	0.4006

Table S16. ^{19}F self-diffusion coefficients vs. temperature for EMIM TFSA isotopologues. D values are in cm^2/s.

Temperature (K)	EMIM MD3	EMIM D2	EMIM TD3	EMIM
298	3.63E-07	3.79E-07	3.83E-07	5.30E-07
306	4.44E-07	4.70E-07	4.72E-07	6.78E-07
313	5.48E-07	5.71E-07	6.50E-07	7.33E-07
319	6.19E-07	6.90E-07	7.49E-07	7.93E-07
327	7.89E-07	8.07E-07	8.26E-07	9.14E-07
334	9.53E-07	9.31E-07	1.11E-06	1.03E-06
341	1.11E-06	1.08E-06	1.14E-06	1.16E-06
348	1.32E-06	1.45E-06	1.28E-06	1.35E-06
355	1.55E-06	1.75E-06	1.42E-06	1.56E-06
362	1.79E-06	1.97E-06	1.65E-06	1.73E-06
367	2.08E-06	2.26E-06	1.84E-06	1.92E-06
373	1.83E-06	2.49E-06	2.01E-06	2.16E-06

Table S17. ^{1}H variable-temperature self-diffusion coefficients for EMIM MD_3 TFSA. D values are in cm^2/s.

Temperature (K)	D EMIM MD3
300	4.34E-07
313	7.94E-07
319	1.04E-06
327	1.24E-06
341	1.60E-06
348	1.90E-06
355	2.40E-06
362	2.70E-06
373	3.36E-06

Table S18. ^{1}H variable-temperature self-diffusion coefficients for EMIM, EMIM D_2 and EMIM TD_3 TFSA. D values are in cm^2/s.

Temperature (K)	D EMIM D2	D EMIM TD3	D EMIM
296	4.56E-07	4.52E-07	4.36E-07
303	5.65E-07	4.86E-07	4.60E-07
310	7.23E-07	5.38E-07	5.30E-07
313	8.30E-07	6.24E-07	5.13E-07
319	9.37E-07	7.02E-07	7.30E-07
327	1.14E-06	8.54E-07	9.19E-07
334	1.35E-06	9.36E-07	1.04E-06
341	1.54E-06	1.32E-06	1.55E-06
348	1.54E-06	1.56E-06	1.91E-06
355	1.65E-06	1.61E-06	2.45E-06
362	1.85E-06	1.61E-06	2.99E-06
367	1.81E-06	2.21E-06	3.15E-06
373	1.93E-06	2.47E-06	3.26E-06

Table S19. Variable-pressure ^2H T_1 relaxation data for EMIM TD_3, MD_3 and D_2 TFSA.

Pressure (Gpa)	Log T1 EMIM MD3	Log T1 (sec) EMIM D2	Log (T1) EMIM TD3	T = 22 °C	
1.00E-04	-0.76462	-1.237	-0.85183		
0.005	-0.79073	-1.258	-0.86678		
0.010	-0.80626	-1.282	-0.87416		
0.015	-0.82518	-1.308	-0.87795		
0.020	-0.84744	-1.332	-0.89282		
0.025	-0.868	-1.351	-0.89884		
0.030	-0.88739	-1.38	-0.90823		
0.035	-0.90507	-1.4	-0.92096		
0.040	-0.92172	-1.422	-0.92475		
0.045	-0.9407	-1.449	-0.93487		
0.050	-0.95924	-1.479	-0.95047		
0.055	-0.97617	-1.49	-0.95125		
0.060	-0.99166	-1.516	-0.95833		
0.065	-1.01046	-1.541	-0.96469		
0.070	-1.02829	-1.546	-0.97277		
0.075	-1.04851	-1.573	-0.98251		
0.080	-1.05549	-1.59	-0.99025		
0.085	-1.0793	-1.62	-0.99405		
0.090	-1.09871	-1.626	-1.00499		
0.095	-1.11663	-1.644	-1.01087		
0.100	-1.13674	-1.659	-1.01566		
0.105	-1.14724	-1.673	-1.02791		
0.110	-1.1683	-1.69	-1.032		
0.115	-1.18964	-1.706	-1.04083		
0.120	-1.19791	-1.726	-1.05518		
0.125	-1.21688	-1.743	-1.06159		
0.130	-1.22983	-1.755	-1.06434		
0.135	-1.2467	-1.765	-1.06818		
0.140	-1.24967	-1.779	-1.09836		
0.145	-1.2611	-1.785	-1.1135		
0.150	-1.27269	-1.798	-1.12856		
0.155	-1.28835	-1.806	-1.10786		
0.160	-1.29344	-1.831	-1.1038		
0.165	-1.31233	-1.829	-1.11572		
0.170	-1.31218	-1.884	-1.11642		
0.175	-1.3193	-1.886	-1.12821		
0.180	-1.32721	-1.875	-1.13051		
0.185	-1.33714	-1.907	-1.13627		
0.190	-1.34525	-1.904	-1.14584		
0.195	-1.35633	-1.904	-1.1545		
0.200	-1.3617	-1.917	-1.1504		
0.205	-1.36665	-1.925	-1.16763		
0.210	-1.37327	-1.935	-1.16231		

Table S20. Variable-pressure ^{1}H and ^{19}F self-diffusion coefficients for EMIM TFSA at 22 °C.

Pressure (Mpa)	1H D (*10^-7 cm^2/s)		Pressure (Mpa)	19F D (*10^-7 cm^2/s)		
0.1	2.557		0.1	2.557		
20	1.872		2.5	2.546		
40	2.240		20	2.472		
60	1.753		40	1.519		
80	1.369		60	0.944		
100	1.370		80	0.721		
120	0.897		80	0.816		
140	0.918		100	0.542		
160	0.728		120	0.570		
180	0.726		140	0.355		
210	0.729		150	0.723		
230	0.586		160	0.429		
250	0.661		170	0.385		
			180	0.275		
			190	0.220		

Table S21. Variable-pressure ^{1}H and ^{19}F self-diffusion coefficients for BMIM TFSA at 22 °C.

Pressure (Mpa)	1H D (*10^-7 cm^2/s)		Pressure (Mpa)	19F (*10^-7 cm^2/s)
0.1	2.557		0.1	2.268
20	2.110		20	2.356
40	1.769		30	1.575
60	1.604		40	1.236
80	1.323		50	1.108
100	0.988		60	0.945
120	0.892		70	0.961
140	0.811		80	0.836
160	0.644		90	0.770
180	0.566		100	0.511
200	0.425		110	0.544
230	0.568		125	0.275
			150	0.337
			175	0.375
			225	0.271
			250	0.385
			250	0.152

Supporting Information (Section 2)

for

Do TFSA Anions Slither?

Pressure Exposes the Role of TFSA Conformational Exchange in Self-Diffusion

Sophia N. Suarez,* Armando Rua, David Cuffari, Kartik Pilar, Jasmine L. Hatcher,

Sharon Ramati and James F. Wishart*

Contents

Table S22. Activation volumes from reported ionic self-diffusion coefficients and viscosities.

Directory of fitted activation volume data

Plots of ionic diffusion constants versus pressure with tabulated data

Plots of ln(fluidity) (inverse viscosity) versus pressure with tabulated data

Table S22. Activation volumes from reported ionic self-diffusion coefficients and viscosities

IL / Reference for diffusion	Temperature °C	$\Delta V^{\ddagger}$(D+) cm^3/mol or molec. vols.	error_$\Delta V^{\ddagger}$(D+) cm^3/mol	$\Delta V^{\ddagger}$(D-) cm^3/mol or molec. vols.	error_$\Delta V^{\ddagger}$(D-) cm^3/mol	$\Delta V^{\ddagger}$(fluidity) cm^3/mol	Reference for fluidity or molec. vols.
		Blue = molecular volumes from Ref. 13					
EMIM TFSA		70.2		95.6			Ref. 13
This work	22	14.6	1.3	28.8	2.5		
	25					26.2 ± 0.7 (25)	Ref. 4
	50					25.7 ± 0.3 (50)	Ref. 4
	70					20.5 ± 0.1 (70)	Ref. 4
BMIM TFSA		90.6		95.6			Ref. 13
This work	22	19.2	1.4	22.6	2.7		
	25					27.7 ± 0.2 (25)	Ref. 5
	50					23.7 ± 0.2 (50)	Ref. 5
	75					21.0 ± 0.3 (75)	Ref. 5
EMIM FSA		70.2		65.0			Ref. 13
This work	22	12.9	0.9	11.0	1.5		
EMIM BF_4		70.2		30.4			Ref. 13
	20					24.7 ± 1.0 (20)	Ref. 6
This work	22	14.0	1.0	15.3	1.4		
	30					23.3 ± 0.9 (30)	Ref. 6
BMIM BF_4		90.6		30.4			Ref. 13
						25.6 ± 0.9 (20)	Ref. 6
Ref. 1	25	22.0	0.4	N/A	N/A	25.0 ± 0.1 (25)	Ref. 7
Ref. 1	50	19.0	0.2	18.9	0.7	21.4 ± 0.2 (50)	Ref. 7
Ref. 1	75	16.8	0.1	17.0	0.4	19.0 ± 0.2 (75)	Ref. 7
HMIM BF_4		111.1		30.4			Ref. 13
	22					32.6 ± 1.2 (22)	Ref. 6
	25					29.5 ± 0.6 (25)	Ref. 4
	50					23.2 ± 0.2 (50)	Ref. 4
	70					21.0 ± 0.2 (70)	Ref. 4
OMIM BF_4		131.6		30.4			Ref. 13
	20					31.3 ± 0.9 (20)	Ref. 6
	25					29.2 ± 0.2 (25)	Ref. 8
Ref. 1	50	25.3	0.8	24.7	0.4	25.5 ± 0.2 (50)	Ref. 8
Ref. 1	60	23.8	0.6	21.5	0.2	24.5 ± 0.3 (60)	Ref. 8
Ref. 1	75	21.8	0.2	20.1	0.3	23.3 ± 0.2 (75)	Ref. 8
BMIM PF_6		90.6		44.7			Ref. 13
	25					33.2 ± 0.9 (25)	Ref. 4
	25					32.6 ± 0.2 (25)	Ref. 9
Ref. 2	50	26.4	0.4	24.6	1.2	28.3 ± 0.2 (50)	Ref. 9
Ref. 2	70	23.6	0.2	24.3	0.3	26.7 ± 0.2 (70)	Ref. 9
HMIM PF_6		111.1		44.7			Ref. 13
	25					35.4 ± 0.2 (25)	Ref. 5
	25					35.9 ± 0.7 (25)	Ref. 4
	50					29.2 ± 0.3 (50)	Ref. 4
Ref. 1	50	25.0	1.1	27.6	0.4	31.0 ± 0.5 (50)	Ref. 5
Ref. 1	60	25.4	0.5	24.9	1.0	29.1 ± 0.3 (60)	Ref. 5
	70					27.2 ± 0.3 (70)	Ref. 4
Ref. 1	75	23.8	0.4	24.6	0.2	27.0 ± 0.4 (75)	Ref. 5
OMIM PF_6		131.6		44.7			Ref. 13
	20					37.0 ± 0.9 (20)	Ref. 10
	25					35.5 ± 0.3 (25)	Ref. 8
	35					34.0 ± 0.3 (35)	Ref. 8
	40					33.8 ± 0.8 (40)	Ref. 10
	60					32.8 ± 1.1 (60)	Ref. 10
	60					30.7 ± 0.3 (60)	Ref. 8
Ref. 1	70	26.9	0.8	N/A	N/A	28.8 ± 0.4 (70)	Ref. 8

Ref. 1	75	26.0	0.4	31.1	2.2		
Ref. 1	80	24.8	0.6	29.1	1.2	33.9 ± 0.7 (80)	Ref. 10
BMpyrr TFSA		101.8		95.6			Ref. 13
	25					31.4 ± 0.2 (25)	Ref. 3
Ref. 3	30	30.5	0.3	27.4	0.5		
	40					28.8 ± 0.3 (40)	Ref. 11
Ref. 3	50	26.0	0.2	25.9	0.3	28.6 ± 0.2 (50)	Ref. 3
Ref. 3	65	24.6	0.2	23.8	0.2		
	70					26.3 ± 0.1 (70)	Ref. 11
Ref. 3	75	23.0	0.1	22.6	0.2	27.3 ± 0.2 (75)	Ref. 3
	90					25.0 ± 0.4 (90)	Ref. 11
(EOM)Mpyrr TFSA		95.3		95.6			Ref. 13
	40					27.0 ± 0.3 (40)	Ref. 11
	70					24.2 ± 0.2 (70)	Ref. 11
	90					23.7 ± 0.3 (90)	Ref. 11
BMMIM TFSA		–		95.6			Ref. 13
	40					29.7 ± 0.3 (40)	Ref. 12
	70					26.3 ± 0.2 (70)	Ref. 12
	90					24.7 ± 0.5 (90)	Ref. 12
HMIM TFSA		111.1		95.6			Ref. 13
	25					27.7 ± 0.2 (25)	Ref. 4
	50					25.7 ± 0.3 (50)	Ref. 4
	70					23.8 ± 0.2 (70)	Ref. 4
C_{10}MIM TFSA		152.1		95.6			Ref. 13
	25					29.8 ± 0.4 (25)	Ref. 4
	50					27.0 ± 0.4 (50)	Ref. 4
	70					27.1 ± 0.3 (70)	Ref. 4
EMIM $EtSO_4$		70.2		58.1			Ref. 13
	40					19.4 ± 0.1 (40)	Ref. 11
BMMIM FAP		–		136.5			
	40					46.0 ± 0.2 (40)	Ref. 12
	70					39.4 ± 0.1 (70)	Ref. 12
(EOM)Mpyrr FAP		95.3		136.5			Ref. 13
	40					42.4 ± 0.2 (40)	Ref. 12
	70					37.4 ± 0.1 (70)	Ref. 12
	90					32.7 ± 0.8 (90)	Ref. 12

Reference list for Spreadsheet of Activation Volumes

(1) Harris, K. R.; Kanakubo, M.; Tsuchihashi, N.; Ibuki, K.; Ueno, M., Effect of pressure on the transport properties of ionic liquids: 1-alkyl-3-methylimidazolium salts. *J. Phys. Chem. B* **2008,** *112*, 9830-9840. http://dx.doi.org/10.1021/jp8021375

(2) Kanakubo, M.; Harris, K. R.; Tsuchihashi, N.; Ibuki, K.; Ueno, M., Effect of pressure on transport properties of the ionic liquid 1-butyl-3-methylimidazolium hexafluorophosphate. *J. Phys. Chem. B* **2007,** *111*, 2062-2069. http://dx.doi.org/10.1021/jp067328k

(3) Harris, K. R.; Woolf, L. A.; Kanakubo, M.; Ruther, T., Transport Properties of N-Butyl-N-methylpyrrolidinium Bis(trifluoromethylsulfonyl)amide. *J. Chem. Eng. Data* **2011,** *56*, 4672-4685. http://dx.doi.org/10.1021/je2006049

(4) Ahosseini, A.; Scurto, A. M., Viscosity of imidazolium-based ionic liquids at elevated pressures: Cation and anion effects. *Int. J. Thermophys.* **2008,** *29*, 1222-1243. http://dx.doi.org/10.1007/s10765-008-0497-7

(5) Harris, K. R.; Kanakubo, M.; Woolf, L. A., Temperature and pressure dependence of the viscosity of the ionic liquids 1-hexyl-3-methylimidazolium hexafluorophosphate and 1-butyl-3-methylimidazolium bis(trifluoromethylsulfonyl)imide. *J. Chem. Eng. Data* **2007,** *52*, 1080-1085. http://dx.doi.org/10.1021/je700032n

(6) Sanmamed, Y. A.; Gonzalez-Salgado, D.; Troncoso, J.; Romani, L.; Baylaucq, A.; Boned, C., Experimental methodology for precise determination of density of RTILs as a function of temperature and pressure using vibrating tube densimeters. *J. Chem. Thermodyn.* **2010,** *42*, 553-563. http://dx.doi.org/10.1016/j.jct.2009.11.014

(7) Harris, K. R.; Kanakubo, M.; Woolf, L. A., Temperature and pressure dependence of the viscosity of the ionic liquid 1-butyl-3-methylimidazolium tetrafluoroborate: Viscosity and density relationships in ionic liquids. *J. Chem. Eng. Data* **2007,** *52*, 2425-2430. http://dx.doi.org/10.1021/je700370z

(8) Harris, K. R.; Kanakubo, M.; Woolf, L. A., Temperature and pressure dependence of the viscosity of the ionic liquids 1-methyl-3-octylimidazolium hexafluorophosphate and 1-methyl-3-octylimidazolium tetrafluoroborate. *J. Chem. Eng. Data* **2006,** *51*, 1161-1167. http://dx.doi.org/10.1021/je060082s

(9) Harris, K. R.; Woolf, L. A.; Kanakubo, M., Temperature and pressure dependence of the viscosity of the ionic liquid 1-butyl-3-methylimidazolium hexaftuorophosphate. *J. Chem. Eng. Data* **2005,** *50*, 1777-1782. http://dx.doi.org/10.1021/je050147b

(10) Tomida, D.; Kumagai, A.; Kenmochi, S.; Qiao, K.; Yokoyama, C., Viscosity of 1-hexyl-3-methylimidazolium hexafluorophosphate and 1-octyl-3-methylimidazolium hexafluorophosphate at high pressure. *J. Chem. Eng. Data* **2007,** *52*, 577-579. http://dx.doi.org/10.1021/je060464y

(11) Gacino, F. M.; Paredes, X.; Comunas, M. J. P.; Fernandez, J., Effect of the pressure on the viscosities of ionic liquids: Experimental values for 1-ethyl-3-methylimidazolium ethylsulfate and two bis(trifluoromethyl-sulfonyl)imide salts. *J. Chem. Thermodyn.* **2012,** *54*, 302-309. http://dx.doi.org/10.1016/j.jct.2012.05.007

(12) Gacino, F. M.; Paredes, X.; Comunas, M. J. P.; Fernandez, J., Pressure dependence on the viscosities of 1-butyl-2,3-dimethylimidazolium bis(trifluoromethylsulfonyl)imide and two tris(pentafluoroethyl)trifluorophosphate based ionic liquids: New measurements and modelling. *J. Chem. Thermodyn.* **2013,** *62*, 162-169. http://dx.doi.org/10.1016/j.jct.2013.02.014

(13) Kaintz, A.; Baker, G.; Benesi, A.; Maroncelli, M., Solute Diffusion in Ionic Liquids, NMR Measurements and Comparisons to Conventional Solvents. *J. Phys. Chem. B* **2013,** *117*, 11697-11708. http://dx.doi.org/10.1021/jp405393d

Directory of fitted activation volume data

Glossary of chemical nomenclature for fitted data

Due to the sheer number of entries and data sets, some designations in the supporting information are different than those used in the manuscript.

BMIM = 1-butyl-3-methylimidazolium cation
BMMIM = 1-butyl-2-methyl-3-methylimidazolium cation
BMpyrr = P_{14} = 1-butyl-1-methylpyrrolidinium cation
C10MIM = 1-decyl-3-methylimidazolium cation
EMIM = 1-ethyl-3-methylimidazolium cation
(EOM)Mpyrr = 1-butyl-1-methoxyethylpyrrolidinium cation
HMIM = 1-hexyl-3-methylimidazolium cation
OMIM = 1-methyl-3-octylimidazolium cation

BF_4 = tetrafluoroborate anion
$EtSO_4$ = ethylsulfate anion
FAP = tris(pentafluoroethyl)trifluorophosphate anion
FSA = bis(fluorosulfonyl)amide anion
PF_6 = hexafluorophosphate anion
TFSA = NTf_2 = bis(trifluoromethylsulfonyl)amide anion

Plots of ionic self-diffusion constants versus pressure (counter-ion in parentheses)

Cations

bmim (BF4) 25C self-diffusion plot p. 9
bmim (BF4) 50C self-diffusion plot p. 10
bmim (BF4) 75C self-diffusion plot p. 11
bmim (PF6) 50C self-diffusion plot p. 12
bmim (PF6) 70C self-diffusion plot p. 13
BMpyrr (TFSA) 30C self-diffusion plot p. 14
BMpyrr (TFSA) 50C self-diffusion plot p. 15
BMpyrr (TFSA) 65C self-diffusion plot p. 16
BMpyrr (TFSA) 75C self-diffusion plot p. 17
hmim (PF6) 50C self-diffusion plot p. 18
hmim (PF6) 60C self-diffusion plot p. 19
hmim (PF6) 75C self-diffusion plot p. 20
omim (BF4) 50C self-diffusion plot p. 21
omim (BF4) 60C self-diffusion plot p. 22
omim (BF4) 75C self-diffusion plot p. 23
omim (PF6) 70C self-diffusion plot p. 24
omim (PF6) 75C self-diffusion plot p. 25
omim (PF6) 80C self-diffusion plot p. 26

Anions

BF4 (bmim) 50C self-diffusion plot p. 27
BF4 (bmim) 75C self-diffusion plot p. 28
BF4 (omim) 50C self-diffusion plot p. 29
BF4 (omim) 60C self-diffusion plot p. 30
BF4 (omim) 75C self-diffusion plot p. 31
PF6 (bmim) 50C self-diffusion plot p. 32
PF6 (bmim) 70C self-diffusion plot p. 33
PF6 (hmim) 50C self-diffusion plot p. 34
PF6 (hmim) 60C self-diffusion plot p. 35
PF6 (hmim) 75C self-diffusion plot p. 36
PF6 (omim) 75C self-diffusion plot p. 37
PF6 (omim) 80C self-diffusion plot p. 38
TFSA (BMpyrr) 30C self-diffusion plot p. 39
TFSA (BMpyrr) 50C self-diffusion plot p. 40
TFSA (BMpyrr) 65C self-diffusion plot p. 41
TFSA (BMpyrr) 75C self-diffusion plot p. 42

Plots of ln(fluidity) (inverse viscosity) versus pressure

bmim BF4 20 C viscosity-pressure plot p. 43
bmim BF4 25 C viscosity-pressure plot p. 44
bmim BF4 50 C viscosity-pressure plot p. 45
bmim BF4 75 C viscosity-pressure plot p. 46
bmim PF6 25 C Ahosseini viscosity-pressure plot p. 47
bmim PF6 25 C Harris viscosity-pressure plot p. 48
bmim PF6 50 C viscosity-pressure plot p. 49
bmim PF6 70 C viscosity-pressure plot p. 50
bmim TFSA 25 C viscosity-pressure plot p. 51
bmim TFSA 50 C viscosity-pressure plot p. 52
bmim TFSA 75 C viscosity-pressure plot p. 53
bmmim FAP 40 C viscosity-pressure plot p. 54
bmmim FAP 70 C viscosity-pressure plot p. 55
bmmim TFSA 40 C viscosity-pressure plot p. 56
bmmim TFSA 70 C viscosity-pressure plot p. 57
bmmim TFSA 90 C viscosity-pressure plot p. 58
BMpyrr TFSA 25 C viscosity-pressure plot p. 59
BMpyrr TFSA 40 C viscosity-pressure plot p. 60
BMpyrr TFSA 50 C viscosity-pressure plot p. 61
BMpyrr TFSA 70 C viscosity-pressure plot p. 62
BMpyrr TFSA 75 C viscosity-pressure plot p. 63
BMpyrr TFSA 90 C viscosity-pressure plot p. 64
C10mim TFSA 25 C viscosity-pressure plot p. 65
C10mim TFSA 50 C viscosity-pressure plot p. 66
C10mim TFSA 70 C viscosity-pressure plot p. 67

emim BF4 20 C viscosity-pressure plot p. 68
emim BF4 30 C viscosity-pressure plot p. 69
emim EtSO4 40 C viscosity-pressure plot p. 70
emim TFSA 25 C viscosity-pressure plot p. 71
emim TFSA 50 C viscosity-pressure plot p. 72
emim TFSA 70 C viscosity-pressure plot p. 73
(EOM)Mpyrr FAP 40 C viscosity-pressure plot p. 74
(EOM)Mpyrr FAP 70 C viscosity-pressure plot p. 75
(EOM)Mpyrr FAP 90 C viscosity-pressure plot p. 76
(EOM)Mpyrr TFSA 40 C viscosity-pressure plot p. 77
(EOM)Mpyrr TFSA 70 C viscosity-pressure plot p. 78
(EOM)Mpyrr TFSA 90 C viscosity-pressure plot p. 79
hmim BF4 22 C viscosity-pressure plot p. 80
hmim BF4 25 C viscosity-pressure plot p. 81
hmim BF4 50 C viscosity-pressure plot p. 82
hmim BF4 70 C viscosity-pressure plot p. 83
hmim PF6 25 C Ahosseini viscosity-pressure plot p. 84
hmim PF6 25 C Harris viscosity-pressure plot p. 85
hmim PF6 50 C Ahosseini viscosity-pressure plot p. 86
hmim PF6 50 C Harris viscosity-pressure plot p. 87
hmim PF6 60 C viscosity-pressure plot p. 88
hmim PF6 70 C viscosity-pressure plot p. 89
hmim PF6 75 C viscosity-pressure plot p. 90
hmim TFSA 25 C viscosity-pressure plot p. 91
hmim TFSA 50 C viscosity-pressure plot p. 92
hmim TFSA 70 C viscosity-pressure plot p. 93
omim BF4 20 C viscosity-pressure plot p. 94
omim BF4 25 C viscosity-pressure plot p. 95
omim BF4 50 C viscosity-pressure plot p. 96
omim BF4 60 C viscosity-pressure plot p. 97
omim BF4 75 C viscosity-pressure plot p. 98
omim PF6 20 C viscosity-pressure plot p. 99
omim PF6 25 C viscosity-pressure plot p. 100
omim PF6 35 C viscosity-pressure plot p. 101
omim PF6 40 C viscosity-pressure plot p. 102
omim PF6 60 C Harris viscosity-pressure plot p. 103
omim PF6 60 C Tomida viscosity-pressure plot p. 104
omim PF6 70 C viscosity-pressure plot p. 105
omim PF6 80 C viscosity-pressure plot p. 106

$\ln(D_+)$ vs. Pressure Plot for BMIM diffusion in BMIM BF_4 at 25 °C

Data from Harris et al. 10.1021/jp8021375

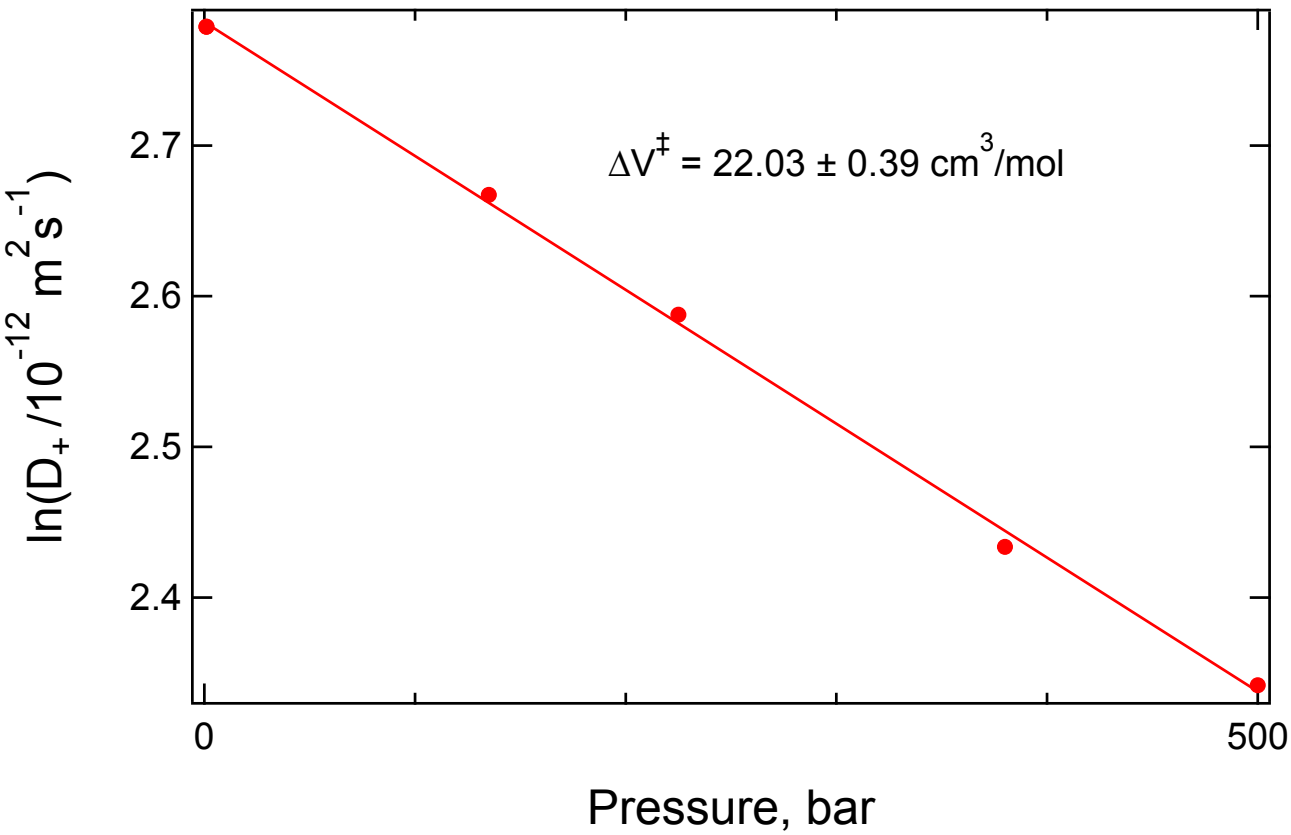

Point	Pressure	D (10^-12 m2/s)	ln(D)
0	1	16.1	2.779
1	1	16.1	2.779
2	135	14.4	2.667
3	225	13.3	2.588
4	380	11.4	2.434
5	500	10.4	2.342

$\ln(D_+)$ vs. Pressure Plot for BMIM diffusion in BMIM BF_4 at 50 °C

Data from Harris et al. 10.1021/jp8021375

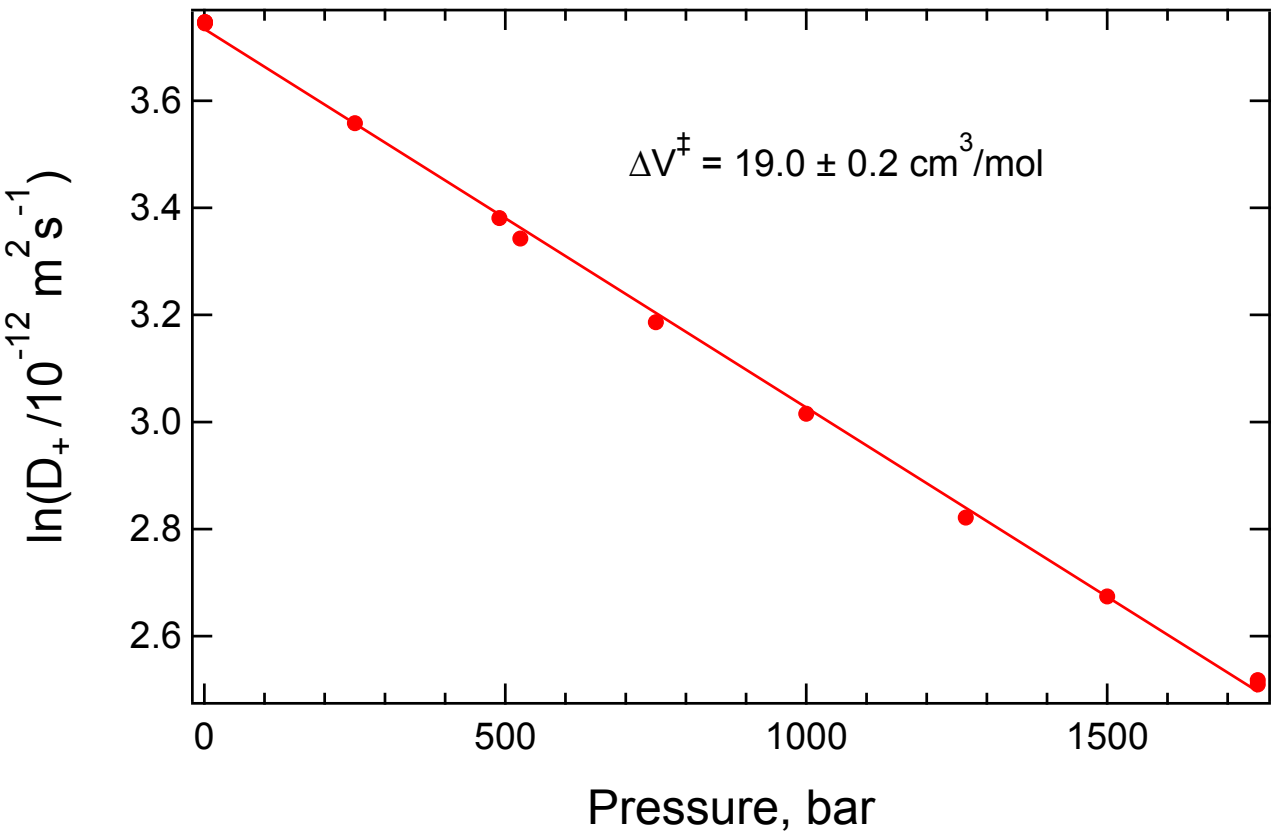

Point	Pressure	D (10^-12 m2/s)	ln(D)
0	1	42.3	3.745
1	1	42.4	3.747
2	1	42.4	3.747
3	250	35.1	3.558
4	490	29.4	3.381
5	525	28.3	3.343
6	750	24.2	3.186
7	1000	20.4	3.016
8	1265	16.8	2.821
9	1500	14.5	2.674
10	1750	12.4	2.518
11	1750	12.3	2.510

$\ln(D_+)$ vs. Pressure Plot for BMIM diffusion in BMIM BF_4 at 75 °C

Data from Harris et al. 10.1021/jp8021375

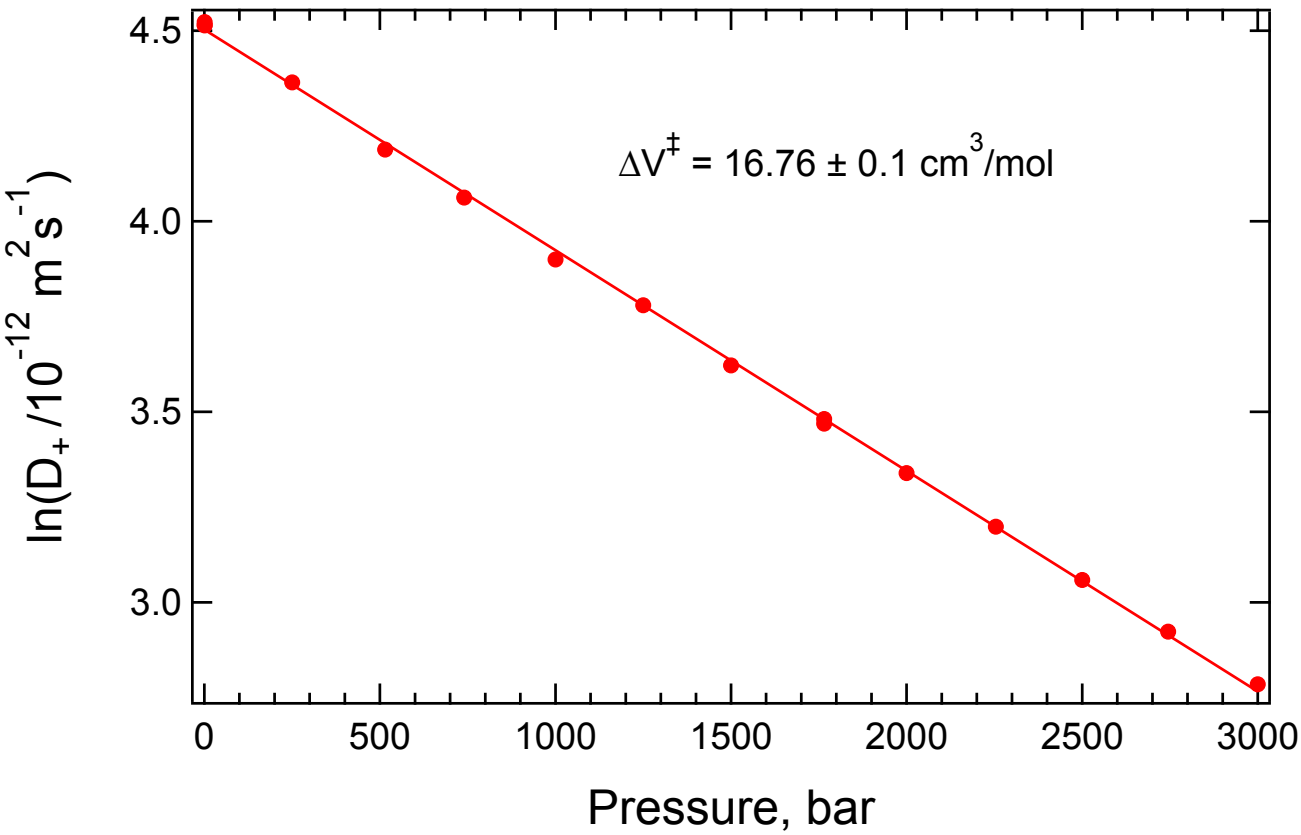

Point	Pressure	D (10^-12 m2/s)	ln(D)
0	1	91.4	4.515
1	1	91.3	4.514
2	1	92.1	4.523
3	250	78.6	4.364
4	515	65.9	4.188
5	740	58.1	4.062
6	1000	49.4	3.900
7	1250	43.8	3.780
8	1500	37.4	3.622
9	1765	32.1	3.469
10	1765	32.5	3.481
11	2000	28.2	3.339
12	2254	24.5	3.199
13	2500	21.3	3.059
14	2745	18.6	2.923
15	3000	16.2	2.785

$\ln(D_+)$ vs. Pressure Plot for BMIM diffusion in BMIM PF_6 at 50 °C

Data from Kanakubo et al. 10.1021/jp063278k

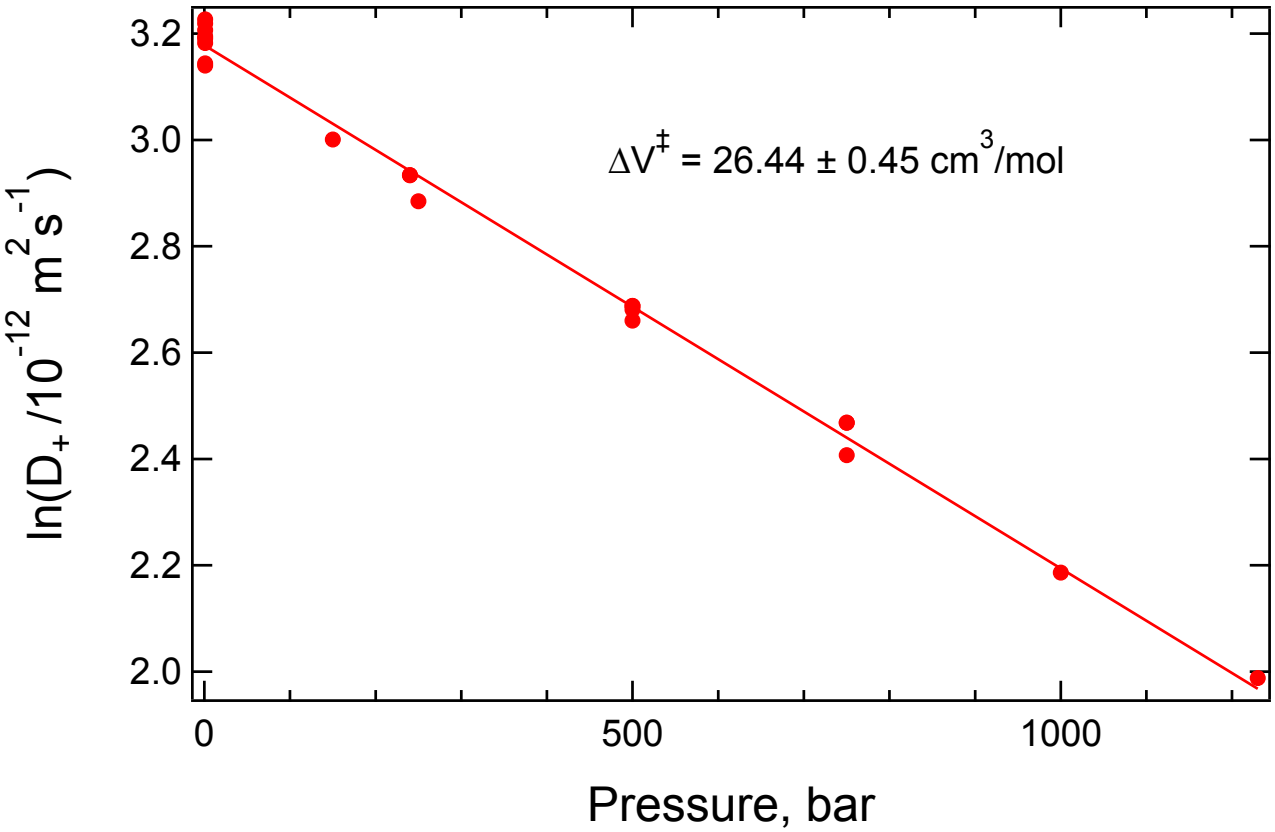

Point	Pressure	D (10^-12 m2/s)	ln(D)	
0	1	24.1	3.182	
1	1	24.4	3.195	
2	1	24.7	3.207	
3	1	23.2	3.144	
4	1	23.1	3.140	
5	1	24.3	3.190	
6	1	25.0	3.219	
7	1	25.2	3.227	
8	150	20.1	3.001	
9	240	18.8	2.934	
10	240	18.8	2.934	
11	250	17.9	2.885	
12	500	14.3	2.660	
13	500	14.7	2.688	
14	500	14.6	2.681	
15	500	14.7	2.688	
16	750	11.1	2.407	
17	750	11.8	2.468	
18	750	11.8	2.468	
19	1000	8.9	2.186	
20	1230	7.3	1.988	

$\ln(D_+)$ vs. Pressure Plot for BMIM diffusion in BMIM PF_6 at 70 °C

Data from Kanakubo et al. 10.1021/jp063278k

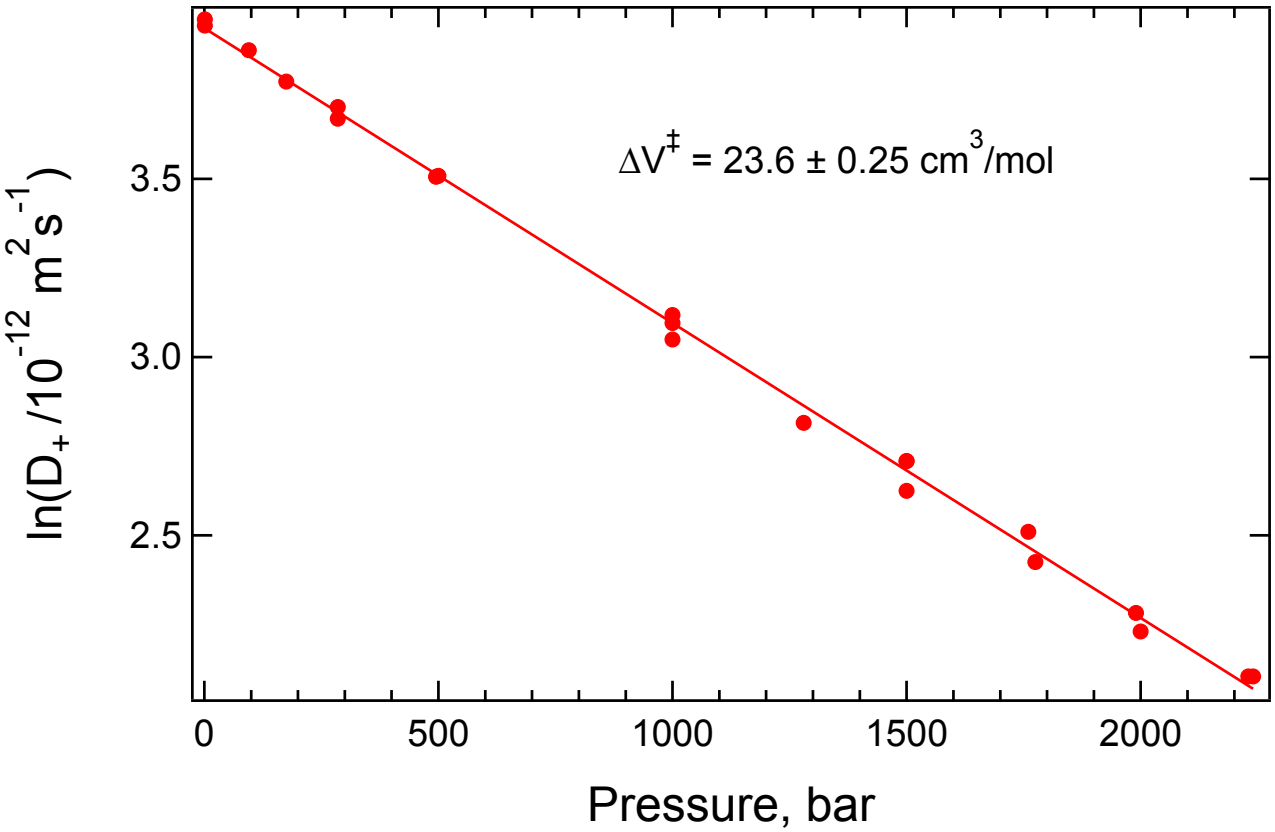

Point	Pressure	D (10^-12 m2/s)	ln(D)
0	1280	16.7	2.815
1	2230	8.2	2.104
2	95	47.5	3.861
3	1000	21.1	3.049
4	1500	13.8	2.625
5	1775	11.3	2.425
6	1990	9.8	2.282
7	2000	9.3	2.230
8	175	43.5	3.773
9	1	50.9	3.930
10	285	39.2	3.669
11	285	40.5	3.701
12	1	51.8	3.947
13	495	33.3	3.506
14	500	33.4	3.509
15	1000	22.6	3.118
16	1000	22.1	3.096
17	1500	15.0	2.708
18	1500	15.0	2.708
19	1760	12.3	2.510
20	2240	8.2	2.104

$\ln(D_+)$ vs. Pressure Plot for BMpyrr diffusion in BMpyrr TFSA at 30 °C

Data from Harris et al. 10.1021/je2006049

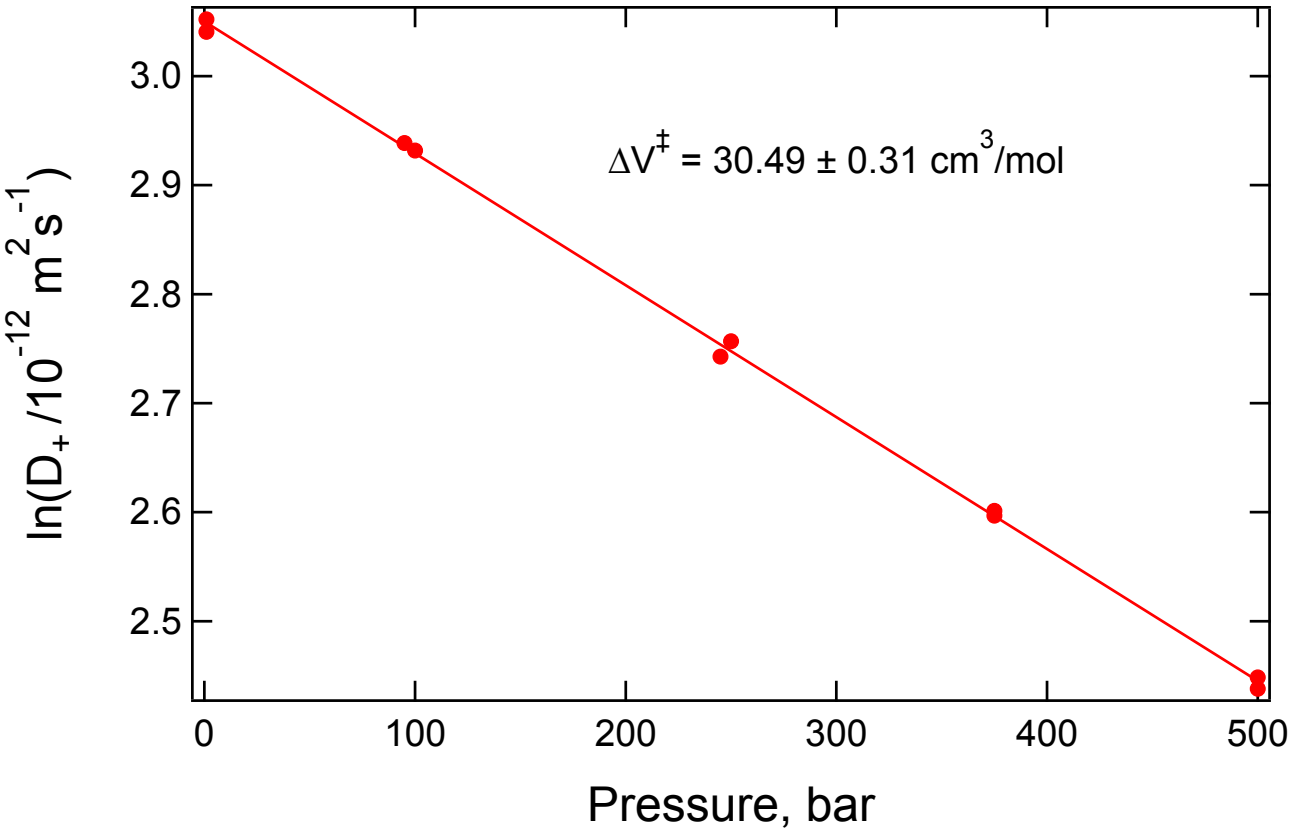

Point	Pressure	D (10^-12 m2/s)	ln(D)
0	1	20.9	3.041
1	1	21.2	3.052
2	95	18.9	2.939
3	100	18.8	2.932
4	245	15.5	2.743
5	250	15.8	2.757
6	375	13.4	2.597
7	375	13.5	2.601
8	500	11.6	2.448
9	500	11.4	2.438

$\ln(D_+)$ vs. Pressure Plot for BMpyrr diffusion in BMpyrr TFSA at 50 °C

Data from Harris et al. 10.1021/je2006049

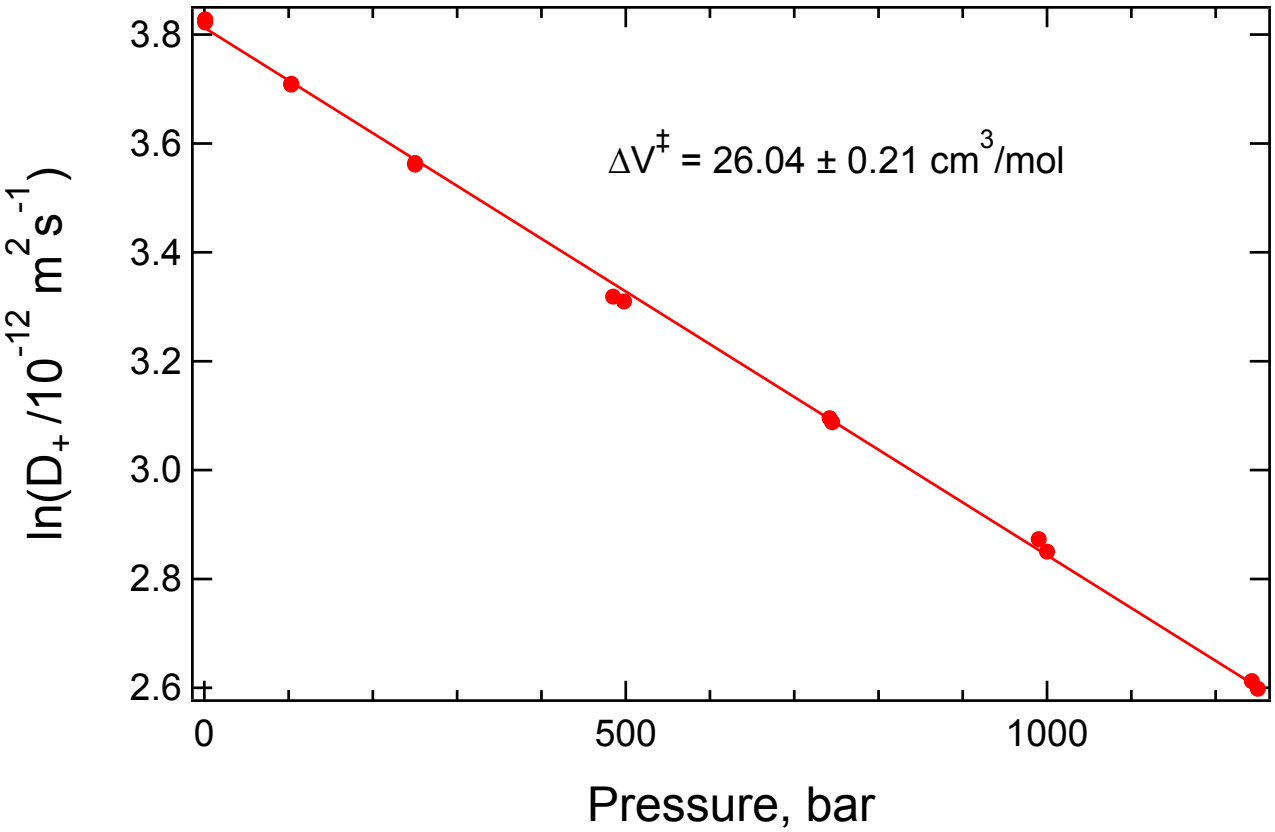

Point	Pressure	D (10^-12 m2/s)	ln(D)
0	1.0	45.9	3.827
1	1.0	45.7	3.823
2	1.0	46.0	3.828
3	103.0	40.8	3.708
4	103.0	40.8	3.709
5	250.0	35.3	3.564
6	250.0	35.2	3.561
7	485.0	27.6	3.319
8	498.0	27.4	3.310
9	742.0	22.1	3.095
10	745.0	21.9	3.088
11	990.0	17.7	2.873
12	1000.0	17.3	2.850
13	1243.0	13.6	2.612
14	1250.0	13.4	2.598

$\ln(D_+)$ vs. Pressure Plot for BMpyrr diffusion in BMpyrr TFSA at 65 °C

Data from Harris et al. 10.1021/je2006049

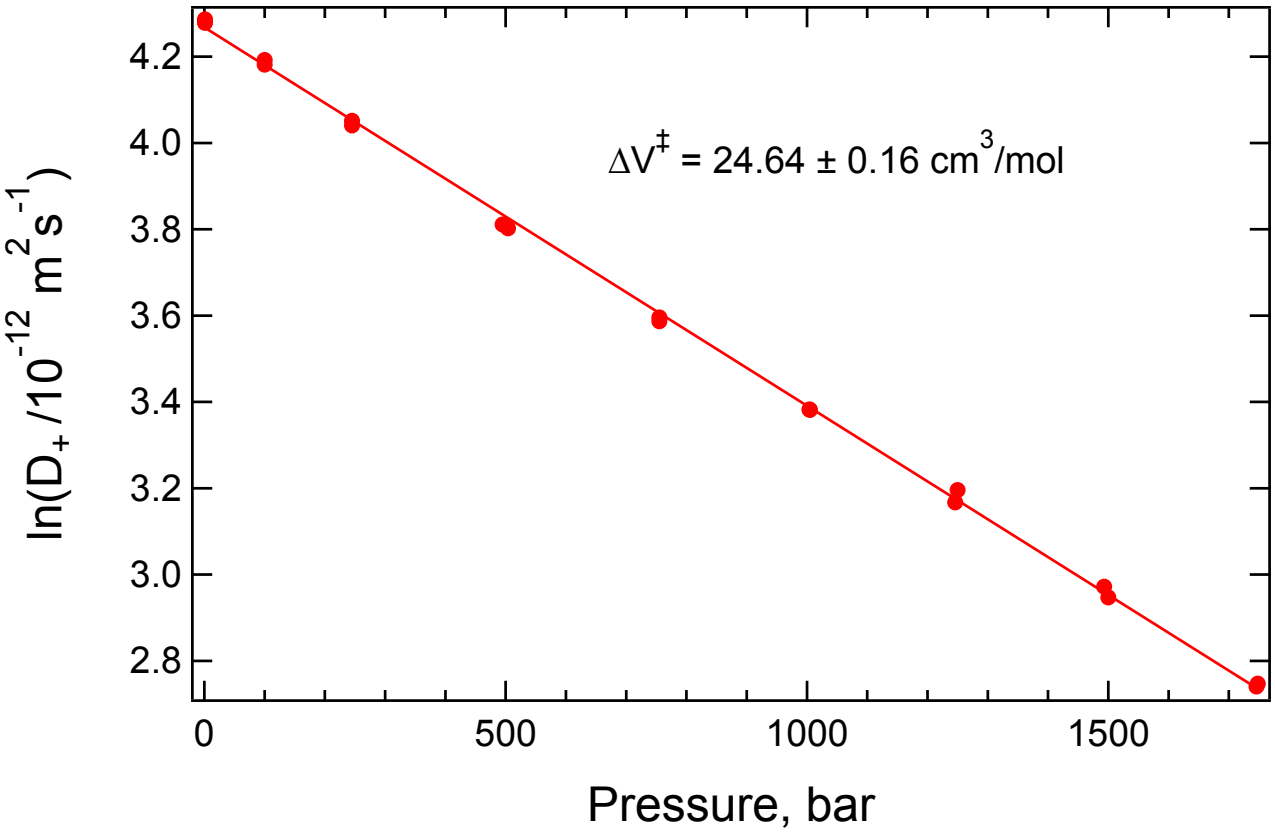

Point	Pressure	D (10^-12 m2/s)	ln(D)
0	1.0	72.7	4.286
1	1.0	72.4	4.283
2	1.0	72.1	4.278
3	100.0	66.2	4.192
4	100.0	65.5	4.181
5	245.0	56.9	4.041
6	245.0	57.5	4.051
7	495.0	45.2	3.811
8	504.0	44.8	3.802
9	755.0	36.4	3.596
10	755.0	36.1	3.587
11	1004.0	29.5	3.383
12	1005.0	29.4	3.382
13	1246.0	23.7	3.167
14	1250.0	24.4	3.196
15	1493.0	19.5	2.972
16	1500.0	19.0	2.947
17	1746.0	15.5	2.741
18	1748.0	15.6	2.747

$\ln(D_+)$ vs. Pressure Plot for BMpyrr diffusion in BMpyrr TFSA at 75 °C

Data from Harris et al. 10.1021/je2006049

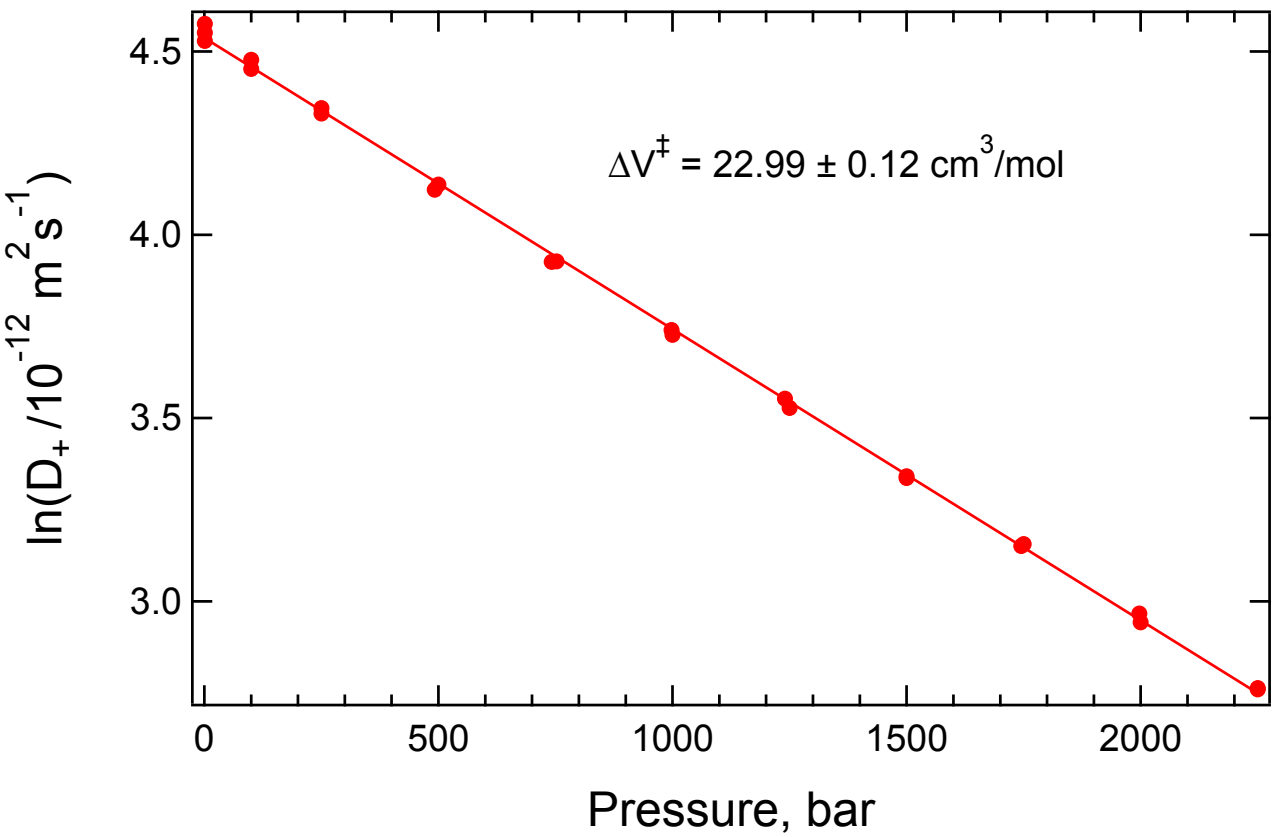

Point	Pressure	D (10^-12 m2/s)	ln(D)
0	1.0	92.6	4.529
1	1.0	94.7	4.551
2	1.0	97.1	4.575
3	100.0	85.8	4.452
4	100.0	88.0	4.477
5	250.0	76.0	4.330
6	250.0	77.1	4.345
7	492.0	61.7	4.123
8	500.0	62.6	4.137
9	742.0	50.7	3.926
10	752.0	50.8	3.928
11	998.0	42.1	3.740
12	1000.0	41.6	3.727
13	1240.0	34.9	3.553
14	1250.0	34.0	3.528
15	1500.0	28.1	3.336
16	1500.0	28.3	3.341
17	1745.0	23.4	3.151
18	1750.0	23.5	3.156
19	1997.0	19.4	2.967
20	2000.0	19.0	2.943
21	2250.0	15.8	2.760
22	2250.0	15.9	2.764

$\ln(D_+)$ vs. Pressure Plot for HMIM diffusion in HMIM PF_6 at 50 °C

Data from Harris et al. 10.1021/jp8021375

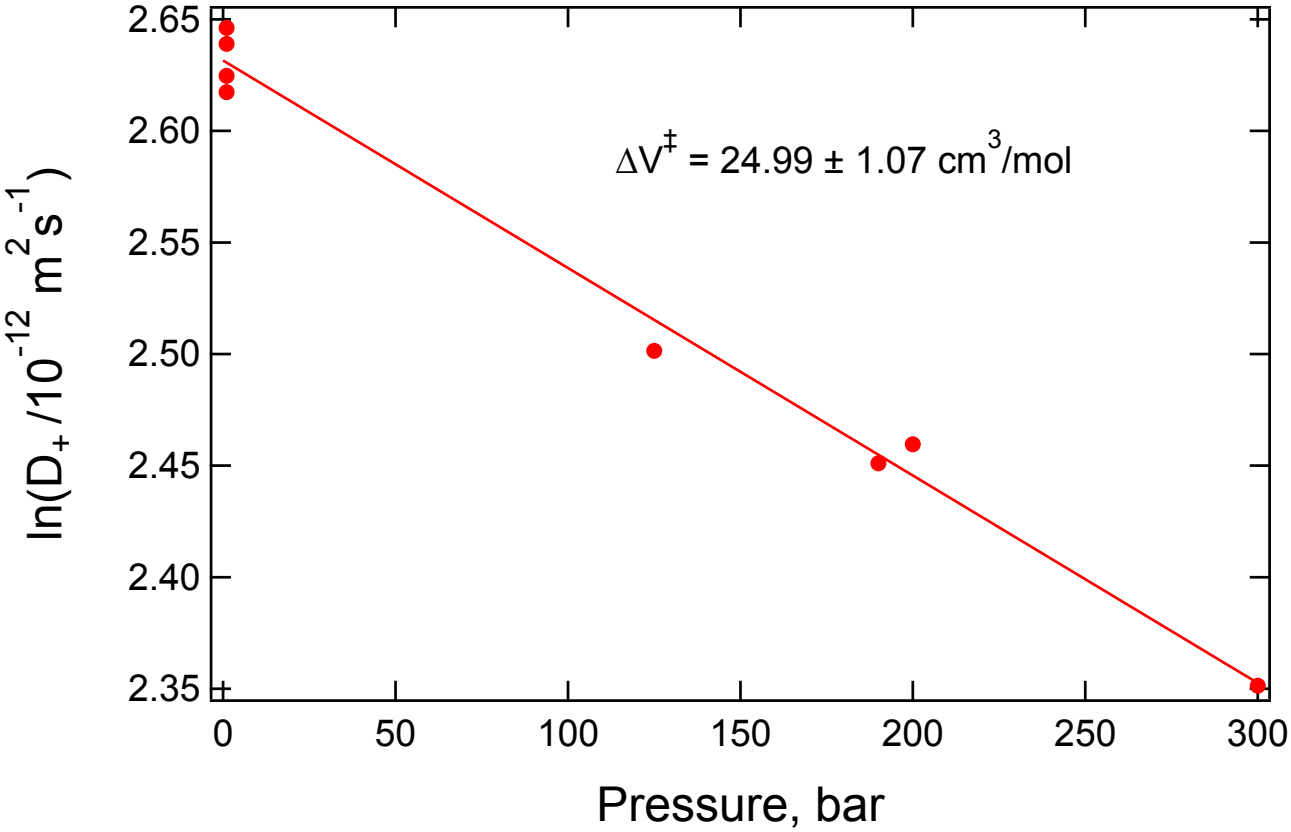

Point	Pressure	D (10^-12 m2/s)	ln(D)
0	1	13.8	2.625
1	1	13.7	2.617
2	1	14.1	2.646
3	1	14.0	2.639
4	125	12.2	2.501
5	190	11.6	2.451
6	200	11.7	2.460
7	300	10.5	2.351

$\ln(D_+)$ vs. Pressure Plot for HMIM diffusion HMIM PF_6 at 60 °C

Data from Harris et al. 10.1021/jp8021375

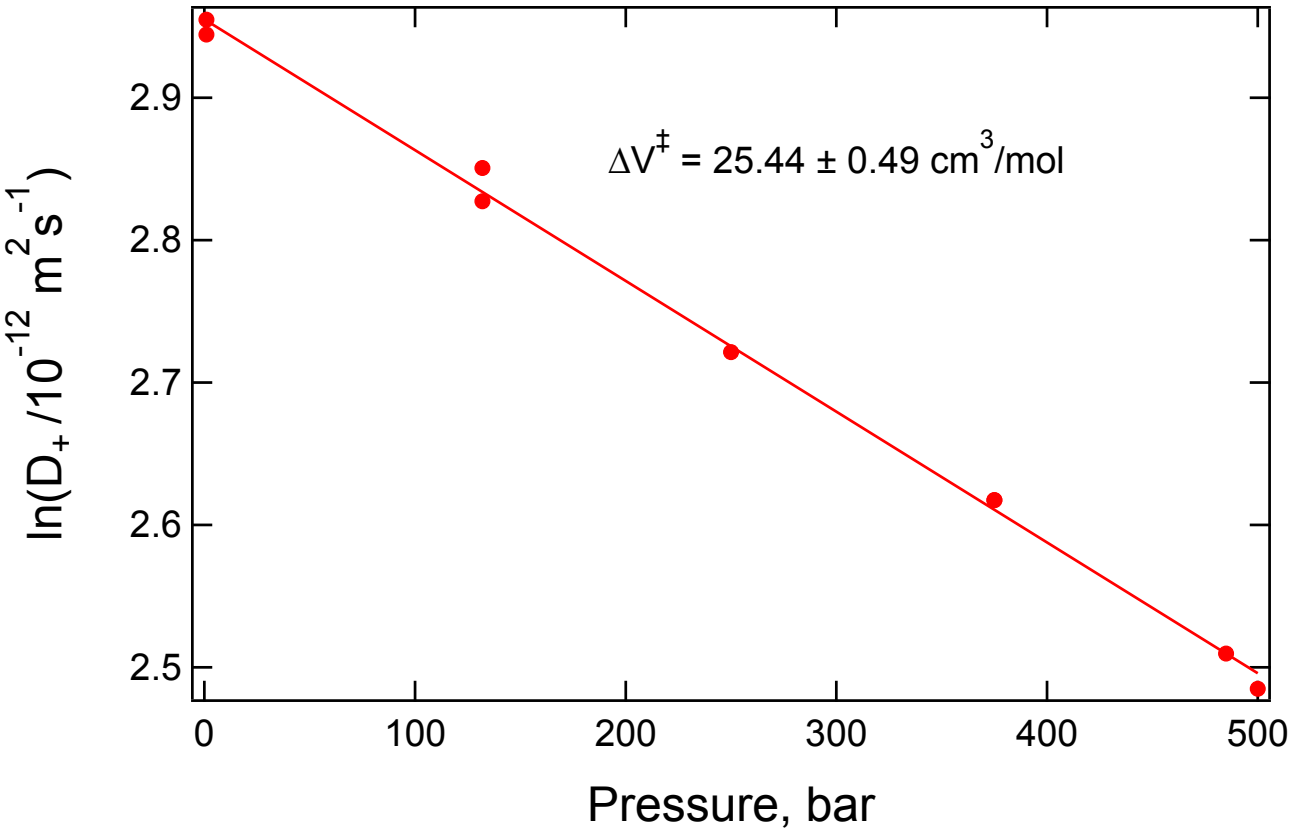

Point	Pressure	D (10^-12 m2/s)	ln(D)
0	1	19.0	2.944
1	1	19.2	2.955
2	132	17.3	2.851
3	132	16.9	2.827
4	250	15.2	2.721
5	375	13.7	2.617
6	375	13.7	2.617
7	485	12.3	2.510
8	500	12.0	2.485

$\ln(D_+)$ vs. Pressure Plot for HMIM diffusion in HMIM PF_6 at 75 °C

Data from Harris et al. 10.1021/jp8021375

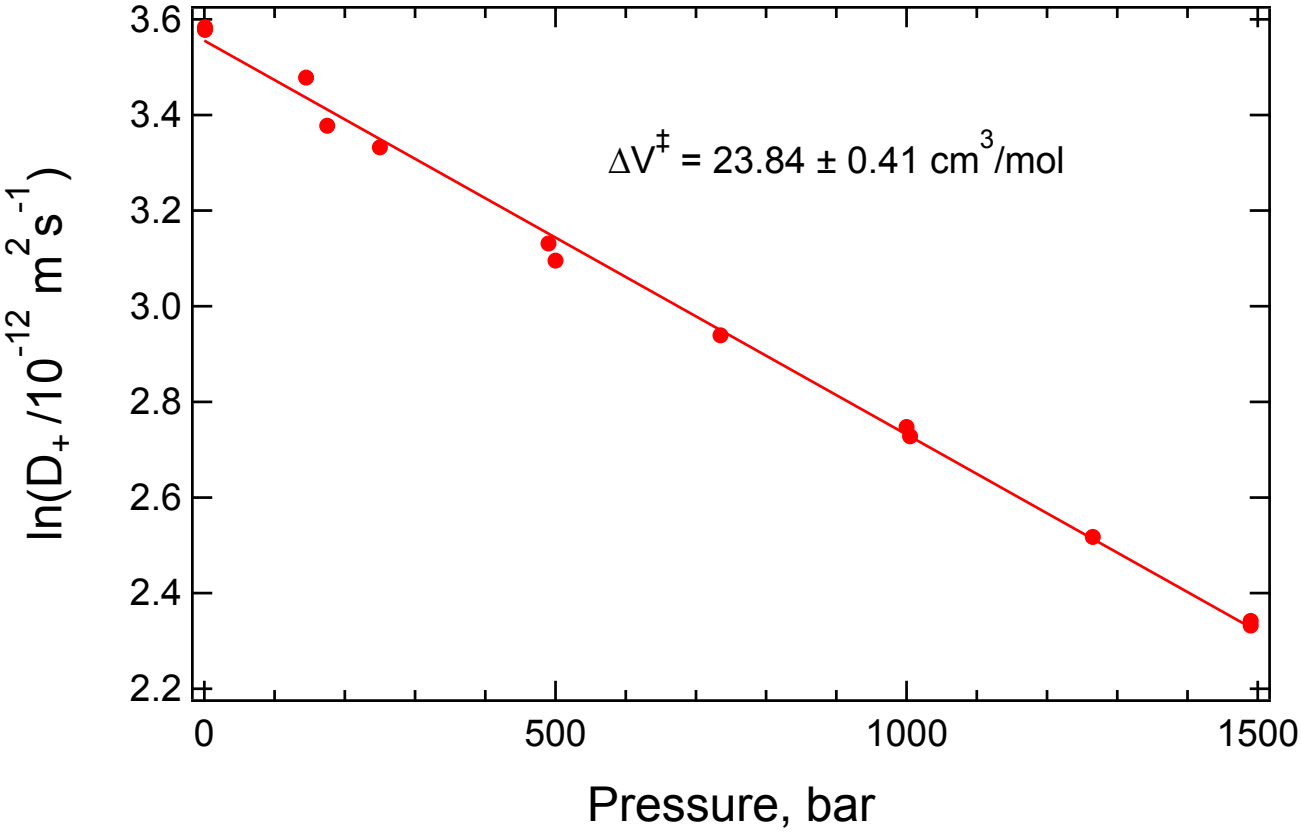

Point	Pressure	D (10^-12 m2/s)	ln(D)
0	1	35.8	3.578
1	1	36.0	3.584
2	145	32.4	3.478
3	175	29.3	3.378
4	250	28.0	3.332
5	490	22.9	3.131
6	500	22.1	3.096
7	735	18.9	2.939
8	1000	15.6	2.747
9	1005	15.3	2.728
10	1265	12.4	2.518
11	1490	10.4	2.342
12	1490	10.3	2.332

$\ln(D_+)$ vs. Pressure Plot for OMIM diffusion in OMIM BF_4 at 50 °C

Data from Harris et al. 10.1021/jp8021375

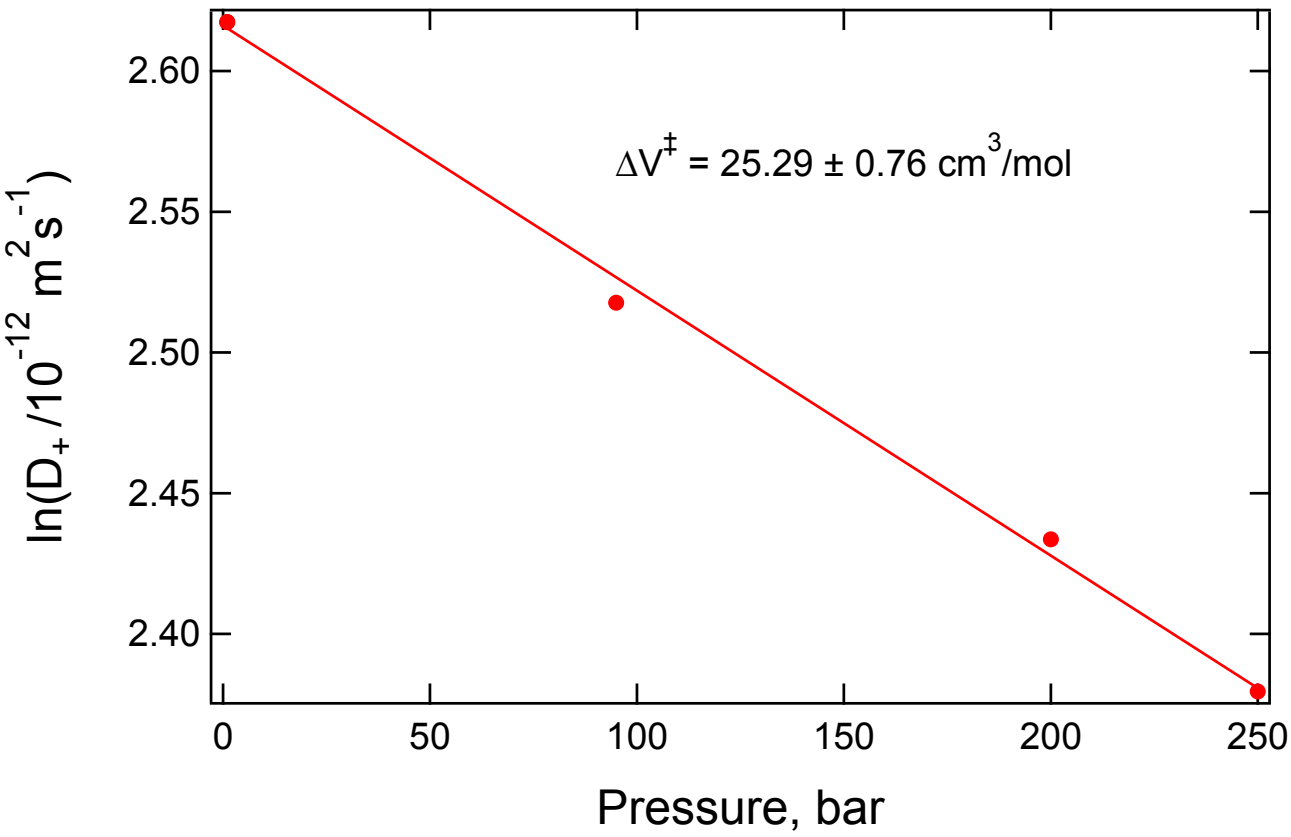

Point	Pressure	D (10^-12 m2/s)	ln(D)
0	1	13.7	2.617
1	1	13.7	2.617
2	95	12.4	2.518
3	200	11.4	2.434
4	250	10.8	2.380

$\ln(D_+)$ vs. Pressure Plot for OMIM diffusion in OMIM BF_4 at 60 °C

Data from Harris et al. 10.1021/jp8021375

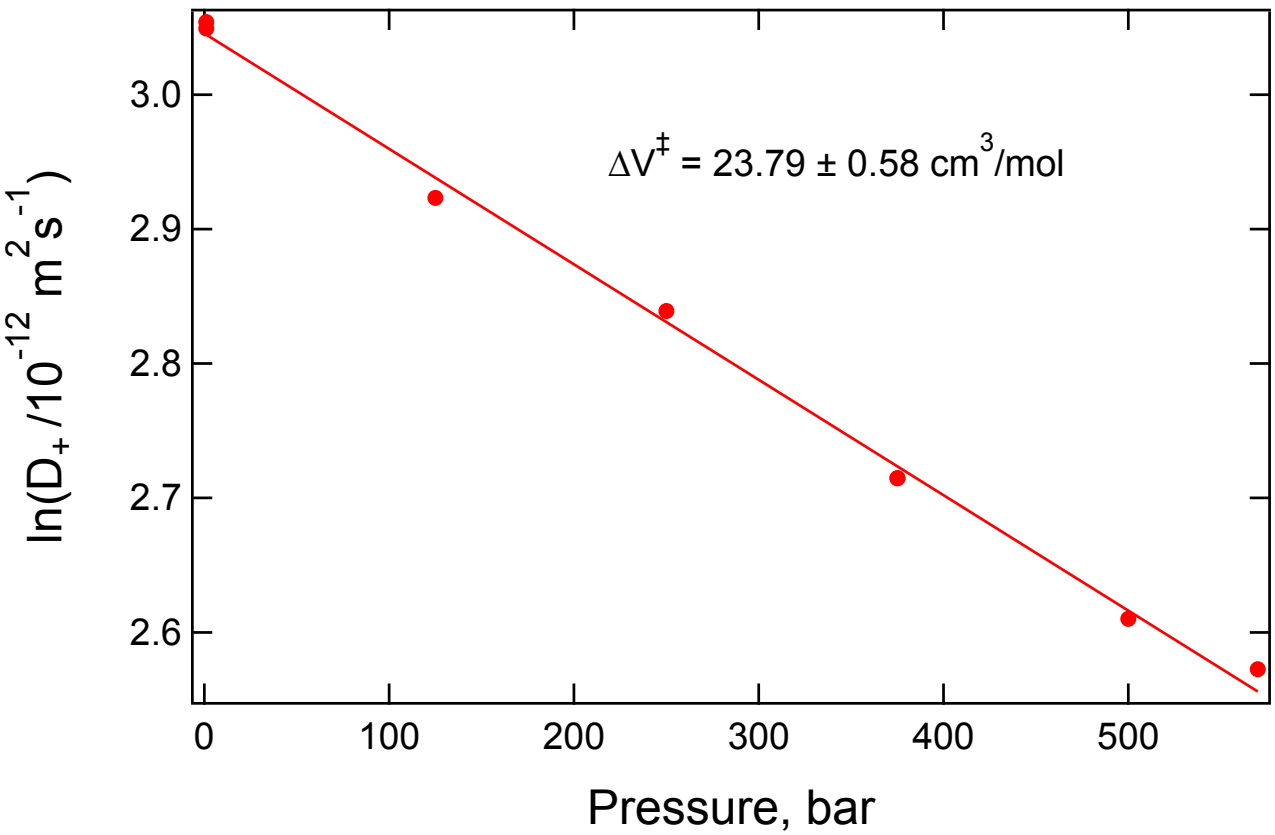

Point	Pressure	D (10^-12 m2/s)	ln(D)
0	1	21.1	3.049
1	1	21.2	3.054
2	125	18.6	2.923
3	250	17.1	2.839
4	375	15.1	2.715
5	375	15.1	2.715
6	500	13.6	2.610
7	570	13.1	2.573

$\ln(D_+)$ vs. Pressure Plot for OMIM diffusion in OMIM BF_4 at 75 °C

Data from Harris et al. 10.1021/jp8021375

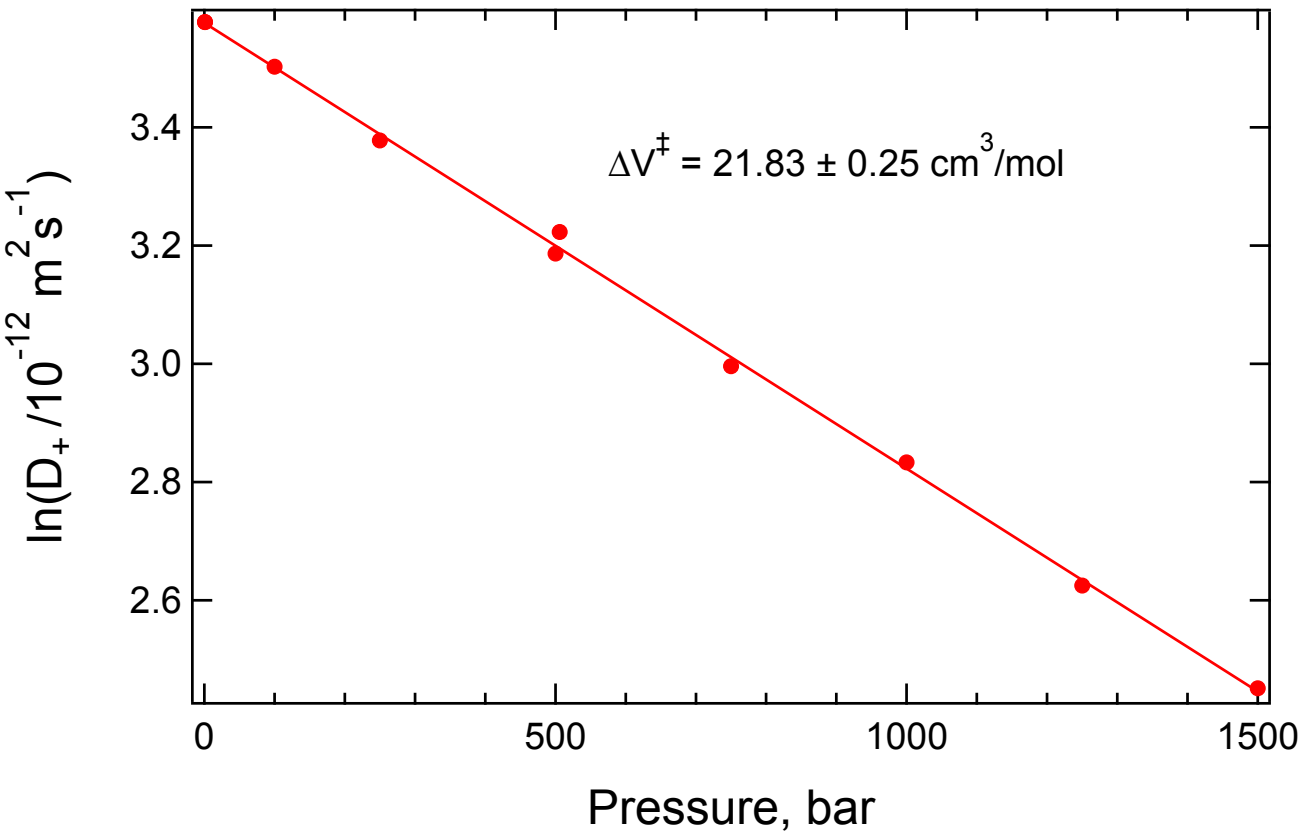

Point	Pressure	D (10^-12 m2/s)	ln(D)
0	1	35.8	3.578
1	1	35.8	3.578
2	100	33.2	3.503
3	250	29.3	3.378
4	500	24.2	3.186
5	506	25.1	3.223
6	750	20.0	2.996
7	1000	17.0	2.833
8	1250	13.8	2.625
9	1500	11.6	2.451

$\ln(D_+)$ vs. Pressure Plot for OMIM diffusion OMIM PF_6 at 70 °C

Data from Harris et al. 10.1021/jp8021375

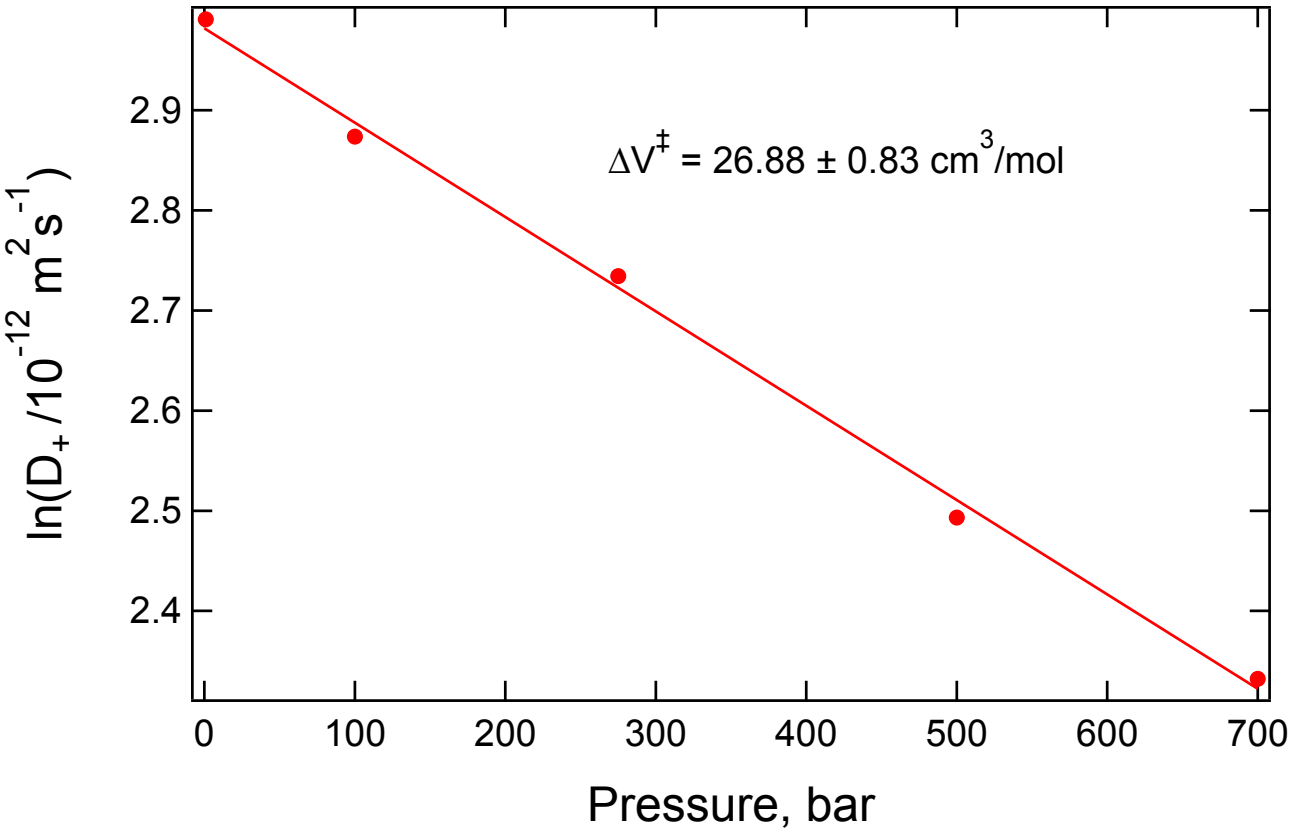

Point	Pressure	D (10^-12 m2/s)	ln(D)
0	1	19.9	2.991
1	100	17.7	2.874
2	275	15.4	2.734
3	500	12.1	2.493
4	700	10.3	2.332

$\ln(D_+)$ vs. Pressure Plot for OMIM diffusion OMIM PF_6 at 75 °C

Data from Harris et al. 10.1021/jp8021375

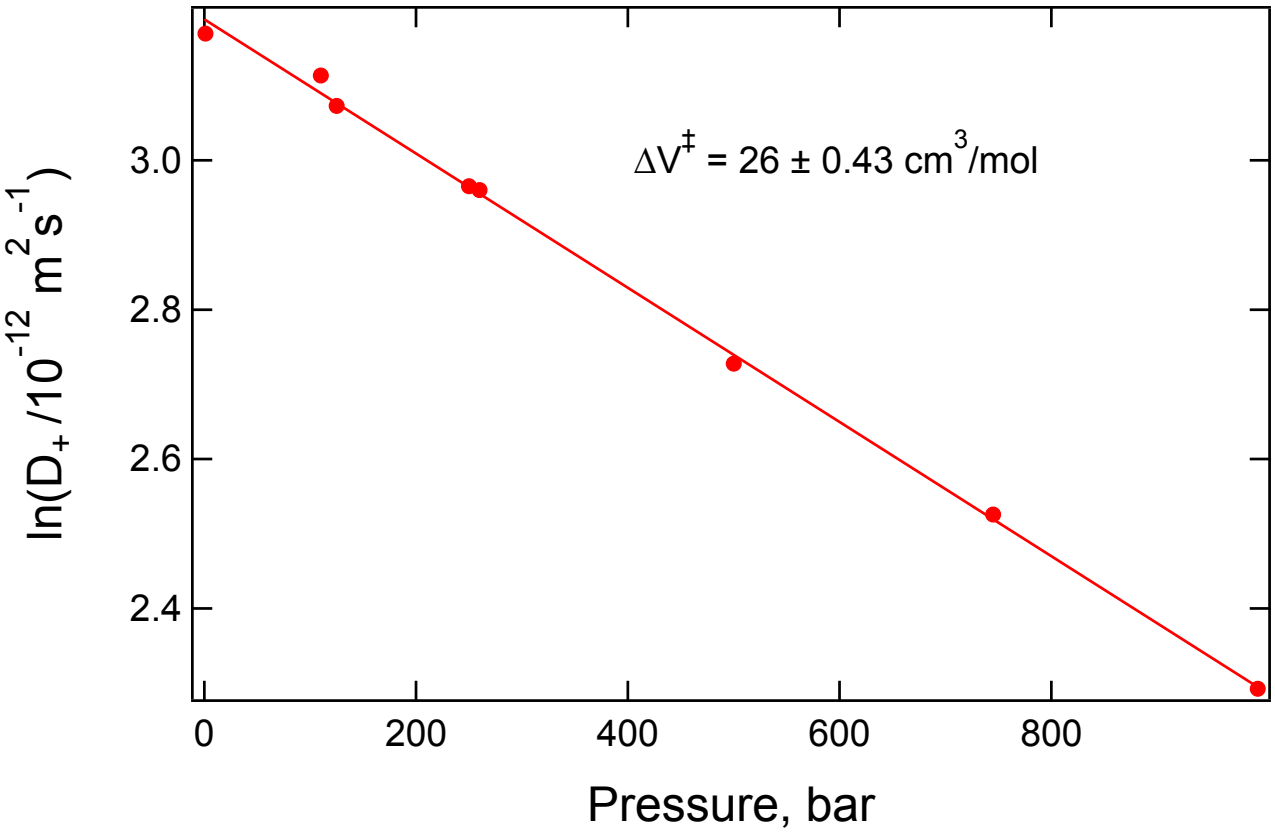

Point	Pressure	D (10^-12 m2/s)	ln(D)
0	1	23.8	3.170
1	110	22.5	3.114
2	125	21.6	3.073
3	250	19.4	2.965
4	260	19.3	2.960
5	500	15.3	2.728
6	745	12.5	2.526
7	995	9.9	2.293

$\ln(D_+)$ vs. Pressure Plot for OMIM diffusion OMIM PF_6 at 80 °C

Data from Harris et al. 10.1021/jp8021375

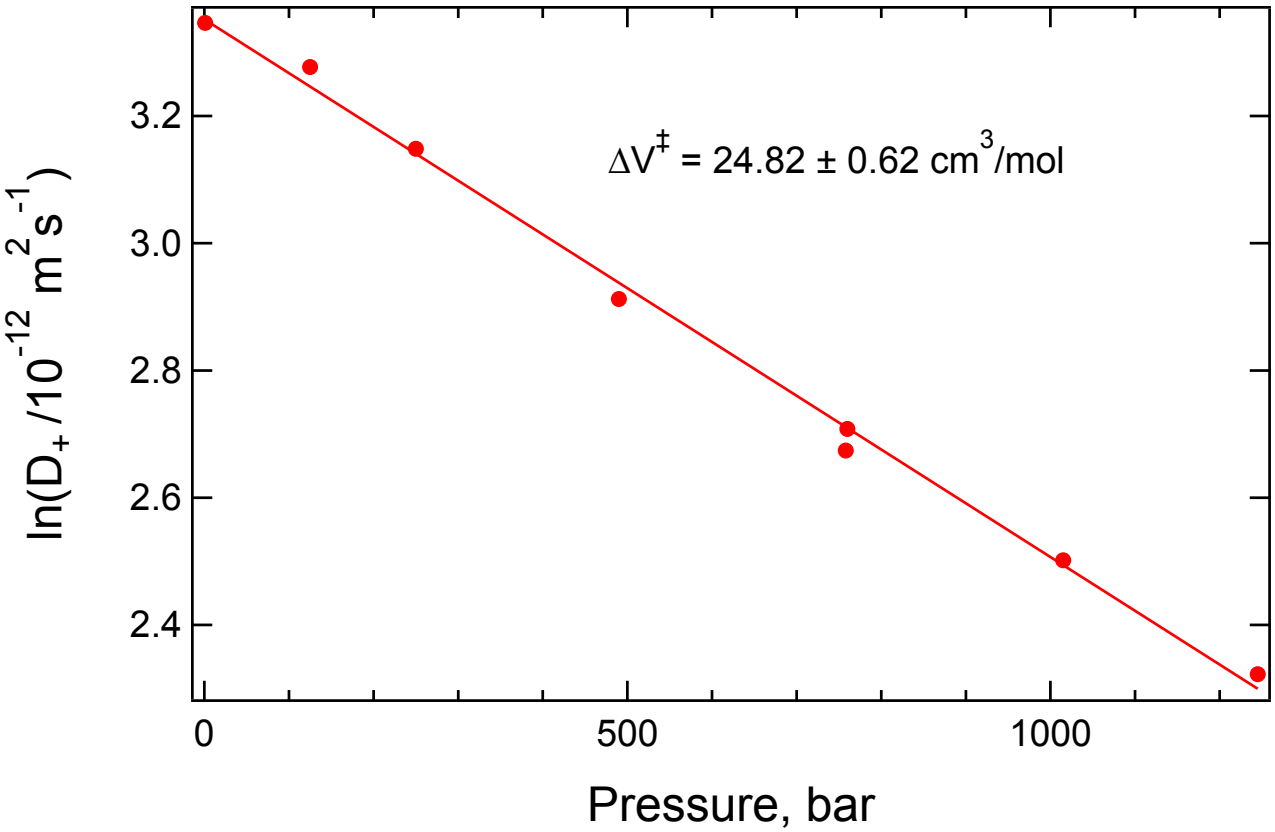

Point	Pressure	D (10^-12 m2/s)	ln(D)
0	1	28.4	3.346
1	125	26.5	3.277
2	250	23.3	3.148
3	490	18.4	2.912
4	758	14.5	2.674
5	760	15.0	2.708
6	1015	12.2	2.501
7	1245	10.2	2.322

ln(D_-) vs. Pressure Plot for BF_4 diffusion in BMIM BF_4 at 50 °C

Data from Harris et al. 10.1021/jp8021375

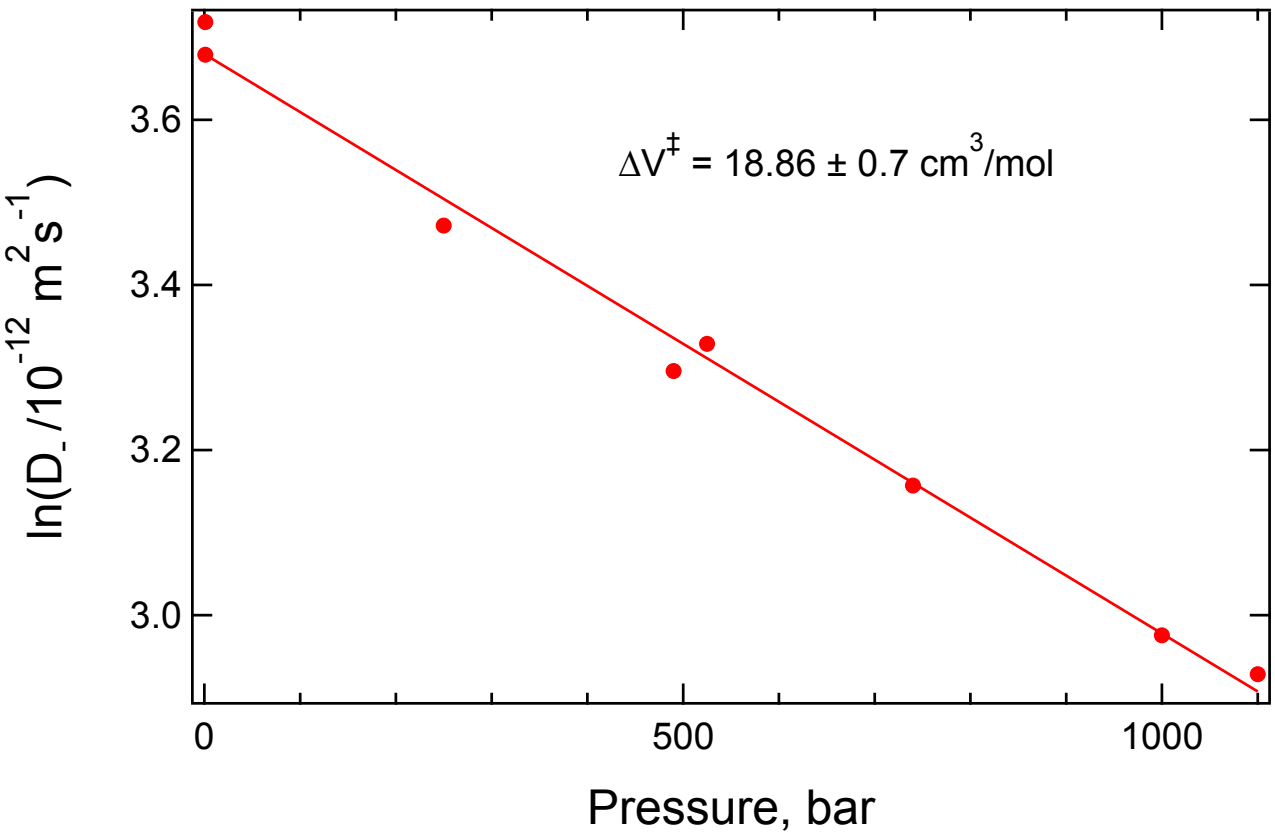

Point	Pressure	D (10^-12 m2/s)	ln(D)
0	1	39.6	3.679
1	1	41.2	3.718
2	250	32.2	3.472
3	490	27.0	3.296
4	525	27.9	3.329
5	740	23.5	3.157
6	1000	19.6	2.976
7	1100	18.7	2.929

ln(D_-) vs. Pressure Plot for BF_4 diffusion in BMIM BF_4 at 75 °C

Data from Harris et al. 10.1021/jp8021375

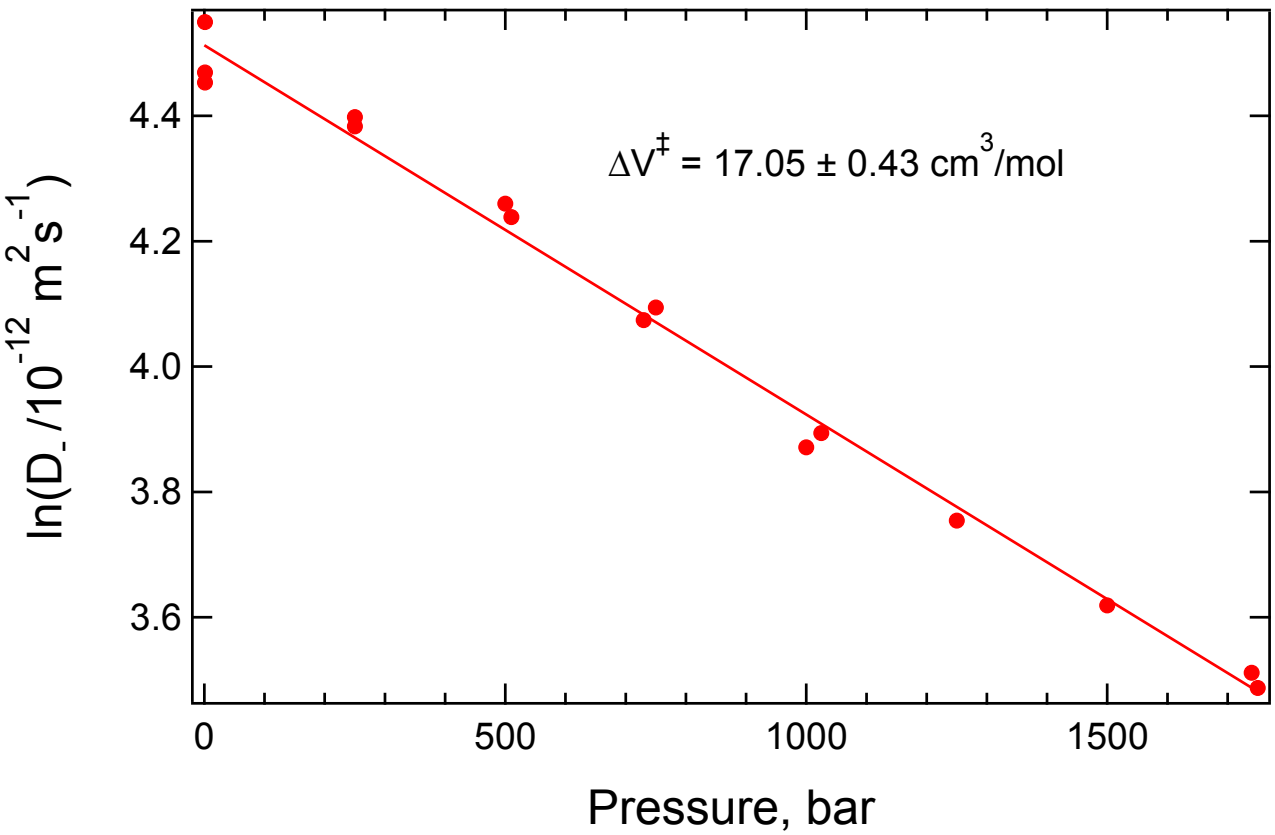

Point	Pressure	D (10^-12 m2/s)	ln(D)
0	1	87.3	4.469
1	1	85.9	4.453
2	1	94.6	4.550
3	250	81.3	4.398
4	250	80.1	4.383
5	500	70.8	4.260
6	510	69.3	4.238
7	730	58.8	4.074
8	750	60.0	4.094
9	1000	48.0	3.871
10	1025	49.1	3.894
11	1250	42.7	3.754
12	1500	37.3	3.619
13	1740	33.5	3.512
14	1750	32.7	3.487

$\ln(D_-)$ vs. Pressure Plot for BF_4 diffusion in OMIM BF_4 at 50 °C

Data from Harris et al. 10.1021/jp8021375

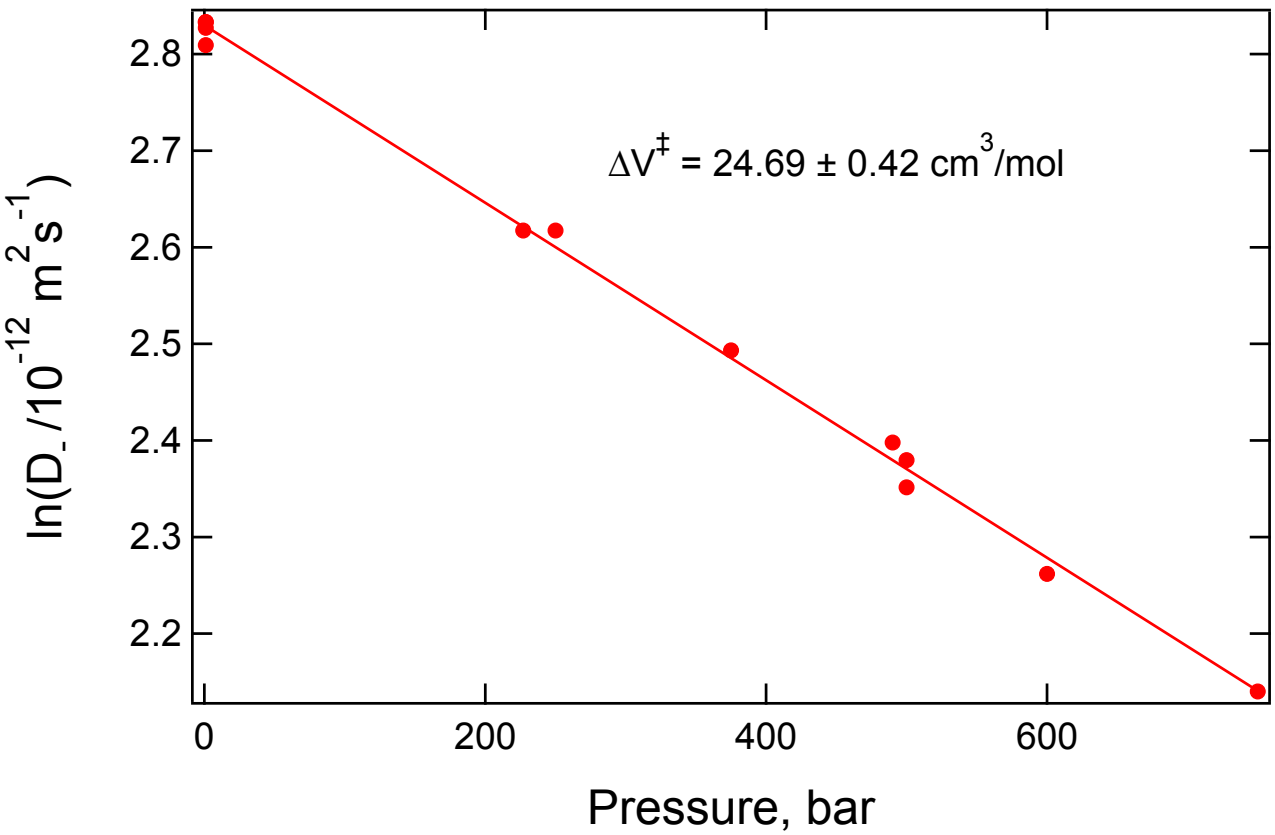

Point	Pressure	D (10^-12 m2/s)	ln(D)
0	1	16.9	2.827
1	1	17.0	2.833
2	250	13.7	2.617
3	375	12.1	2.493
4	490	11.0	2.398
5	500	10.8	2.380
6	1	16.6	2.809
7	1	17.0	2.833
8	227	13.7	2.617
9	500	10.5	2.351
10	600	9.6	2.262
11	750	8.5	2.140

$\ln(D_-)$ vs. Pressure Plot for BF_4 diffusion in OMIM BF_4 at 60 °C

Data from Harris et al. 10.1021/jp8021375

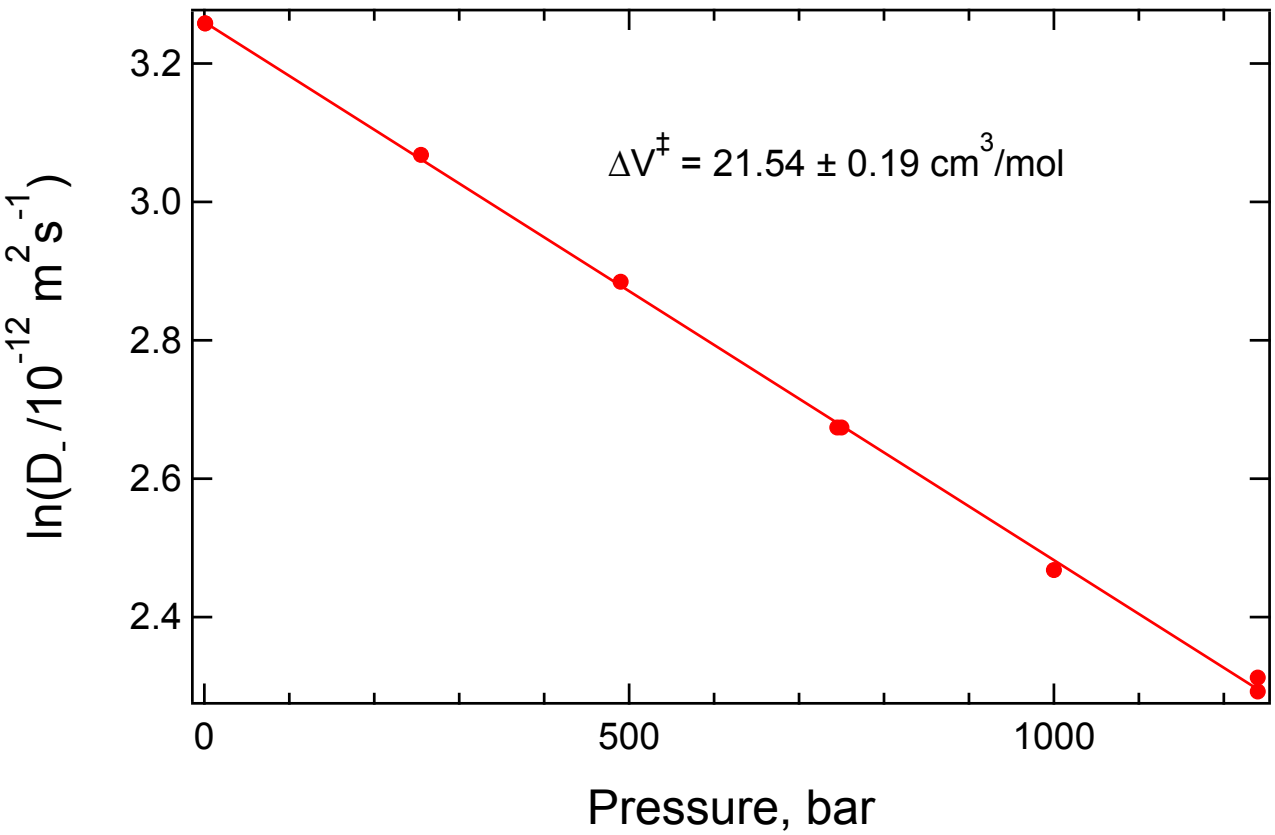

Point	Pressure	D (10^-12 m2/s)	ln(D)
0	1	26.0	3.258
1	1	26.0	3.258
2	255	21.5	3.068
3	490	17.9	2.885
4	745	14.5	2.674
5	750	14.5	2.674
6	1000	11.8	2.468
7	1240	10.1	2.313
8	1240	9.9	2.293

$\ln(D_-)$ vs. Pressure Plot for BF_4 diffusion in OMIM BF_4 at 75 °C

Data from Harris et al. 10.1021/jp8021375

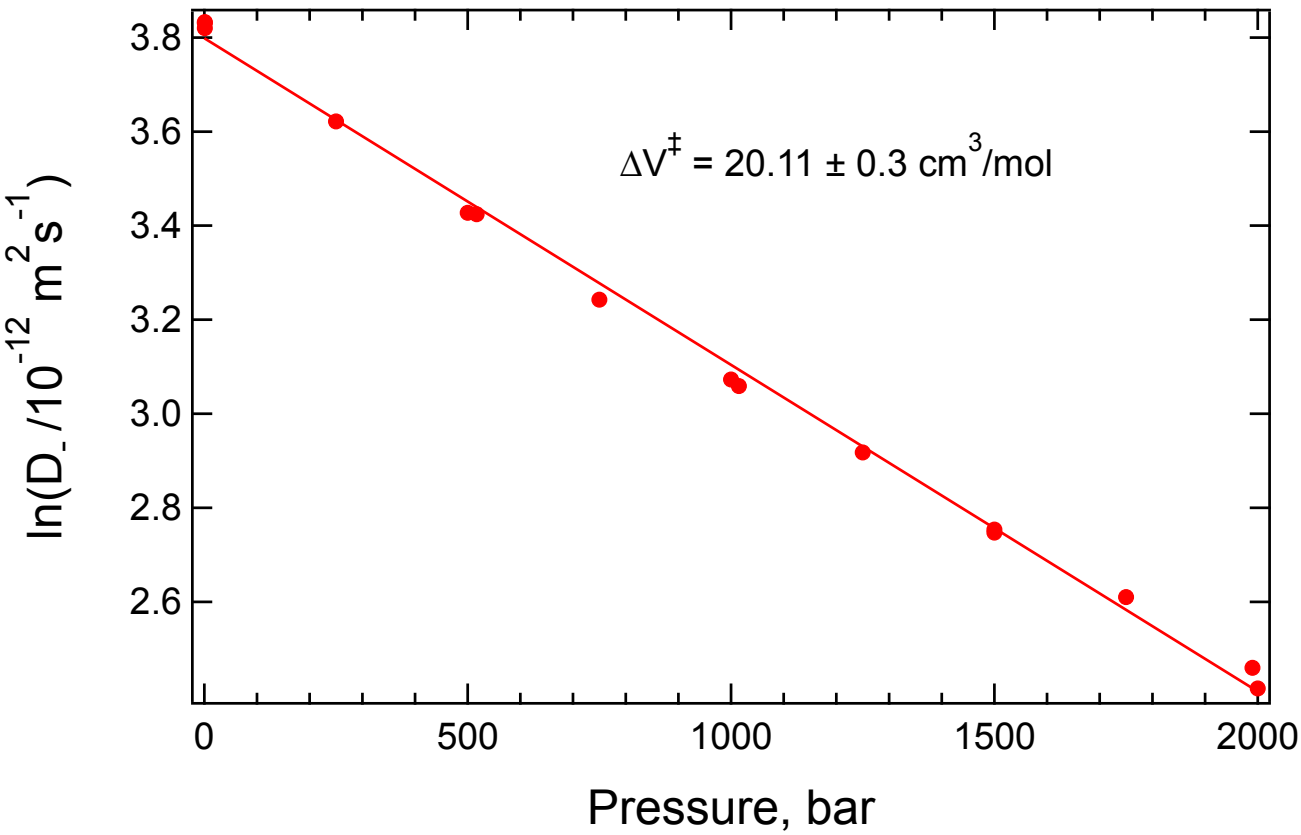

Point	Pressure	D (10^-12 m2/s)	ln(D)
0	1	46.2	3.833
1	1	45.6	3.820
2	1	46.1	3.831
3	250	37.4	3.622
4	500	30.8	3.428
5	517	30.7	3.424
6	750	25.6	3.243
7	1000	21.6	3.073
8	1015	21.3	3.059
9	1250	18.5	2.918
10	1500	15.7	2.754
11	1500	15.6	2.747
12	1750	13.6	2.610
13	1990	11.7	2.460
14	2000	11.2	2.416

ln(D_-) vs. Pressure Plot for PF_6 diffusion in BMIM PF_6 at 50 °C

Data from Kanakubo et al. 10.1021/jp063278k

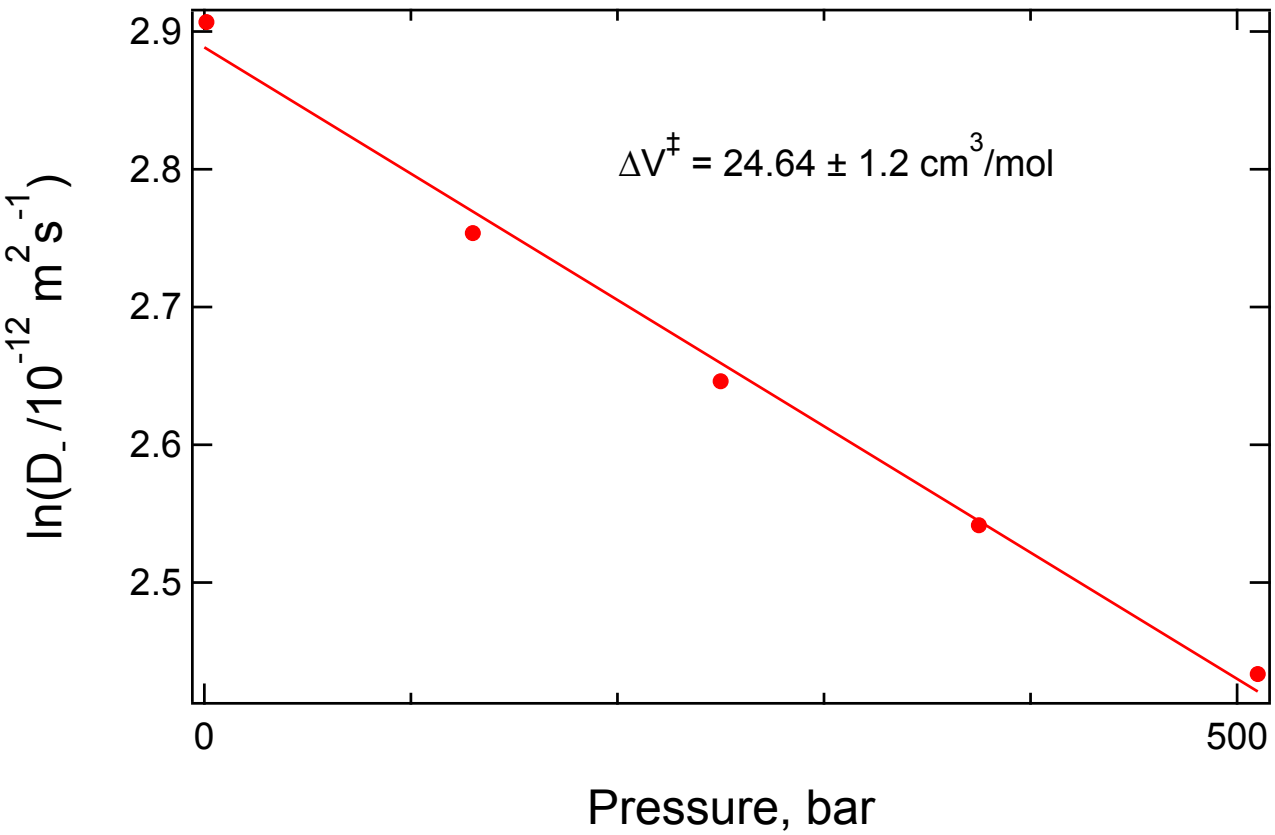

Point	Pressure	D (10^-12 m2/s)	ln(D)
0	1	18.3	2.907
1	130	15.7	2.754
2	250	14.1	2.646
3	375	12.7	2.542
4	510	11.4	2.434

ln(D_-) vs. Pressure Plot for PF_6 diffusion in BMIM PF_6 at 70 °C

Data from Kanakubo et al. 10.1021/jp063278k

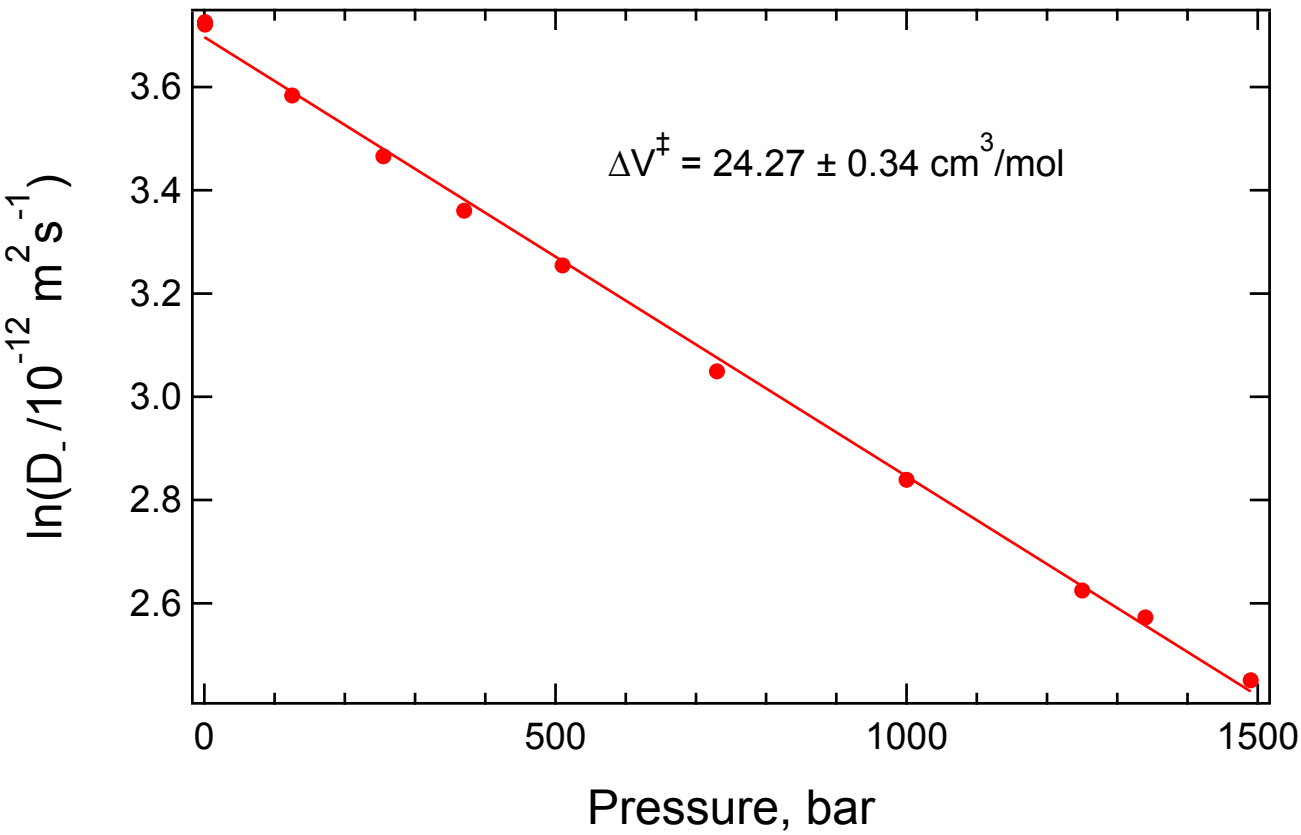

Point	Pressure	D (10^-12 m2/s)	ln(D)
0	1	41.3	3.721
1	1	41.5	3.726
2	125	36.0	3.584
3	255	32.0	3.466
4	370	28.8	3.360
5	510	25.9	3.254
6	730	21.1	3.049
7	1000	17.1	2.839
8	1250	13.8	2.625
9	1340	13.1	2.573
10	1490	11.6	2.451

ln(D_-) vs. Pressure Plot for PF_6 diffusion in hmim PF_6 at 50 °C

Data from Harris et al. 10.1021/jp8021375

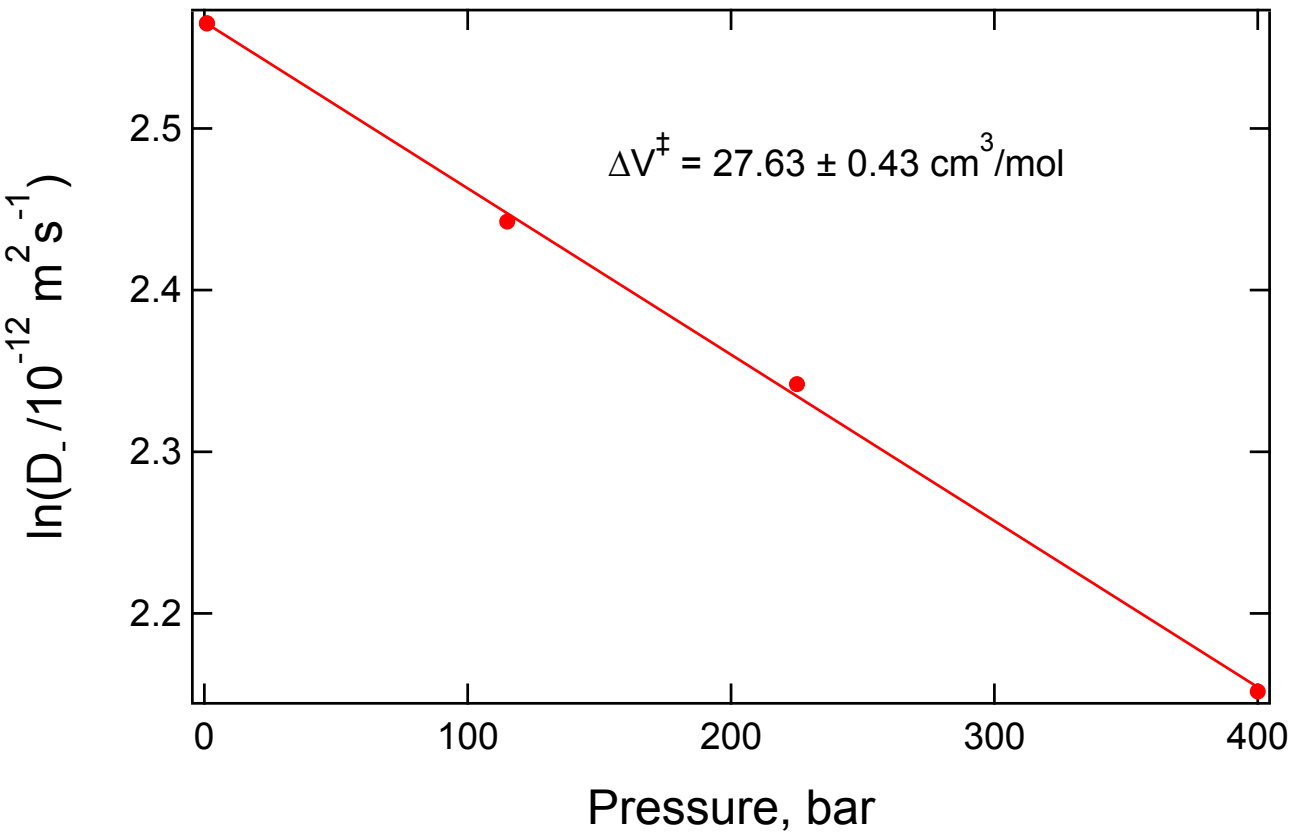

Point	Pressure	D (10^-12 m2/s)	ln(D)
0	1	13.0	2.565
1	1	13.0	2.565
2	115	11.5	2.442
3	225	10.4	2.342
4	400	8.6	2.152

ln(D_-) vs. Pressure Plot for PF_6 diffusion in hmim PF_6 at 60 °C

Data from Harris et al. 10.1021/jp8021375

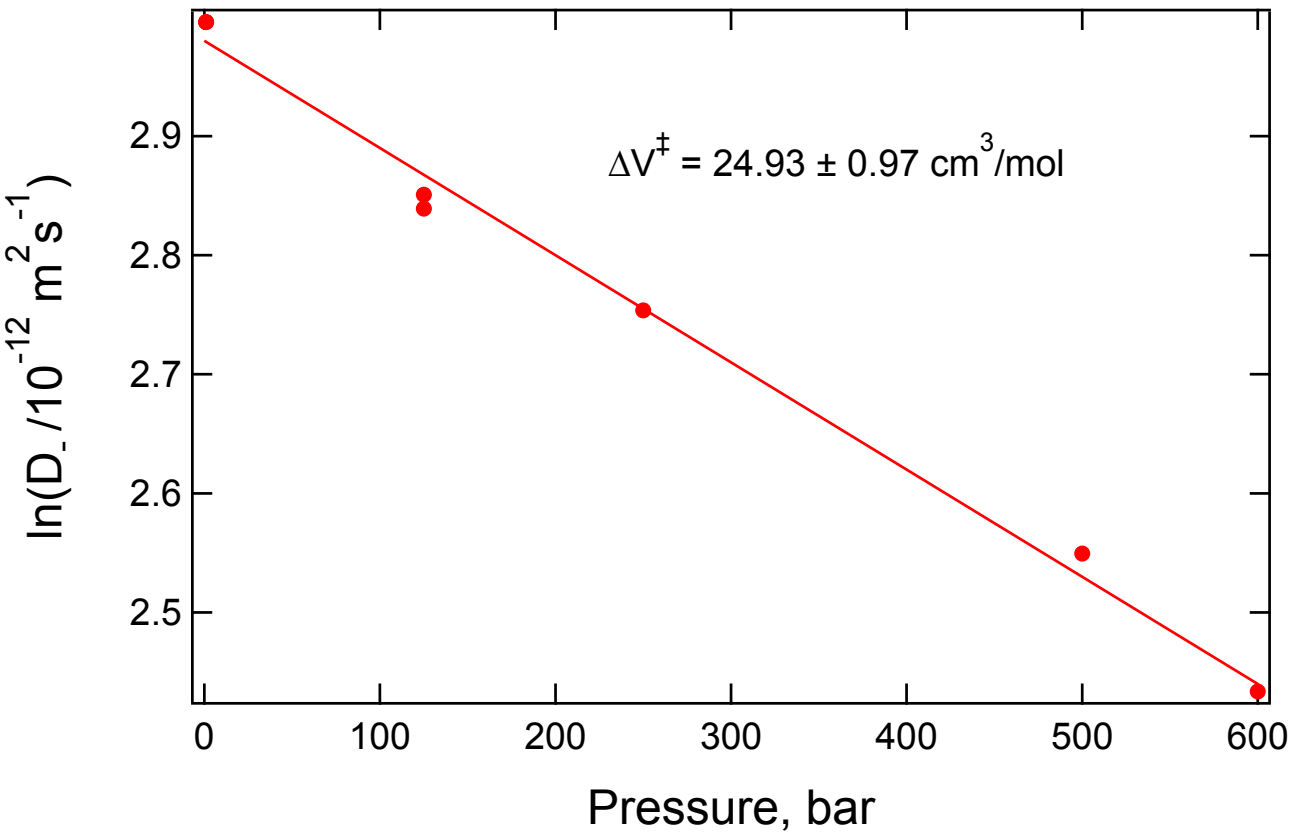

Point	Pressure	D (10^-12 m2/s)	ln(D)
0	1	20.0	2.996
1	1	20.0	2.996
2	125	17.1	2.839
3	125	17.3	2.851
4	250	15.7	2.754
5	500	12.8	2.549
6	600	11.4	2.434

ln(D_-) vs. Pressure Plot for PF_6 diffusion in hmim PF_6 at 75 °C

Data from Harris et al. 10.1021/jp8021375

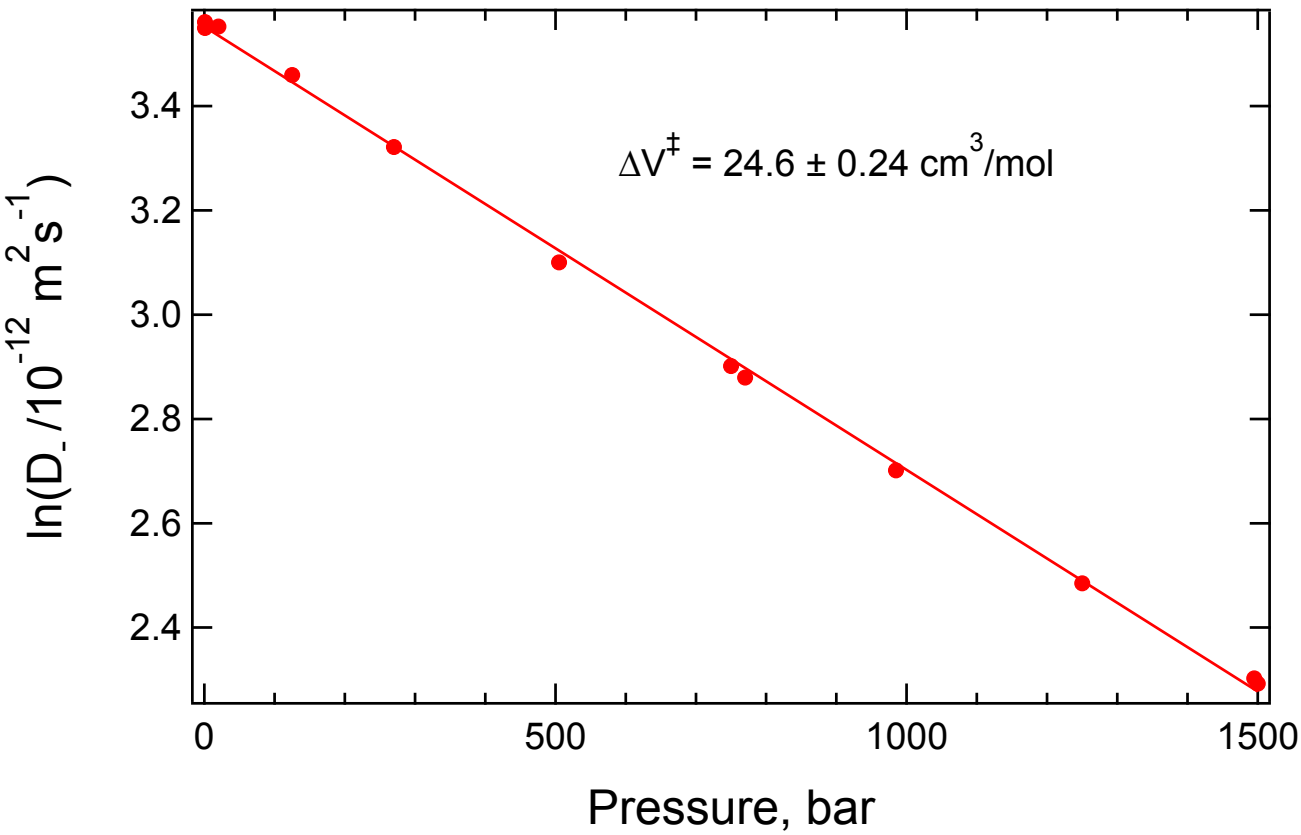

Point	Pressure	D (10^-12 m2/s)	ln(D)
0	1	35.2	3.561
1	1	34.8	3.550
2	20	34.9	3.552
3	125	31.8	3.459
4	270	27.7	3.321
5	505	22.2	3.100
6	750	18.2	2.901
7	770	17.8	2.879
8	985	14.9	2.701
9	1250	12.0	2.485
10	1495	10.0	2.303
11	1500	9.9	2.293

ln(D_-) vs. Pressure Plot for PF_6 diffusion in OMIM PF_6 at 75 °C

Data from Harris et al. 10.1021/jp8021375

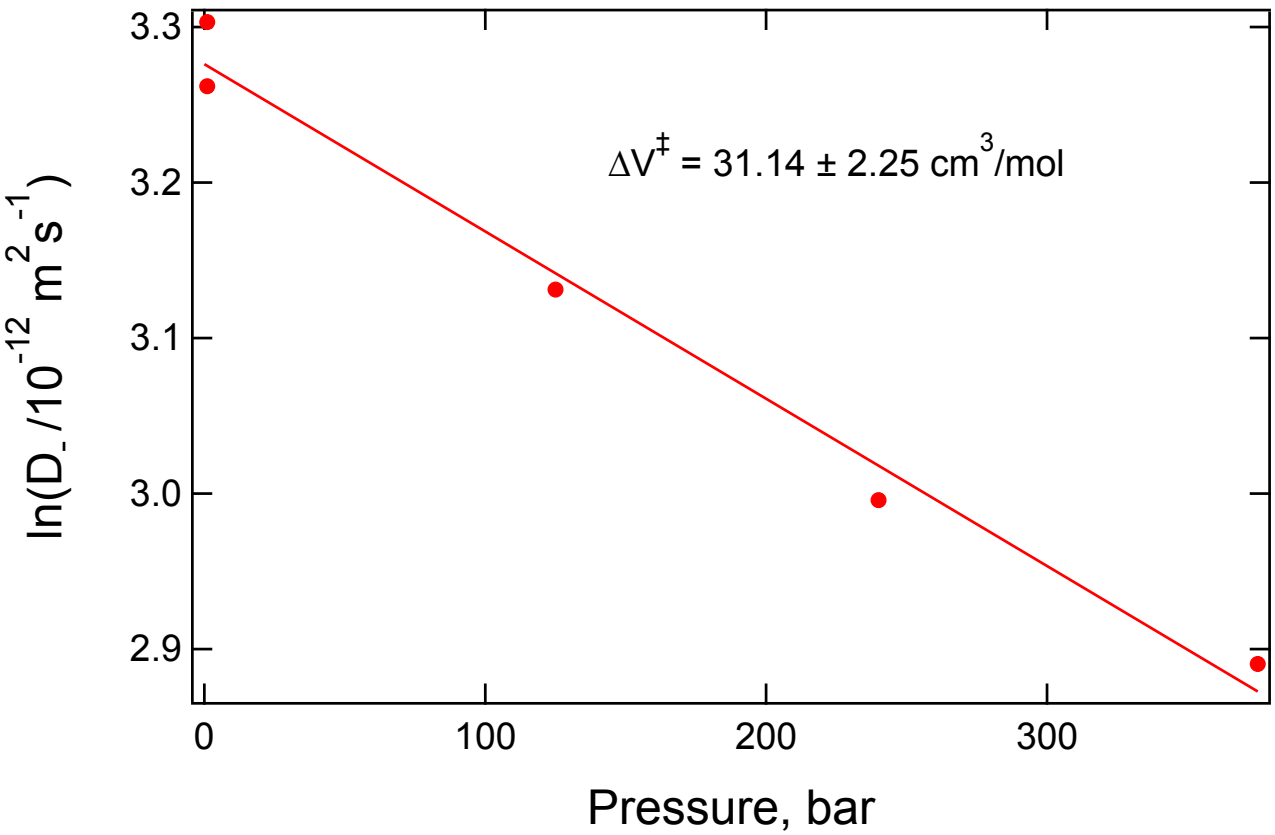

Point	Pressure	D (10^-12 m2/s)	ln(D)
0	1	26.1	3.262
1	1	27.2	3.303
2	125	22.9	3.131
3	240	20.0	2.996
4	375	18.0	2.890

$\ln(D_-)$ vs. Pressure Plot for PF_6 diffusion in OMIM PF_6 at 80 °C

Data from Harris et al. 10.1021/jp8021375

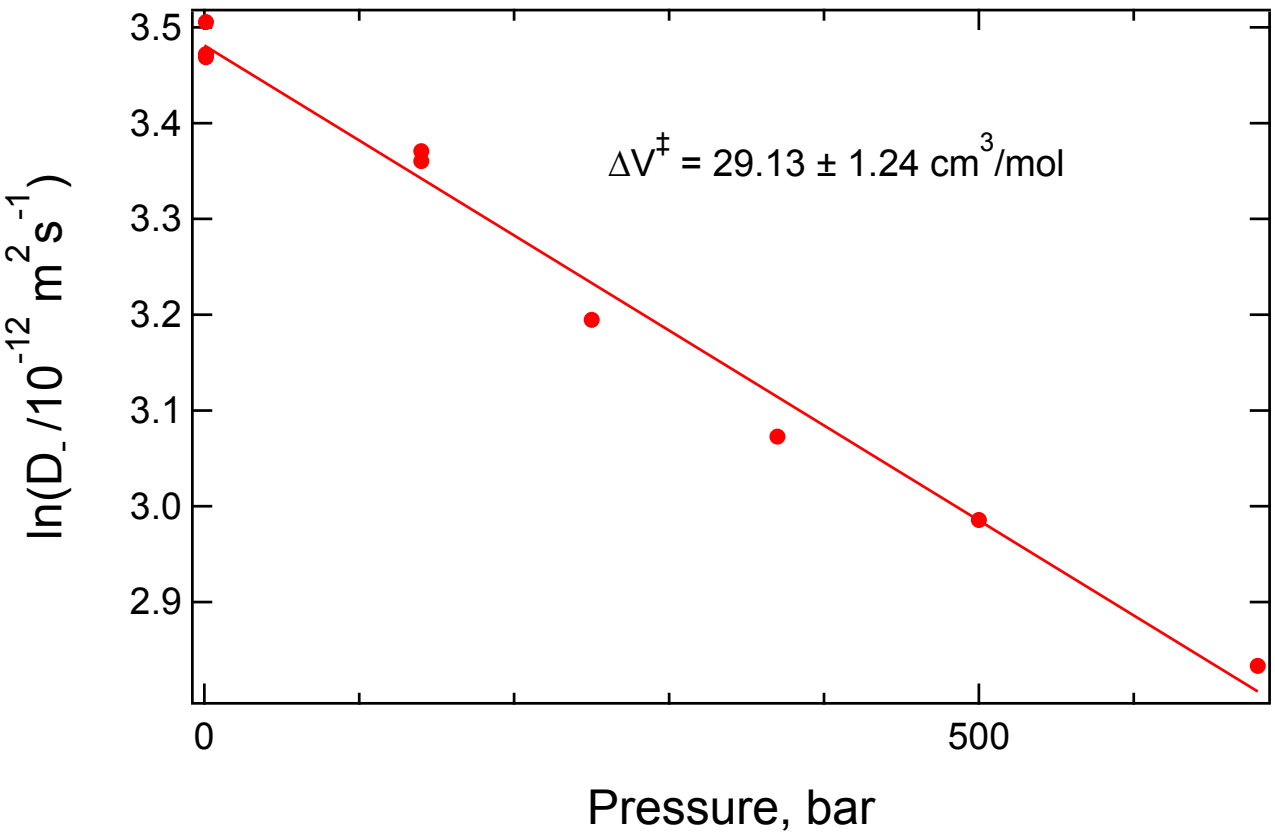

Point	Pressure	D (10^-12 m2/s)	ln(D)
0	1	32.2	3.472
1	1	32.1	3.469
2	1	33.3	3.506
3	140	29.1	3.371
4	140	28.8	3.360
5	250	24.4	3.195
6	370	21.6	3.073
7	500	19.8	2.986
8	680	17.0	2.833

ln(D_-) vs. Pressure Plot for TFSA diffusion in BMpyrr TFSA at 30 °C

Data from Harris et al. 10.1021/je2006049

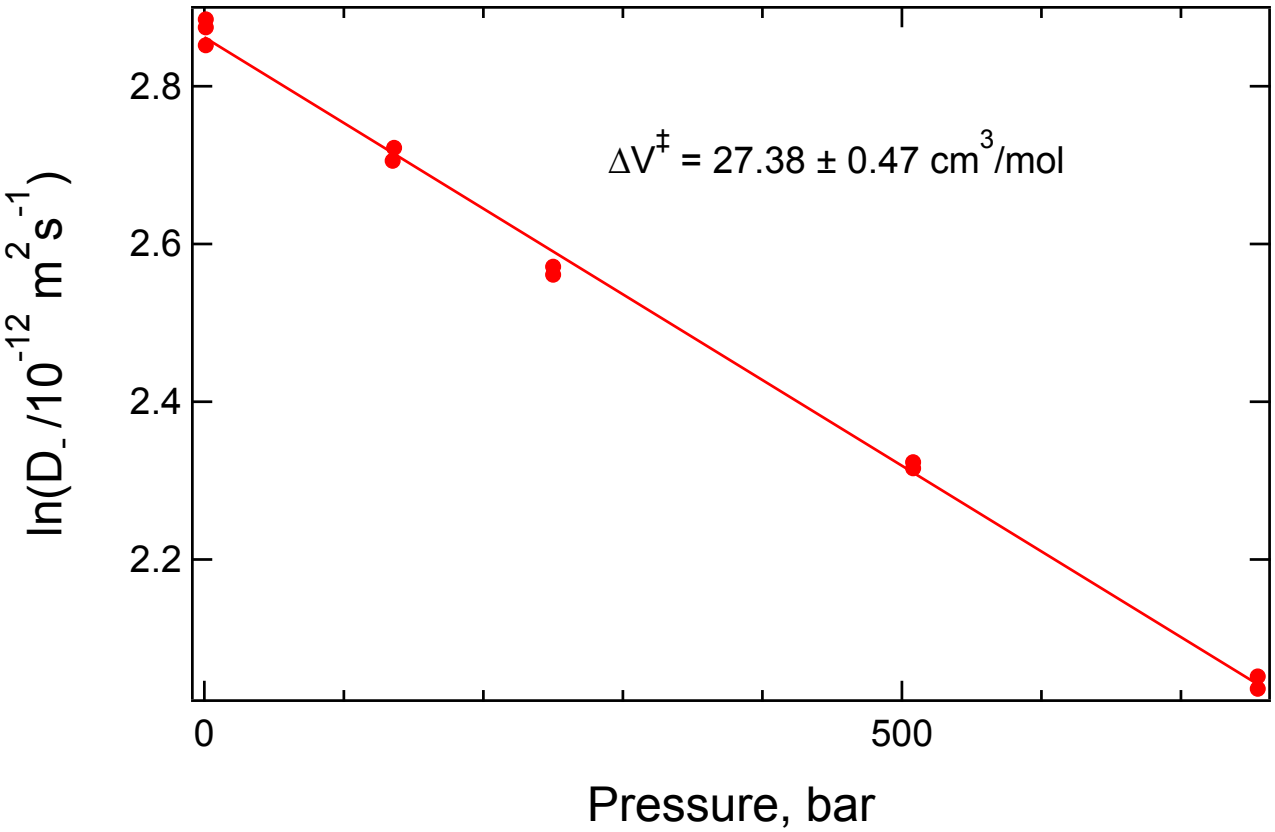

Point	Pressure	D (10^-12 m2/s)	ln(D)
0	1	17.9	2.885
1	1	17.7	2.875
2	1	17.3	2.852
3	135	15.0	2.705
4	136	15.2	2.722
5	250	12.9	2.561
6	250	13.1	2.571
7	508	10.2	2.323
8	508	10.1	2.316
9	755	7.7	2.036
10	755	7.8	2.052

ln(D_-) vs. Pressure Plot for TFSA diffusion in BMpyrr TFSA at 50 °C

Data from Harris et al. 10.1021/je2006049

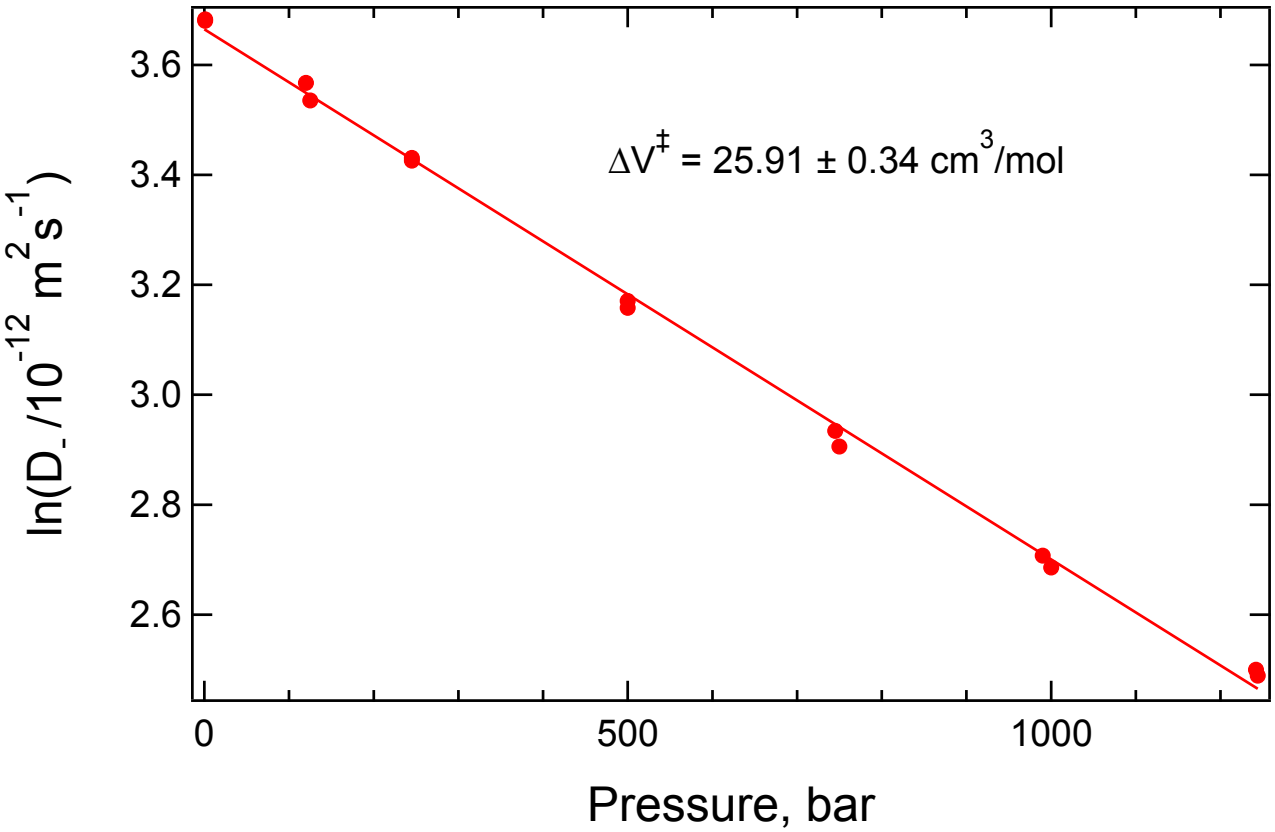

Point	Pressure	D (10^-12 m2/s)	ln(D)
0	1	39.8	3.683
1	1	39.7	3.680
2	120	35.4	3.567
3	125	34.3	3.535
4	245	30.9	3.431
5	245	30.8	3.426
6	500	23.8	3.171
7	500	23.5	3.158
8	745	18.8	2.934
9	750	18.3	2.906
10	990	15.0	2.707
11	1000	14.7	2.686
12	1242	12.2	2.500
13	1244	12.1	2.489

ln(D_-) vs. Pressure Plot for TFSA diffusion in BMpyrr TFSA at 65 °C

Data from Harris et al. 10.1021/je2006049

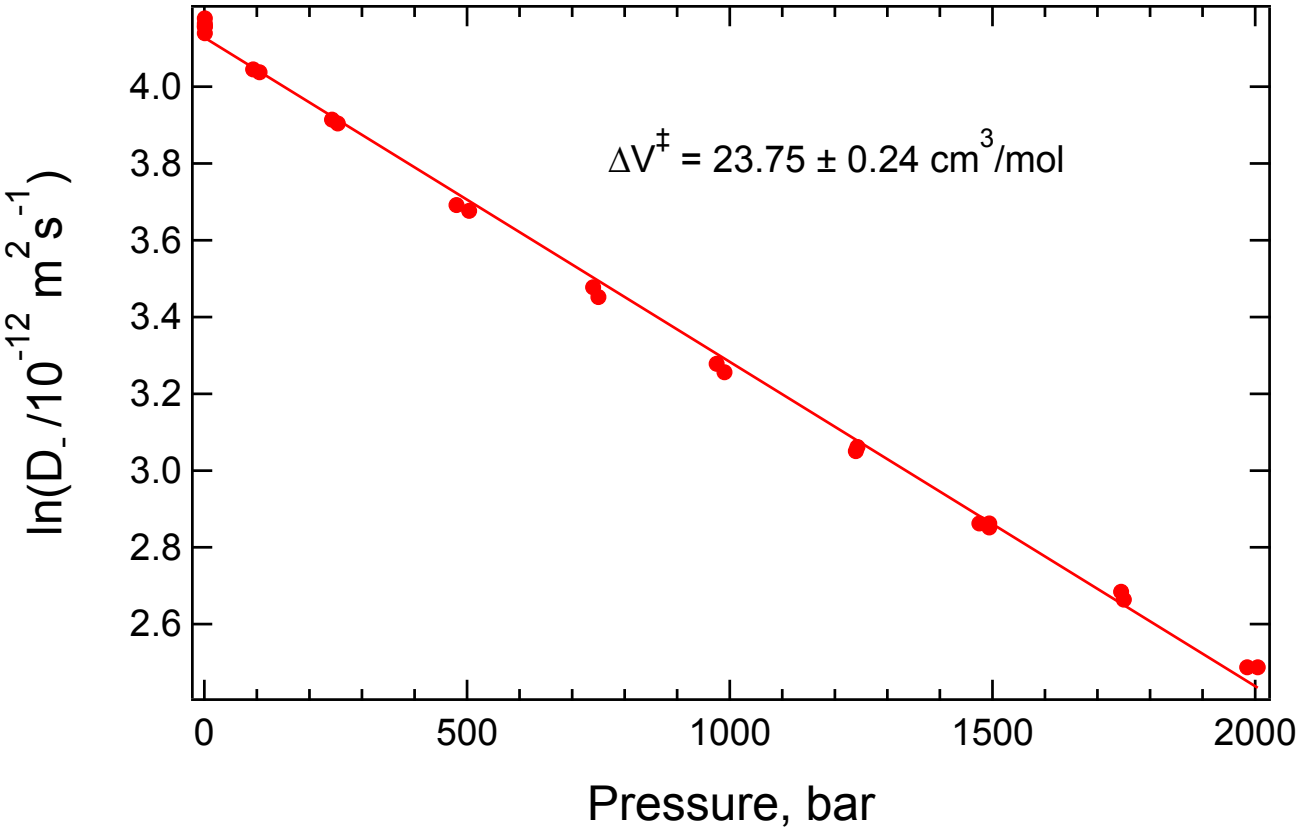

Point	Pressure	D (10^-12 m2/s)	ln(D)
0	1	63.9	4.158
1	1	63.8	4.156
2	1	62.8	4.139
3	1	65.2	4.178
4	1	64.3	4.164
5	93	57.1	4.045
6	105	56.7	4.038
7	243	50.1	3.914
8	254	49.6	3.904
9	480	40.1	3.692
10	504	39.5	3.677
11	740	32.4	3.478
12	750	31.6	3.452
13	975	26.5	3.278
14	990	26.0	3.256
15	1240	21.1	3.051
16	1243	21.4	3.062
17	1475	17.5	2.862
18	1494	17.5	2.862
19	1494	17.3	2.852
20	1745	14.6	2.684
21	1750	14.4	2.664
22	1985	12.0	2.487
23	2005	12.0	2.487

ln(D_-) vs. Pressure Plot for TFSA diffusion in BMpyrr TFSA at 75 °C

Data from Harris et al. 10.1021/je2006049

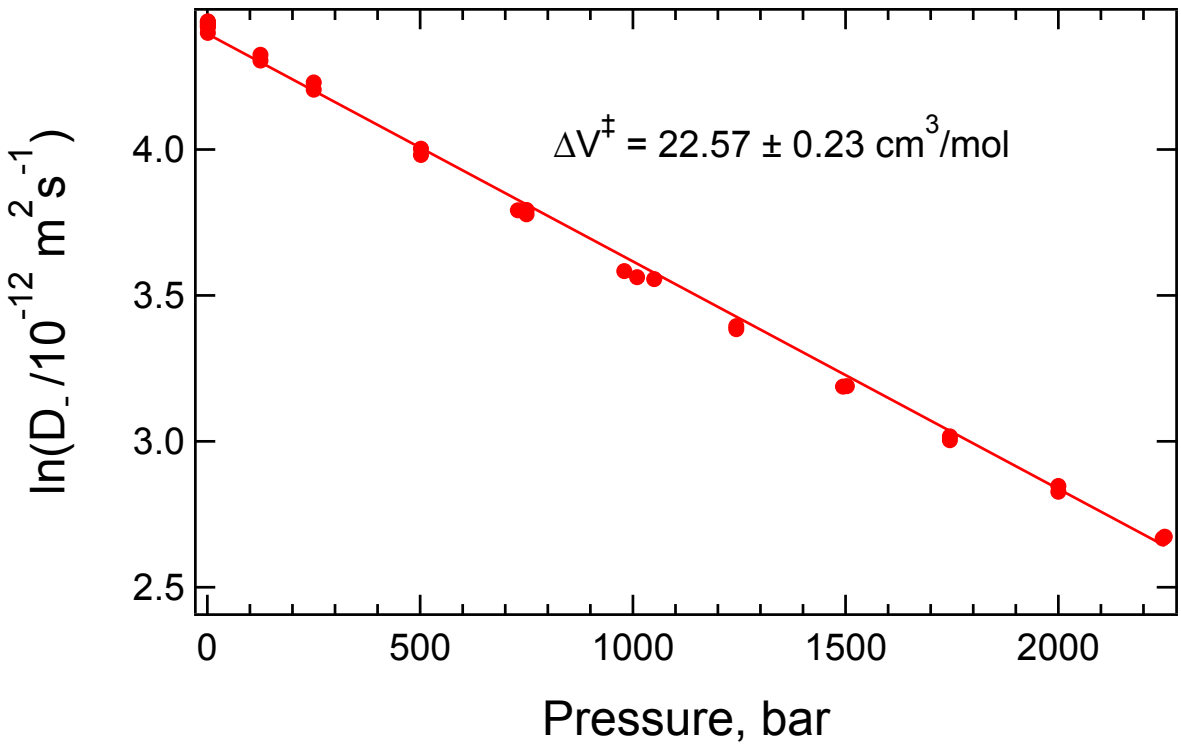

Point	Pressure	D (10^-12 m2/s)	ln(D)
0	1	83.4	4.423
1	1	83.9	4.430
2	1	81.4	4.400
3	1	82.9	4.418
4	1	84.6	4.438
5	1	84.7	4.439
6	125	75.5	4.324
7	125	74.1	4.305
8	250	67.0	4.205
9	250	68.7	4.229
10	502	54.8	4.003
11	502	53.6	3.982
12	730	44.3	3.792
13	750	44.4	3.793
14	750	43.7	3.778
15	980	36.0	3.584
16	1010	35.3	3.563
17	1050	35.0	3.556
18	1243	29.8	3.395
19	1243	29.5	3.384
20	1494	24.2	3.188
21	1503	24.3	3.189
22	1745	20.4	3.017
23	1745	20.2	3.004
24	2000	17.2	2.847
25	2000	16.9	2.827
26	2245	14.4	2.667
27	2250	14.5	2.673
28	2500	12.4	2.521
29	2500	12.4	2.519

1/Viscosity vs. Pressure Plot for BMIM BF_4 at 20 °C

Data from Sanmamed et al. 10.1016/j.jct.2009.11.014

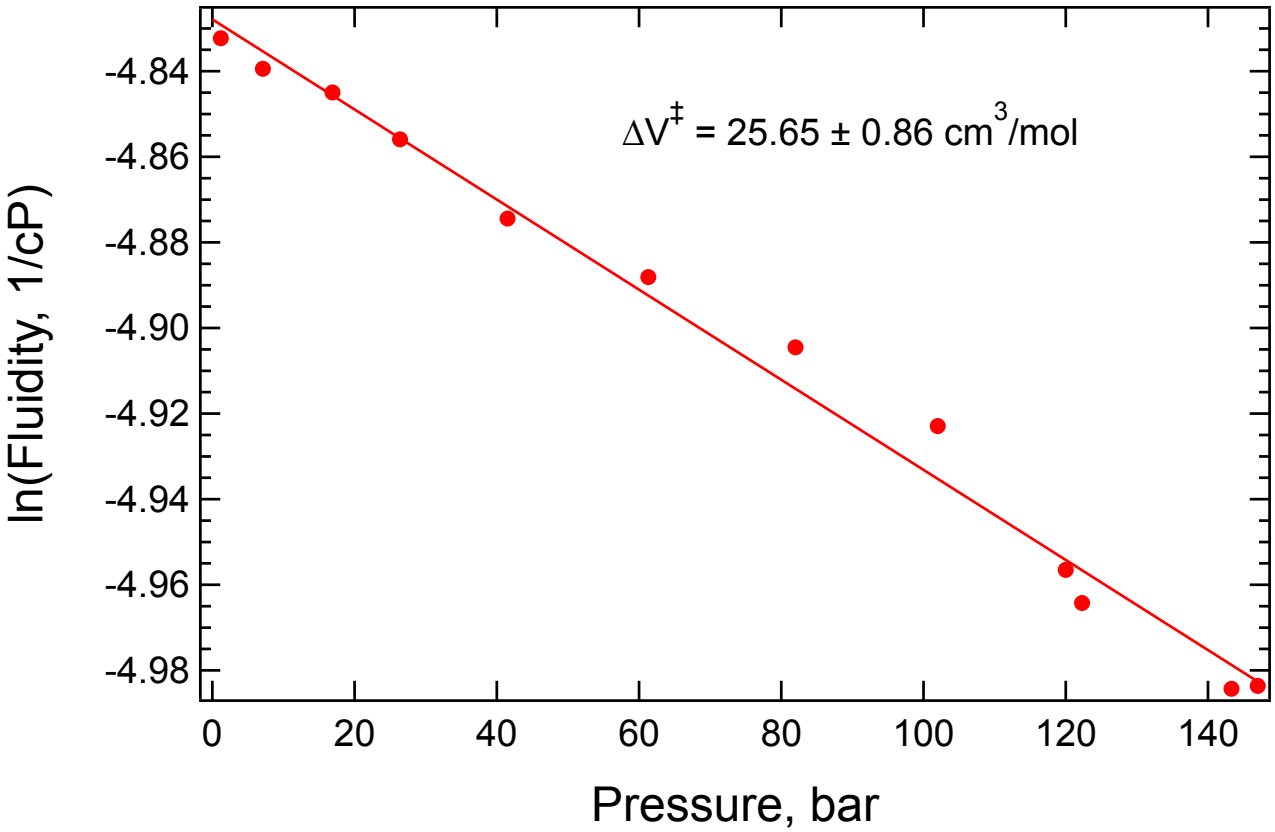

Point	Pressure	Visc, cP	ln(Fluidity)
0	1.2	125.5	-4.832
1	7.1	126.4	-4.839
2	16.9	127.1	-4.845
3	26.4	128.5	-4.856
4	41.5	130.9	-4.874
5	61.3	132.7	-4.888
6	82	134.9	-4.905
7	102	137.4	-4.923
8	120	142.1	-4.957
9	122.3	143.2	-4.964
10	143.3	146.1	-4.984
11	147	146	-4.984

1/Viscosity vs. Pressure Plot for BMIM BF_4 at 25 °C

Data from Harris et al. 10.1021/je700370z
J. Chem. Eng. Data 2007, 52, 2425-2430

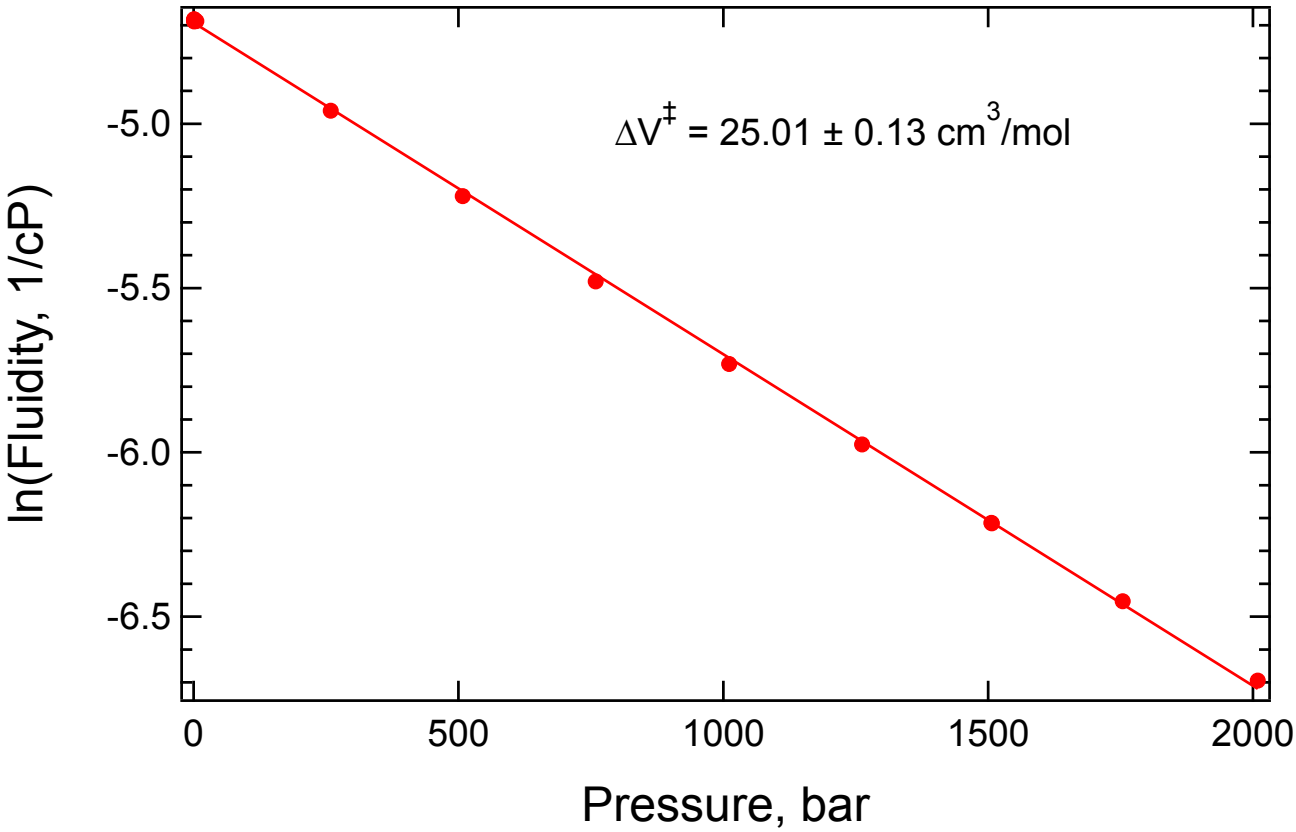

Point	Pressure	Visc, cP	ln(Fluidity)
0	1	108	-4.682
1	1	108	-4.682
2	1	108.5	-4.687
3	1	108.7	-4.689
4	5	108.6	-4.688
5	259	142.6	-4.960
6	508	185	-5.220
7	759	239.8	-5.480
8	1011	308.3	-5.731
9	1262	393.9	-5.976
10	1506	499.9	-6.214
11	1507	500.6	-6.216
12	1754	634.7	-6.453
13	2009	808.3	-6.695

1/Viscosity vs. Pressure Plot for BMIM BF_4 at 50 °C

Data from Harris et al. 10.1021/je700370z
J. Chem. Eng. Data 2007, 52, 2425-2430

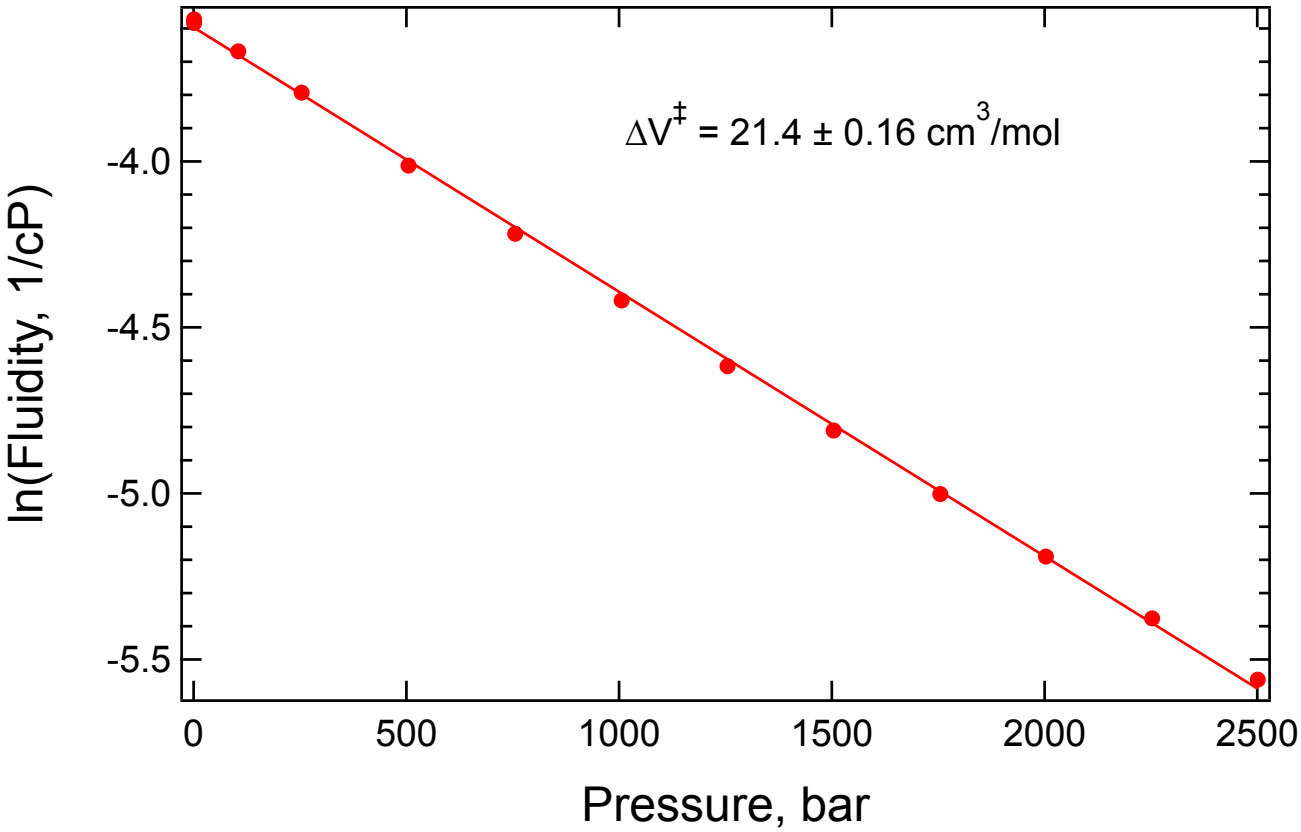

Point	Pressure	Visc, cP	ln(Fluidity)
0	1	35.6	-3.572
1	1	36	-3.584
2	105	39.2	-3.669
3	254	44.4	-3.793
4	505	55.3	-4.013
5	756	67.9	-4.218
6	1006	83	-4.419
7	1255	101.2	-4.617
8	1504	122.8	-4.811
9	1755	148.7	-5.002
10	2003	179.5	-5.190
11	2253	216.2	-5.376
12	2501	260	-5.561

1/Viscosity vs. Pressure Plot for BMIM BF_4 at 75 °C

Data from Harris et al. 10.1021/je700370z
J. Chem. Eng. Data 2007, 52, 2425-2430

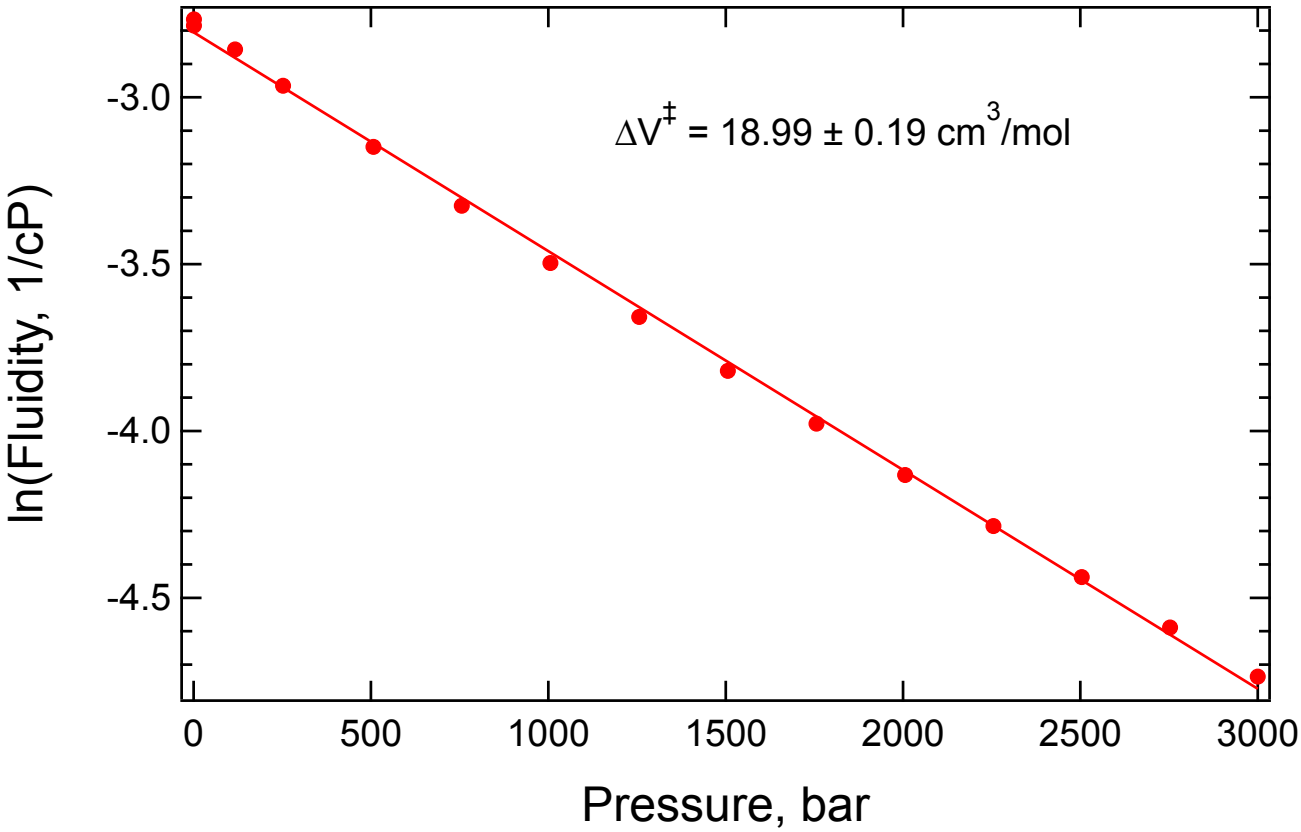

Point	Pressure	Visc, cP	ln(Fluidity)
0	1	16.2	-2.785
1	1	15.9	-2.766
2	117	17.4	-2.856
3	252	19.4	-2.965
4	507	23.3	-3.148
5	756	27.8	-3.325
6	1006	33	-3.497
7	1256	38.8	-3.658
8	1506	45.6	-3.820
9	1756	53.4	-3.978
10	2006	62.3	-4.132
11	2255	72.6	-4.285
12	2504	84.6	-4.438
13	2753	98.4	-4.589
14	3000	114	-4.736

1/Viscosity vs. Pressure Plot for BMIM PF_6 at 25 °C

Data from Ahosseini and Scurto 10.1007/s10765-008-0497-7

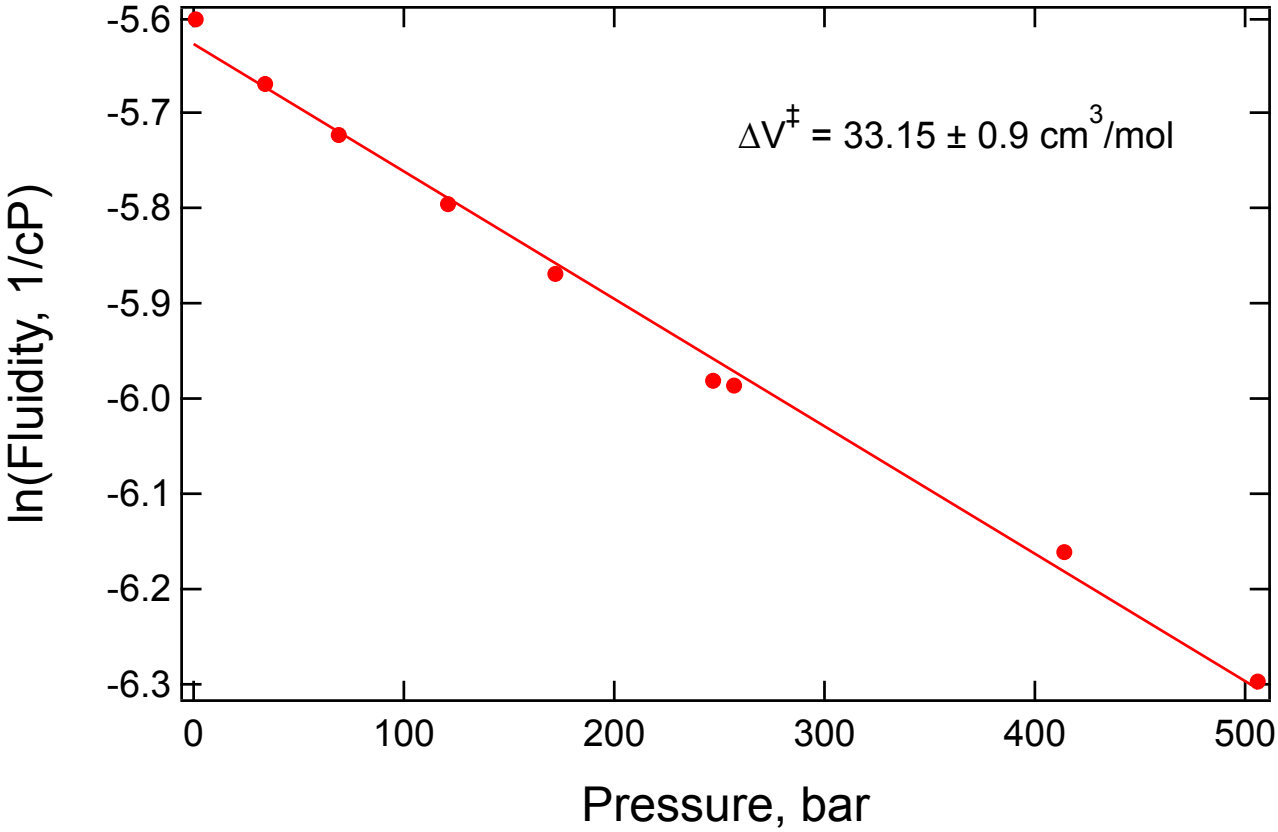

Point	Pressure	Visc, cP	ln(Fluidity)
0	1	271	-5.602
1	34	290	-5.670
2	69	306	-5.724
3	121	329	-5.796
4	172	354	-5.869
5	247	396	-5.981
6	257	398	-5.986
7	414	474	-6.161
8	506	543	-6.297

1/Viscosity vs. Pressure Plot for BMIM PF_6 at 25 °C

Data from Harris et al. 10.1021/je050147b

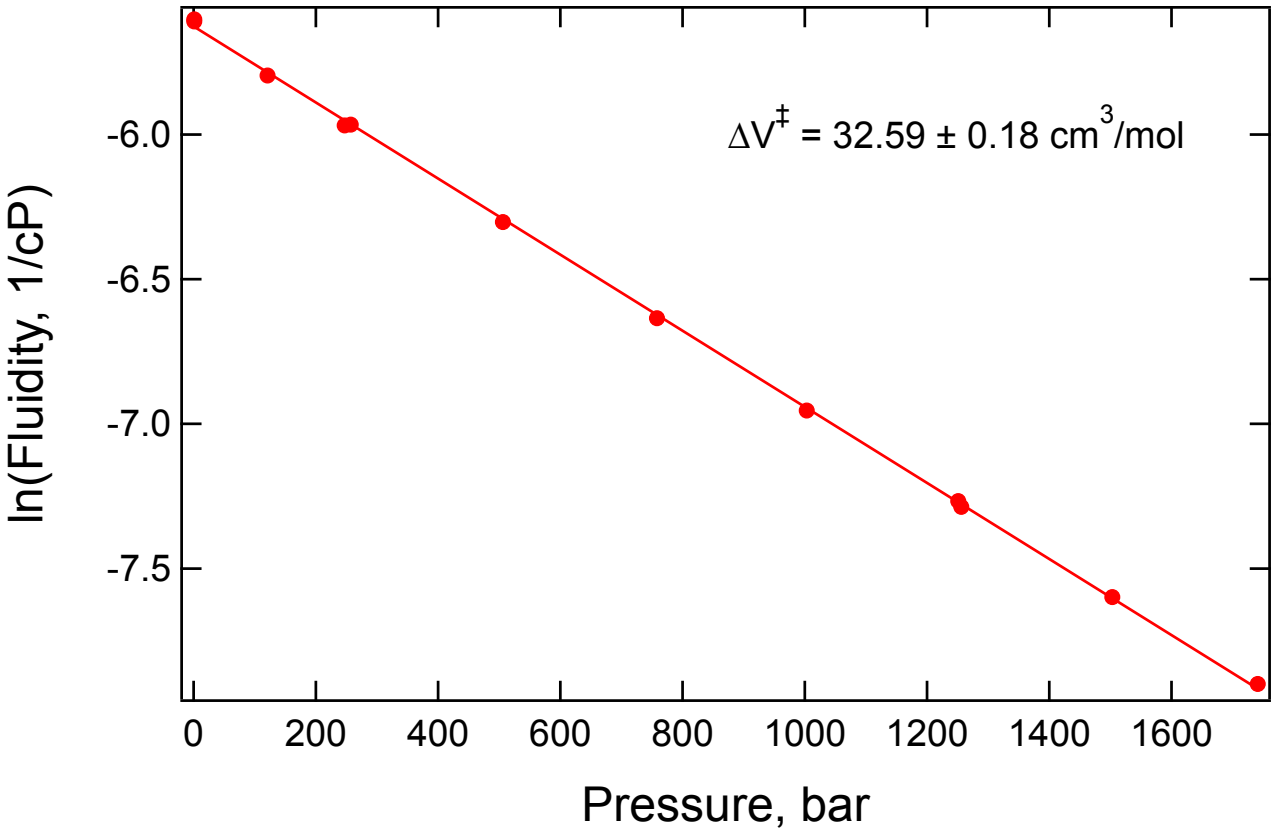

Point	Pressure	Visc, cP	ln(Fluidity)
0	1	273	-5.609
1	1	271	-5.602
2	121	329	-5.796
3	247	391	-5.969
4	257	390	-5.966
5	506	546	-6.303
6	758	761	-6.635
7	1003	1047	-6.954
8	1251	1432	-7.267
9	1256	1461	-7.287
10	1503	1995	-7.598
11	1741	2694	-7.899

1/Viscosity vs. Pressure Plot for BMIM PF_6 at 50 °C

Data from Harris et al. 10.1021/je050147b

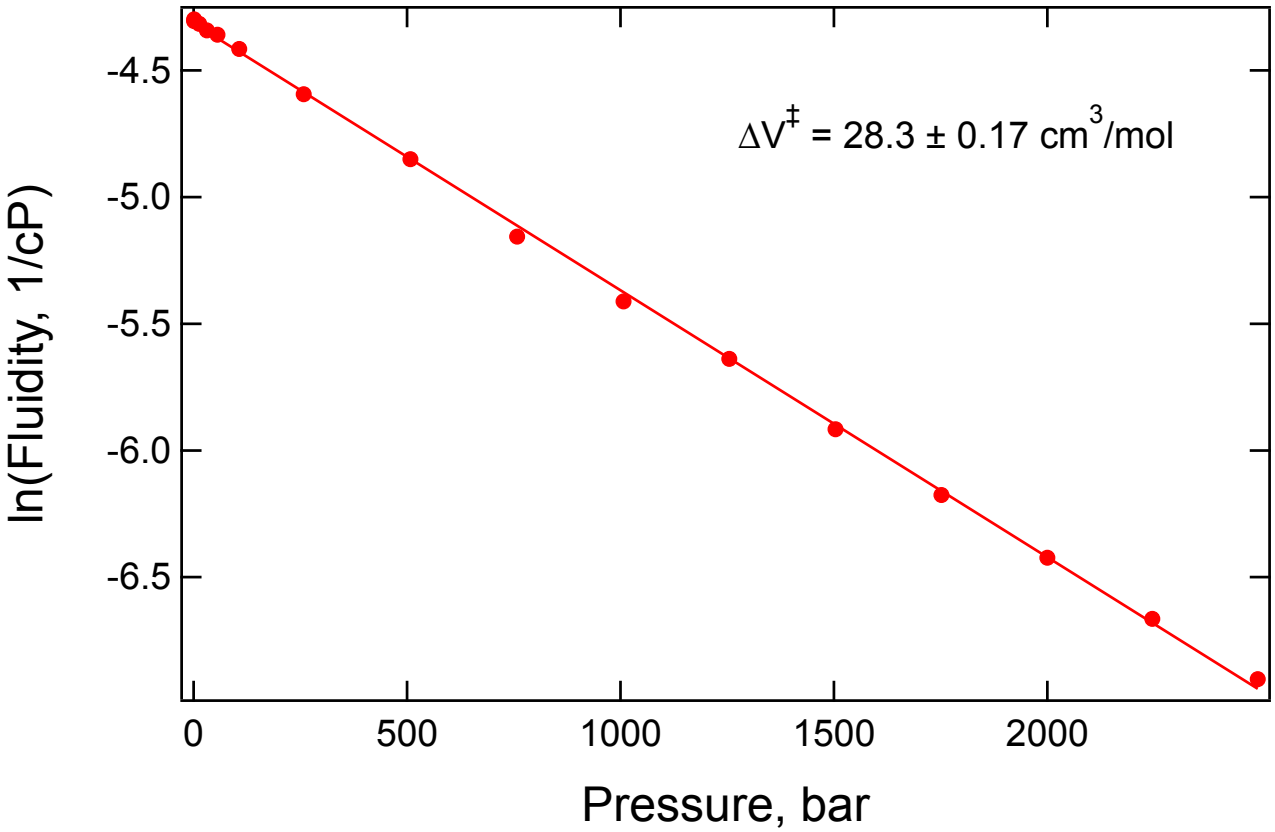

Point	Pressure	Visc, cP	ln(Fluidity)
0	1	73.6	-4.299
1	1	74.1	-4.305
2	13	74.9	-4.316
3	31	76.9	-4.343
4	56	78.2	-4.359
5	107	82.7	-4.415
6	258	98.9	-4.594
7	508	127.8	-4.850
8	758	173.5	-5.156
9	1007	224	-5.412
10	1255	281	-5.638
11	1504	371	-5.916
12	1752	481	-6.176
13	2000	616	-6.423
14	2246	784	-6.664
15	2493	995	-6.903

1/Viscosity vs. Pressure Plot for BMIM PF_6 at 70 °C

Data from Harris et al. 10.1021/je050147b

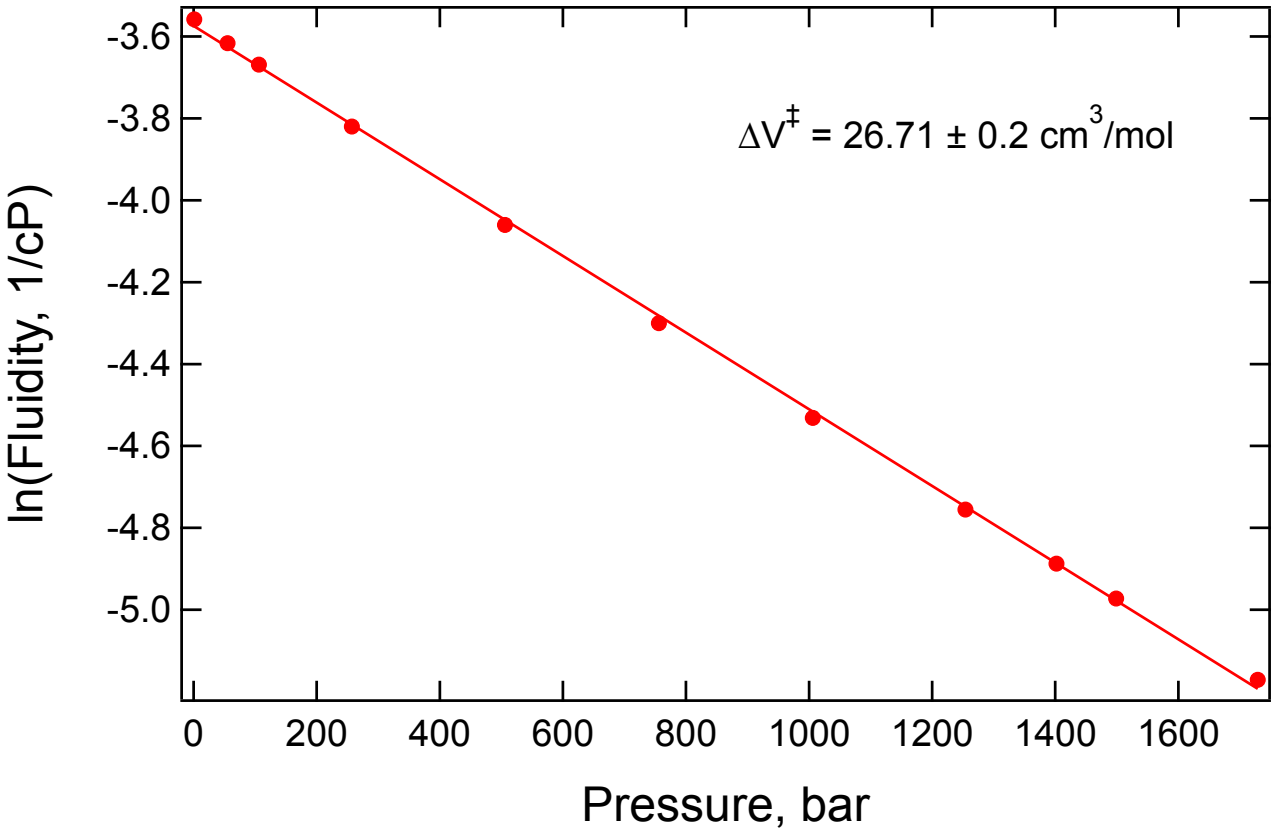

Point	Pressure	Visc, cP	ln(Fluidity)
0	1	35.1	-3.558
1	55	37.2	-3.616
2	106	39.2	-3.669
3	257	45.6	-3.820
4	506	58	-4.060
5	756	73.7	-4.300
6	1006	92.9	-4.532
7	1254	116.2	-4.755
8	1402	132.6	-4.887
9	1499	144.4	-4.973
10	1729	176.1	-5.171

1/Viscosity vs. Pressure Plot for BMIM TFSA at 25 °C

Data from Harris et al. 10.1021/je700032n
J. Chem. Eng. Data 2007, 52, 1080-1085

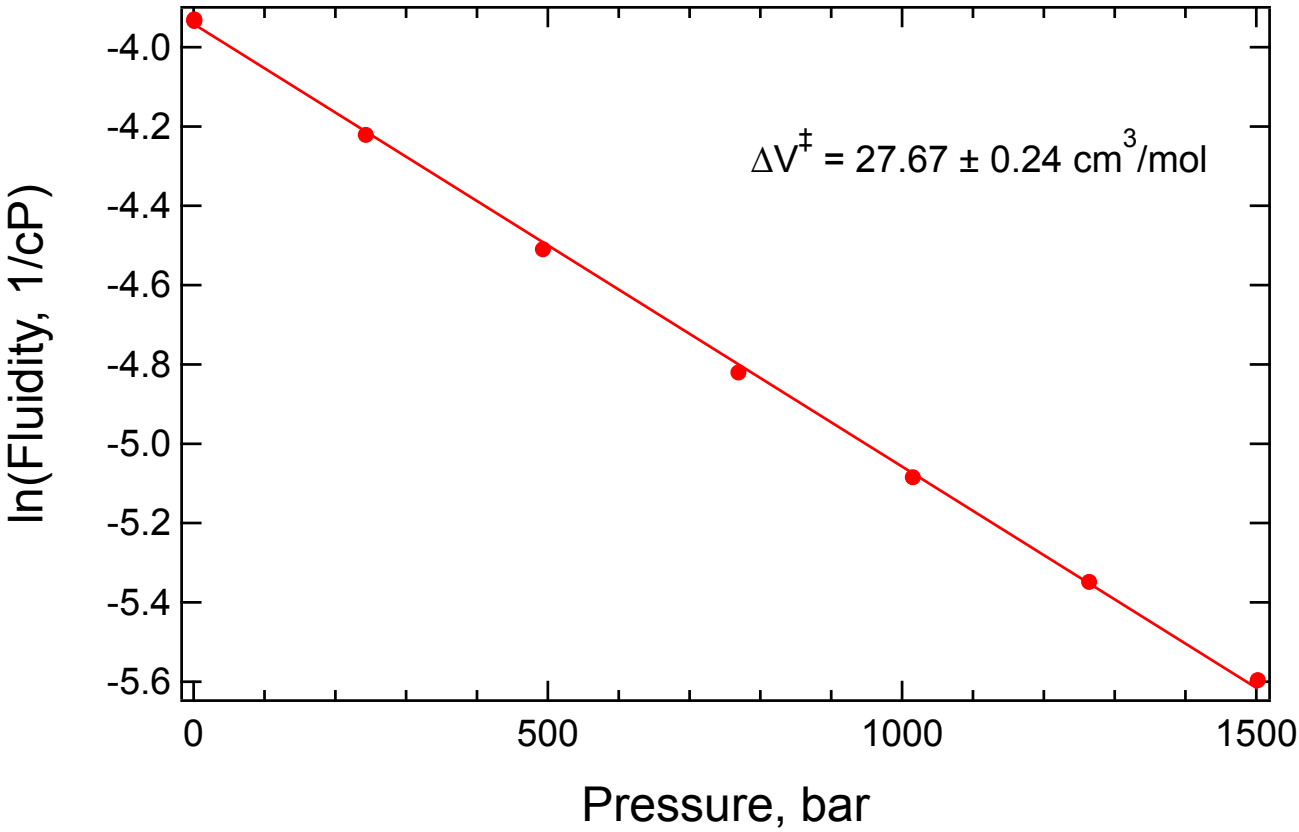

Point	Pressure	Visc, cP	ln(Fluidity)
0	1	51	-3.932
1	1	51.1	-3.934
2	1	50.9	-3.930
3	243	68.1	-4.221
4	493	90.9	-4.510
5	769	124	-4.820
6	1015	161.5	-5.085
7	1264	210.3	-5.349
8	1502	269.4	-5.596

1/Viscosity vs. Pressure Plot for BMIM TFSA at 50 °C

Data from Harris et al. 10.1021/je700032n
J. Chem. Eng. Data 2007, 52, 1080-1085

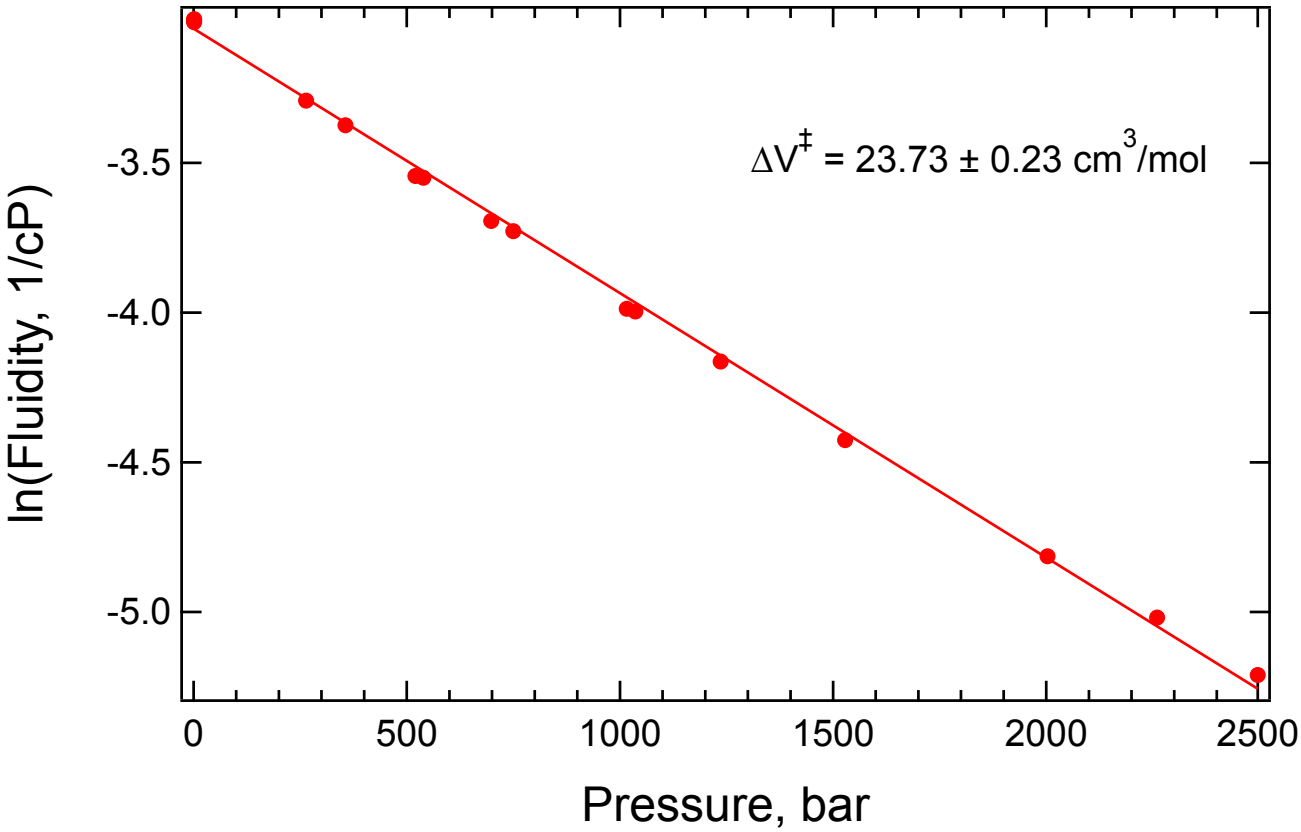

Point	Pressure	Visc, cP	ln(Fluidity)
0	1	20.5	-3.020
1	1	20.5	-3.020
2	264	26.9	-3.292
3	520	34.6	-3.544
4	750	41.6	-3.728
5	1016	53.9	-3.987
6	1528	83.6	-4.426
7	2003	123.2	-4.814
8	2260	151.2	-5.019
9	2496	183.2	-5.211
10	1	20.6	-3.025
11	1	20.7	-3.030
12	1	20.6	-3.025
13	356	29.2	-3.374
14	539	34.8	-3.550
15	698	40.2	-3.694
16	1036	54.4	-3.996
17	1236	64.3	-4.164

1/Viscosity vs. Pressure Plot for BMIM TFSA at 75 °C

Data from Harris et al. 10.1021/je700032n
J. Chem. Eng. Data 2007, 52, 1080-1085

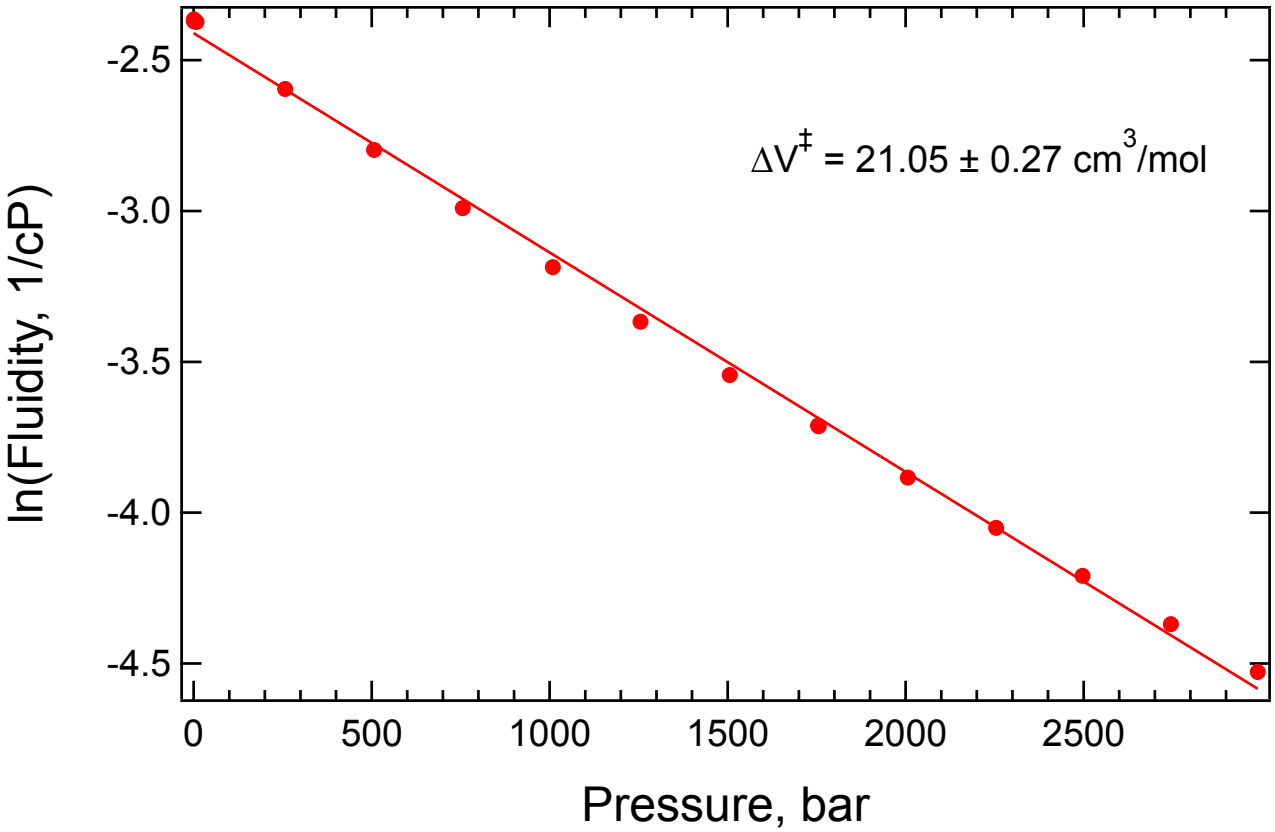

Point	Pressure	Visc, cP	ln(Fluidity)
0	1	10.64	-2.365
1	1	10.71	-2.371
2	8	10.73	-2.373
3	257	13.4	-2.595
4	507	16.4	-2.797
5	756	19.9	-2.991
6	1009	24.2	-3.186
7	1255	29	-3.367
8	1506	34.6	-3.544
9	1754	40.9	-3.711
10	1756	41	-3.714
11	2006	48.6	-3.884
12	2254	57.4	-4.050
13	2497	67.3	-4.209
14	2745	79	-4.369
15	2989	92.6	-4.528

1/Viscosity vs. Pressure Plot BMMIM FAP at 40 °C

Data from Gacino et al. 10.1016/j.jct.2013.02.014
J. Chem. Thermodynamics 62 (2013) 162–169

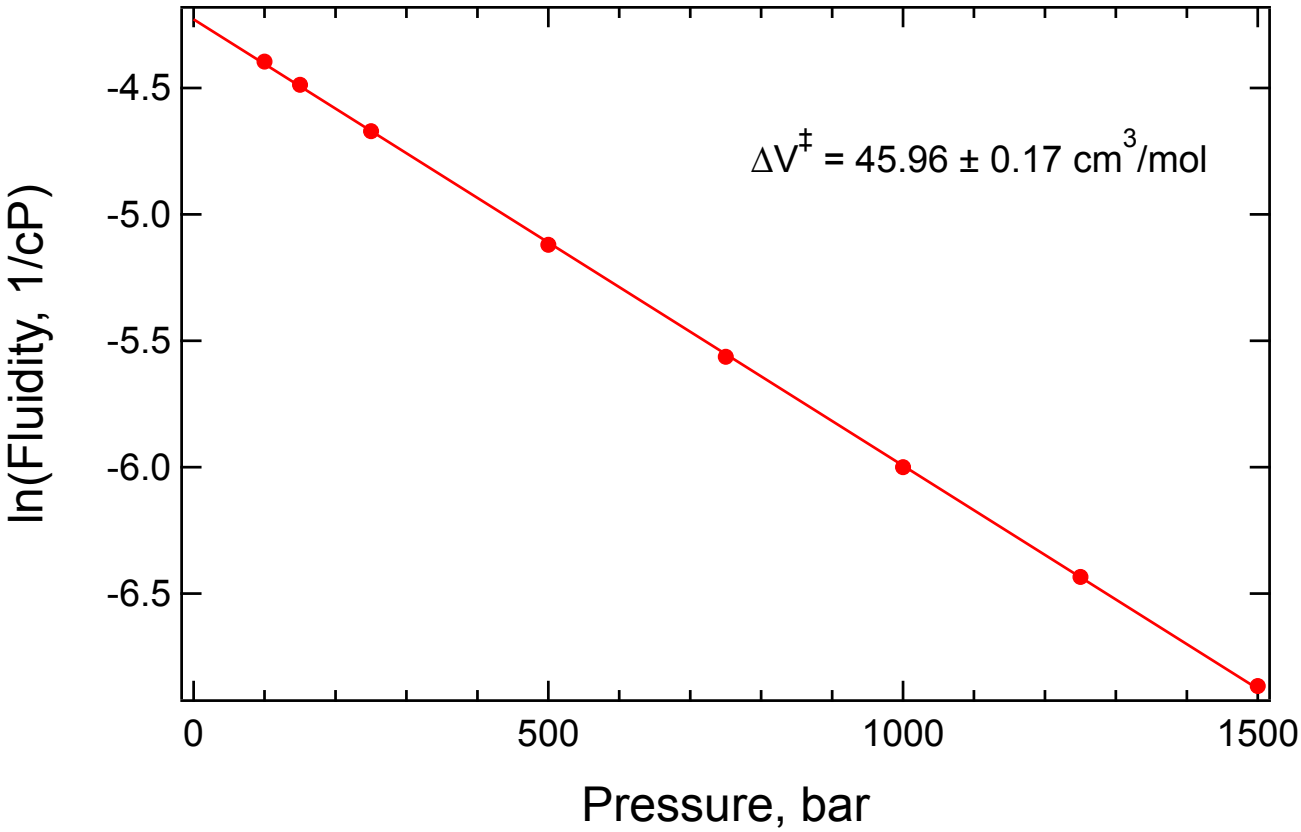

Point	Pressure	Visc, cP	ln(Fluidity)
0	100	81.1	-4.396
1	150	88.9	-4.488
2	250	106.8	-4.671
3	500	167.4	-5.120
4	750	260.6	-5.563
5	1000	403.5	-6.000
6	1250	622.7	-6.434
7	1500	958.7	-6.866

1/Viscosity vs. Pressure Plot BMMIM FAP at 70 °C

Data from Gacino et al. 10.1016/j.jct.2013.02.014
J. Chem. Thermodynamics 62 (2013) 162–169

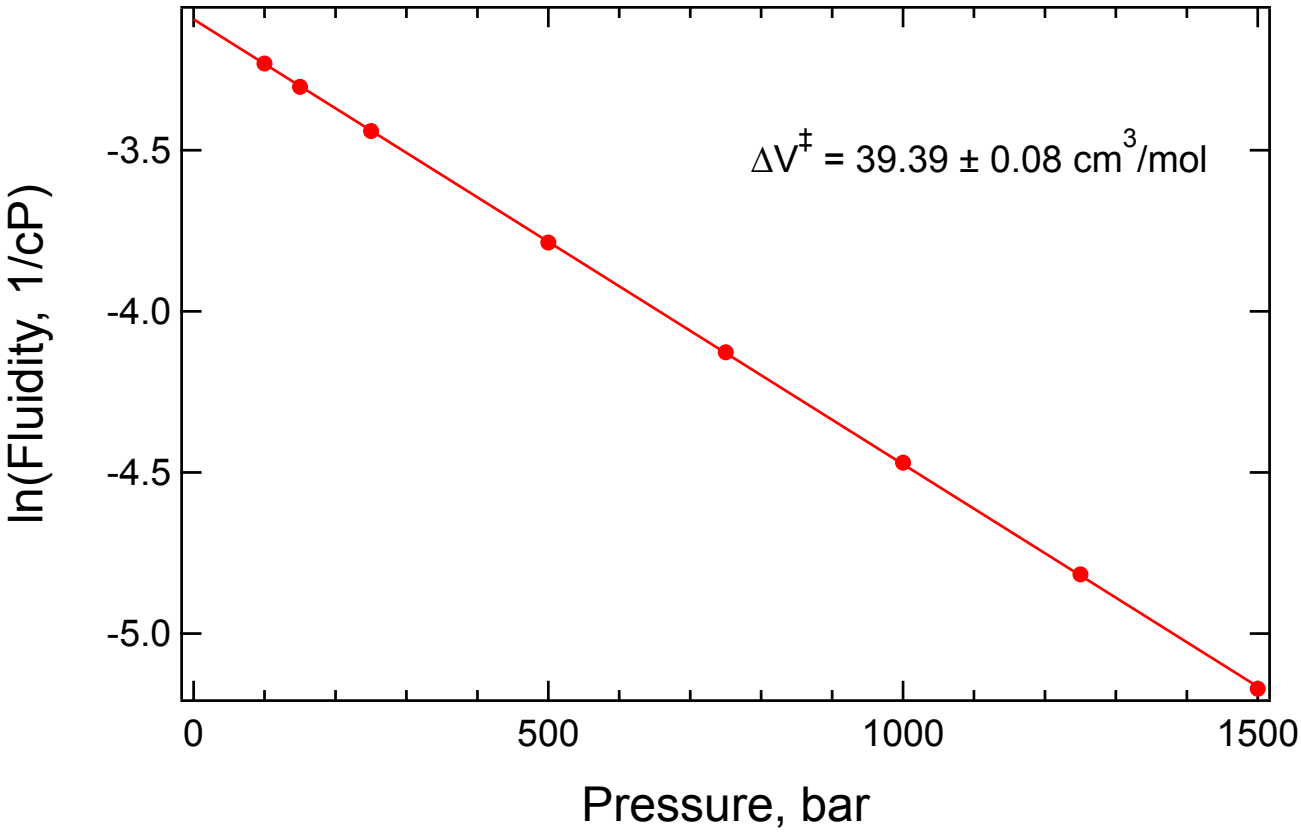

Point	Pressure	Visc, cP	ln(Fluidity)
0	100	25.3	-3.231
1	150	27.2	-3.303
2	250	31.2	-3.440
3	500	44.1	-3.786
4	750	62	-4.127
5	1000	87.3	-4.469
6	1250	123.5	-4.816
7	1500	176.1	-5.171

1/Viscosity vs. Pressure Plot BMMIM TFSA at 40 °C

Data from Gacino et al. 10.1016/j.jct.2013.02.014
J. Chem. Thermodynamics 62 (2013) 162–169

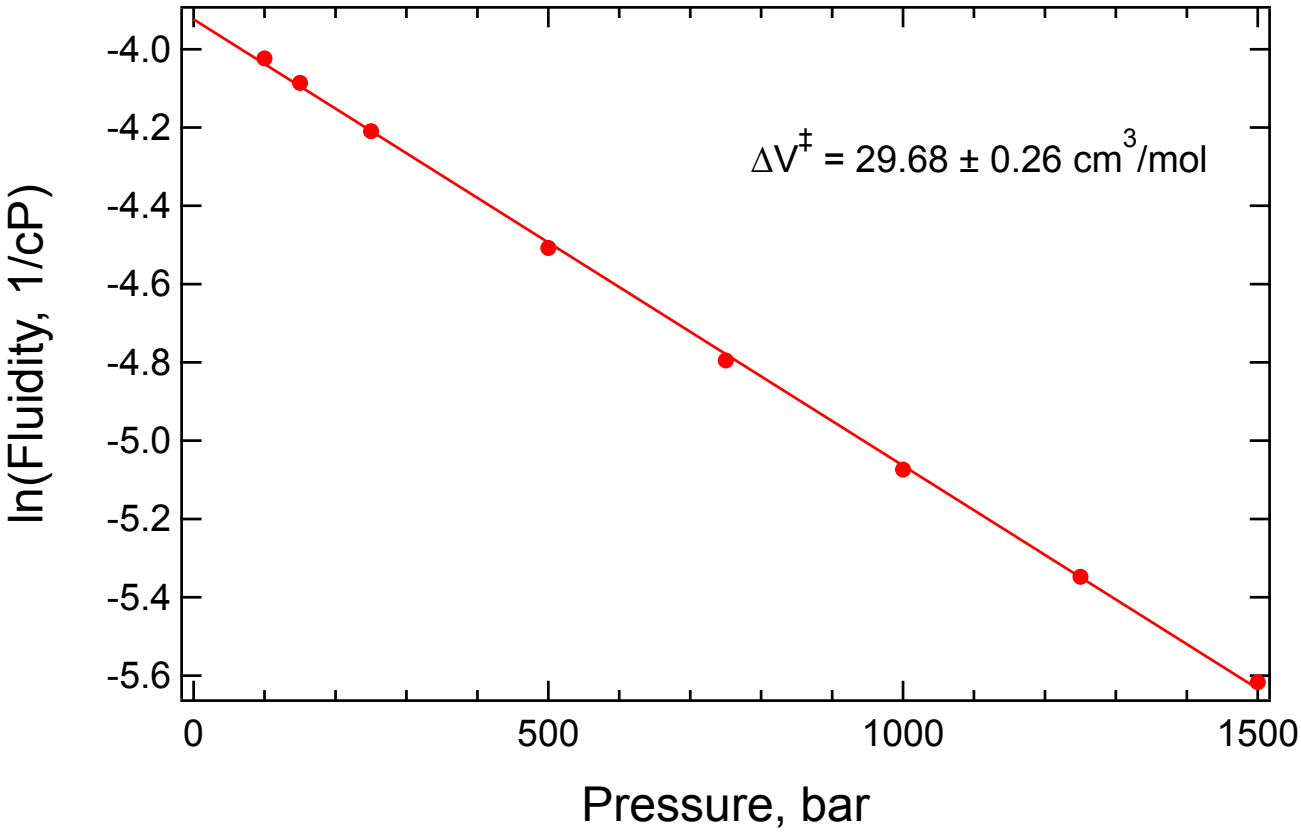

Point	Pressure	Visc, cP	ln(Fluidity)
0	100	55.9	-4.024
1	150	59.5	-4.086
2	250	67.3	-4.209
3	500	90.7	-4.508
4	750	120.9	-4.795
5	1000	159.8	-5.074
6	1250	210.1	-5.348
7	1500	275	-5.617

1/Viscosity vs. Pressure Plot BMMIM TFSA at 70 °C

Data from Gacino et al. 10.1016/j.jct.2013.02.014
J. Chem. Thermodynamics 62 (2013) 162–169

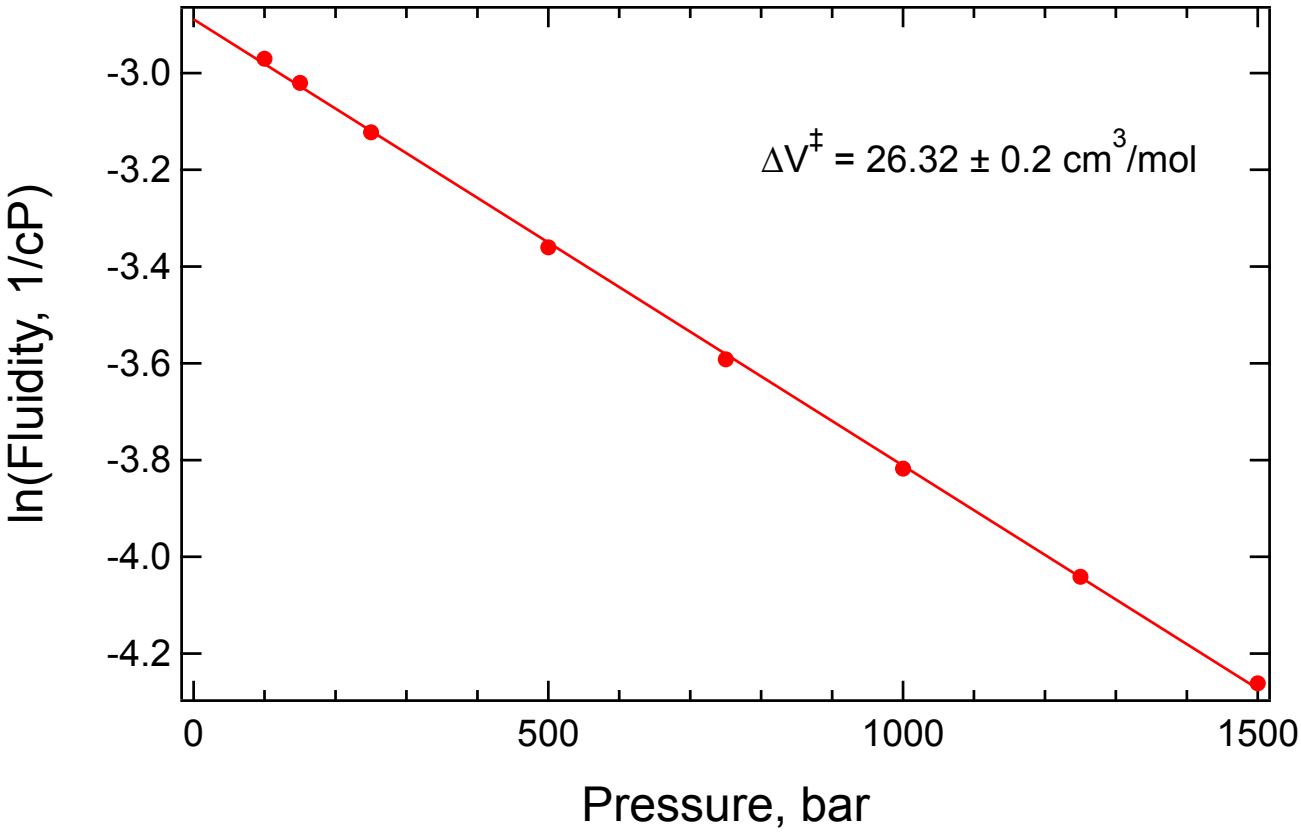

Point	Pressure	Visc, cP	ln(Fluidity)
0	100	19.5	-2.970
1	150	20.5	-3.020
2	250	22.7	-3.122
3	500	28.8	-3.360
4	750	36.3	-3.592
5	1000	45.5	-3.818
6	1250	56.9	-4.041
7	1500	70.9	-4.261

1/Viscosity vs. Pressure Plot BMMIM TFSA at 90 °C

Data from Gacino et al. 10.1016/j.jct.2013.02.014
J. Chem. Thermodynamics 62 (2013) 162–169

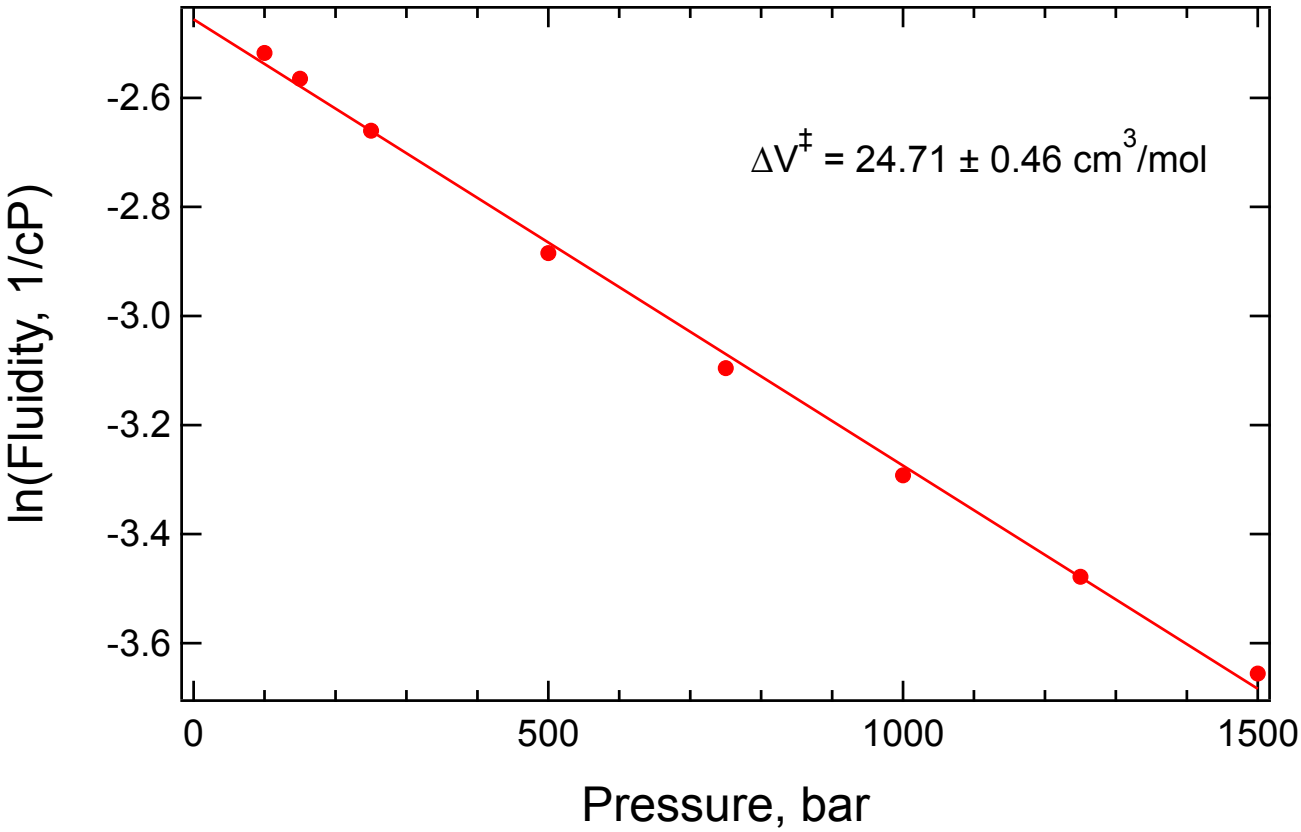

Point	Pressure	Visc, cP	ln(Fluidity)
0	100	12.4	-2.518
1	150	13	-2.565
2	250	14.3	-2.660
3	500	17.9	-2.885
4	750	22.1	-3.096
5	1000	26.9	-3.292
6	1250	32.4	-3.478
7	1500	38.7	-3.656

1/Viscosity vs. Pressure Plot for BMpyrr TFSA at 25 °C

Data from Harris et al. 10.1021/je2006049

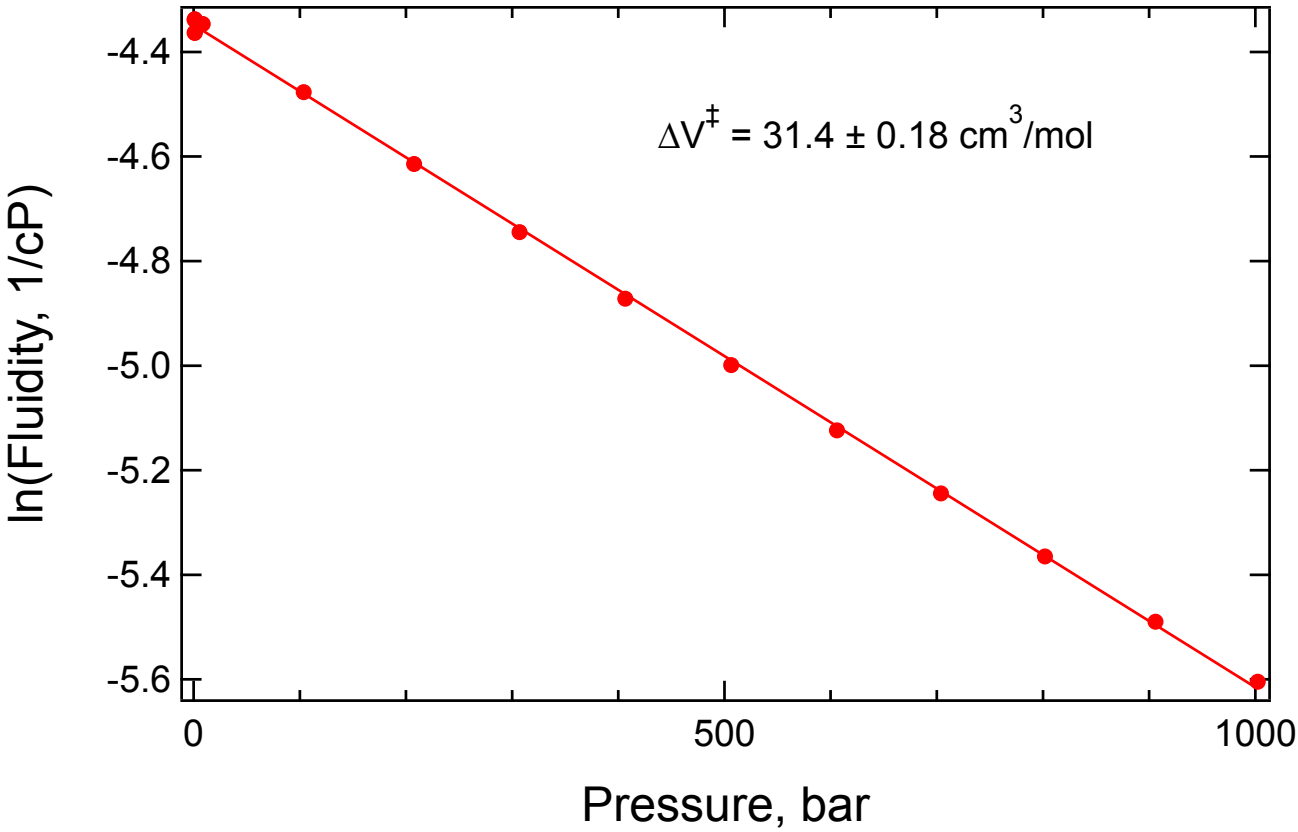

Point	Pressure	Visc, cP	ln(Fluidity)
0	1	76.54	-4.338
1	1	78.55	-4.364
2	1	78.48	-4.363
3	1	76.53	-4.338
4	1	76.63	-4.339
5	8.6	77.22	-4.347
6	103.7	87.96	-4.477
7	207.6	100.93	-4.614
8	307	114.96	-4.745
9	406.6	130.58	-4.872
10	506.3	148.26	-4.999
11	606	167.95	-5.124
12	703.9	189.46	-5.244
13	801.8	213.75	-5.365
14	906	242.18	-5.490
15	1002.3	271.62	-5.604

1/Viscosity vs. Pressure Plot for BMpyrr TFSA at 40 °C

Data from Gacino et al. 10.1016/j.jct.2012.05.007

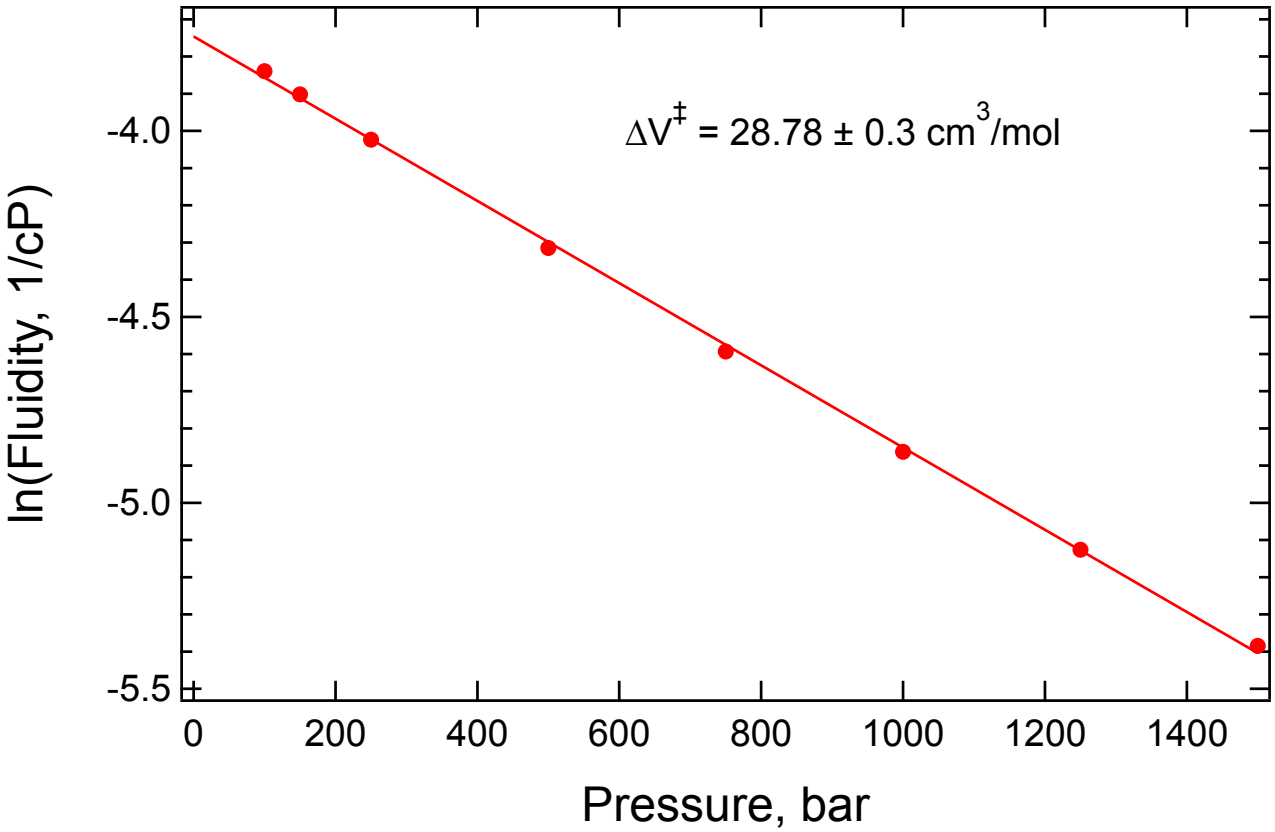

Point	Pressure	Visc, cP	ln(Fluidity)
0	100	46.5	-3.839
1	150	49.5	-3.902
2	250	55.9	-4.024
3	500	74.8	-4.315
4	750	98.8	-4.593
5	1000	129.4	-4.863
6	1250	168.4	-5.126
7	1500	218	-5.384

1/Viscosity vs. Pressure Plot for BMpyrr TFSA at 50 °C

Data from Harris et al. 10.1021/je2006049

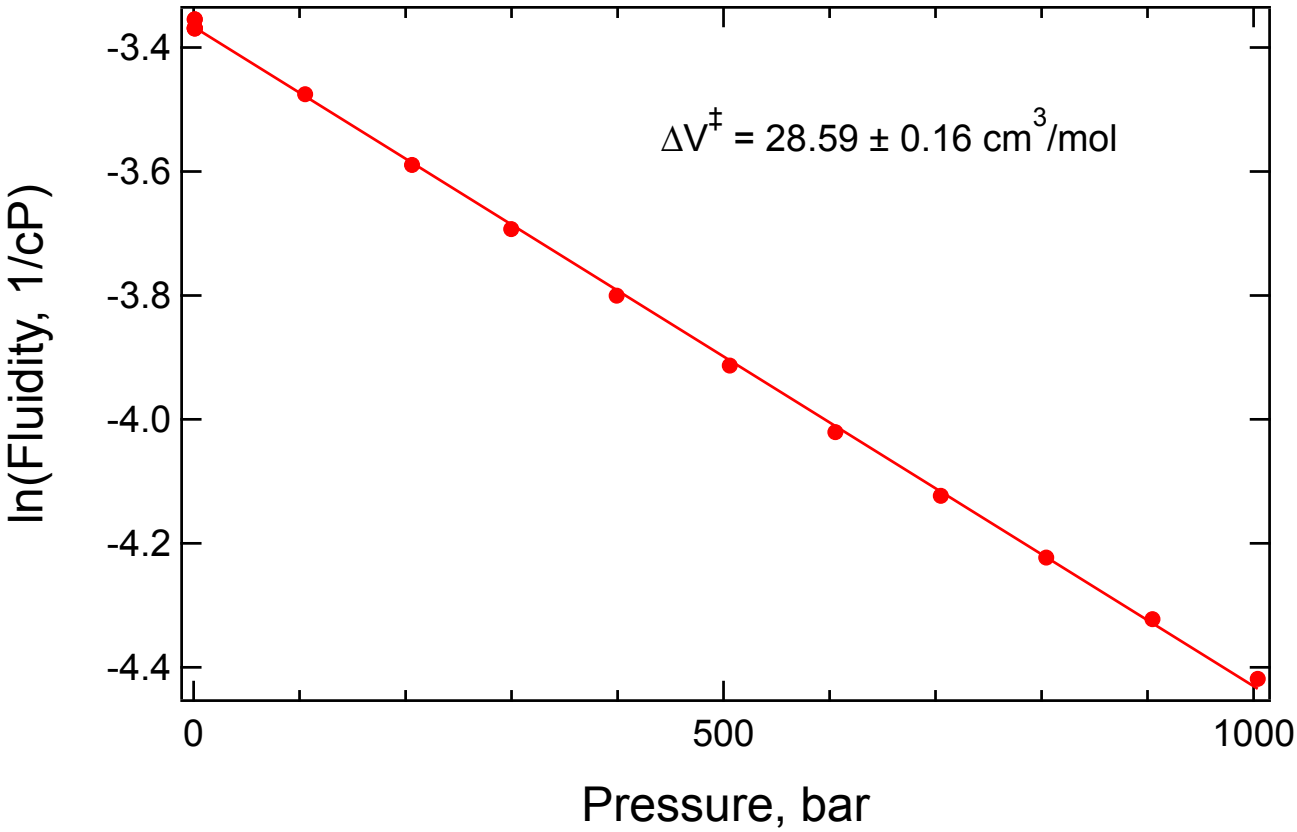

Point	Pressure	Visc, cP	ln(Fluidity)
0	1	29.06	-3.369
1	1	29.04	-3.369
2	1	28.63	-3.354
3	1	29.05	-3.369
4	1	29.03	-3.368
5	1	28.63	-3.354
6	105.2	32.31	-3.475
7	206	36.21	-3.589
8	299.7	40.16	-3.693
9	399.1	44.72	-3.800
10	505.9	50.06	-3.913
11	605.5	55.73	-4.021
12	704.9	61.77	-4.123
13	804.5	68.24	-4.223
14	904.7	75.36	-4.322
15	1004	82.99	-4.419

1/Viscosity vs. Pressure Plot for BMpyrr TFSA at 70 °C

Data from Gacino et al. 10.1016/j.jct.2012.05.007

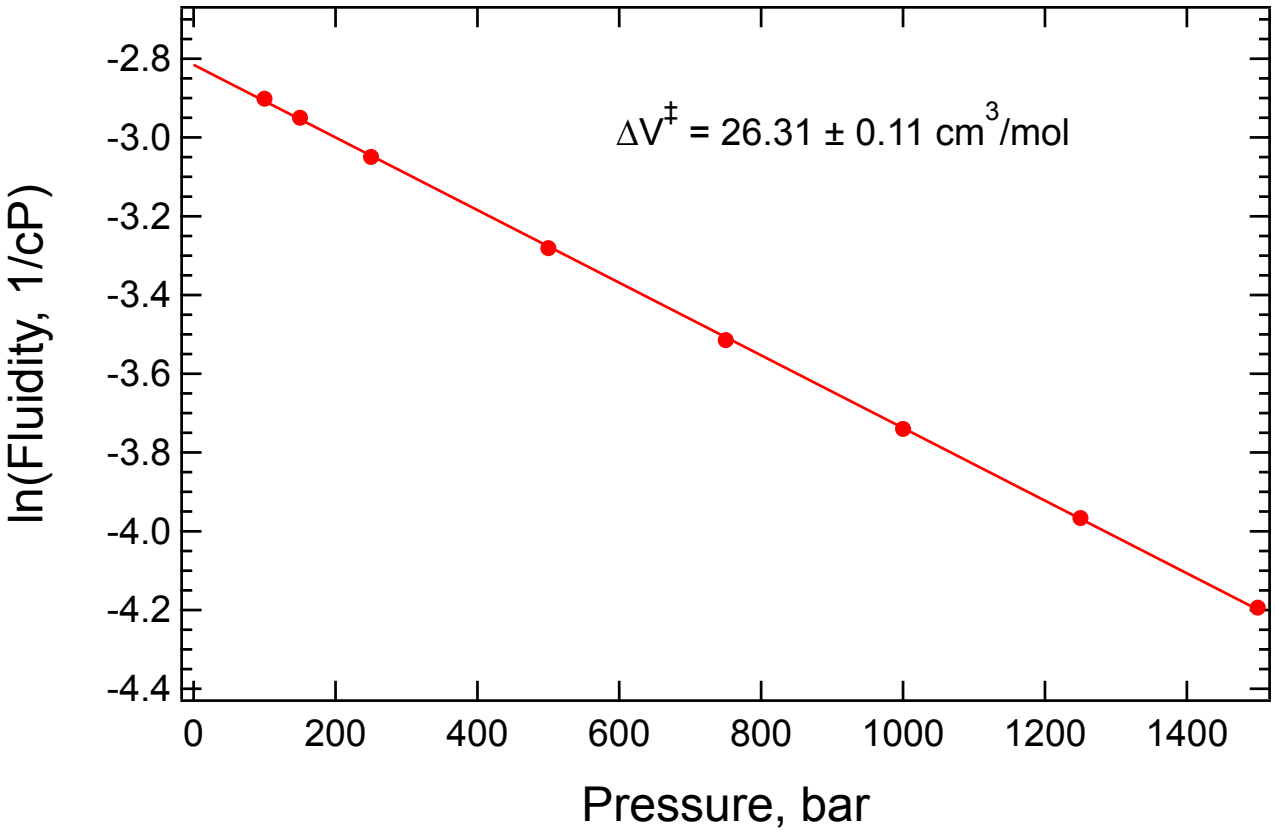

Point	Pressure	Visc, cP	ln(Fluidity)
0	100	18.2	-2.901
1	150	19.1	-2.950
2	250	21.1	-3.049
3	500	26.6	-3.281
4	750	33.6	-3.515
5	1000	42.1	-3.740
6	1250	52.8	-3.967
7	1500	66.3	-4.194

1/Viscosity vs. Pressure Plot for BMpyrr TFSA at 75 °C

Data from Harris et al. 10.1021/je2006049

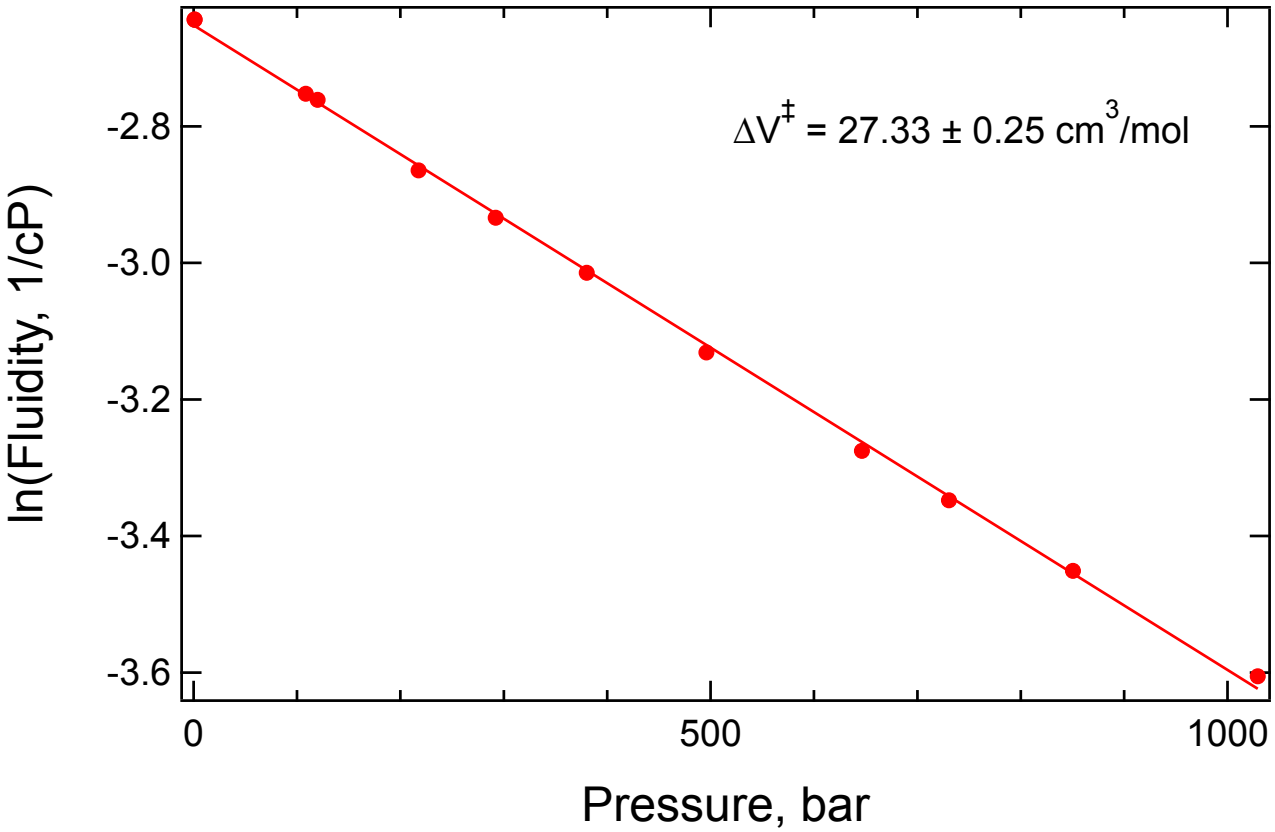

Point	Pressure	Visc, cP	ln(Fluidity)
0	1	14.07	-2.644
1	1	14.06	-2.643
2	108.5	15.68	-2.752
3	119.9	15.82	-2.761
4	217.6	17.54	-2.864
5	292.1	18.8	-2.934
6	380.2	20.38	-3.015
7	496	22.9	-3.131
8	646.3	26.45	-3.275
9	730.6	28.44	-3.348
10	850.4	31.53	-3.451
11	1029.2	36.8	-3.605

1/Viscosity vs. Pressure Plot for BMpyrr TFSA at 90 °C

Data from Gacino et al. 10.1016/j.jct.2012.05.007

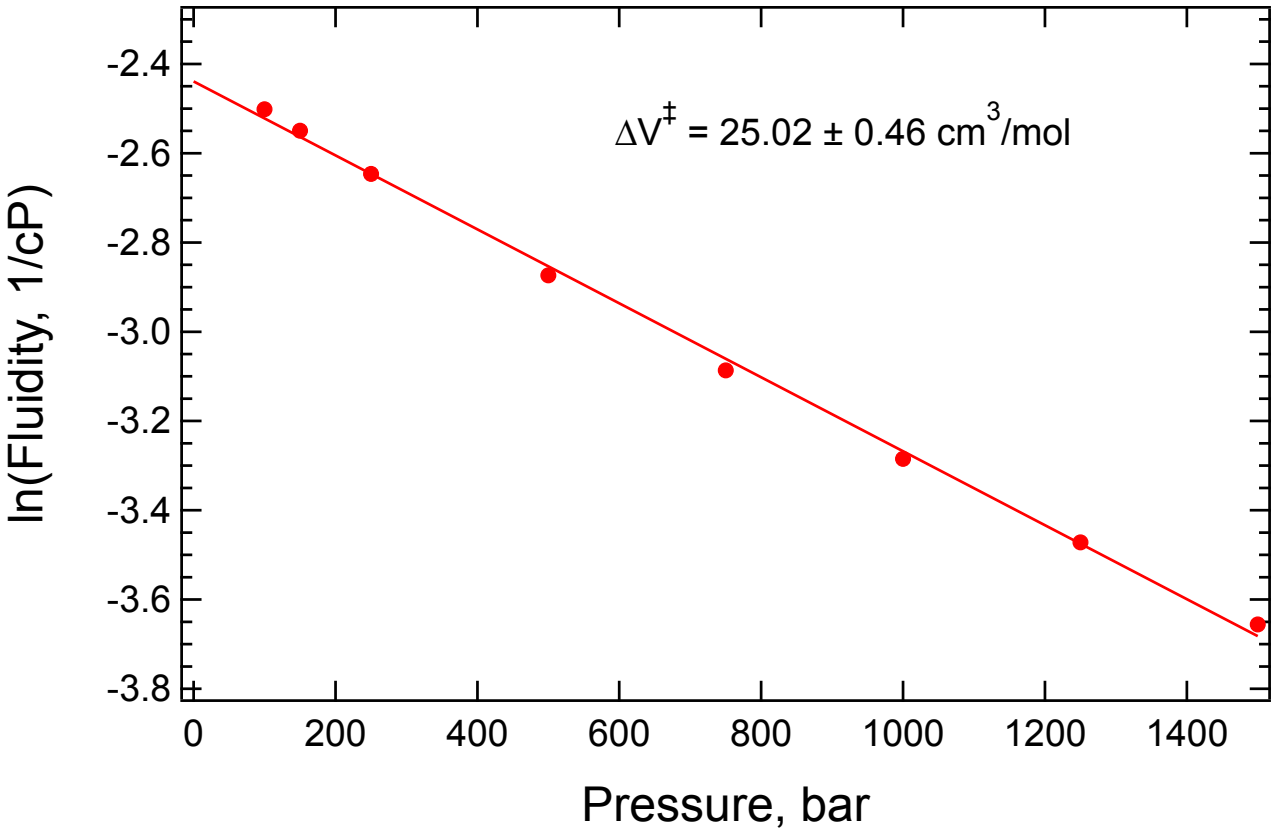

Point	Pressure	Visc, cP	ln(Fluidity)
0	100	12.2	-2.501
1	150	12.8	-2.549
2	250	14.1	-2.646
3	500	17.7	-2.874
4	750	21.9	-3.086
5	1000	26.7	-3.285
6	1250	32.2	-3.472
7	1500	38.7	-3.656

1/Viscosity vs. Pressure Plot C_{10}MIM TFSA at 25 °C

Data from Ahosseini and Scurto 10.1007/s10765-008-0497-7
Int J Thermophys (2008) 29:1222–1243

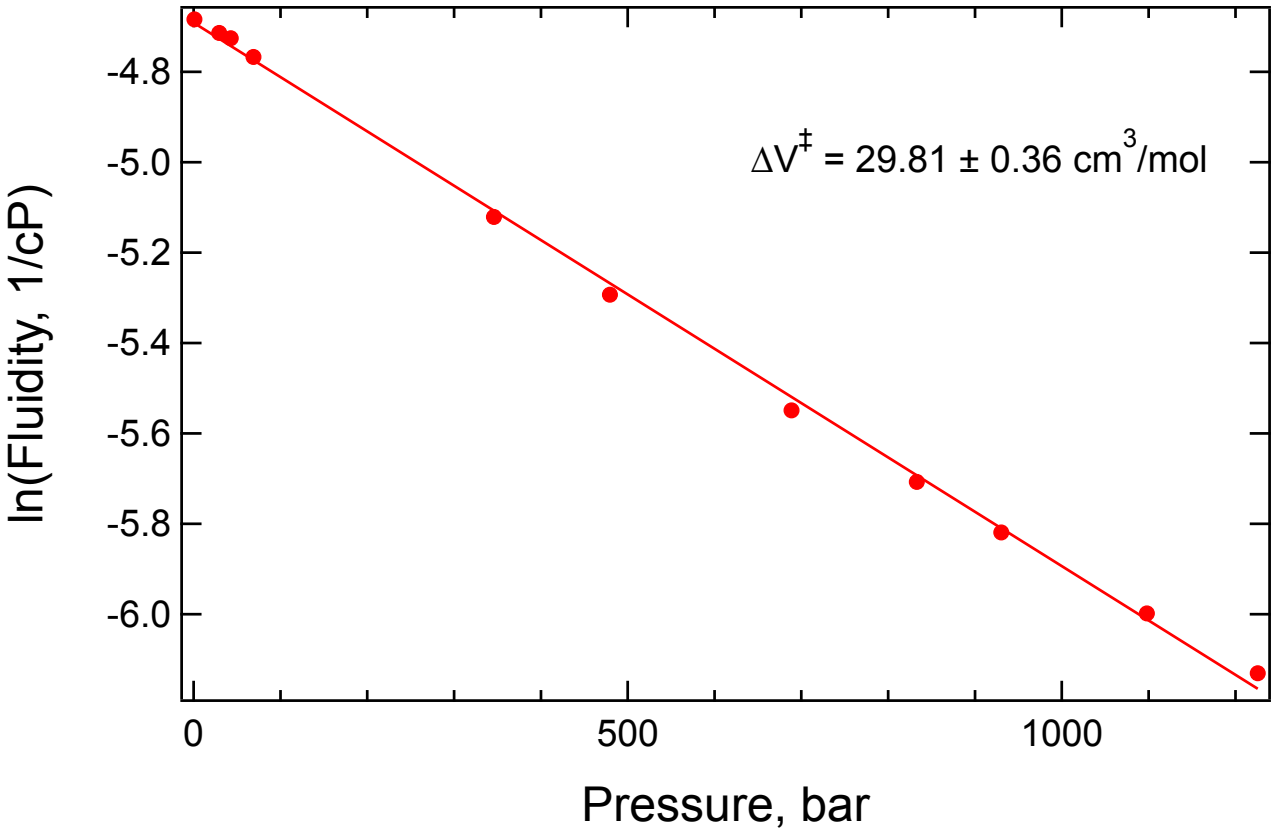

Point	Pressure	Visc, cP	ln(Fluidity)
0	1	108.2	-4.684
1	29.5	111.5	-4.714
2	42.7	112.8	-4.726
3	69	117.6	-4.767
4	346	167.5	-5.121
5	479.6	199	-5.293
6	688.7	257	-5.549
7	832.9	301.1	-5.707
8	930.3	336.7	-5.819
9	1098	402.7	-5.998
10	1225.7	459.8	-6.131

1/Viscosity vs. Pressure Plot C_{10}MIM TFSA at 50 °C

Data from Ahosseini and Scurto 10.1007/s10765-008-0497-7
Int J Thermophys (2008) 29:1222–1243

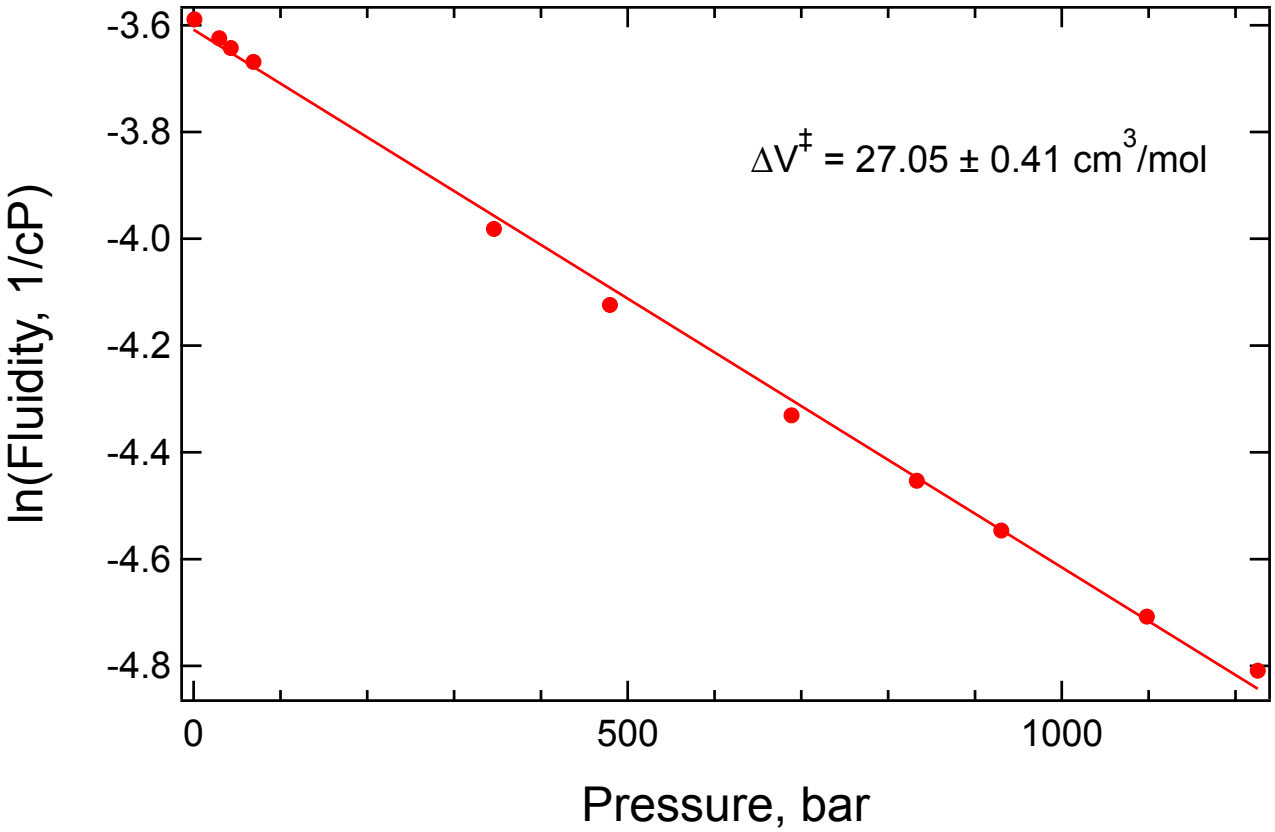

Point	Pressure	Visc, cP	ln(Fluidity)
0	1	36.2	-3.589
1	29.5	37.5	-3.624
2	42.7	38.2	-3.643
3	69	39.2	-3.669
4	346	53.6	-3.982
5	479.6	61.8	-4.124
6	688.7	76	-4.331
7	832.9	85.9	-4.453
8	930.3	94.3	-4.546
9	1098	110.8	-4.708
10	1225.7	122.6	-4.809

1/Viscosity vs. Pressure Plot C_{10}MIM TFSA at 70 °C

Data from Ahosseini and Scurto 10.1007/s10765-008-0497-7
Int J Thermophys (2008) 29:1222–1243

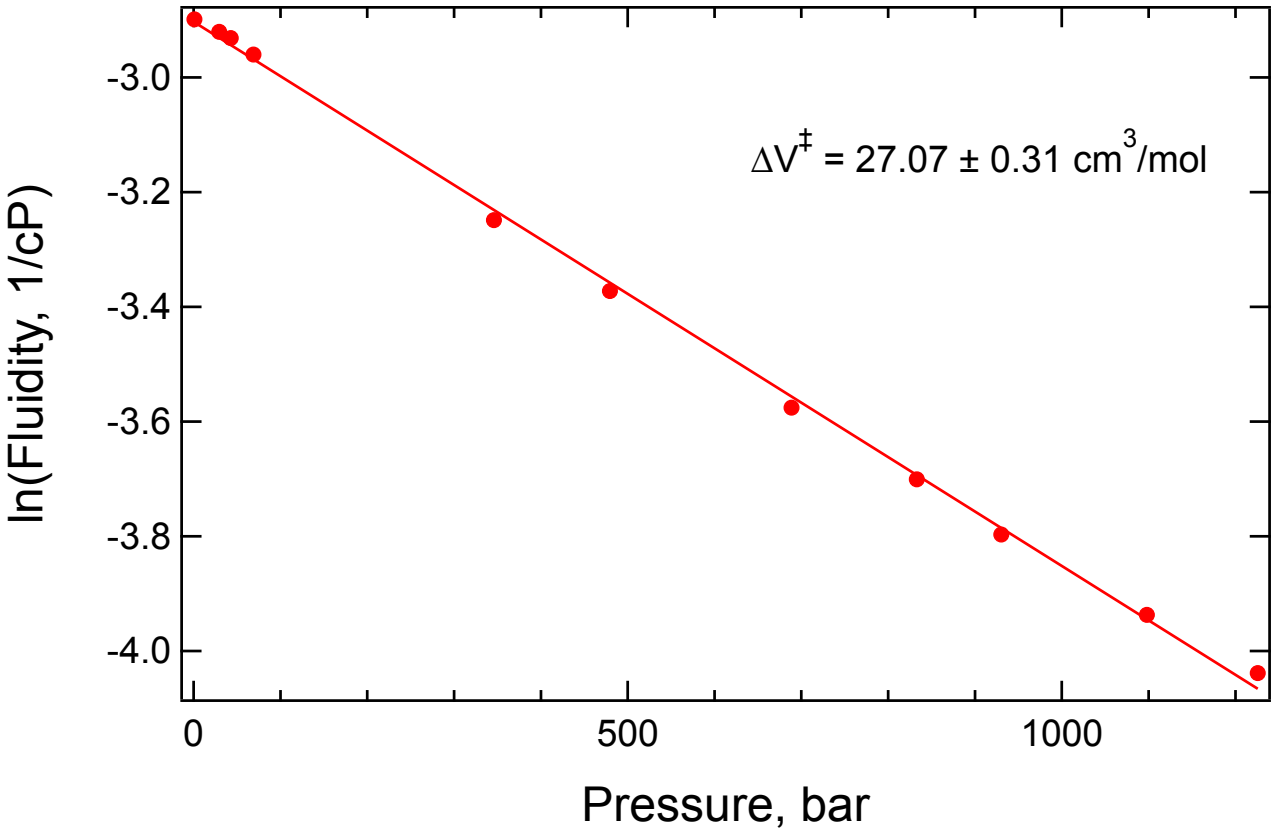

Point	Pressure	Visc, cP	ln(Fluidity)
0	1	18.15	-2.899
1	29.5	18.55	-2.920
2	42.7	18.75	-2.931
3	69	19.3	-2.960
4	346	25.76	-3.249
5	479.6	29.15	-3.372
6	688.7	35.72	-3.576
7	832.9	40.47	-3.701
8	930.3	44.56	-3.797
9	1098	51.26	-3.937
10	1225.7	56.74	-4.038

1/Viscosity vs. Pressure Plot for EMIM BF_4 at 20 °C

Data from Sanmamed et al. 10.1016/j.jct.2009.11.014

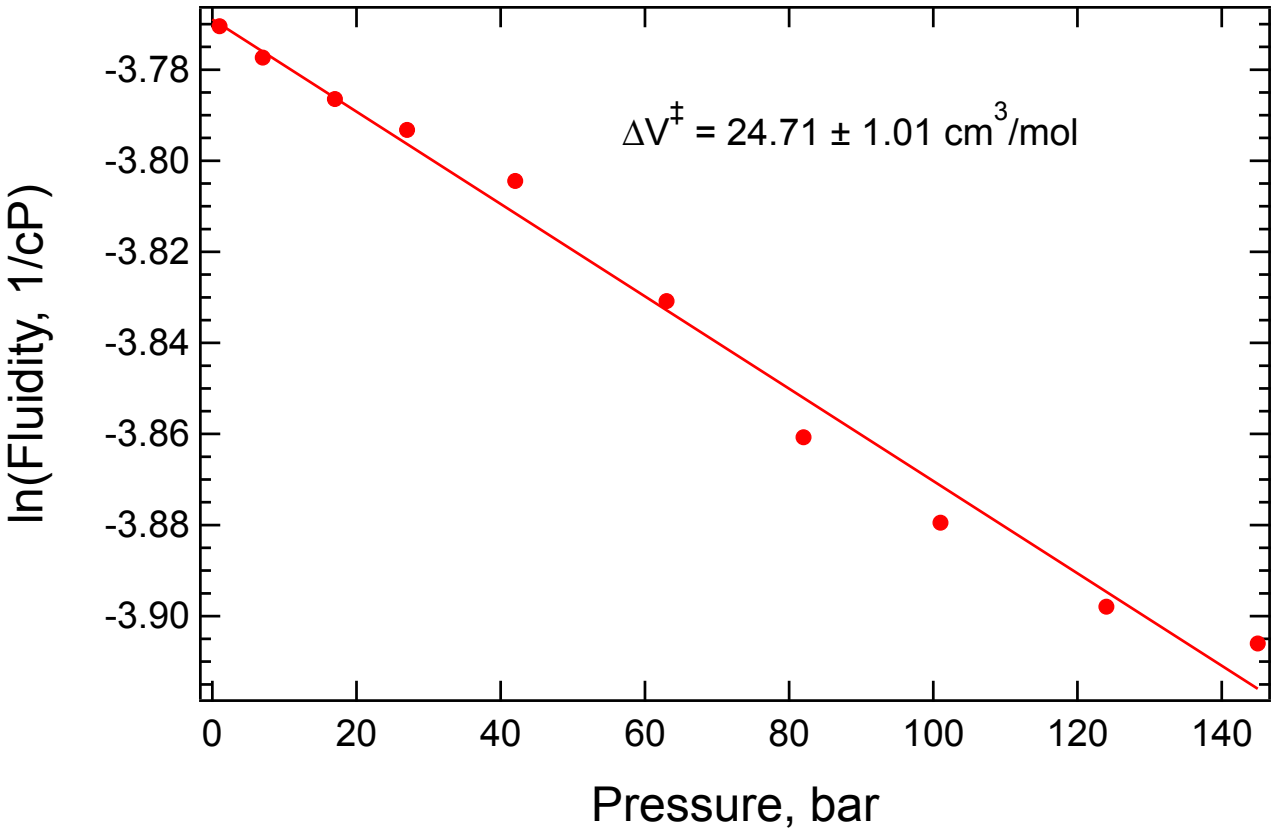

Point	Pressure	Visc, cP	ln(Fluidity)
0	1	43.4	-3.770
1	7	43.7	-3.777
2	17	44.1	-3.786
3	27	44.4	-3.793
4	42	44.9	-3.804
5	63	46.1	-3.831
6	82	47.5	-3.861
7	101	48.4	-3.879
8	124	49.3	-3.898
9	145	49.7	-3.906

1/Viscosity vs. Pressure Plot for EMIM BF_4 at 30 °C

Data from Sanmamed et al. 10.1016/j.jct.2009.11.014

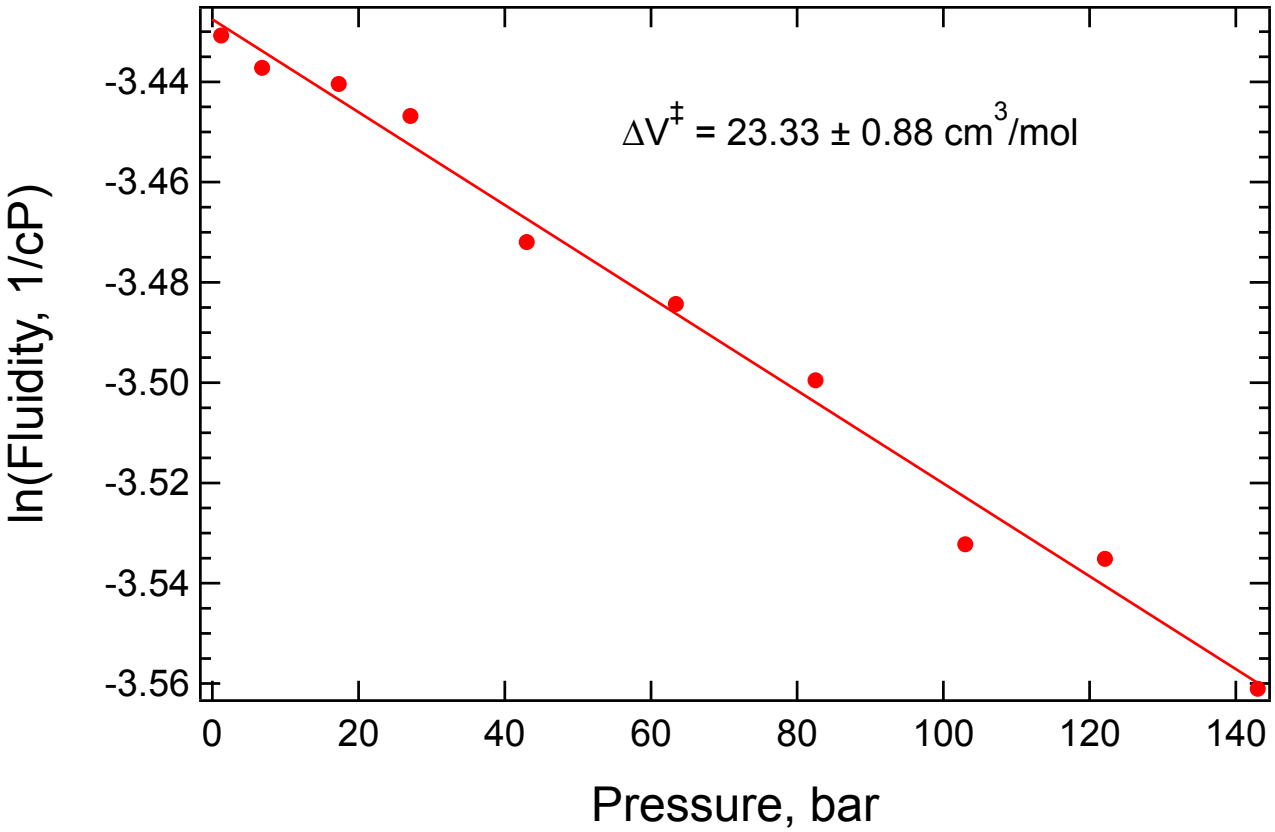

Point	Pressure	Visc, cP	ln(Fluidity)
0	1.2	30.9	-3.431
1	6.8	31.1	-3.437
2	17.3	31.2	-3.440
3	27.1	31.4	-3.447
4	43	32.2	-3.472
5	63.4	32.6	-3.484
6	82.5	33.1	-3.500
7	103	34.2	-3.532
8	122.1	34.3	-3.535
9	143	35.2	-3.561

1/Viscosity vs. Pressure Plot for EMIM $EtSO_4$ at 40 °C

Data from Gacino et al. 10.1016/j.jct.2012.05.007

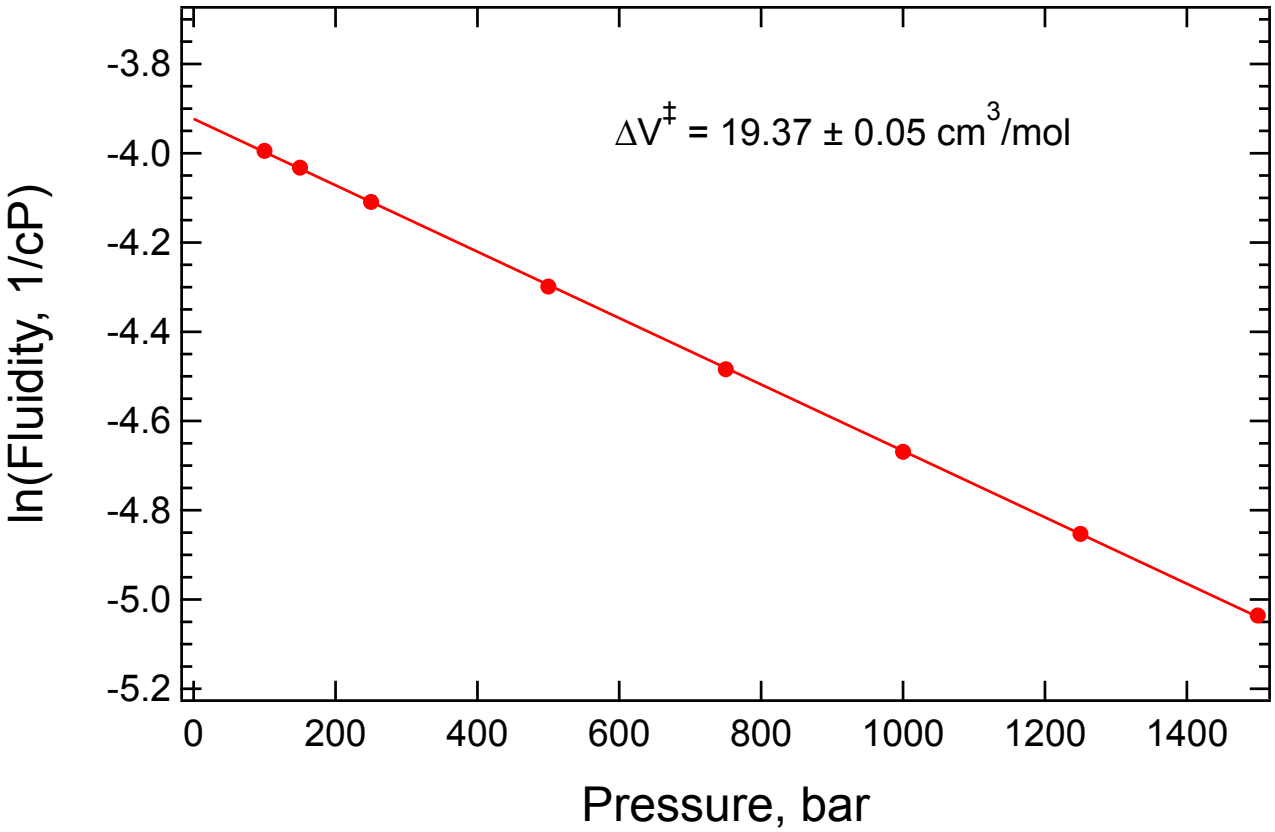

Point	Pressure	Visc, cP	ln(Fluidity)
0	100	54.3	-3.995
1	150	56.4	-4.032
2	250	60.9	-4.109
3	500	73.6	-4.299
4	750	88.6	-4.484
5	1000	106.6	-4.669
6	1250	128.1	-4.853
7	1500	153.8	-5.036

1/Viscosity vs. Pressure Plot EMIM TFSA at 25 °C

Data from Ahosseini and Scurto 10.1007/s10765-008-0497-7

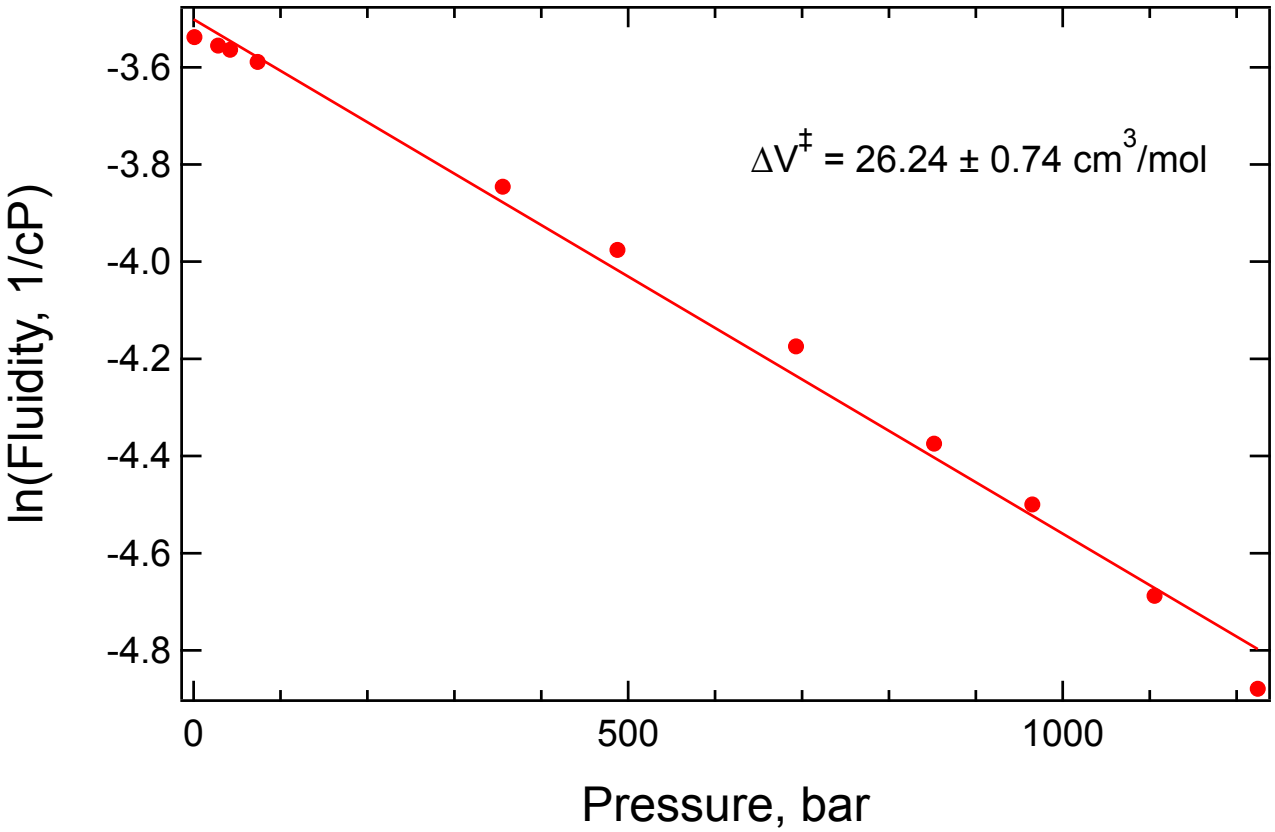

Point	Pressure	Visc, cP	ln(Fluidity)
0	1	34.4	-3.538
1	28.2	35	-3.555
2	41.9	35.3	-3.564
3	73.6	36.2	-3.589
4	355.6	46.8	-3.846
5	487.6	53.3	-3.976
6	693	65	-4.174
7	852	79.4	-4.374
8	965	90	-4.500
9	1105.5	108.6	-4.688
10	1224.3	131.5	-4.879

1/Viscosity vs. Pressure Plot EMIM TFSA at 50 °C

Data from Ahosseini and Scurto 10.1007/s10765-008-0497-7

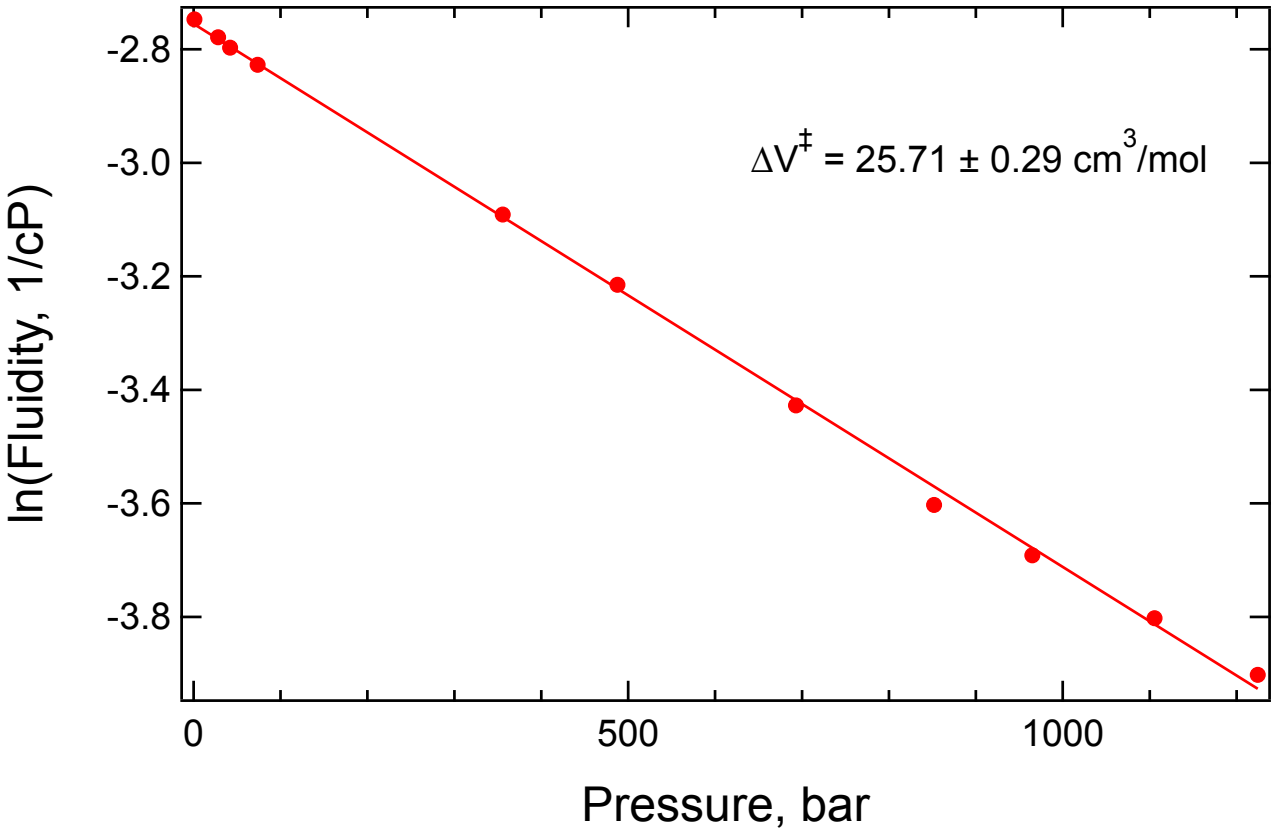

Point	Pressure	Visc, cP	ln(Fluidity)
0	1	15.6	-2.747
1	28.2	16.1	-2.779
2	41.9	16.4	-2.797
3	73.6	16.9	-2.827
4	355.6	22	-3.091
5	487.6	24.9	-3.215
6	693	30.8	-3.428
7	852	36.7	-3.603
8	965	40.1	-3.691
9	1105.5	44.8	-3.802
10	1224.3	49.5	-3.902

1/Viscosity vs. Pressure Plot EMIM TFSA at 70 °C

Data from Ahosseini and Scurto 10.1007/s10765-008-0497-7

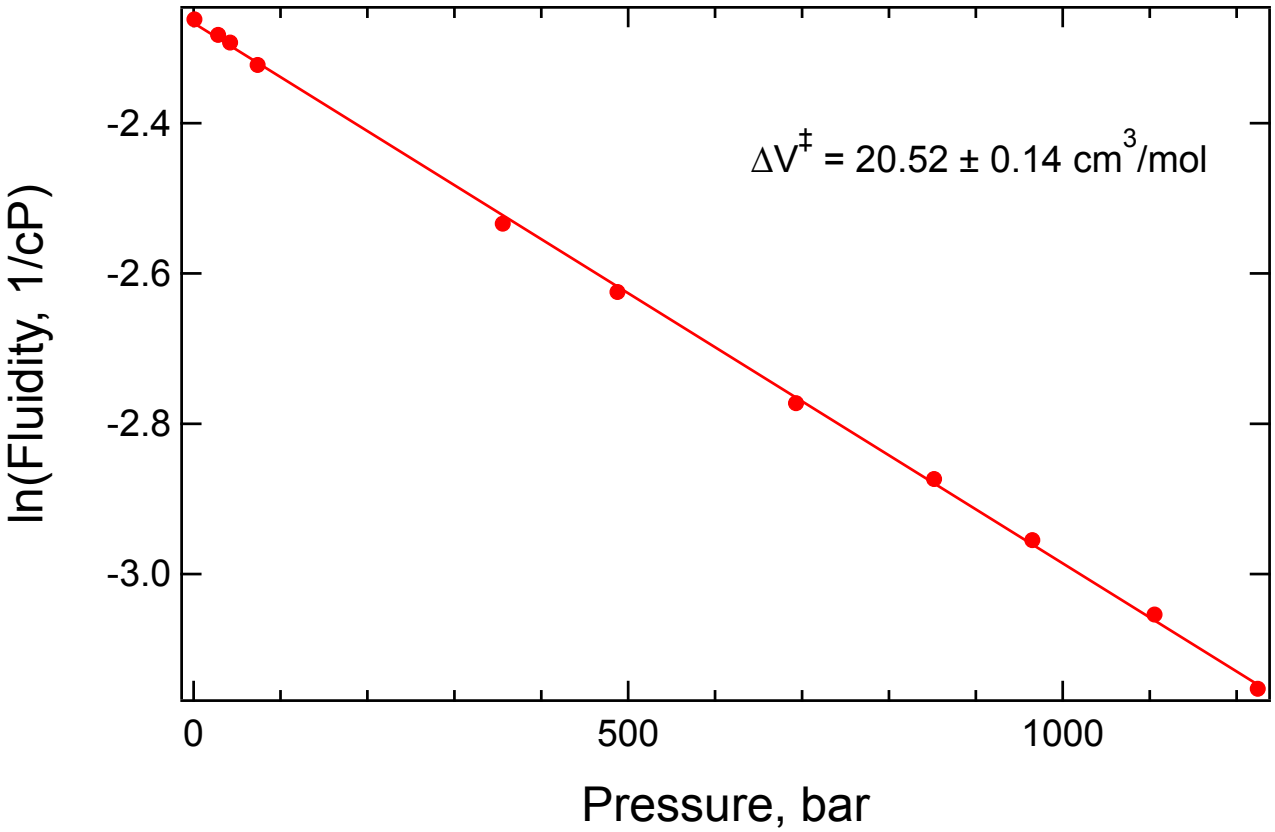

Point	Pressure	Visc, cP	ln(Fluidity)
0	1	9.6	-2.262
1	28.2	9.8	-2.282
2	41.9	9.9	-2.293
3	73.6	10.2	-2.322
4	355.6	12.6	-2.534
5	487.6	13.8	-2.625
6	693	16	-2.773
7	852	17.7	-2.874
8	965	19.2	-2.955
9	1105.5	21.2	-3.054
10	1224.3	23.4	-3.153

1/Viscosity vs. Pressure Plot (EOM)Mpyrr FAP at 40 °C

Data from Gacino et al. 10.1016/j.jct.2013.02.014

J. Chem. Thermodynamics 62 (2013) 162–169

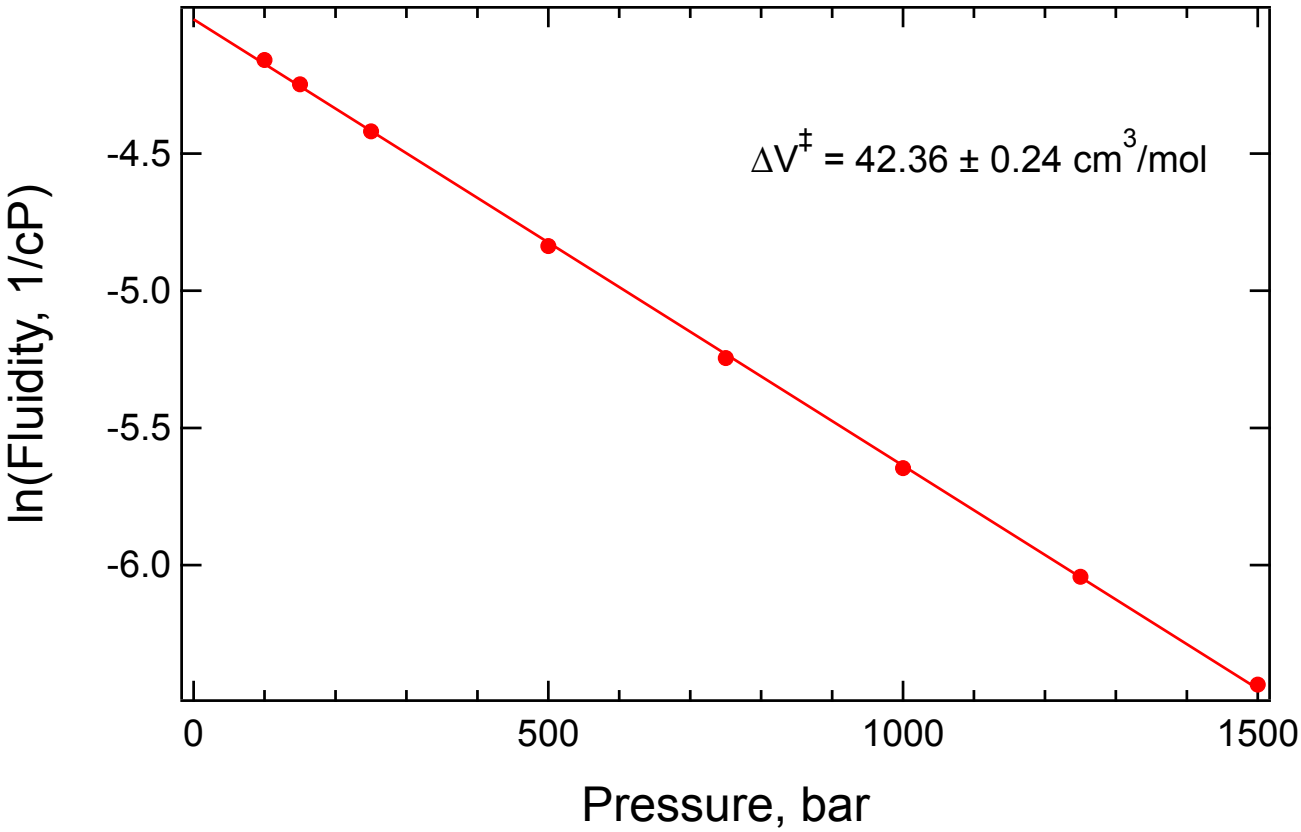

Point	Pressure	Visc, cP	ln(Fluidity)
0	100	64	-4.159
1	150	69.9	-4.247
2	250	83	-4.419
3	500	126.1	-4.837
4	750	189.7	-5.245
5	1000	283.3	-5.647
6	1250	421.1	-6.043
7	1500	623.8	-6.436

1/Viscosity vs. Pressure Plot (EOM)Mpyrr FAP at 70 °C

Data from Gacino et al. 10.1016/j.jct.2013.02.014
J. Chem. Thermodynamics 62 (2013) 162–169

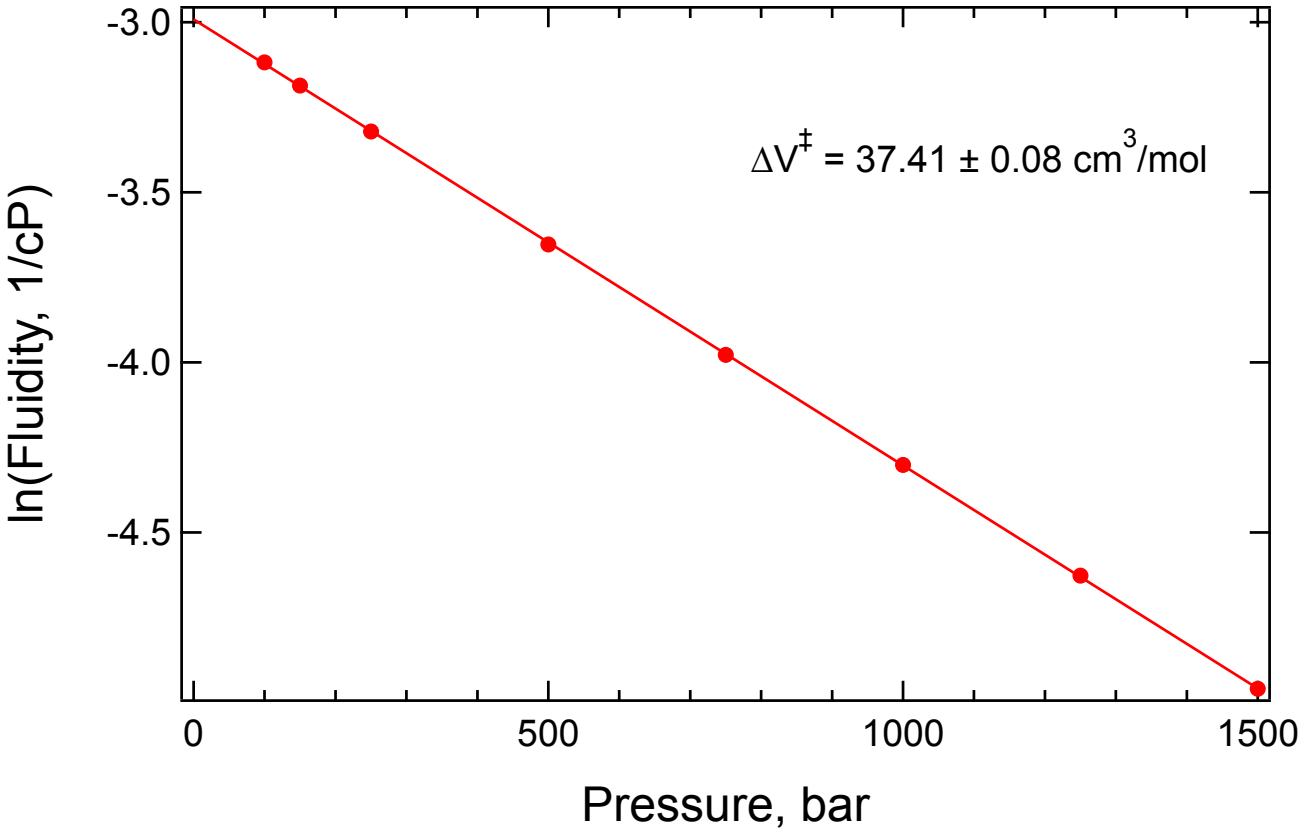

Point	Pressure	Visc, cP	ln(Fluidity)
0	100	22.6	-3.118
1	150	24.2	-3.186
2	250	27.7	-3.321
3	500	38.6	-3.653
4	750	53.4	-3.978
5	1000	73.8	-4.301
6	1250	102.2	-4.627
7	1500	142.5	-4.959

1/Viscosity vs. Pressure Plot (EOM)Mpyrr FAP at 90 °C

Data from Gacino et al. 10.1016/j.jct.2013.02.014
J. Chem. Thermodynamics 62 (2013) 162–169

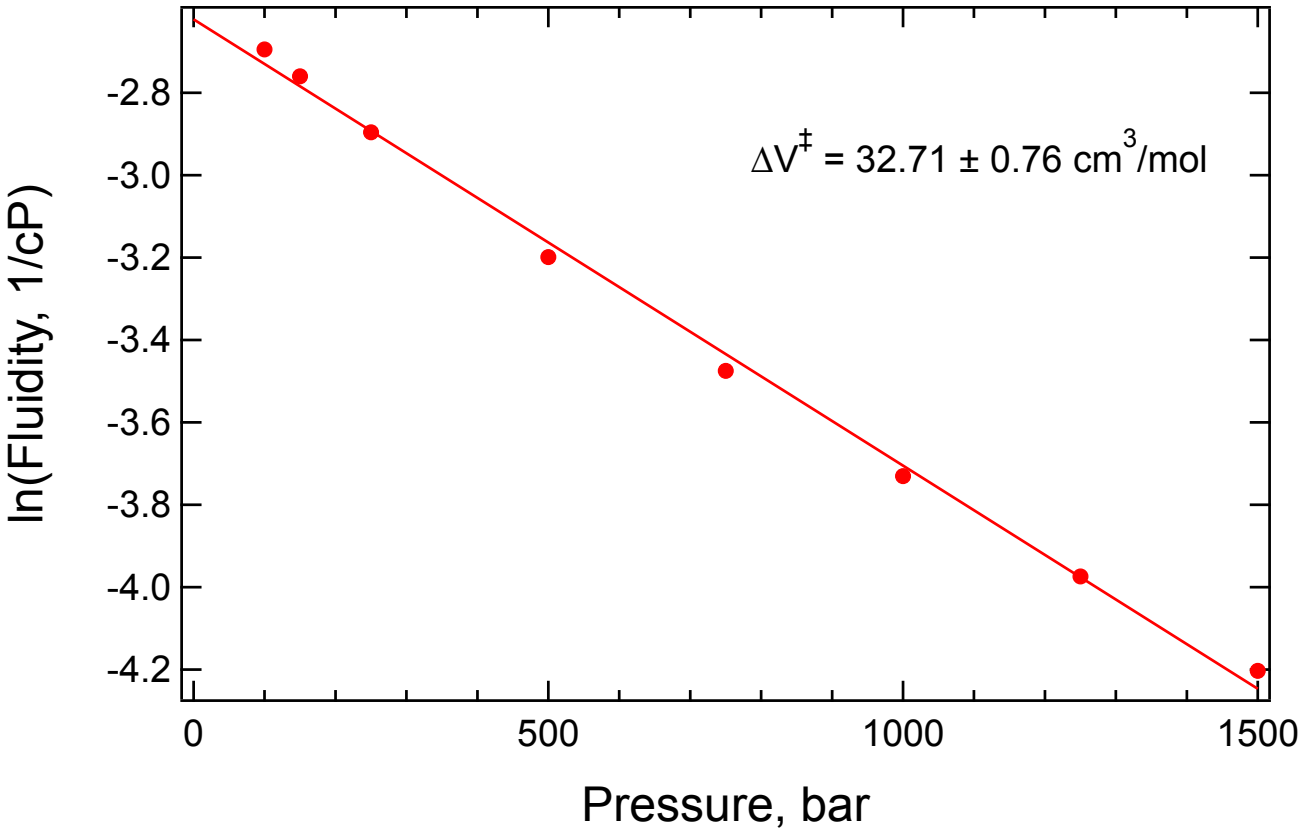

Point	Pressure	Visc, cP	ln(Fluidity)
0	100	14.8	-2.695
1	150	15.8	-2.760
2	250	18.1	-2.896
3	500	24.5	-3.199
4	750	32.3	-3.475
5	1000	41.7	-3.731
6	1250	53.2	-3.974
7	1500	66.9	-4.203

1/Viscosity vs. Pressure Plot for (EOM)Mpyrr TFSA at 40 °C

Data from Gacino et al. 10.1016/j.jct.2012.05.007

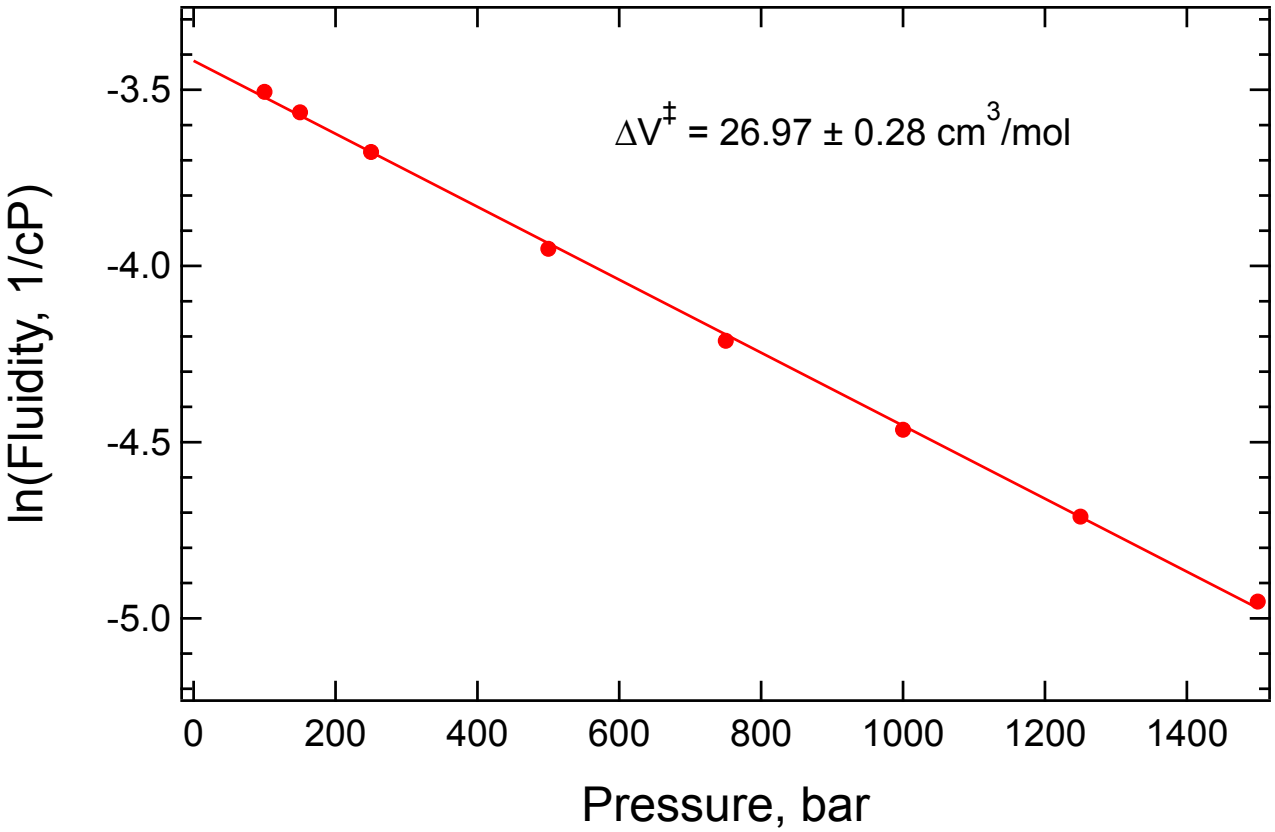

Point	Pressure	Visc, cP	ln(Fluidity)
0	100	33.3	-3.506
1	150	35.3	-3.564
2	250	39.5	-3.676
3	500	52	-3.951
4	750	67.5	-4.212
5	1000	86.9	-4.465
6	1250	111.2	-4.711
7	1500	141.5	-4.952

1/Viscosity vs. Pressure Plot for (EOM)Mpyrr TFSA at 70 °C

Data from Gacino et al. 10.1016/j.jct.2012.05.007

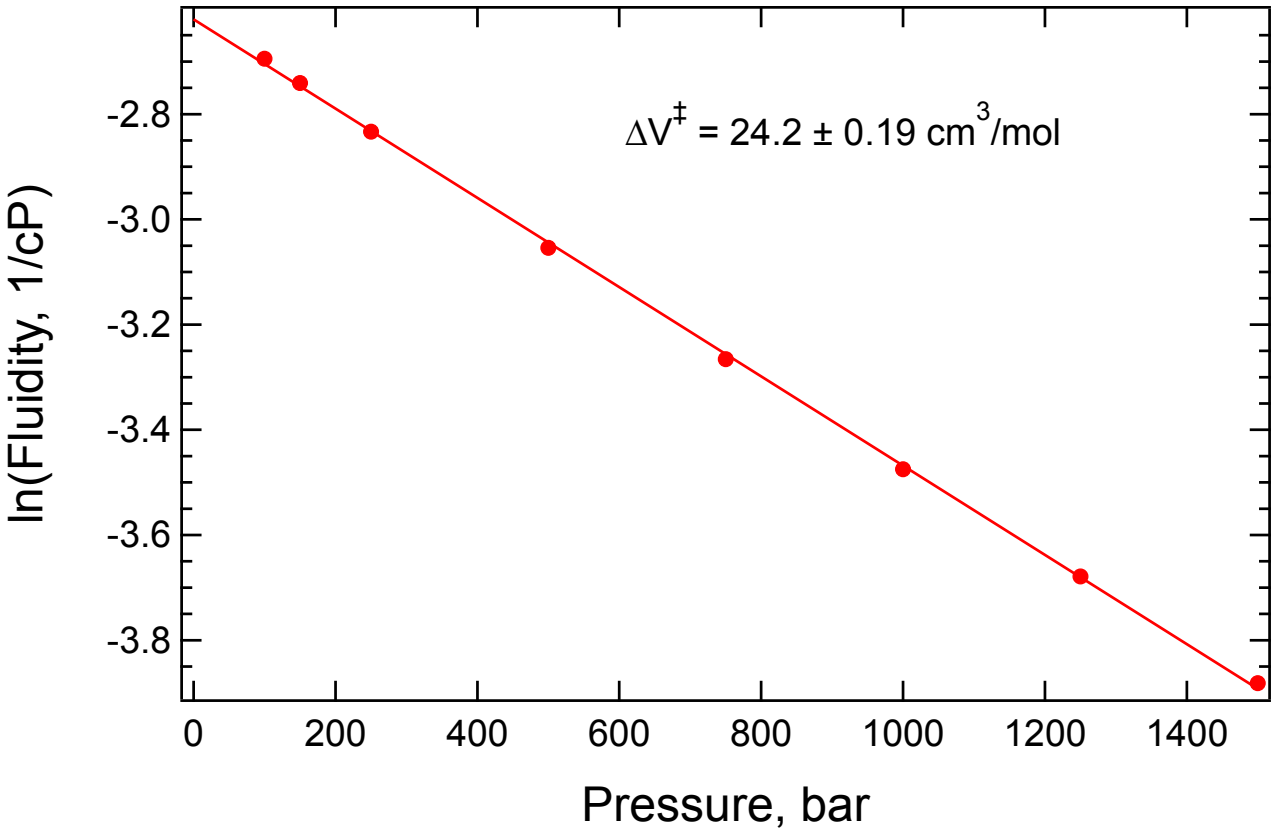

Point	Pressure	Visc, cP	ln(Fluidity)
0	100	14.8	-2.695
1	150	15.5	-2.741
2	250	17	-2.833
3	500	21.2	-3.054
4	750	26.2	-3.266
5	1000	32.3	-3.475
6	1250	39.6	-3.679
7	1500	48.5	-3.882

1/Viscosity vs. Pressure Plot for (EOM)Mpyrr TFSA at 90 °C

Data from Gacino et al. 10.1016/j.jct.2012.05.007

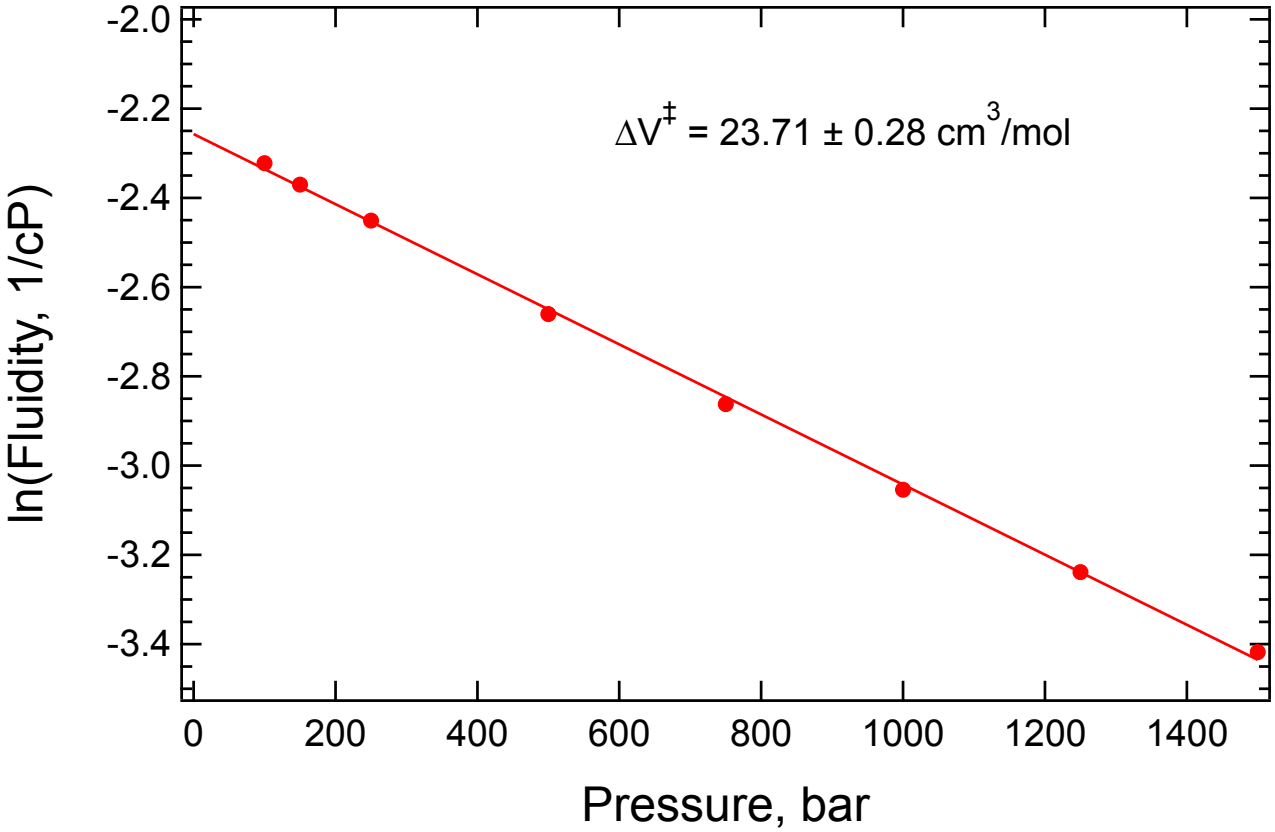

Point	Pressure	Visc, cP	ln(Fluidity)
0	100	10.2	-2.322
1	150	10.7	-2.370
2	250	11.6	-2.451
3	500	14.3	-2.660
4	750	17.5	-2.862
5	1000	21.2	-3.054
6	1250	25.5	-3.239
7	1500	30.5	-3.418

1/Viscosity vs. Pressure Plot for HMIM BF_4 at 21.7 °C

Data from Sanmamed et al. 10.1016/j.jct.2009.11.014

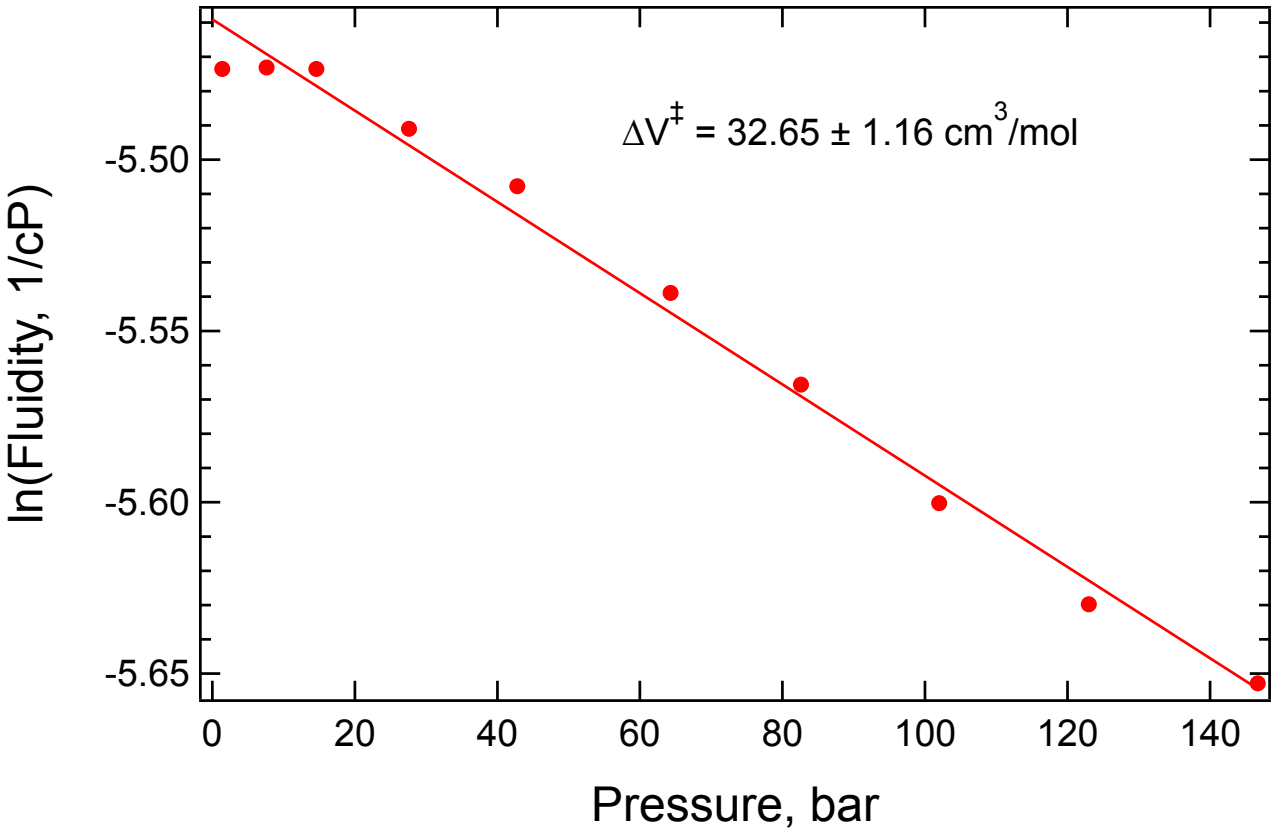

Point	Pressure	Visc, cP	ln(Fluidity)
0	1.4	238.3	-5.474
1	7.6	238.2	-5.473
2	14.6	238.3	-5.474
3	27.6	242.5	-5.491
4	42.8	246.6	-5.508
5	64.3	254.4	-5.539
6	82.6	261.3	-5.566
7	102	270.5	-5.600
8	123	278.6	-5.630
9	146.7	285.1	-5.653

1/Viscosity vs. Pressure Plot for HMIM BF_4 at 25 °C

Data from Ahosseini and Scurto 10.1007/s10765-008-0497-7

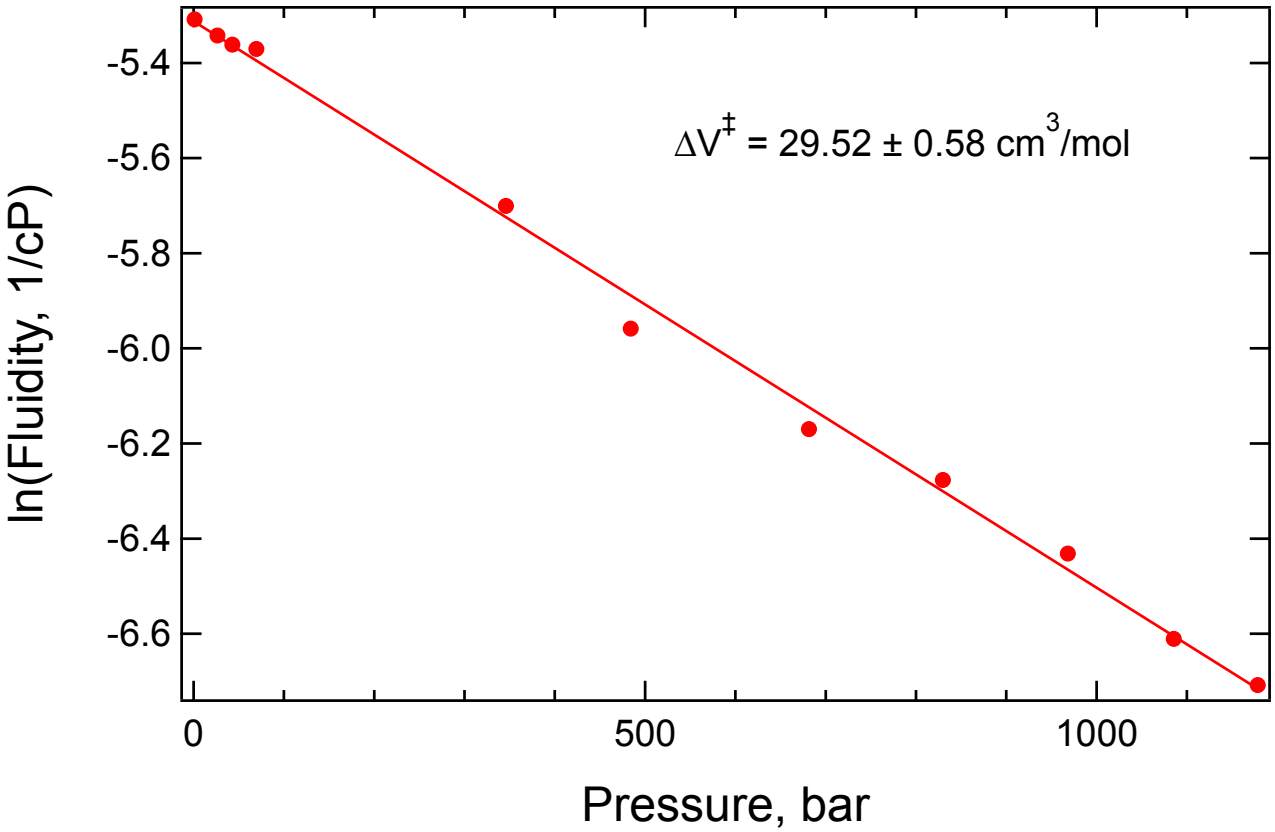

Point	Pressure	Visc, cP	ln(Fluidity)
0	1	2.02e+02	-5.308
1	26.4	2.09e+02	-5.342
2	42.9	2.13e+02	-5.361
3	69.5	2.15e+02	-5.371
4	345.9	2.99e+02	-5.700
5	484	3.87e+02	-5.958
6	681.4	4.78e+02	-6.170
7	829.7	5.32e+02	-6.277
8	968.2	6.21e+02	-6.431
9	1085.5	7.43e+02	-6.611
10	1178.5	8.19e+02	-6.708

1/Viscosity vs. Pressure Plot for HMIM BF_4 at 50 °C

Data from Ahosseini and Scurto 10.1007/s10765-008-0497-7

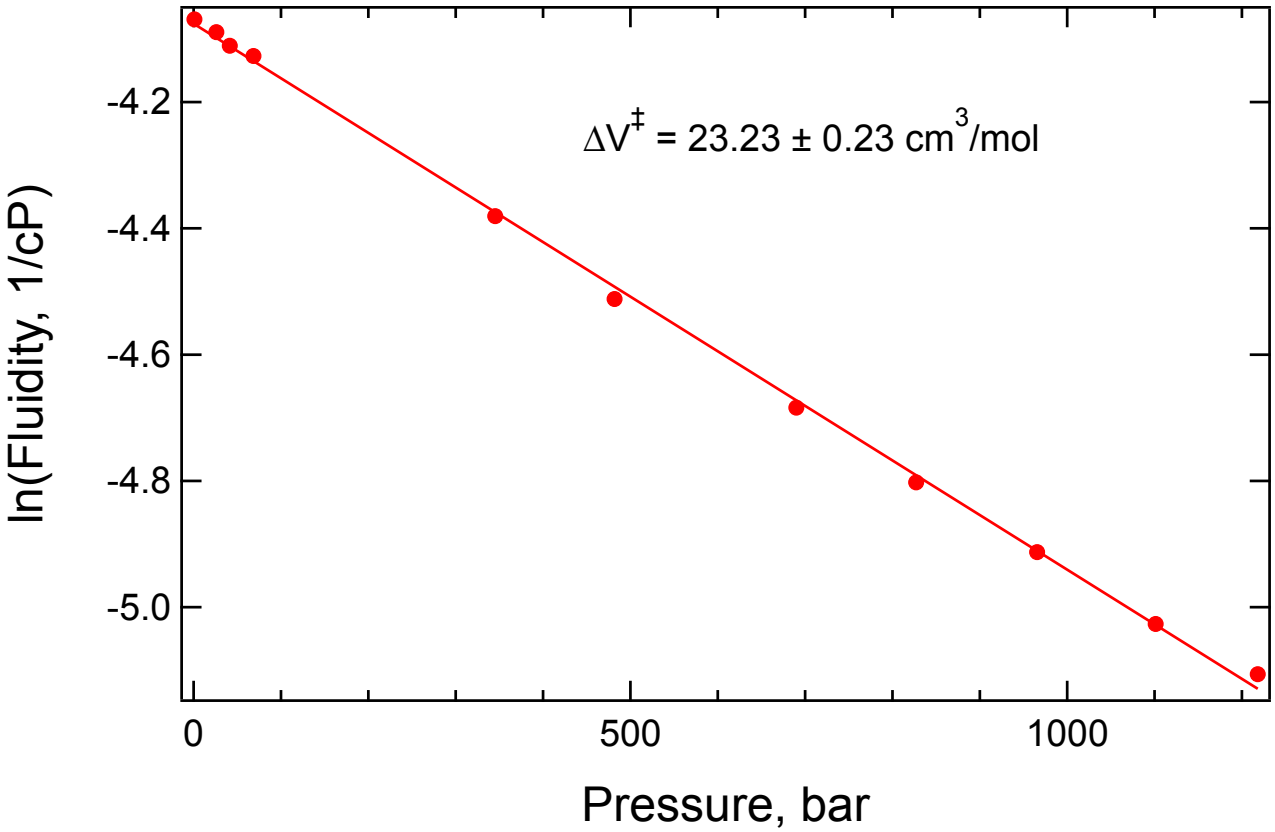

Point	Pressure	Visc, cP	ln(Fluidity)
0	1	58.5	-4.069
1	26	59.7	-4.089
2	41.3	61	-4.111
3	68.5	62	-4.127
4	345.2	79.9	-4.381
5	481.8	91.1	-4.512
6	689.9	108.2	-4.684
7	827.1	121.8	-4.802
8	965.5	136	-4.913
9	1101.2	152.4	-5.027
10	1218.1	165	-5.106

1/Viscosity vs. Pressure Plot for HMIM BF_4 at 70 °C

Data from Ahosseini and Scurto 10.1007/s10765-008-0497-7

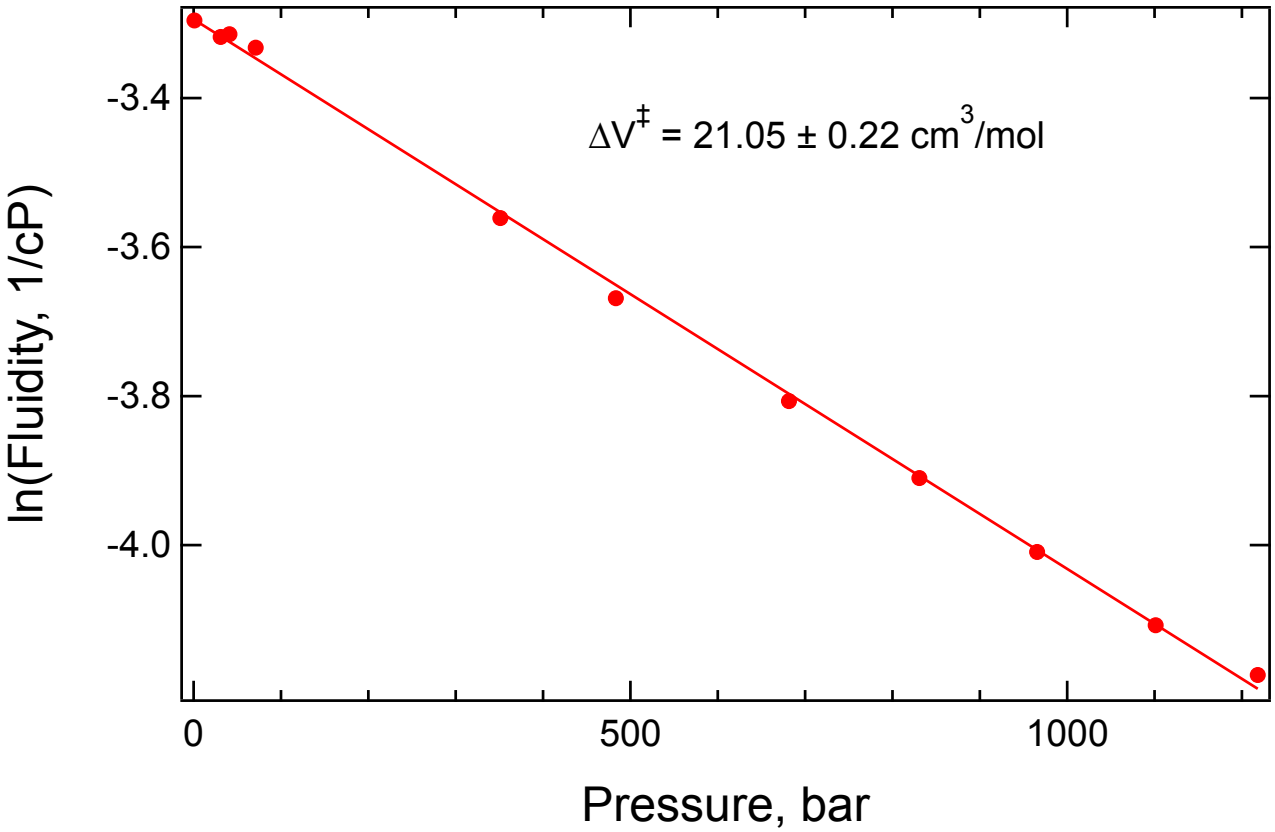

Point	Pressure	Visc, cP	ln(Fluidity)
0	1	27	-3.296
1	31	27.6	-3.318
2	41	27.5	-3.314
3	71	28	-3.332
4	351	35.2	-3.561
5	483.4	39.2	-3.669
6	681.4	45	-3.807
7	830.8	49.9	-3.910
8	965.5	55.1	-4.009
9	1101.2	60.8	-4.108
10	1218.1	65	-4.174

1/Viscosity vs. Pressure Plot for HMIM PF_6 at 25 °C

Data from Ahosseini and Scurto 10.1007/s10765-008-0497-7

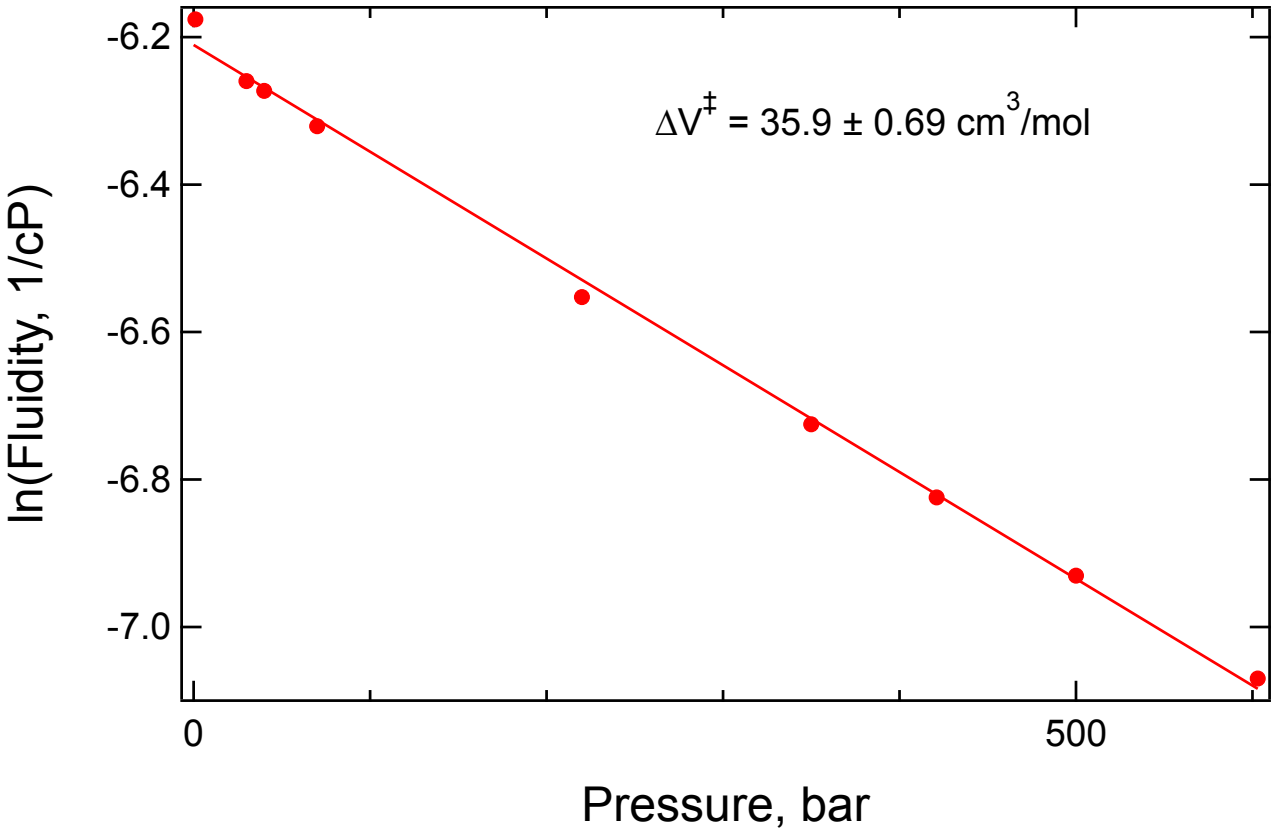

Point	Pressure	Visc, cP	ln(Fluidity)
0	1	481	-6.176
1	29.9	523	-6.260
2	40	530	-6.273
3	70	556	-6.321
4	220	701	-6.553
5	350	833	-6.725
6	421	920	-6.824
7	500	1023	-6.930
8	603	1176	-7.070

1/Viscosity vs. Pressure Plot for HMIM PF_6 at 25 °C

Data from Harris et al. 10.1021/je700032n
J. Chem. Eng. Data 2007, 52, 1080-1085

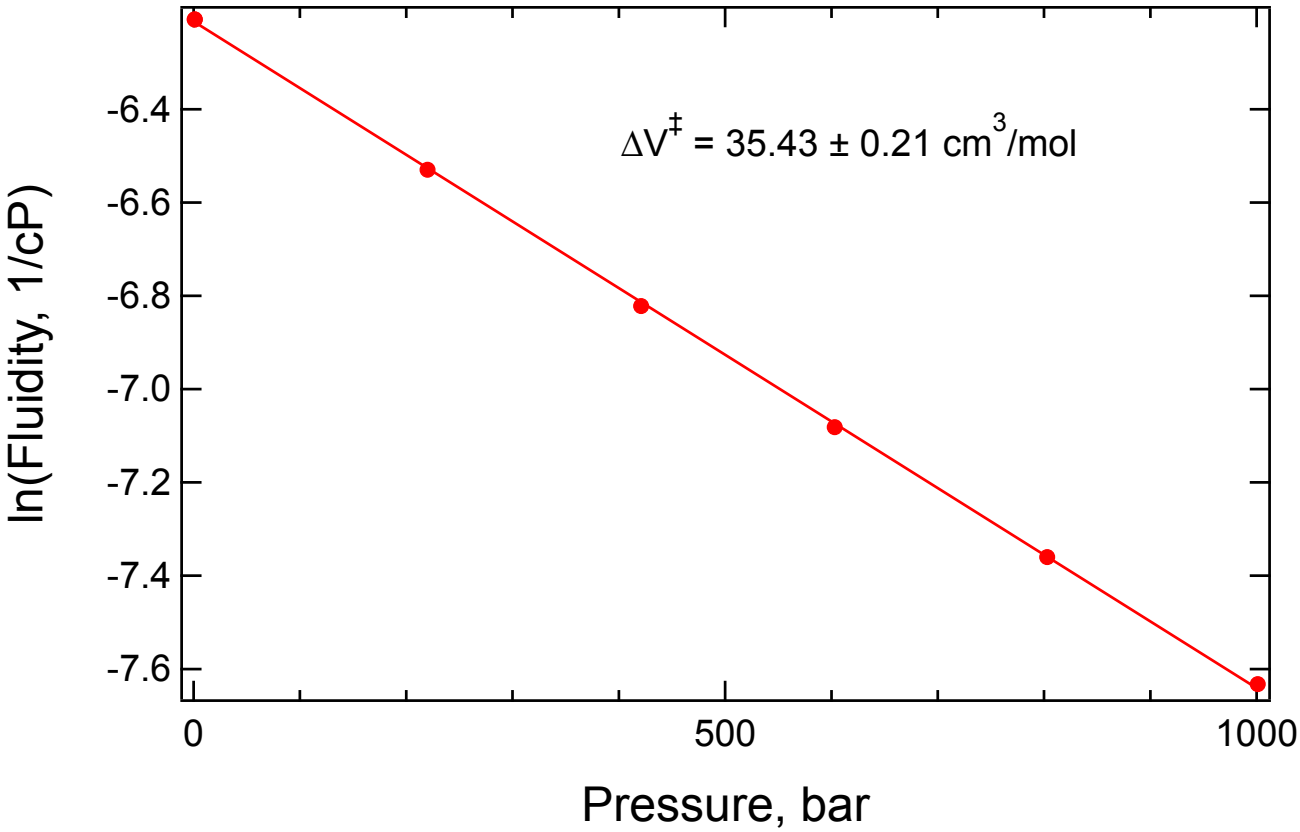

Point	Pressure	Visc, cP	ln(Fluidity)
0	1	496.5	-6.208
1	1	496.4	-6.207
2	220	685.3	-6.530
3	421	917.7	-6.822
4	603	1190	-7.082
5	803	1572	-7.360
6	1001	2064	-7.632

1/Viscosity vs. Pressure Plot for HMIM PF_6 at 50 °C

Data from Ahosseini and Scurto 10.1007/s10765-008-0497-7

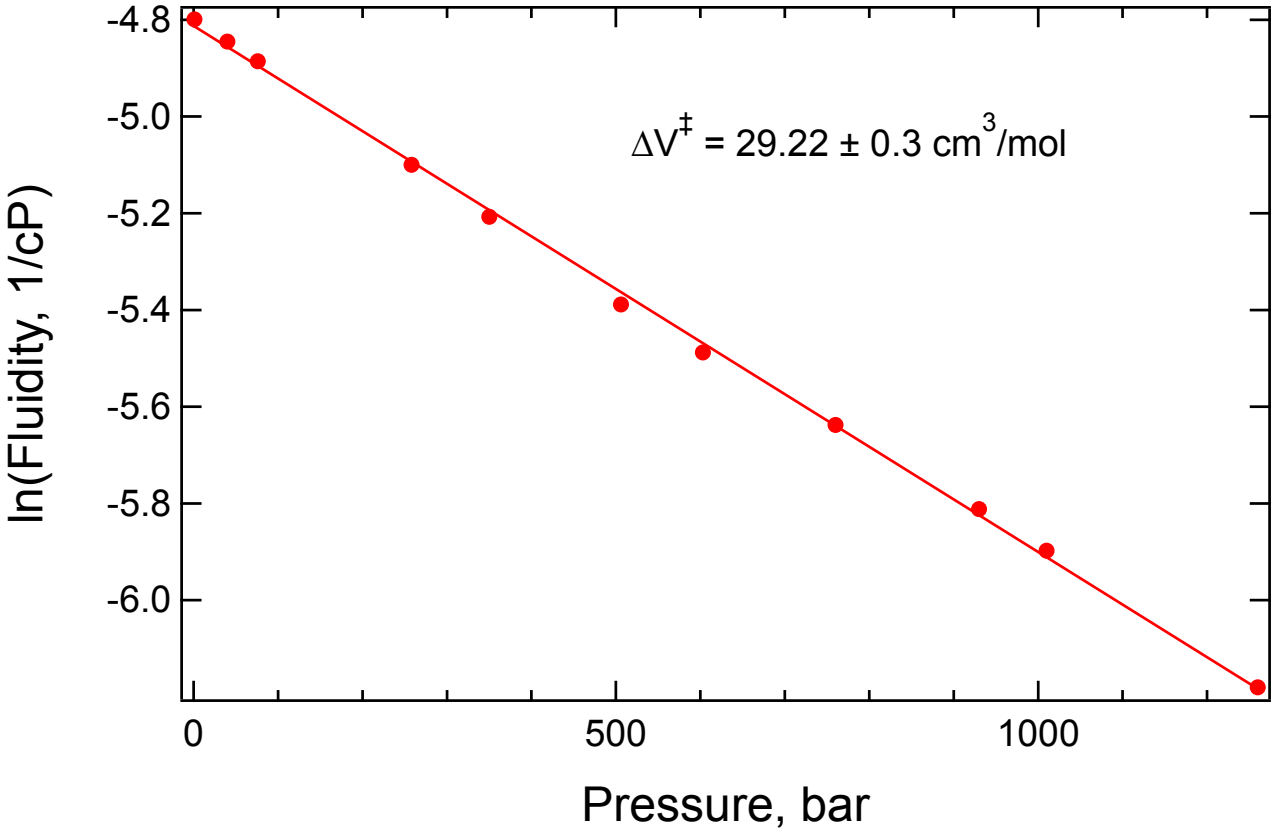

Point	Pressure	Visc, cP	ln(Fluidity)
0	1	121.4	-4.799
1	40	127.1	-4.845
2	76	132.4	-4.886
3	258	164	-5.100
4	350	182.6	-5.207
5	506	218.9	-5.389
6	603	241.7	-5.488
7	760	280.8	-5.638
8	930	334.2	-5.812
9	1010	364.2	-5.898
10	1260	483.1	-6.180

1/Viscosity vs. Pressure Plot for HMIM PF_6 at 50 °C

Data from Harris et al. 10.1021/je700032n
J. Chem. Eng. Data 2007, 52, 1080-1085

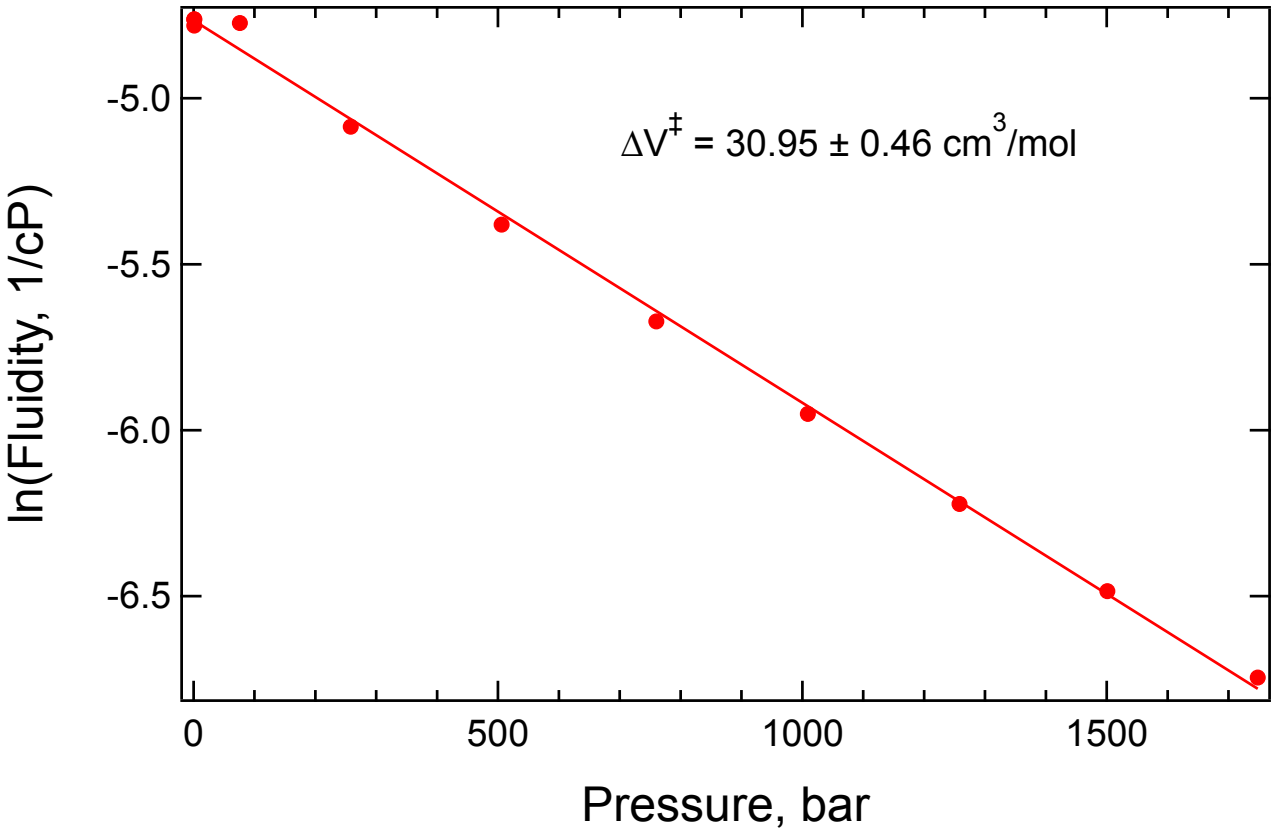

Point	Pressure	Visc, cP	ln(Fluidity)
0	1	119.2	-4.781
1	1	117	-4.762
2	1	117	-4.762
3	76	118.3	-4.773
4	258	161.7	-5.086
5	506	217.1	-5.380
6	760	290.7	-5.672
7	1009	384	-5.951
8	1258	503.9	-6.222
9	1501	655	-6.485
10	1748	850.1	-6.745

1/Viscosity vs. Pressure Plot for HMIM PF_6 at 60 °C

Data from Harris et al. 10.1021/je700032n
J. Chem. Eng. Data 2007, 52, 1080-1085

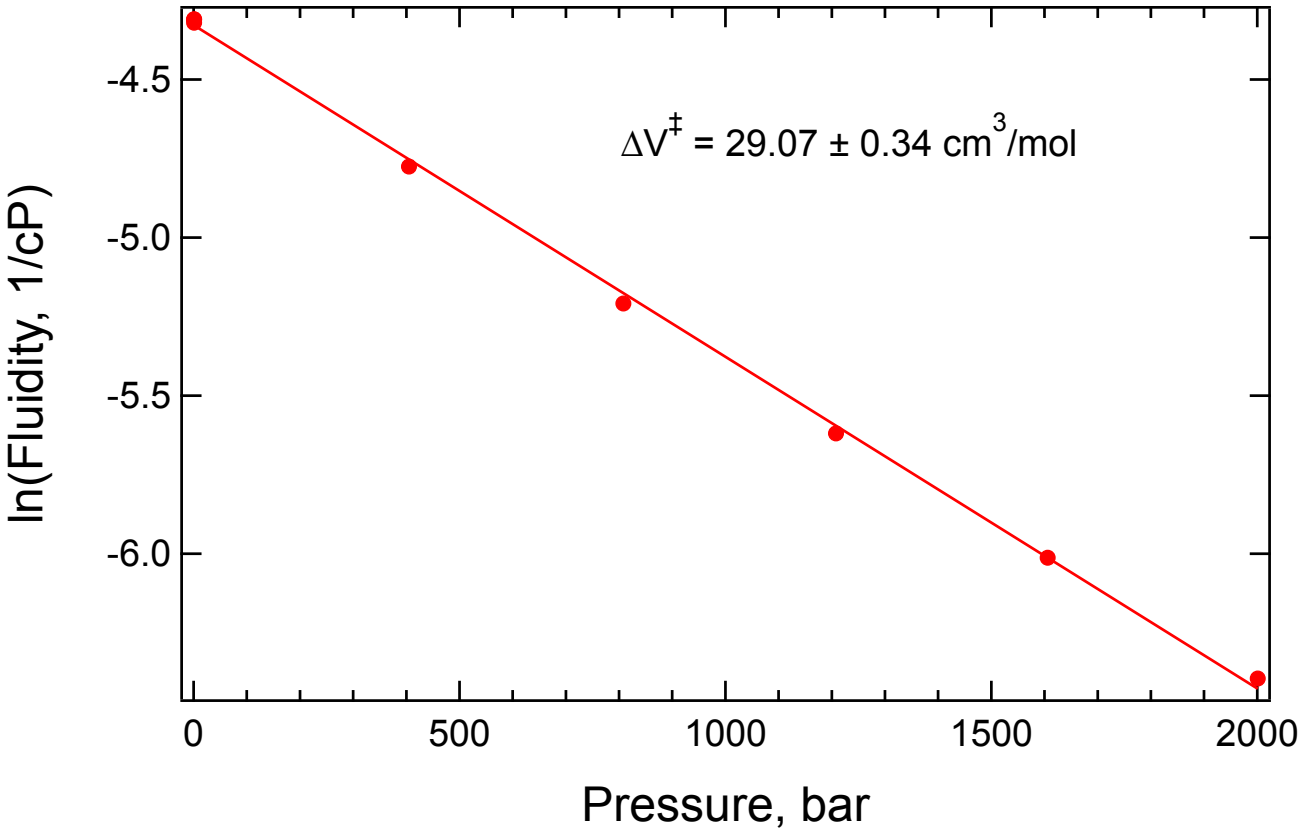

Point	Pressure	Visc, cP	ln(Fluidity)
0	1	75.2	-4.320
1	1	74.4	-4.309
2	1	74.4	-4.309
3	405	118.5	-4.775
4	808	182.8	-5.208
5	1208	275.7	-5.619
6	1606	408.7	-6.013
7	2001	598.9	-6.395

1/Viscosity vs. Pressure Plot for HMIM PF_6 at 70 °C

Data from Ahosseini and Scurto 10.1007/s10765-008-0497-7

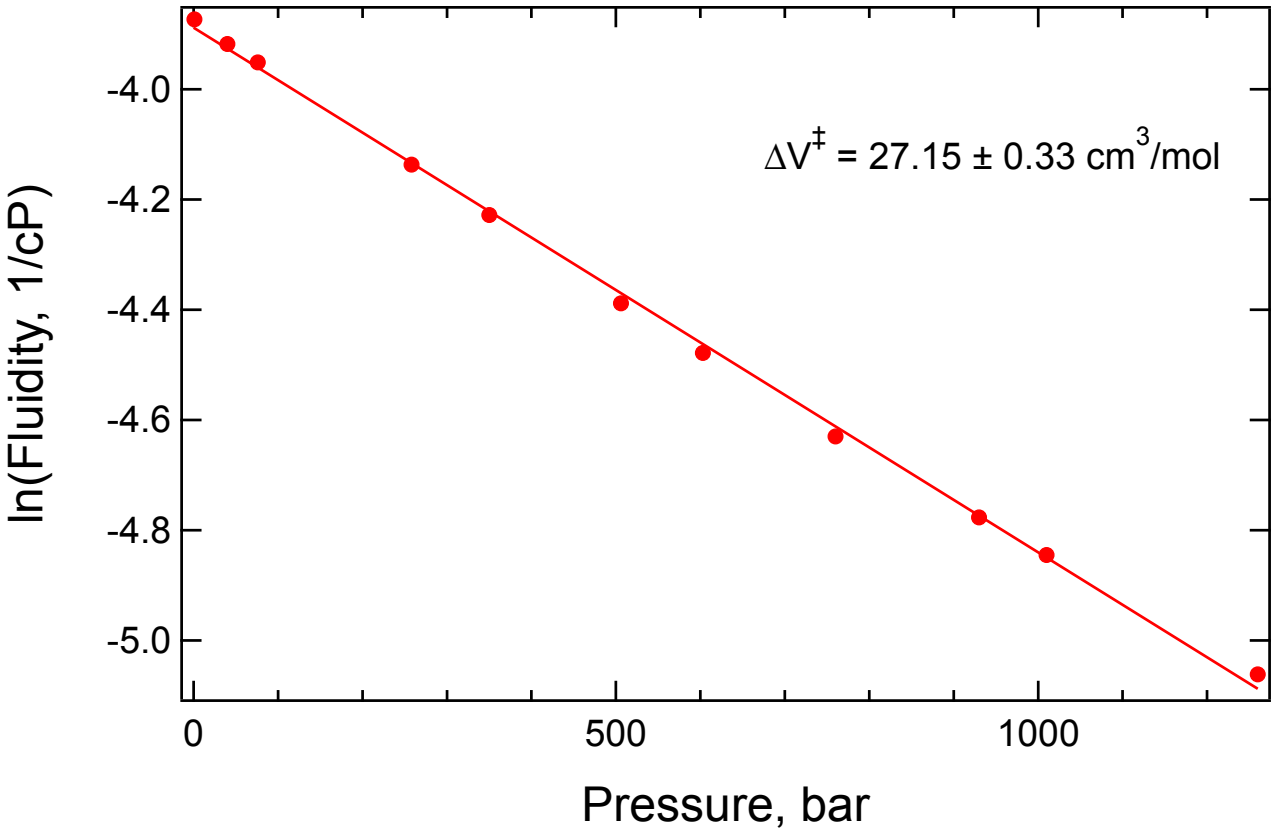

Point	Pressure	Visc, cP	ln(Fluidity)
0	1	48.1	-3.873
1	40	50.3	-3.918
2	76	52	-3.951
3	258	62.6	-4.137
4	350	68.6	-4.228
5	506	80.5	-4.388
6	603	88.1	-4.478
7	760	102.5	-4.630
8	930	118.7	-4.777
9	1010	127.1	-4.845
10	1260	157.8	-5.061

1/Viscosity vs. Pressure Plot for HMIM PF_6 at 75 °C

Data from Harris et al. 10.1021/je700032n
J. Chem. Eng. Data 2007, 52, 1080-1085

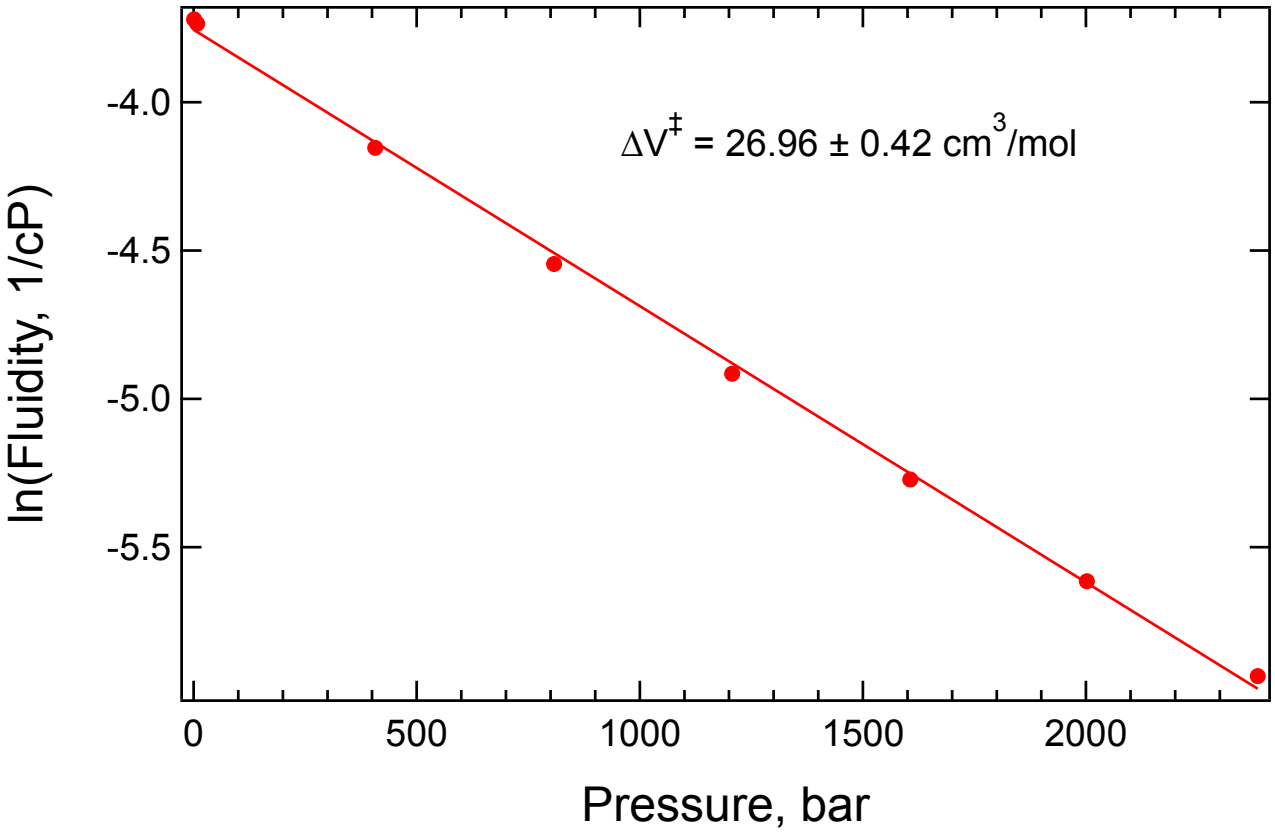

Point	Pressure	Visc, cP	ln(Fluidity)
0	1	41.3	-3.721
1	8	41.9	-3.735
2	407	63.7	-4.154
3	808	94.2	-4.545
4	1207	136.4	-4.916
5	1606	194.8	-5.272
6	2002	274.5	-5.615
7	2385	378	-5.935

1/Viscosity vs. Pressure Plot for HMIM TFSA at 25 °C

Data from Ahosseini and Scurto 10.1007/s10765-008-0497-7

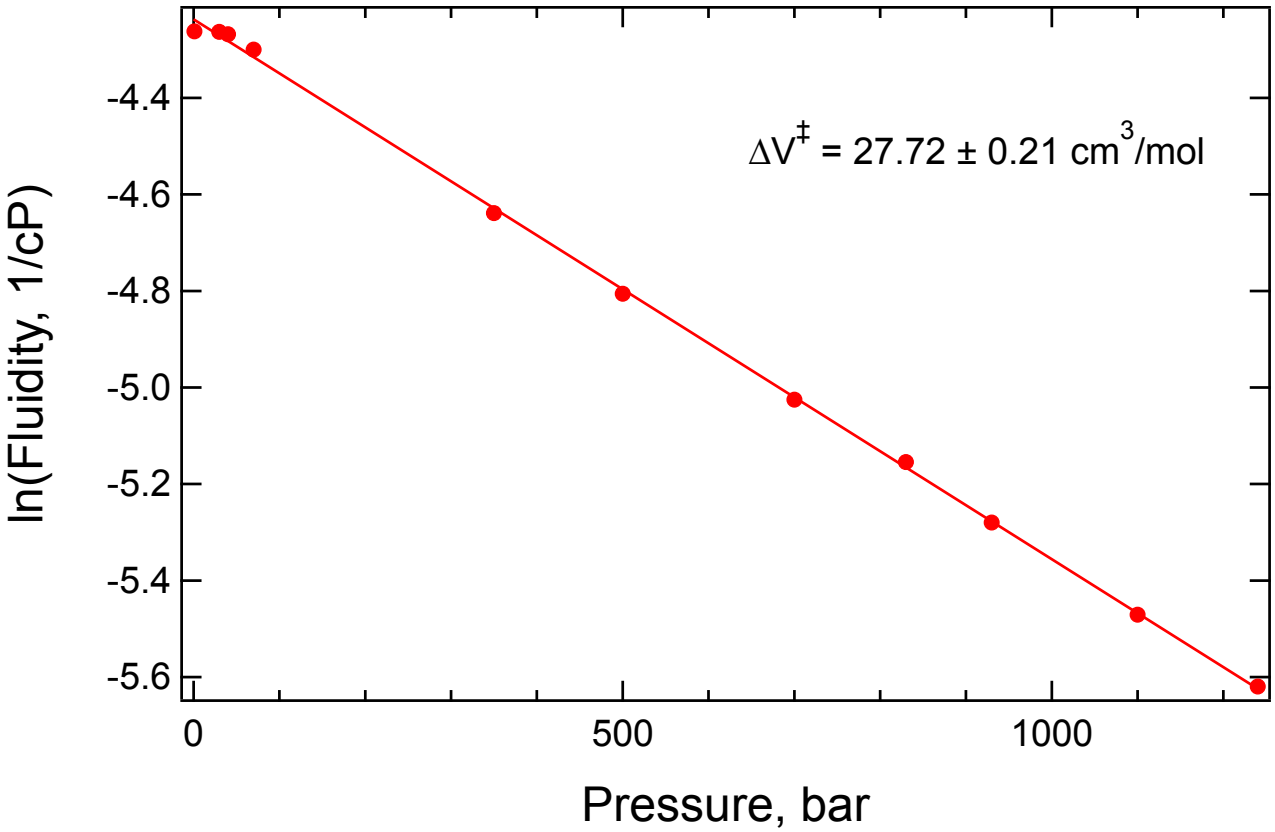

Point	Pressure	Visc, cP	ln(Fluidity)
0	1	70.96	-4.262
1	29.9	71.04	-4.263
2	40	71.38	-4.268
3	70	73.71	-4.300
4	350	103.4	-4.639
5	500	122.2	-4.806
6	700	152.2	-5.025
7	830	173.2	-5.154
8	930	196.3	-5.280
9	1100	237.6	-5.471
10	1240	275.7	-5.619

1/Viscosity vs. Pressure Plot for HMIM TFSA at 50 °C

Data from Ahosseini and Scurto 10.1007/s10765-008-0497-7

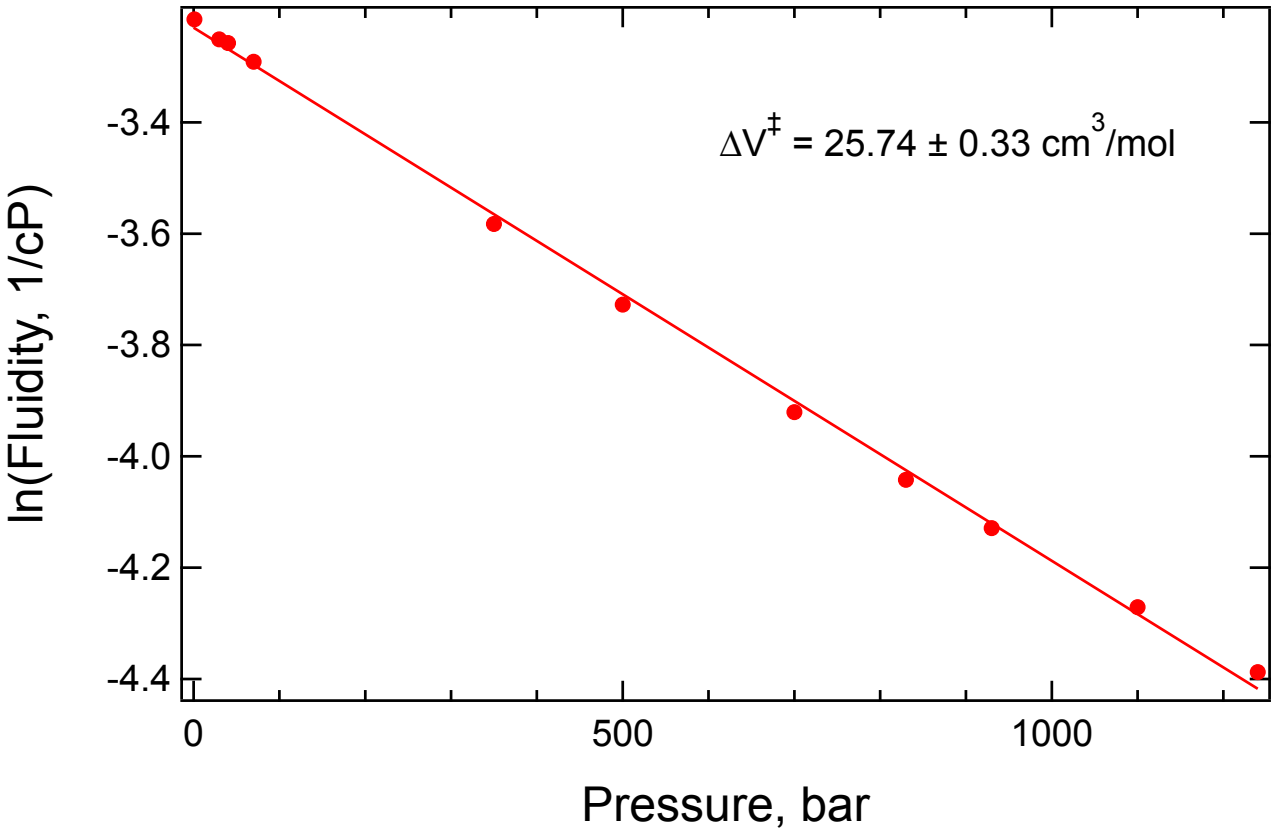

Point	Pressure	Visc, cP	ln(Fluidity)
0	1	24.9	-3.215
1	29.9	25.81	-3.251
2	40	25.98	-3.257
3	70	26.87	-3.291
4	350	35.96	-3.582
5	500	41.57	-3.727
6	700	50.43	-3.921
7	830	56.96	-4.042
8	930	62.11	-4.129
9	1100	71.6	-4.271
10	1240	80.46	-4.388

1/Viscosity vs. Pressure Plot for HMIM TFSA at 70 °C

Data from Ahosseini and Scurto 10.1007/s10765-008-0497-7

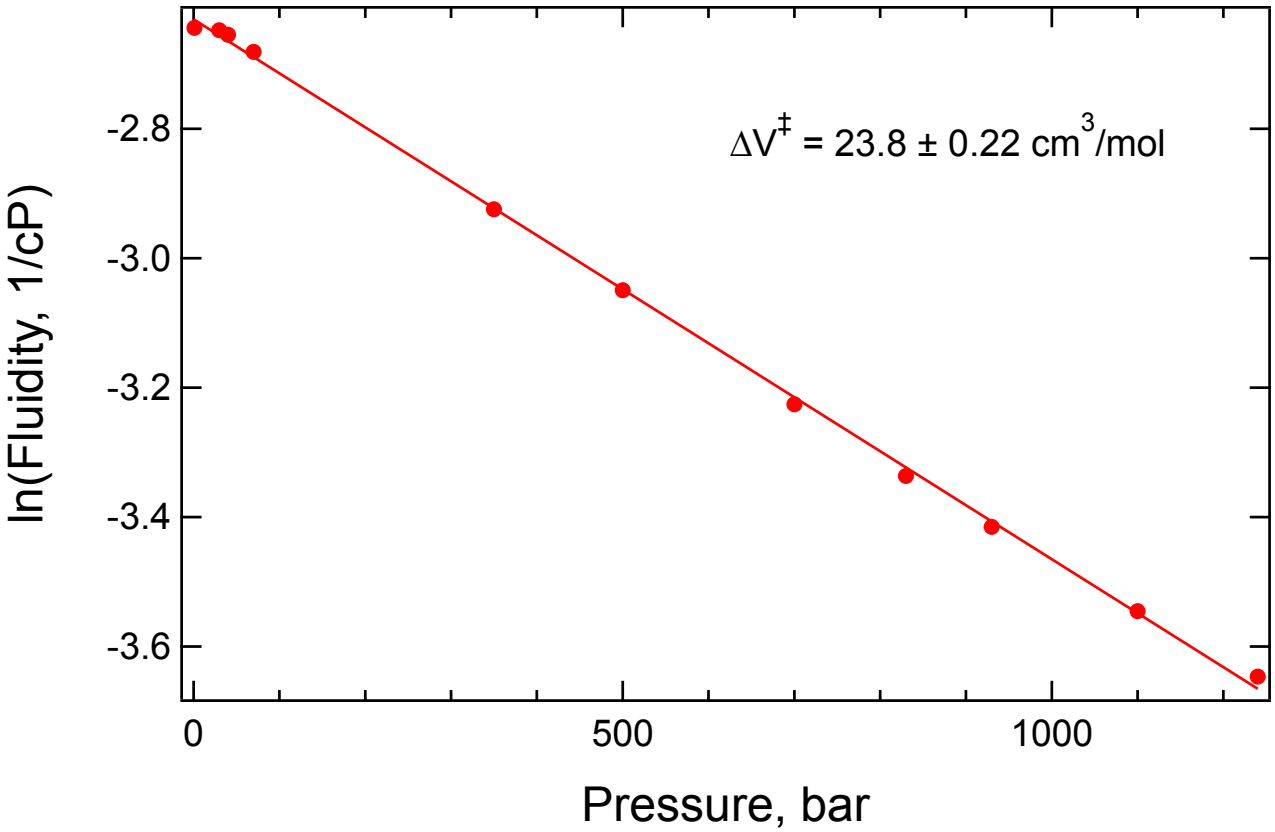

Point	Pressure	Visc, cP	ln(Fluidity)
0	1	14.07	-2.644
1	29.9	14.12	-2.648
2	40	14.22	-2.655
3	70	14.6	-2.681
4	350	18.62	-2.924
5	500	21.1	-3.049
6	700	25.17	-3.226
7	830	28.12	-3.336
8	930	30.42	-3.415
9	1100	34.65	-3.545
10	1240	38.34	-3.646

1/Viscosity vs. Pressure Plot for OMIM BF_4 at 20.5 °C

Data from Sanmamed et al. 10.1016/j.jct.2009.11.014

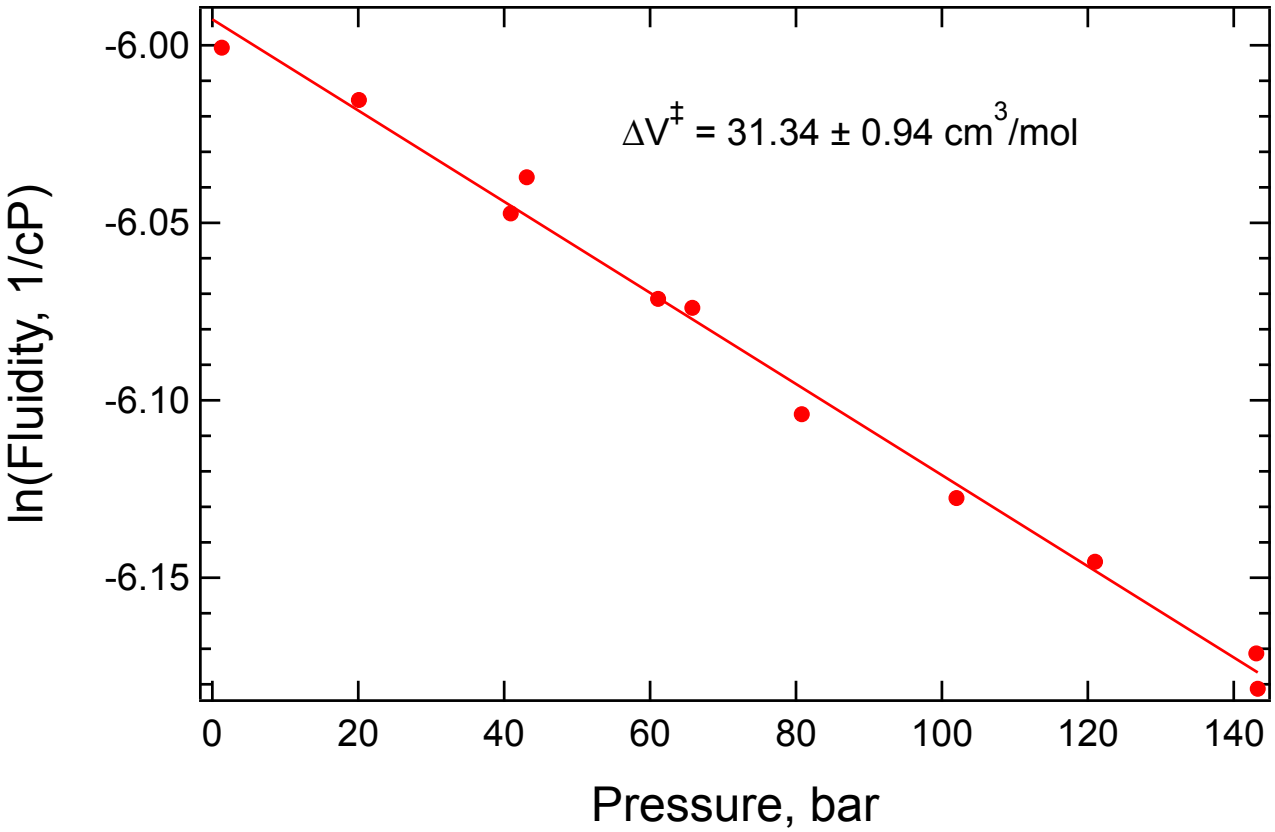

Point	Pressure	Visc, cP	ln(Fluidity)
0	1.3	403.7	-6.001
1	20.1	409.7	-6.015
2	40.9	423	-6.047
3	43.1	418.7	-6.037
4	61.1	433.3	-6.071
5	65.8	434.4	-6.074
6	80.8	447.6	-6.104
7	102	458.3	-6.128
8	121	466.6	-6.145
9	143.1	478.8	-6.171
10	143.3	483.6	-6.181

1/Viscosity vs. Pressure Plot for OMIM BF_4 at 25 °C

Data from Harris et al. 10.1021/je060082s

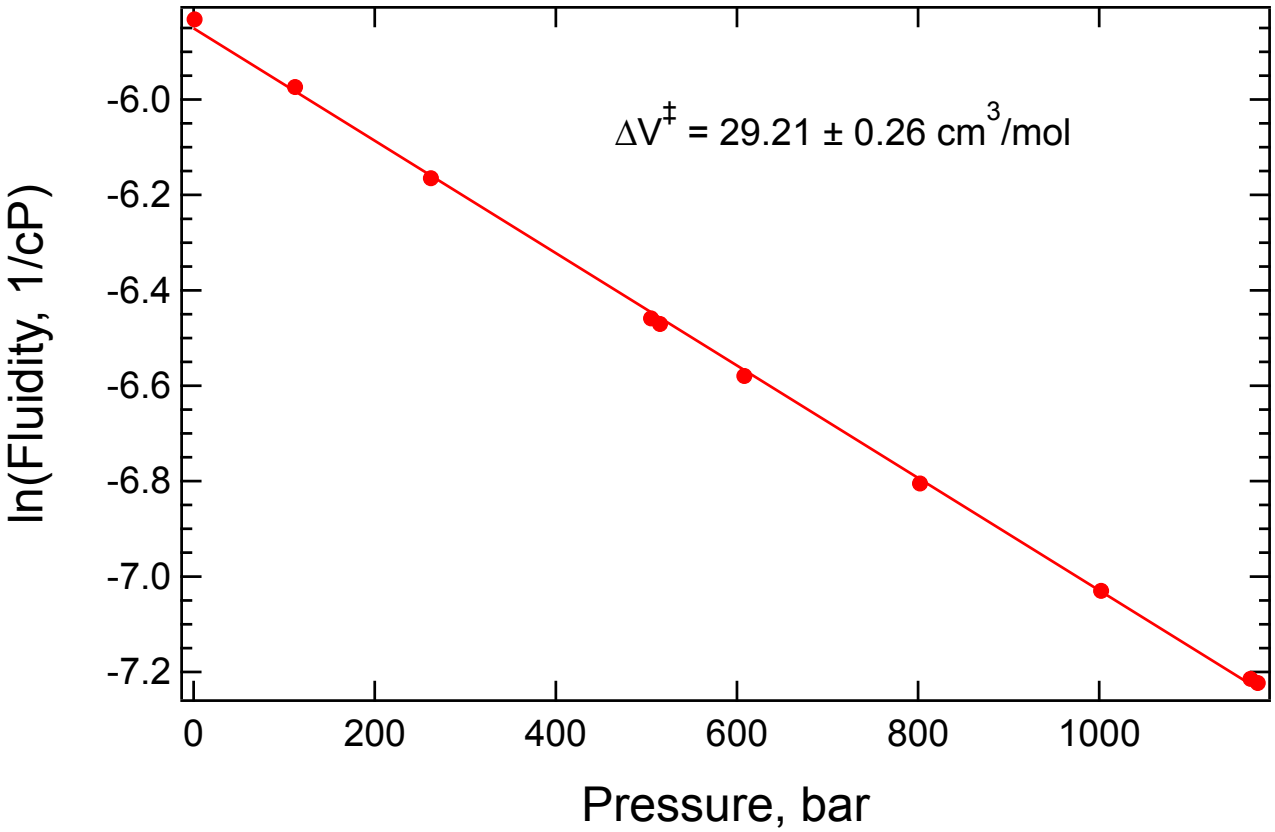

Point	Pressure	Visc, cP	ln(Fluidity)
0	1	341	-5.832
1	112	393	-5.974
2	262	475.7	-6.165
3	505	638.3	-6.459
4	515	645.9	-6.471
5	608	720.1	-6.579
6	802	902.3	-6.805
7	1002	1130	-7.030
8	1167	1359	-7.215
9	1175	1371	-7.223

1/Viscosity vs. Pressure Plot for OMIM BF_4 at 50 °C

Data from Harris et al. 10.1021/je060082s

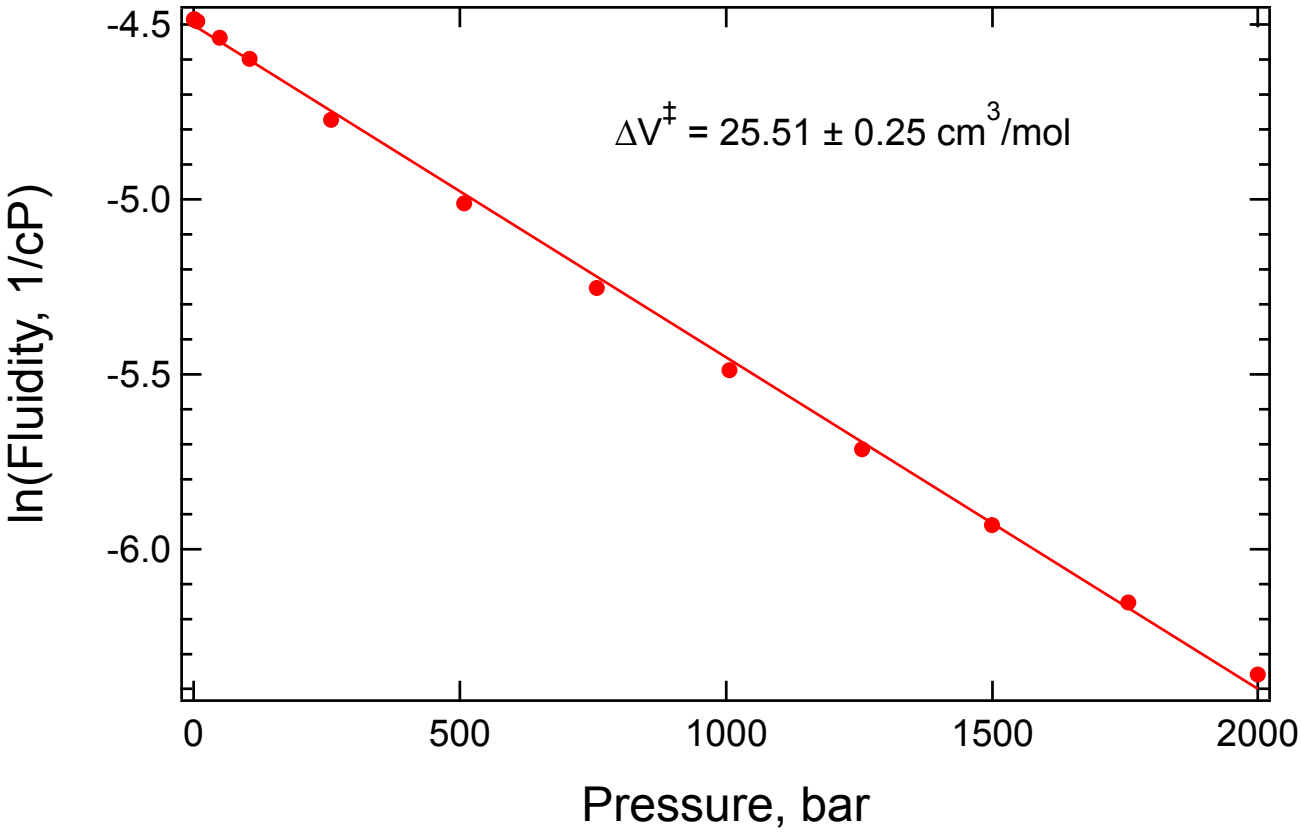

Point	Pressure	Visc, cP	ln(Fluidity)
0	1	88.8	-4.486
1	1	88.7	-4.485
2	1	88.7	-4.485
3	7	89.2	-4.491
4	49	93.5	-4.538
5	105	99.3	-4.598
6	258	118.2	-4.772
7	508	150.1	-5.011
8	757	191.2	-5.253
9	1006	241.8	-5.488
10	1255	303.1	-5.714
11	1499	376.5	-5.931
12	1755	469.8	-6.152
13	1998	577.3	-6.358

1/Viscosity vs. Pressure Plot for OMIM BF_4 at 60 °C

Data from Harris et al. 10.1021/je060082s

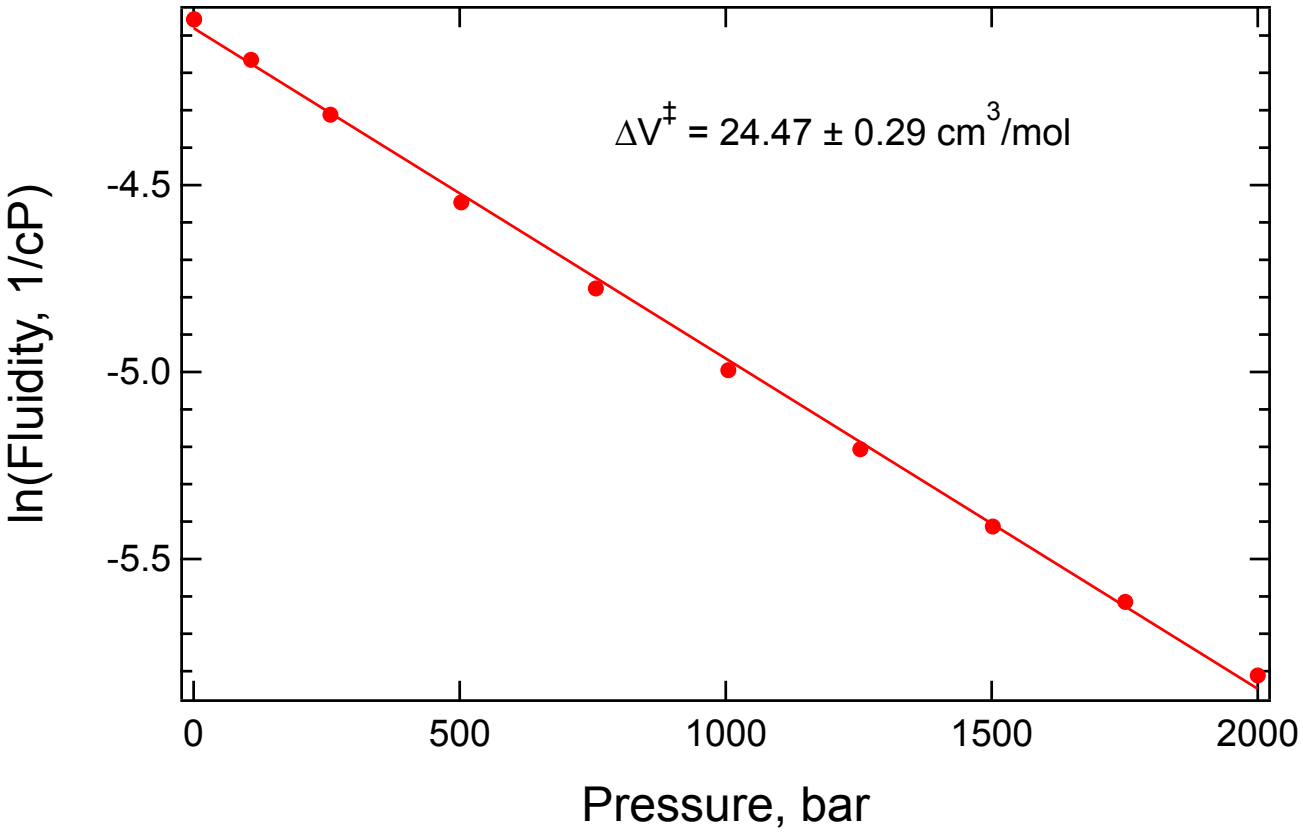

Point	Pressure	Visc, cP	ln(Fluidity)
0	1	57.8	-4.057
1	1	57.8	-4.057
2	108	64.4	-4.165
3	257	74.6	-4.312
4	503	94.3	-4.546
5	756	118.7	-4.777
6	1005	147.7	-4.995
7	1253	182.5	-5.207
8	1502	224.3	-5.413
9	1751	274.4	-5.615
10	2000	334.1	-5.811

1/Viscosity vs. Pressure Plot for OMIM BF_4 at 75 °C

Data from Harris et al. 10.1021/je060082s

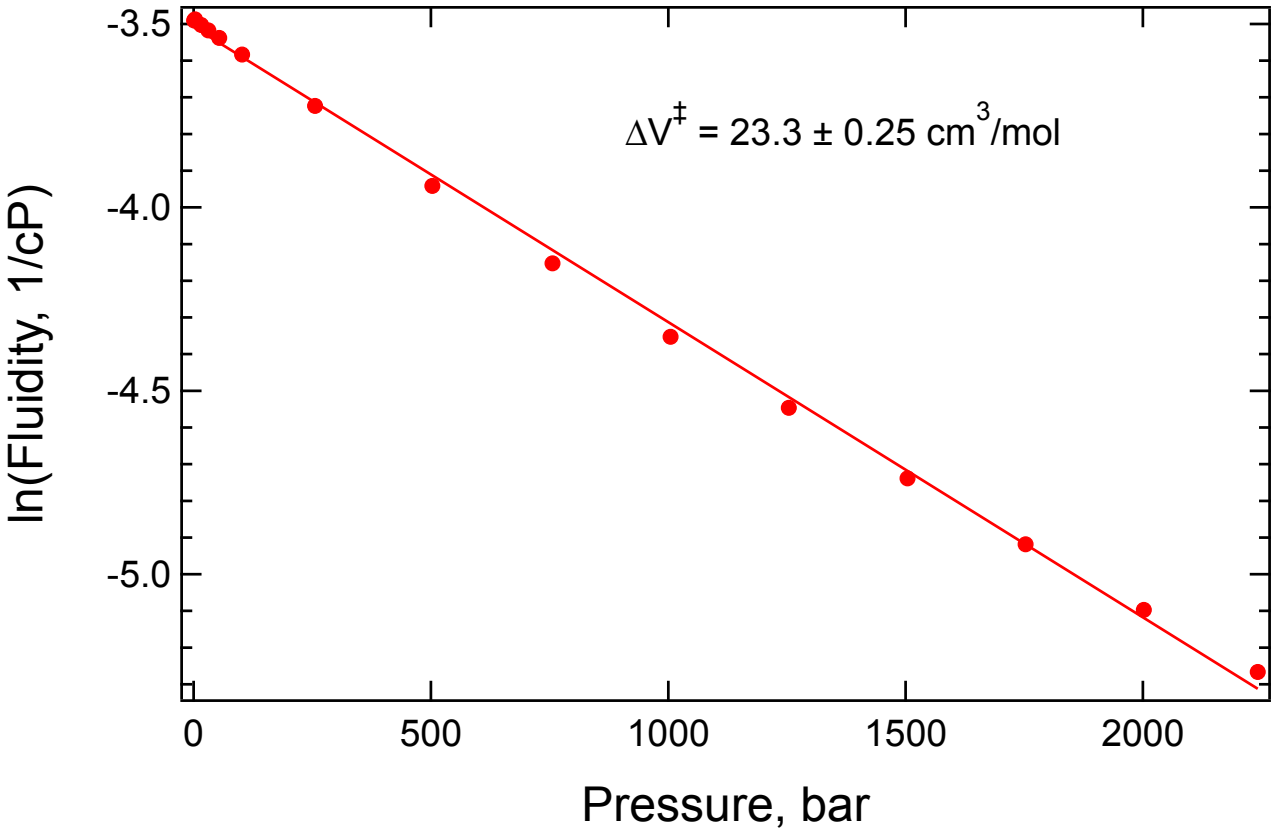

Point	Pressure	Visc, cP	ln(Fluidity)
0	1	32.8	-3.490
1	3	32.7	-3.487
2	16	33.2	-3.503
3	31	33.7	-3.517
4	54	34.4	-3.538
5	102	36	-3.584
6	256	41.4	-3.723
7	503	51.5	-3.942
8	756	63.6	-4.153
9	1005	77.7	-4.353
10	1254	94.3	-4.546
11	1504	114.3	-4.739
12	1753	136.8	-4.919
13	2002	163.6	-5.097
14	2242	193.7	-5.266

1/Viscosity vs. Pressure Plot for OMIM PF_6 at 20 °C

Data from Tomida et al. 10.1021/je060464y
J. Chem. Eng. Data 2007, 52, 577-579

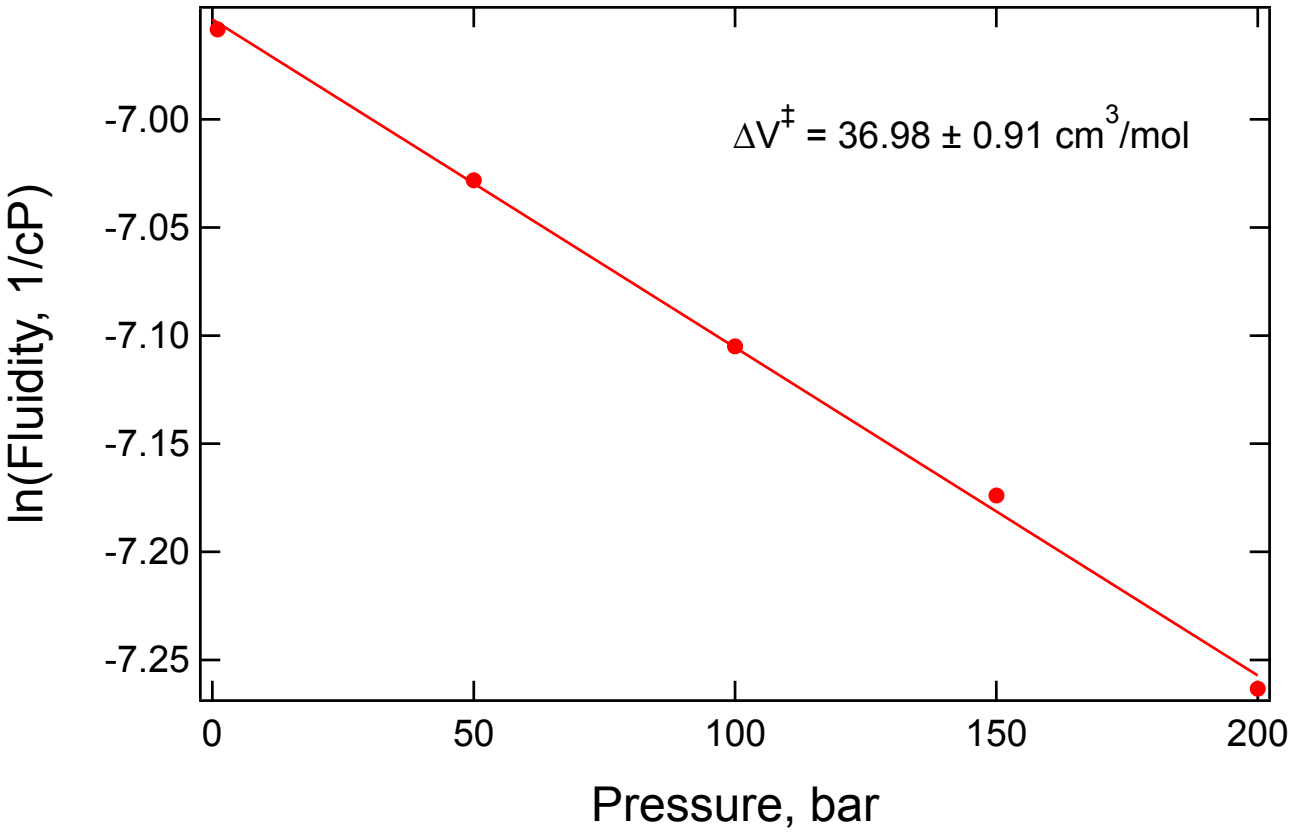

Point	Pressure	Visc, cP	ln(Fluidity)
0	1	1052	-6.958
1	50	1128	-7.028
2	100	1218	-7.105
3	150	1305	-7.174
4	200	1427	-7.263

1/Viscosity vs. Pressure Plot for OMIM PF_6 at 25 °C

Data from Harris et al. 10.1021/je060082s
J. Chem. Eng. Data 2006, 51, 1161-1167

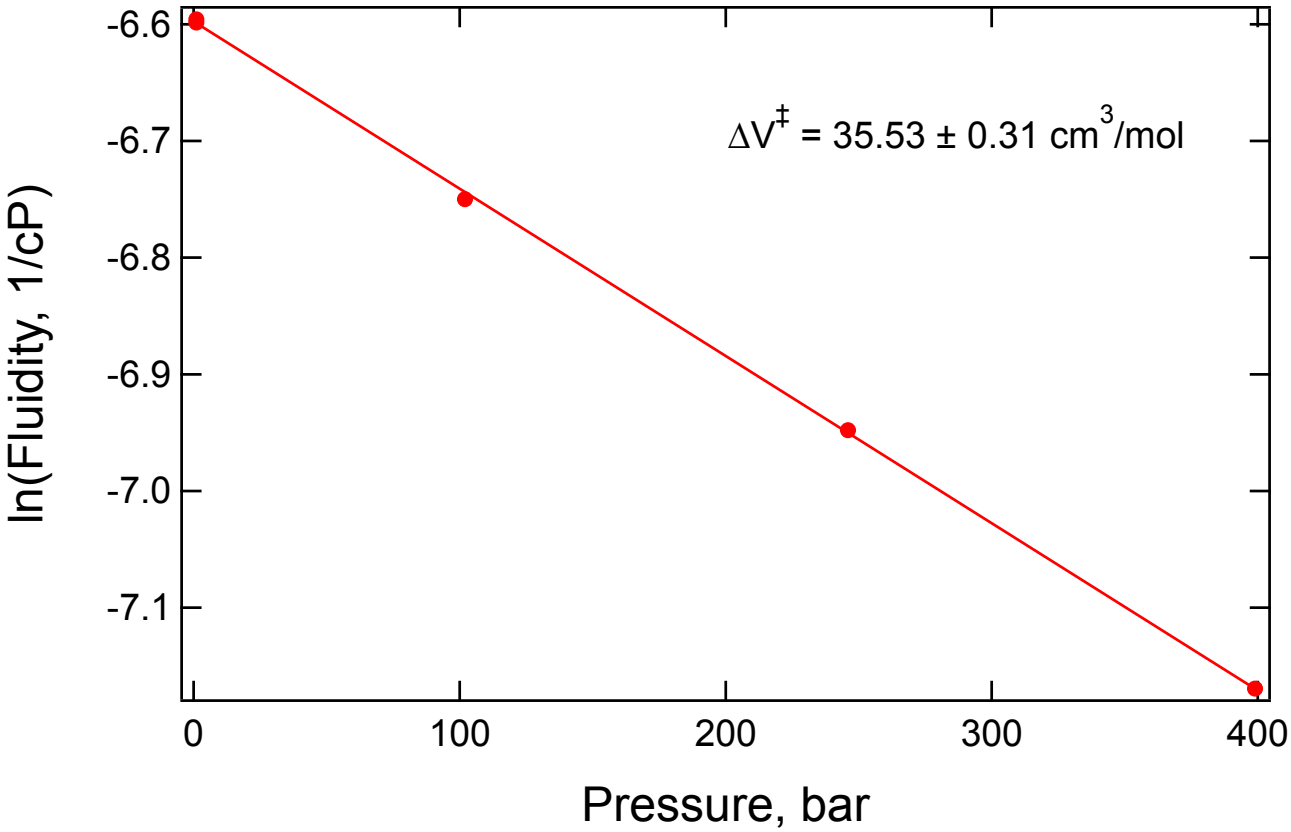

Point	Pressure	Visc, cP	ln(Fluidity)
0	1	734	-6.599
1	1	732	-6.596
2	102	854	-6.750
3	246	1041	-6.948
4	399	1299	-7.169

1/Viscosity vs. Pressure Plot for OMIM PF_6 at 35 °C

Data from Harris et al. 10.1021/je060082s
J. Chem. Eng. Data 2006, 51, 1161-1167

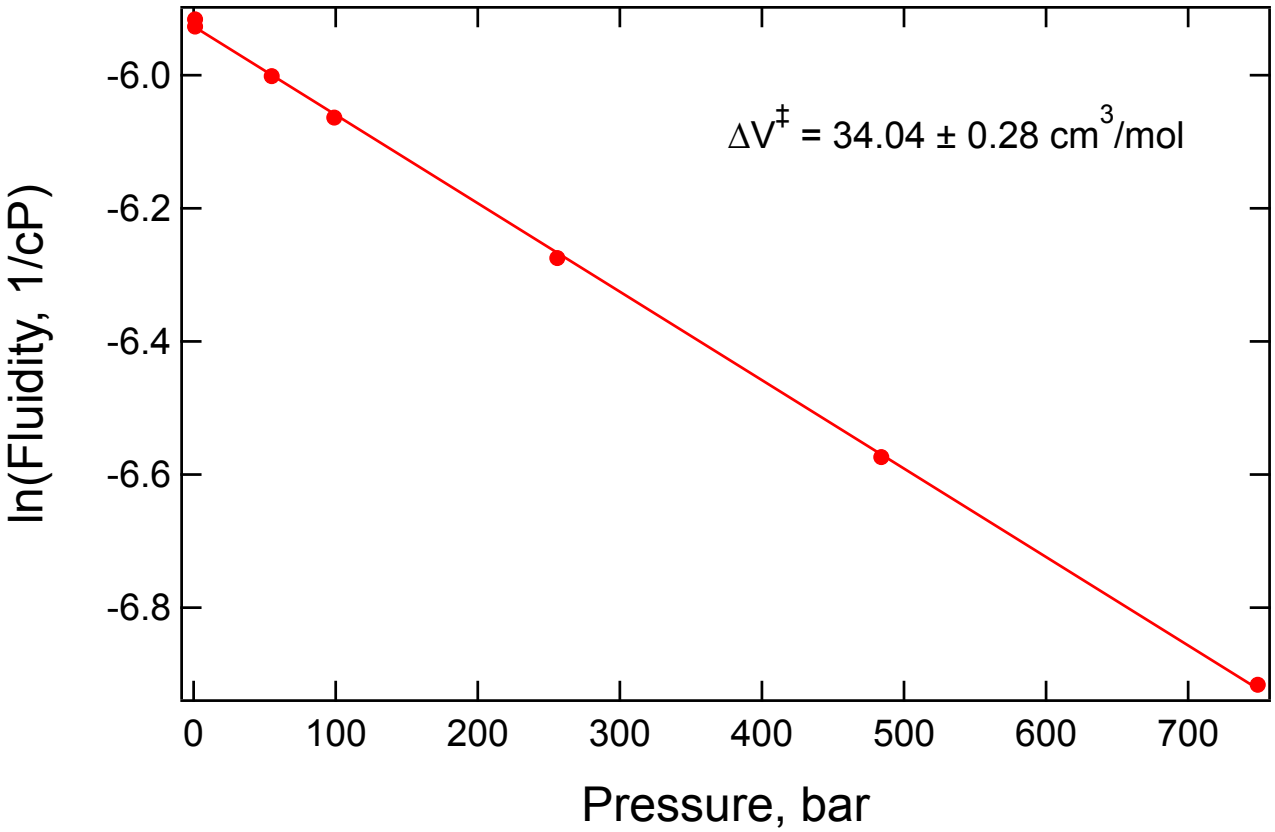

Point	Pressure	Visc, cP	ln(Fluidity)
0	1	375	-5.927
1	1	371	-5.916
2	55	404	-6.001
3	99	430	-6.064
4	256	531	-6.275
5	484	716	-6.574
6	749	1008	-6.916

1/Viscosity vs. Pressure Plot for OMIM PF_6 at 40 °C

Data from Tomida et al. 10.1021/je060464y
J. Chem. Eng. Data 2007, 52, 577-579

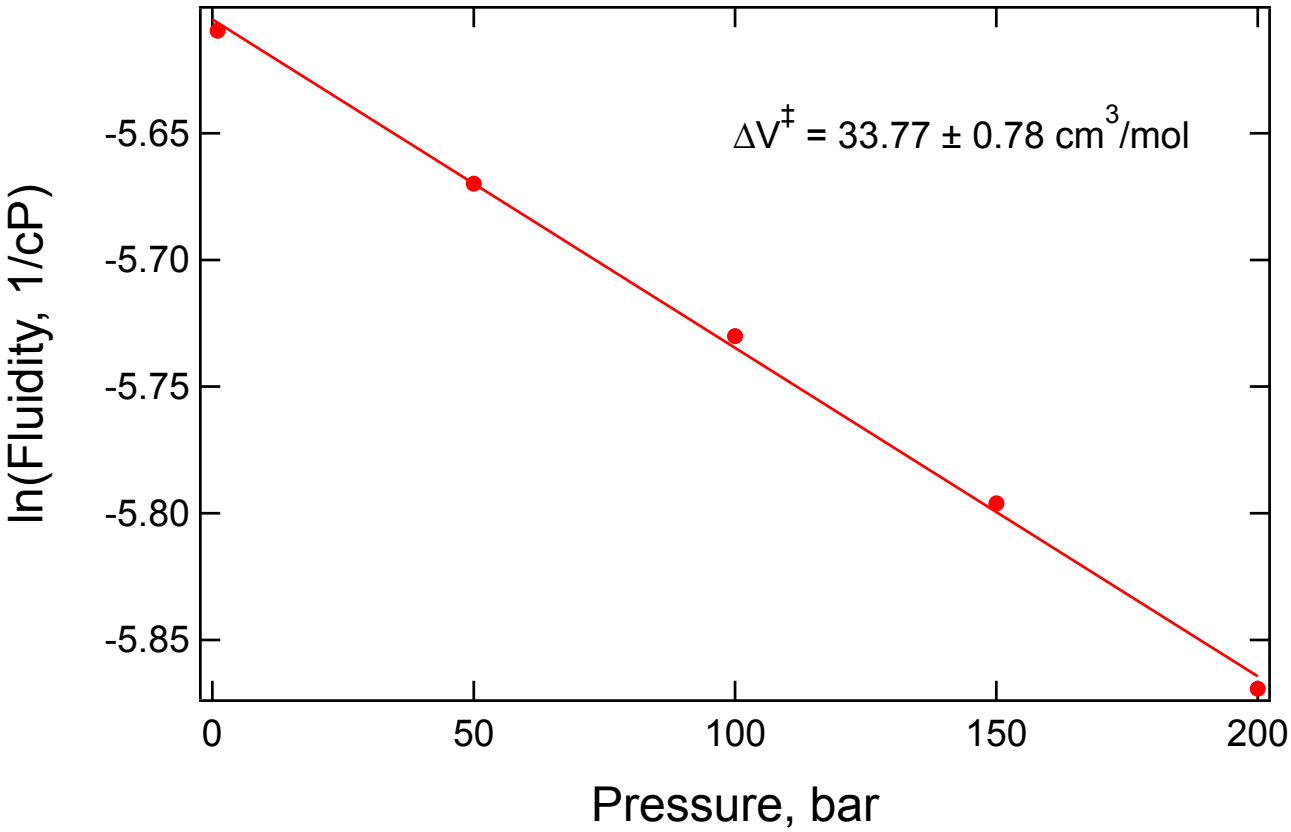

Point	Pressure	Visc, cP	ln(Fluidity)
0	1	273	-5.609
1	50	290	-5.670
2	100	308	-5.730
3	150	329	-5.796
4	200	354	-5.869

1/Viscosity vs. Pressure Plot for OMIM PF_6 at 60 °C

Data from Harris et al. 10.1021/je060082s
J. Chem. Eng. Data 2006, 51, 1161-1167

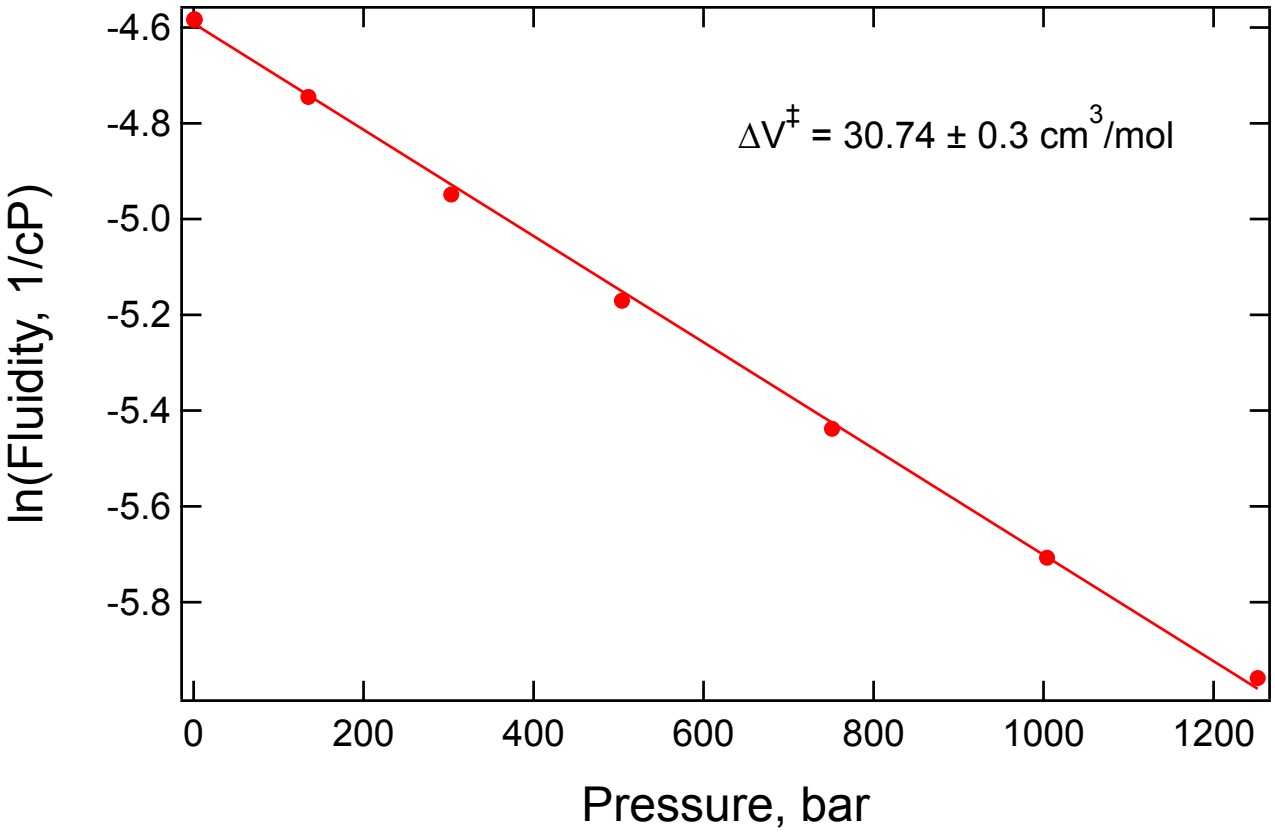

Point	Pressure	Visc, cP	ln(Fluidity)
0	1	97.9	-4.584
1	1	97.8	-4.583
2	1	97.9	-4.584
3	1	97.8	-4.583
4	135	115	-4.745
5	303	141	-4.949
6	504	176	-5.170
7	751	230	-5.438
8	1004	301	-5.707
9	1252	387	-5.958

1/Viscosity vs. Pressure Plot for OMIM PF_6 at 60 °C

Data from Tomida et al. 10.1021/je060464y
J. Chem. Eng. Data 2007, 52, 577-579

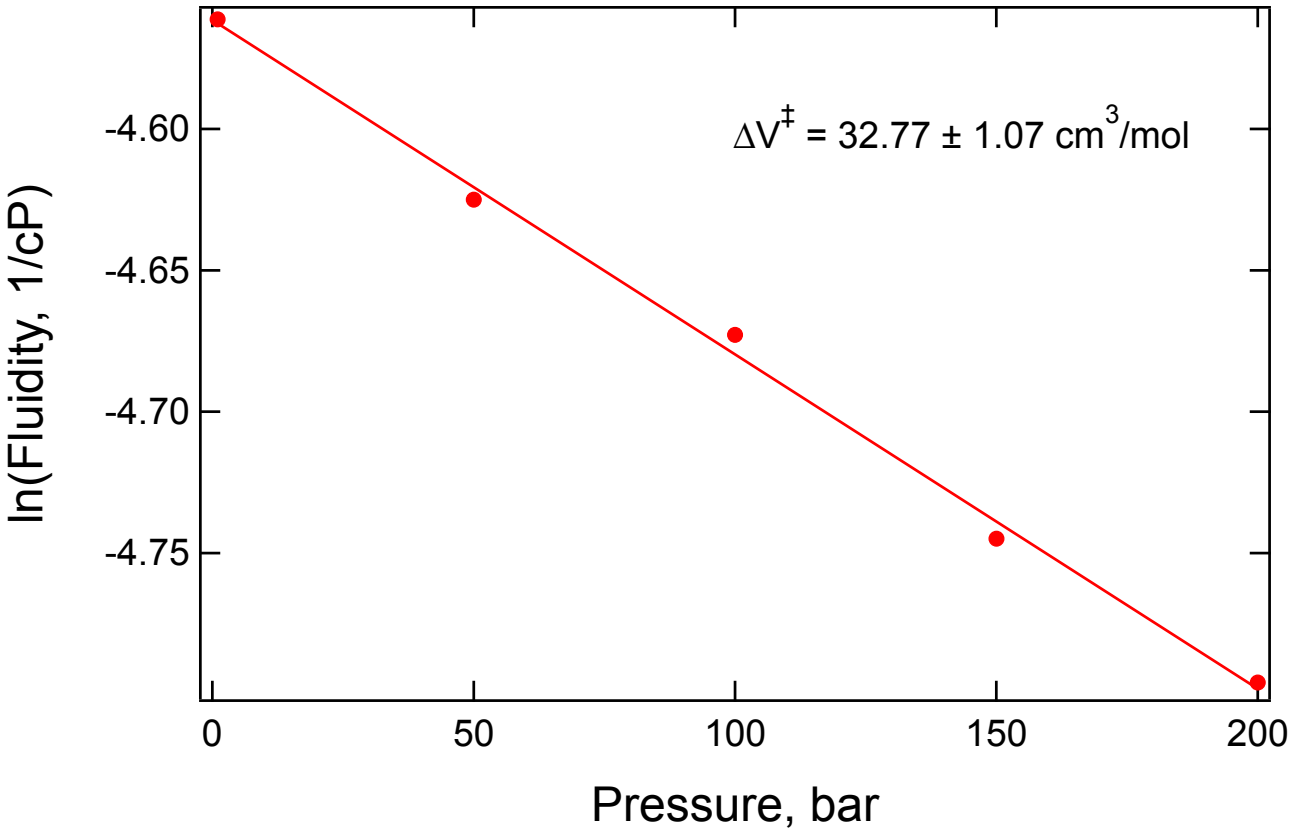

Point	Pressure	Visc, cP	ln(Fluidity)
0	1	95.7	-4.561
1	50	102	-4.625
2	100	107	-4.673
3	150	115	-4.745
4	200	121	-4.796

1/Viscosity vs. Pressure Plot for OMIM PF_6 at 70 °C

Data from Harris et al. 10.1021/je060082s
J. Chem. Eng. Data 2006, 51, 1161-1167

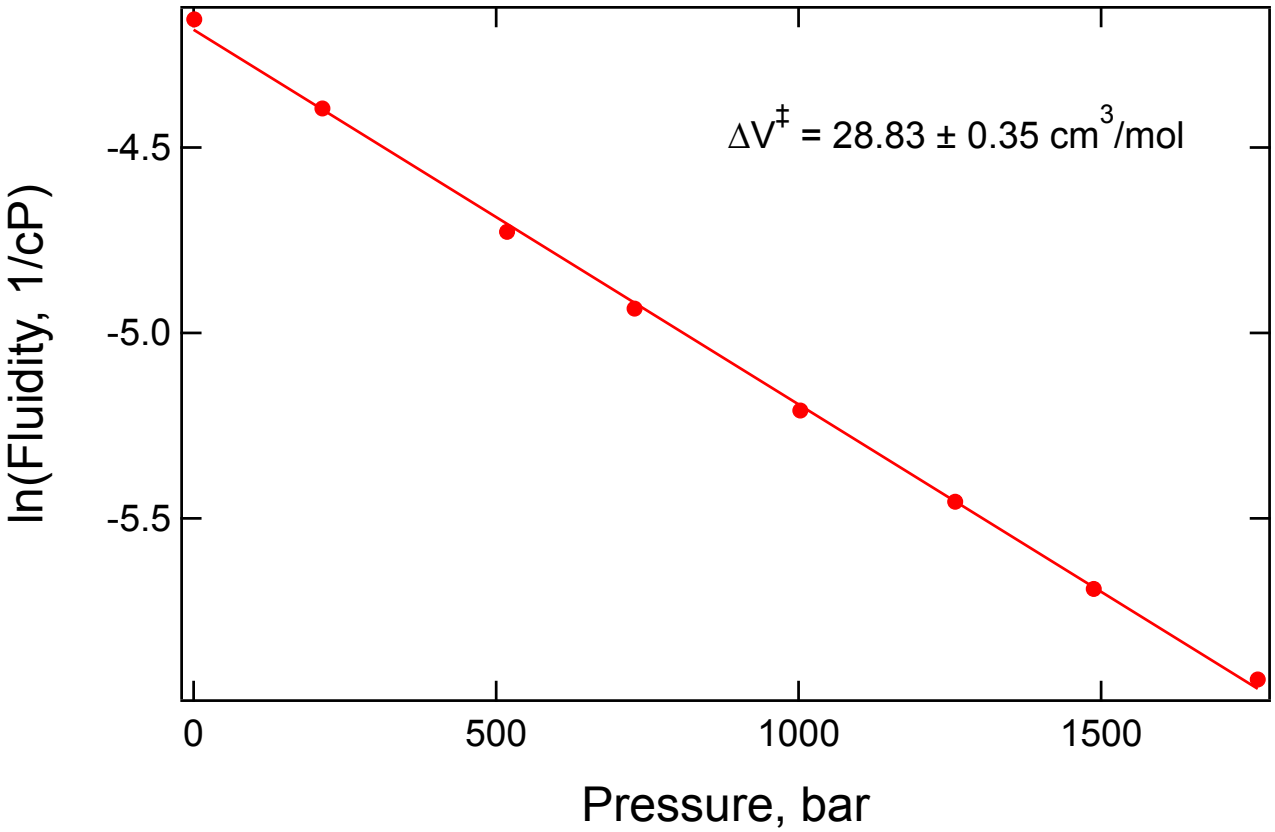

Point	Pressure	Visc, cP	ln(Fluidity)
0	1	63.7	-4.154
1	213	81	-4.394
2	518	113	-4.727
3	729	139	-4.934
4	1003	183	-5.209
5	1259	234	-5.455
6	1488	296	-5.690
7	1759	378	-5.935

1/Viscosity vs. Pressure Plot for OMIM PF_6 at 80 °C

Data from Tomida et al. 10.1021/je060464y
J. Chem. Eng. Data 2007, 52, 577-579

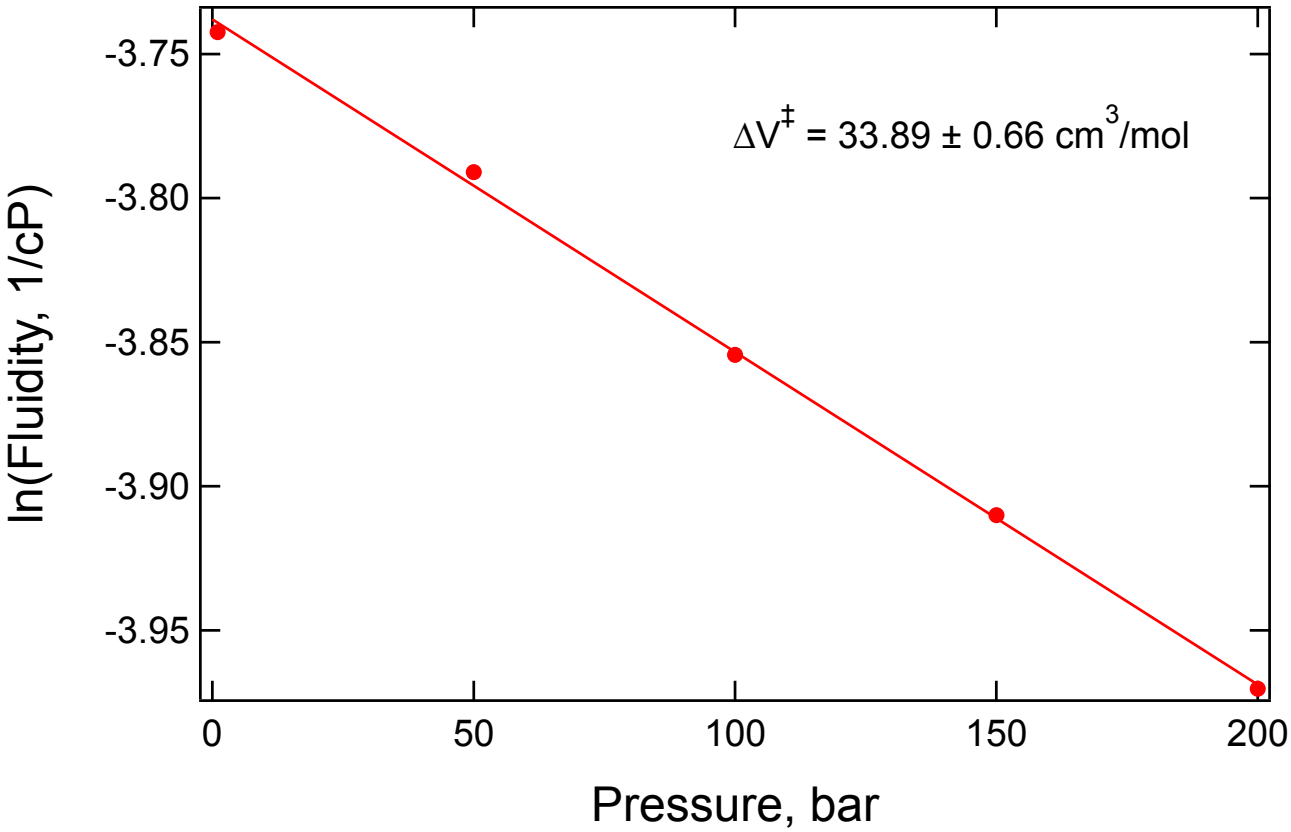

Point	Pressure	Visc, cP	ln(Fluidity)
0	1	42.2	-3.742
1	50	44.3	-3.791
2	100	47.2	-3.854
3	150	49.9	-3.910
4	200	53	-3.970